Master's Thesis

Investigating the 4-point truncation of the JIMWLK evolution equation

by:

Mohammad Faaris Alam

Supervisor: Associate Professor Heribert Weigert

A thesis submitted in fulfilment of the requirements for the Master of Science in Theoretical Physics

of the

Department of Physics,
Faculty of Science,
University of Cape Town

"One day the world may end
But there's still plenty to discover"

- Portugal. The Man, from *So Young*

Abstract

The Colour Glass Condensate (CGC) is a dense gluonic state that dominates in-state hadrons in deep inelastic scattering (DIS). The JIMWLK equation describes the rapidity evolution of Wilson line correlators in the CGC framework, which are crucial for computing cross-sections in DIS. However, JIMWLK generates an infinite hierarchy of coupled integro-differential equations (the Balitsky hierarchy), for which no analytical or numerical solutions exist. To address this, R. Moerman and H. Weigert introduced a parameterisation scheme that reparameterises the rapidity dependence of Wilson line correlators into n-point colour structure functions while preserving JIMWLK symmetry, gauge invariance, and finiteness for N_c. Since this involves an infinite sum, truncation at some order p is necessary. While 2- and 3-point truncations have been studied extensively, this thesis extends the framework to 4-point truncations to capture the physics of 4-point Wilson line correlators. We first refine the parameterisation scheme, identifying an additional term required at the 4-point level. We then construct a suitable basis for adjoint singlet states, which may help isolate iterated 2-point contributions, and leverage Hermitian Young Projection Operators and transition operators—key tools in the 4-point truncation studied by J. Alcock-Zeilinger and H. Weigert. Applying the 4-point truncation to Wilson line correlators, we aimed to derive an update equation for the 4-point colour structure functions, facilitating numerical implementation. Although significant progress has been made, the unresolved complexities suggest the need for new techniques and frameworks. This thesis provides an outlook on potential approaches to overcoming these challenges and advancing our understanding of high-energy QCD.

Acknowledgements

Firstly, I would like to thank the SA-CERN programme for awarding me the SA-CERN Excellence Bursary which was the primary source of funding that allowed me to complete my MSc degree.

Furthermore, I must thank my supervisor Associate Professor Heribert Weigert for guiding me throughout this Master's and allowing for its completion. I am eternally grateful to him for his seemingly infinite patience in explaining complex mathematical and physical concepts to me over and over again and for his expert supervision throughout my Master's. Through him, I have not only learned a great deal of mathematical physics but I also learned what it is like to conduct research in physics. I've learnt invaluable lessons in conducting research not only in physics but science as a whole and I have come out of this Master's with a much deeper understanding of what research in theoretical physics entails, which will surely aid me in the future. I would also like to thank him for going through multiple drafts of my thesis and providing excellent feedback which greatly improved my thesis and resulted in the superior version you are reading now.

I'd also like to thank Judith Alcock-Zeilinger for providing me with the birdtrack diagrams and corresponding TikZ code that I needed during the last stretch of write-up of this thesis. By doing so, she potentially saved me weeks of having to learn how to create birdtrack diagrams myself, and I cannot thank her enough for being willing to share her diagrams and code with me.

Then of course, I must thank my friends for keeping me sane these past 2 years and getting me through this thesis. In no particular order, I'd like to thank Miles Kidson, Zayd Pandit, Cole Faraday, Ben Bert, Kaylie Chernotsky, Samantha Parle, Alice McKnight, Stephan Potgieter, Salmaan Barday and Joshua Browne. I am grateful for the many lunches, tea times and fooling around in-between that we had over these years; you have no idea how much I needed some of those moments when I was really going through the most. Thank you guys, you're all amazing and wonderful people and I would not have finished this MSc without you :) Special shout out to Cole Faraday, Zayd Pandit and Ben Bert for carefully reading through my introduction and giving me great feedback on it and Stephan Potgieter, Salmaan Barday and Joshua Browne for letting me use their ALICE office.

I'd like to especially thank one of my closest friends, Carl Brann, for his sage advice that

led me to pursue this MSc. He has been an encouraging and supportive presence in my life throughout the years and I have truly come to value our friendship over the years. Thank you for being genuinely interested in the work that I do, even as someone who is not in the field of theoretical physics. Your interest and words of encouragement are also what kept me going through the trying times of this thesis.

Finally, I'd like to thank my parents and my brother, Maarij Alam. My parents for affording me the privilege which allowed me to pursue a degree in physics, and my brother, whom I lived with during the course of this MSc, for the many late night chats we had which made me grateful to be here at UCT.

Contents

Chapter 1

Introduction

1.1 High-Energy Physics

Quantum field theories, specifically quantum chromodynamics (QCD), are essential in describing the strong force that mediates interactions between quarks and gluons [1–4]. While QCD has been successful in explaining a range of phenomena, such as deep inelastic scattering and quark confinement [1, 2], much remains unknown about its high-energy behavior, such as the properties of the quark-gluon plasma (QGP) [5]. Understanding this behavior is crucial, as it could provide insights into the early universe, where a QGP is thought to have existed [6], and enable precise predictions for high-energy scattering experiments. High-energy scattering, both experimentally and theoretically, remains the primary method for testing the predictions of quantum field theories like QCD.

High-energy scattering experiments are conducted at facilities like the Large Hadron Collider (LHC) at CERN, the Relativistic Heavy Ion Collider (RHIC) at Brookhaven National Lab (BNL), and the HERA (Hadron-Electron Ring Accelerator) particle accelerator at DESY (Deutsches Elektronen-Synchrotron) in Hamburg, Germany. These experiments generally fall into two categories, which can be illustrated with a simple analogy to studying the internal structure of a watermelon[1]. One can either smash the watermelon to break it into its constituent parts or slice it to examine its internal structure. In high-energy physics, the first method corresponds to colliding heavy nuclei or protons at high energies, as done at RHIC and the LHC, to observe their constituents. The second method involves deep inelastic scattering (DIS) experiments, where an electron, commonly referred to as the probe, collides with a nucleus or proton to probe its internal structure via the strong force. This thesis focuses on the latter method, investigating electron-nucleus or electron-proton collisions.

As the energy of high-energy scattering experiments increases, the gluon occupation in nuclei (as observed by the probe) grows, eventually surpassing that of quarks. This leads

[1] This analogy was adapted from Asmita Mukherjee's UCT (University of Cape Town) CTMP (Centre for Theoretical and Mathematical Physics) seminar titled "Probing matter in three dimensions" (13 September 2024, University of Cape Town, available at: https://www.youtube.com/watch?v=r8zRBCigWTw).

to gluon saturation, where the effective size of gluons becomes large enough to limit further occupation [7–10]. The resulting state of matter is described by the colour glass condensate (CGC) [10–14], which is thought to be the initial state before a DIS event. The CGC evolves into the glasma, which then transitions into the QGP [15, 16]. Understanding the CGC is crucial for exploring the stages of the early universe and gaining insights into these high-energy processes.

An essential tool for understanding the CGC is the JIMWLK evolution equation, a renormalization group (RG) equation that describes the rapidity evolution of observables in the CGC [13, 17]. It governs the evolution of n-point Wilson line correlators, which are central to the CGC and DIS. These correlators describe the scattering amplitude of n partons with a dense gluonic target at n specific transverse coordinates, under the eikonal approximation which assumes soft gluon emission[2] [18]. A Wilson line correlator is constructed from two key components, which will be discussed throughout this thesis:

- **Wilson lines**: Summing all Feynman diagrams for quarks emitting and absorbing soft gluons eikonally to all orders along a straight line [19, 20].
- **Singlet states of SU(N)**: Color-neutral states formed by the combination of color-charged objects (Wilson lines) due to color confinement [2].

These correlators play a crucial role in total cross-sections for processes such as dijet production in DIS and pA (proton-nucleus) collisions [21], as well as medium-induced gluon radiation in forward parton scattering [22]. Determining their rapidity evolution is essential for calculating cross-sections, providing a direct test of QCD's predictive power. This makes understanding Wilson line correlators a key objective in high-energy physics.

Significant effort has been dedicated to constructing Wilson line correlators, as identifying useful forms of these correlators is non-trivial [23]. A major contribution in this area was made in the PhD thesis of J. Alcock-Zeilinger [23], which led to publications on constructing Wilson line correlators that simplify in specific coincidence limits—where quarks are brought onto anti-quarks or (anti)-quarks onto (anti)-quarks [24–26]. Simplifications in these limits are essential, as QCD calculations often involve configurations where parton separations become negligible. Alcock-Zeilinger's work focused on finding suitable bases for the space of color singlet states of SU(N), leveraging representation theory to develop an algorithm that constructs correlator matrices simplifying in both quark/anti-quark and (anti)-quark/(anti)-quark coincidence limits.

In this thesis, we extend this work by presenting a new basis of singlet states that allows for the construction of Wilson line correlator matrices simplifying under *combined* quark/anti-

[2] Soft gluon emissions occur when emitted gluons have much lower energy than the emitting parton, without altering its travel direction.

quark and (anti)-quark/(anti)-quark coincidence limits. To our knowledge, this basis and the resulting simplifications are new contributions to the literature. Such a basis may prove easier to work with in the future when considering the JIMWLK evolution of a Wilson line correlator constructed in this basis.

Applying the JIMWLK evolution equation to Wilson line correlators generates an infinite hierarchy of coupled integro-differential equations. This hierarchy, known as the Balitsky-Kovchegov (BK) hierarchy, is a hierarchy in the sense that it involves the evolution of n-point correlators that depend on $(n+1)$-point correlators [13]. This hierarchy cannot be solved exactly, posing significant challenges in determining the rapidity evolution of Wilson line correlators. Various approaches have been explored to tackle this problem, including numerical methods [27] and analytical solutions in the large-N_c limit [28–32]. However, these methods often break gauge invariance or fail to remain finite in N_c, limiting their applicability—especially for observables in DIS that require gauge invariance and N_c finiteness [17, 33].

To address these limitations, R. Moerman and H. Weigert proposed a gauge-invariant, symmetry-preserving parameterization of the JIMWLK equation [33]. In this approach, the rapidity dependence of Wilson line correlators is re-expressed in terms of ***n*-point color structure functions**—the new primary objects solved by the JIMWLK equation. Since this parameterization forms an infinite sum over all possible n-point functions, practical calculations require truncating the sum at a finite order, referred to as the ***n*-point truncation of JIMWLK**.

These color structure functions are the central focus of this thesis. Analogous to structure functions in the DGLAP framework, which parameterize the hadronic tensor in deep inelastic electron-proton scattering [34–36], n-point color structure functions encode the physics of n-wise interactions within Wilson line correlators. For example, 2-point functions describe pairwise interactions, while 3-point and higher functions capture multi-particle correlations. Higher-order interactions become relevant only in systems with sufficient particle number, making these functions key to understanding complex QCD dynamics. Extensive work has been done on 2-point and 3-point color structure functions, derived from Gaussian and 3-point truncations [17, 33, 37–39]. However, these functions only capture up to 3-body interactions, while the Wilson line correlators relevant to the total cross-sections in DIS—such as dijet production and medium-induced gluon radiation—are **4-point correlators** [21, 22]. To fully describe the physics of these observables, it is necessary to study the JIMWLK evolution of 4-point correlators, which requires deriving the corresponding **4-point color structure functions**.

This thesis focuses on investigating the **4-point truncation** of the JIMWLK equation, aiming to construct these higher-order structure functions. Extending the truncation to 4-

point interactions is expected to improve the accuracy of rapidity evolution predictions for Wilson line correlators when compared to experimental data. Testing this hypothesis will help determine whether pursuing even higher-order truncations is worthwhile for future studies.

To apply the 4-point truncation, we must incorporate a critical element in the JIMWLK truncation framework: the **color adjoint singlet states**. These colour adjoint singlet states, composed purely of gluons, are essential for maintaining color neutrality in the Wilson line correlator matrix during the parameterization and truncation processes. Identifying a suitable basis for these adjoint singlet states is non-trivial and was the focus of J. Rayner's MSc thesis [40]. In his work, he proposed a basis with advantageous symmetry properties, which can transfer to the color structure functions, simplifying complex expressions through symmetry exploitation.

In this thesis, we adopt J. Rayner's basis for the 4-point truncation, with modifications aimed at subtracting redundant contributions from the squared Gaussian truncation. Since the Gaussian truncation squared can mimic certain 4-point effects, isolating and removing these overlaps will help highlight genuine 4-point contributions.

Furthermore, during the 4-point truncation, we discovered that the parameterization ansatz introduced by R. Moerman and H. Weigert was no longer the most general form. At this level, an additional term emerges that satisfies all required properties and extends the parameterization beyond what has been previously documented. We generalize the ansatz to accommodate this new term at the 4-point level, presenting a novel contribution to the literature.

While beyond the immediate scope of this thesis, deriving the 4-point color structure functions connects directly with the jet-JIMWLK correspondence explored in J. Bohra's MSc thesis [41], the development of Soft Collinear Effective Theory by T. Becher [42], and advancements in parton shower Monte Carlo codes by S. Platzer [43]. These connections highlight the broader relevance of our work to ongoing research in high-energy physics.

Since the 4-point truncation of the JIMWLK evolution equation has not yet been explored in the literature, this thesis is dedicated to its development and application. To this end, we present the theoretical framework necessary for understanding and deriving the 4-point truncation. This involves summarizing key contributions from J. Alcock-Zeilinger and H. Weigert on **constructing Wilson line correlators from singlet states**, R. Moerman and H. Weigert on **symmetry-preserving, gauge-invariant truncations of JIMWLK**, and J. Rayner and H. Weigert on developing a suitable basis for the space of **colour adjoint singlet states**. This thesis brings together these foundational works, extending them toward the derivation of the 4-point colour structure functions. The structure of this thesis, outlined in the following section, follows this progression.

1.2 How to read this thesis

Chapter 2 introduces the theoretical foundations of the Color Glass Condensate (CGC) in Quantum Chromodynamics (QCD), focusing on Deep Inelastic Scattering experiments (**Chapter 2.1**), the Regge-Gribov limit (**Chapter 2.2**), and the role of Wilson lines in the JIMWLK evolution equation (**Chapter 2.3**). This chapter lays the groundwork for understanding the high-energy physics underlying the JIMWLK evolution equation and motivates the need for truncation schemes explored in this thesis.

In **Chapter 3**, we explore the construction of Wilson line correlators, pivotal for understanding the JIMWLK equation's rapidity evolution. We begin by introducing birdtracks, a graphical notation that simplifies group-theoretical computations (**Chapter 3.1**). The reader should note that the birdtrack notation used throughout this thesis is somewhat non-standard compared to other birdtrack literature; for example [44]. We then delve into the construction of correlator matrices, discussing the roles of Hermitian Young Projection Operators, transition operators, the Fierz basis and color singlet states (**Chapter 3.2**). The chapter also presents new work on an alternative basis for singlet states, enabling the construction of Wilson line correlator matrices suited for various combinations of coincidence limits. This foundation is crucial for the systematic representation of Wilson line correlators in our study (**Chapter 3.2**). For a deeper dive into the theoretical foundations and mathematical formalism, readers are encouraged to explore the references provided in this chapter.

In **Chapter 4**, we present a gauge-invariant, symmetry-preserving truncation framework for the JIMWLK evolution equation, as developed by R. Moerman and H. Weigert. We begin by discussing a novel parameterization of JIMWLK, which necessitates constructing a basis for the adjoint color singlet states in $A^{\otimes m}$ (**Chapter 4.1**). Following J. Rayner's methodology, we construct these bases to elucidate the adjoint color structures within the truncation scheme (**Chapter 4.2**). Finally, we combine the Wilson line correlator matrices, the truncations of JIMWLK, and the adjoint color singlet state basis to demonstrate how they all fit together with the JIMWLK evolution equation (**Chapter 4.3**). We then show how the symmetry properties of the colour adjoint singlet states can imprint themselves onto the colour structure functions, the G's as we will refer to them throughout this thesis and how these symmetry properties can be exploited (**Chapter 4.3**).

Chapter 5 presents the application and analysis of the 4-point truncation of the JIMWLK equation. It refines the framework for truncations by introducing necessary modifications and focusing on obtaining simplified expressions for the evolution of the amplitude matrix of two quark-antiquark pairs. The chapter is structured into three main parts: generalizing the parameterisation to accommodate an extra term that only appears in the 4-point truncation (**Chapter 5.1**), refining the basis for adjoint color singlet states to isolate genuine 4-point effects (**Chapter 5.2**), and applying the truncation to the JIMWLK evolution equations,

simplifying the resulting expressions and addressing related challenges (**Chapter 5.3**).

Chapter 6 serves as the concluding section of this thesis. In **Chapter 6.1**, we provide a summary of the main results, revisiting key findings related to the 4-point truncation of the JIMWLK evolution equation. Despite the progress made, several challenges remain, particularly in simplifying the expressions for the JIMWLK evolution equations and obtaining a numerically solvable update equation. In **Chapter 6.2**, we discuss the outlook and open questions, highlighting potential strategies for overcoming these challenges. The section explores future avenues for improvement, such as the development of more methods of simplifying the obtained JIMWLK evolution equation and further refinements of the truncation approach.

Chapter 2

The JIMWLK Equation

2.1 Deep Inelastic Scattering Experiments

We shall initiate our discussion by scrutinizing high-energy scattering experiments. These experiments currently represent the foremost methodology for investigating the intricate structure of nuclei and their fundamental constituents. In particular, the JIMWLK evolution equation is intrinsically linked to these investigations.

In most high-energy scattering experiments, the primary axis of collision in the center of mass frame is identified (commonly referred to as the z or x^3 -axis). The collision kinematics are then studied relative to this axis, as well as the two perpendicular axes, known respectively as the x^1-(x)-axis and the x^2-(y)-axis. One can, of course, do all calculations in high-energy physics using the standard Cartesian coordinates with the extra spacetime dimension added. However, it is much more convenient to work in light-cone coordinates, where

$$x^{\pm} := \frac{1}{\sqrt{2}}(x^0 \pm x^3) \quad \text{and} \quad x := (x^1, x^2)^t. \tag{2.1}$$

The reason why light-cone coordinates are more convenient to work with is easy to see from Eq. 2.1 in the context of high-energy collisions. When a projectile and a target (the two objects involved in a high-energy collision) collide at very high energies, i.e. very high values of x^0, their worldlines approach the x^+ and x^- axis (depending on which direction we choose x^3 to be positive), and they will therefore have a large rapidity separation. This is illustrated in Figure 2.1.

In high-energy collisions conducted in experiments around the world, we focus specifically on interactions between a dilute probe, such as an electron, and a dense object, such as a lead nucleus. In this context, the electron is referred to as the projectile and the dense object as the target. Both objects travel along the x^3-axis at high energies. As a result, one of the light-cone coordinates, x^+, becomes very large for one object and very small for the other, with a similar situation for x^-. In effect, one object moves primarily along the x^+-axis and

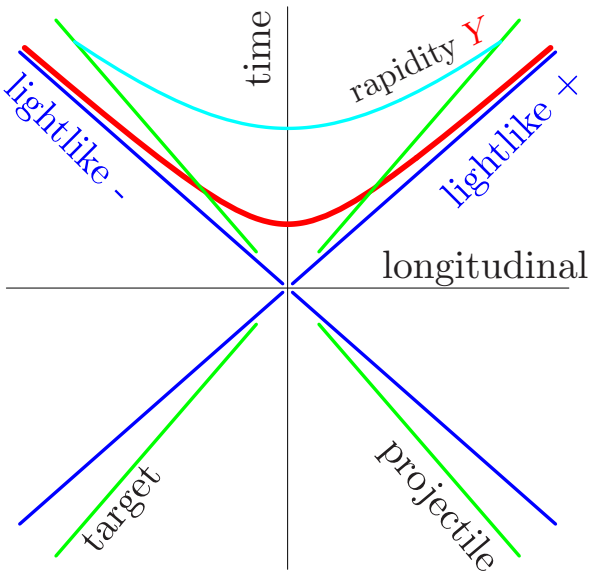

FIGURE 2.1: At high energies, the worldlines of the target and projectile in this Minkowski diagram approach the x^+ and x^- axes in lightcone coordinates, reflecting their near-lightlike motion. The projectile and the target are separated by a large boost factor given by e^Y. This behavior highlights the relativistic effects where both objects move at velocities close to the speed of light, causing their worldlines to become nearly parallel to the lightcone. Taken from Figure 2 of [13].

the other along the x^--axis (see Figure 2.1) [13]. By convention, we assume that the projectile moves in the x^--direction and the target in the x^+-direction. This is illustrated in Figure 2.2.

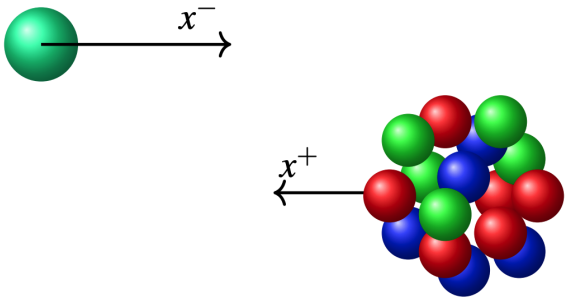

FIGURE 2.2: High-energy collision showing the projectile along the x^--axis and the target along the x^+-axis in lightcone coordinates. Taken from [23].

In the projectile's rest frame, the high-energy target appears Lorentz contracted, with its support almost a δ-function in the x^--direction due to high rapidity separation. Furthermore, the effects of time dilation at such high speeds essentially mean that the color field of the target [1] will be constant in x^+ in the rest frame of the projectile. The way that one can

[1] Remember that the target in general consists of protons and neutrons and will therefore consist of quarks and gluons, thus giving rise to a color field of sorts [45].

think about this is that in the rest frame of the projectile, the target essentially looks like a flat disc with a constant color field. Furthermore, since the projectile is small in relation to the target, the flat disc that the projectile sees is very large in diameter, essentially infinite. Although this is a somewhat simplistic picture of what is happening, it does allow us the following considerations for b where b describes the color field of the target [13]

$$b^i = b^- = 0, \quad b^+ = \beta(\boldsymbol{x})\delta(x^-), \tag{2.2}$$

where $\beta(\boldsymbol{x})$ is the distribution of the color charges in the transverse plane [13].

In this scenario, a deep-inelastic scattering (DIS) event occurs. This type of event involves a dilute probe interacting with a dense target, resulting in the target being shattered upon collision; hence the term "deep inelasticity." Thus, in order to better understand what is happening in the high-energy collision in Figure 2.2, it is prudent to explore more in-detail how DIS works. The following short review summarizes the work in [13, 14].

The projectile will interact with the target, as illustrated in Figure 2.3

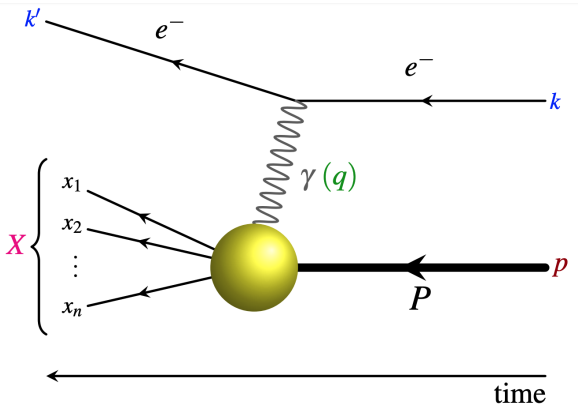

FIGURE 2.3: Dilute probe interacting with a dense target in a deep-inelastic scattering experiment in high-energy physics. Here, the dense target is labelled as P. Figure taken from Figure 1.2 in [23] and the arguments follow that in [13, 14].

Here, we take the dilute probe to be an electron with an incoming momentum k and an outgoing momentum k'. The dense target has an incoming momentum p and is shattered into n-constituents, each with momenta x_i and total momentum X. We assume that the electron interacts with the dense target via an exchange of a photon and that the interaction occurs in the t-channel. The electron exchanges momentum q through the photon. There are four

Lorentz invariants that are of interest to us in this picture, namely:

$$\begin{aligned} s &:= (k+p)^2, \\ Q^2 &:= -q^2, \\ x_{\mathrm{Bj}} &:= \frac{Q^2}{2p\cdot q}, \\ y &:= \frac{2p\cdot q}{s}. \end{aligned} \tag{2.3}$$

We briefly describe each of these Lorentz invariants:

- s is the total energy of the interaction,
- Q^2 is the virtuality of the photon (q is the spacelike momentum of the photon),
- x_{Bj} is the momentum fraction Bjorken-x,
- y is the inelasticity of the collision.

Now, due to momentum conservation at each vertex, we have that the sum of the outgoing momenta of all the constituents that the target breaks up into, i.e. X, is given by $X = (p+q)$. Thus, we get $X^2 = (p+q)^2 = p^2 + 2p\cdot q + q^2$. Since the incoming target is on-shell, we have $p^2 = m_P^2$ where m_P is the mass of the target. Factoring out $2p\cdot q$ in each term in X^2 gives us

$$\begin{aligned} X^2 &= 2p\cdot q\left(\frac{m_P^2}{2p\cdot q} + 1 + \frac{q^2}{2p\cdot q}\right) \\ &= 2p\cdot q\left(\frac{m_P^2}{2p\cdot q} + 1 - x_{\mathrm{Bj}}\right), \end{aligned} \tag{2.4}$$

where in the last line, we have used the fact that $Q^2 = -q^2$ and the definition of x_{Bj}. The quantity X^2 in various limits tells us the nature of the interaction between the probe and the target in DIS. Each different limit describes a certain part of the QCD phase space diagram in Figure 2.4.

In the realm of high-energy physics, numerous segments of the QCD phase space diagram displayed in Figure 2.4 are of significant interest and are currently active research areas. Each segment of the QCD phase-space diagram represents different kinematic limits of a DIS event. The specific area we are focusing on is the top left region, which corresponds to the color glass condensate (CGC). A detailed review of the other regions within the QCD phase-space diagram and the processes that produce them is beyond the scope of this thesis; readers seeking more information should refer to [46].

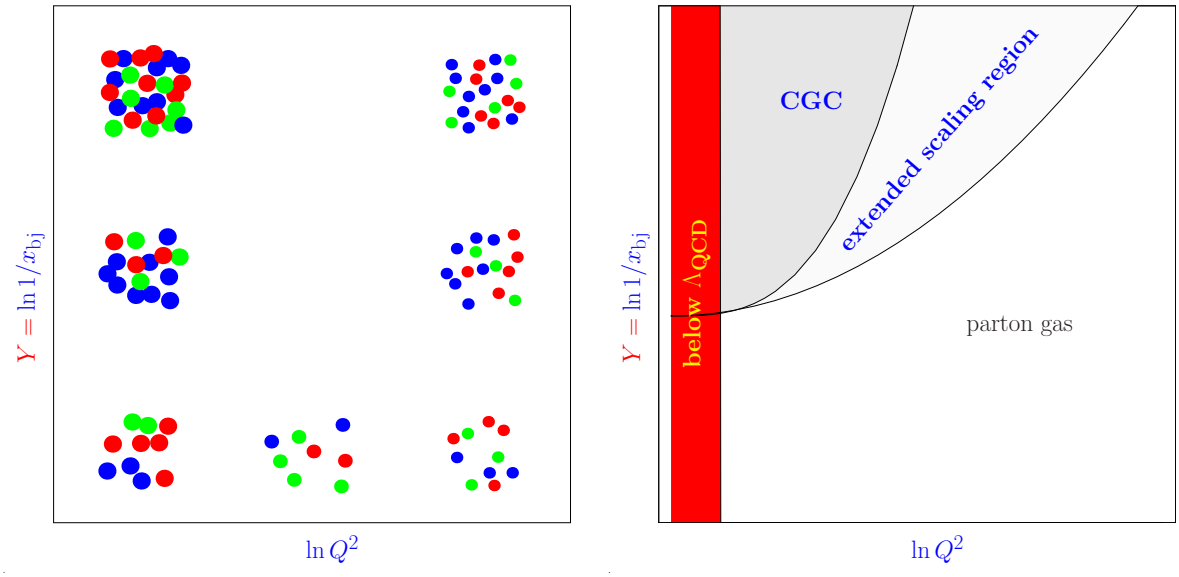

FIGURE 2.4: A diagram which illustrates the particle distribution and quantity in the dense target (left), and the phase space regions of interest exhibiting distinct qualitative behaviors in high-energy physics (right) as a function of $\ln Q^2$. This thesis will primarily focus on the top-left area of the phase diagram, which represents the CGC. As illustrated in the left figure, the CGC is a dense medium composed of color-charged partons. This figure is taken from [13].

2.2 The Regge-Gribov Limit and the Colour Glass Condensate

The CGC arises when we take the Regge-Gribov limit for X^2 in Eq. 2.4. The Regge-Gribov limit is the case in which the $p \cdot q$-term in X^2 is the dominant contribution. Looking at Eq. 2.4, we see that this happens when Bjorken-x is small, that is, $x_{\rm Bj} \ll 1$. This limit, in-turn, is achieved when:

$$x_{\rm Bj} \to 0,\ s \to \infty, \quad \text{while } Q^2 \text{ remains fixed.} \tag{2.5}$$

Looking at Eq. 2.3, we see that as $x_{\rm Bj} \to 0$, $p \cdot q \gg Q^2, m_P^2$. Thus, this allows us to write $x_{\rm Bj}$ as

$$x_{\rm Bj} \approx \frac{Q^2}{X^2}, \tag{2.6}$$

We can therefore interpret Bjorken-x as the fractional momentum transfer from the probe to the target in the DIS event.

As $x_{\rm Bj}$ decreases, the target becomes more and more populated with colour charges as the fractional momentum transfer to the target decreases. This is somewhat similar to the Rutherford gold foil experiment, where higher energy alpha particles encounter a less dense medium to penetrate [47]. However, since Q^2 remains fixed, Figure 3 of [48] demonstrated that the overall target size remains the same despite an increase in the collision energy. Consequently,

these colour charges begin to overlap within the probe's reference frame. Subsequently, this leads to recombination effects, and eventually, the recombination of colour charges equates to the generation of new gluons, resulting in the medium reaching a saturation point. This newly saturated medium is known as the color glass condensate. Therefore, in the small x_{Bj} limit, the probe does not encounter a parton or collection of partons but rather a dense colour field and hence, we move from the individual degrees of freedom that the probe encounters to collective degrees of freedom. Furthermore, since the target is highly Lorentz contracted, the interaction between the probe and the target is eikonal which means that the probe and the target only interact through soft gluon exchange, which does not change the direction of the probe and, therefore, the probe can only experience a rotation in colour space [13, 14]. However, since the photon (through which the probe is interacting) is colour neutral, the photon itself first has to split into a color neutral combination of color-carrying partons before any interaction can take place [2, 4]. We assume, for the sake of simplicity, that the photon splits into a $q\bar{q}$-pair, commonly referred to as a $q\bar{q}$-dipole, and interacts with the target from there (see Figure 2.5 for an illustration).

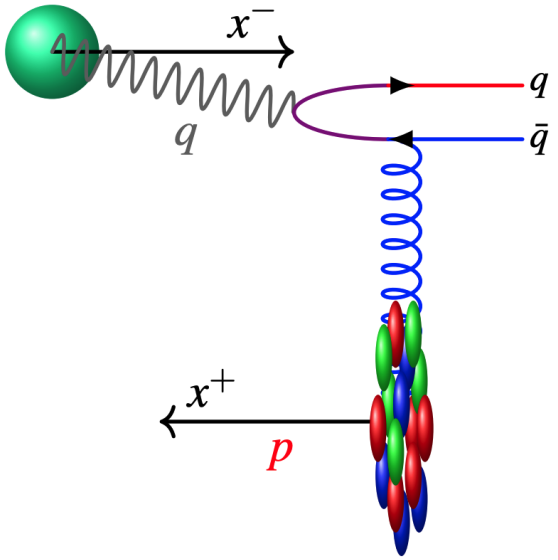

FIGURE 2.5: $q\bar{q}$-dipole interacting with the dense, gluonic target. Taken from Eq. 1.5 in [23].

Before we move on, let us now try to give a qualitative description of what the CGC is. From what we have seen, the CGC is a dense, gluonic state of matter composed of partons that carry a color charge (the "colour" in CGC). Furthermore, the CGC essentially appears frozen in time because of time-dilation effects, and thus is static over large short time scales. Likewise, glass is a material that is unchanging over short time scales but behaves like a liquid on long time scales; hence the "glass" in CGC. And because CGC is a saturated medium in which recombination effects balance the production of new gluons, it is a condensate (hence

the "condensate" in CGC) [13, 15, 16]. The CGC is thought to be the initial state that leads to the formation of glasma, which, in turn, leads to the formation of the quark-gluon plasma [15, 16]. The way in which these processes work is still an active area of research in high-energy physics.

2.3 Wilson Lines and their Role in the JIMWLK Equation

The interaction between the target and the nucleus is naturally described by Wilson lines. The physics interpretation of a Wilson line is a quark that emits and absorbs a multitude of soft gluons where the gluons are summed over [19]. Thus, we see how Wilson lines naturally describe the interaction between the target and the projectile in the Regge-Gribov limit in DIS: the projectile emits a photon which, in turn, splits into a $q\overline{q}$ pair that then interacts eikonally with the target via an emission/absorption of soft gluons. Wilson lines therefore describe these quark/anti-quarks that interact with the dense gluonic target. The mathematical definition of a Wilson line is a path-ordered exponential [2] given by:

$$U_{[\gamma(\tau),x,y]} = \mathrm{Pexp}\left\{-ig\int_{y}^{x} \mathrm{d}\tau \frac{\mathrm{d}\gamma^{\mu}}{\mathrm{d}\tau} A_{\mu}(\gamma(\tau))\right\}, \tag{2.7}$$

where $\gamma\left(\tau\right)$ is the curve, parametrised by τ which goes from y at $\tau = 0$ to x at $\tau = 1$, i.e.

$$\gamma : [0,1] \to \mathbb{M} \quad \text{where} \quad \gamma(0) = y\,,\, \gamma(1) = x, \tag{2.8}$$

A^{μ} represents the gauge field of the non-Abelian gauge theory; g is the coupling constant.

Using the eikonal approximation and the relevant Feynman rules, one can show that the sum of all Feynman diagrams describing a quark emitting and absorbing any number of soft gluons along a straight-line trajectory, γ^{μ}, parametrized by τ, results in a path-ordered exponential of the form given in Eq. 2.7 [19, 20]. The quark's trajectory is given by

$$\gamma^{\mu}\left(\tau\right) = x_{\perp}^{\mu} + \eta^{\mu}\tau, \tag{2.9}$$

where

$$x_{\perp}^{\mu} = \begin{pmatrix} 0 \\ \boldsymbol{x} \\ 0 \end{pmatrix}, \tag{2.10}$$

[2] This path-ordered exponential satisfies a parallel transport equation which parallel transports a field component $\psi(y)$, where $\psi(y)$ is a fermion field residing in Fock space under the gauge-transformed Dirac Lagrangian, to another field $\psi(x)$ where x lies on the Minkowski manifold. This is the geometric interpretation of a Wilson line [3, 34, 49].

is the transverse coordinate where the quark interacts with the target, and η^μ defines the direction of motion from $\tau = -\infty$ to $\tau = \infty$. This leads to the Wilson line expression:

$$U_{[\gamma(\tau),x,y]} \quad \rightarrow \quad U_{\boldsymbol{x}} = \text{Pexp}\left\{-ig\int\limits_{-\infty}^{\infty} \mathrm{d}\tau\, \eta \cdot A_\mu(\gamma(\tau))\right\}. \tag{2.11}$$

Due to the target's δ function support from Lorentz contraction in the probe's rest frame, Wilson lines are gauge equivalent to unity except at the probe's worldline intersection with the $x^- = 0$ plane [23]. Therefore, specifying the transverse coordinate where the interaction occurs is sufficient to describe a Wilson line, denoted $U_{\boldsymbol{x}}$. Note that this transverse coordinate is a 2D spatial vector, unlike the 4-vector x in Eq. 2.7. Therefore, the Wilson lines that we are specifically interested in in this thesis will be expressed in this form since we are primarily interested in quarks and anti-quarks interacting eikonally with the target.

The important point is that the Wilson lines take the form of Eq. 2.7 where they can be expressed as a path-ordered exponential; from this form of a Wilson line, we can deduce their most important property, which is crucial to this thesis: they are elements of SU(N) as shown in [19]. What this means is that instead of working with Wilson lines as path-ordered exponentials in the form of Eq. 2.7, we can instead work with them as elements of SU(N). This, in turn, means that we can use all the group-theoretic machinery of SU(N) in-order to investigate the properties of Wilson lines and hence the properties of the CGC. Using the group-theoretic machinery of SU(N) is, and has proven to be, much easier to work with and lends itself to easier physical interpretations which is why we emphasize this point and why, for the vast majority of this thesis we shall treat Wilson lines as elements of SU(N) as opposed to using the path-ordered exponential form in Eq. 2.7. The path-ordered definition of a Wilson line in Eq. 2.7 holds in all representations; for the purposes of this thesis, we shall restrict ourselves to Wilson lines in the fundamental, anti-fundamental and adjoint representations.

- A Wilson line in the fundamental representation (corresponding to a quark) with transverse coordinate, $\boldsymbol{x}$, will be denoted by

$$U_{\boldsymbol{x}}.$$

- A Wilson line in the anti-fundamental representation with transverse coordinate, $\boldsymbol{y}$, (corresponding to an anti-quark) will be denoted by

$$U^\dagger_{\boldsymbol{y}},$$

and note that

$$U^\dagger_{\boldsymbol{y}} U_{\boldsymbol{y}} = \mathbb{1}.$$

- A Wilson line in the adjoint representation with transverse coordinate, $\boldsymbol{z}$, (corresponding to a gluon) will be given by

$$\widetilde{U}^{ab}_{\boldsymbol{z}},$$

where a and b are colour indices. Also note that such a Wilson line in the adjoint representation will be given by:

$$\widetilde{U}^{ab}_{\boldsymbol{z}} = 2\mathrm{tr}\left(t^a U_{\boldsymbol{z}} t^b U^{\dagger}_{\boldsymbol{z}}\right), \tag{2.12}$$

where the t^a's are the generators of SU(N).

With this important fact in mind now, let us turn to the JIMWLK equation which describes the rapidity evolution of Wilson line correlators (more on that in a bit). A complete derivation is given in [13, 27] and the MSc theses of R. Moerman and D. Adamiak [33, 37], as well as the Ph.D. thesis of J. Alcock-Zeilinger [23] also give a good recount of the derivation of the JIMWLK evolution equation. To leading logarithmic order, the JIMWLK equation is given by:

$$\frac{d}{dY} Z_Y[U] = -H_{\mathrm{JIMWLK}}\, Z_Y[U], \tag{2.13}$$

where Y is the rapidity, H_{JIMWLK} is the JIMWLK Hamiltonian, and U is a Wilson line (an SU(N) element) that depends on a transverse coordinate of the target in the DIS event, $\boldsymbol{x}$, where the Wilson line interacts with the target at $x^- = 0$.

The term $Z_Y[U]$ represents the functional weight that is averaged to compute the expectation values of the operators in the CGC regime. Such expectation values are given by:

$$\langle \cdots \rangle_Y = \int \mathcal{D}[U] \cdots Z_Y[U], \tag{2.14}$$

where $\mathcal{D}[U]$ is a functional Haar measure on SU(N). To compute expectation values of operators in the CGC regime, a functional integration over all SU(N) elements must be performed. Note that the expectation value of an operator in this context depends on the rapidity, Y.

The JIMWLK Hamiltonian is defined as (note that we are dealing with 2D spatial vectors $\boldsymbol{x}, \boldsymbol{z}$ and $\boldsymbol{y}$ now):

$$H_{\mathrm{JIMWLK}} := -\frac{\alpha_s}{2\pi^2} \int\limits_{\boldsymbol{xzy}} \mathcal{K}_{\boldsymbol{xzy}} \left(i\overline{\nabla}^a_{\boldsymbol{x}} i\nabla^a_{\boldsymbol{y}} + i\overline{\nabla}^a_{\boldsymbol{x}} i\overline{\nabla}^a_{\boldsymbol{y}} + \widetilde{U}^{ab}_{\boldsymbol{z}} \left(i\overline{\nabla}^a_{\boldsymbol{x}} \nabla^b_{\boldsymbol{y}} + i\nabla^a_{\boldsymbol{x}} \overline{\nabla}^b_{\boldsymbol{y}} \right) \right), \tag{2.15}$$

where $\widetilde{U}^{ab}_{\boldsymbol{z}}$ is a Wilson line in the adjoint representation.

$\mathcal{K}_{\boldsymbol{xzy}}$ is the JIMWLK kernel defined as

$$\mathcal{K}_{\boldsymbol{xzy}} := \frac{(\boldsymbol{x}-\boldsymbol{z})\cdot(\boldsymbol{z}-\boldsymbol{y})}{(\boldsymbol{x}-\boldsymbol{z})^2(\boldsymbol{z}-\boldsymbol{y})^2}, \tag{2.16}$$

and the operators $i\nabla^a_{\boldsymbol{x}}$ and $i\overline{\nabla}^a_{\boldsymbol{x}}$ is defined as[3]:

$$i\nabla^a_{\boldsymbol{x}} := [U_{\boldsymbol{x}}t^a]_{ij}\frac{\delta}{\delta U_{\boldsymbol{x},ij}}, \qquad i\overline{\nabla}^a_{\boldsymbol{x}} := -[t^a U_{\boldsymbol{x}}]_{ij}\frac{\delta}{\delta U_{\boldsymbol{x},ij}}. \tag{2.17}$$

Equation 2.17 gives the left- and right-invariant vector fields on SU(N) respectively [13, 14]. What these left- and right-invariant vector fields essentially do is insert a generator next to a Wilson line; the left-invariant vector field inserts a generator on the left of a Wilson line and the right-invariant vector field inserts a generator on the right of a Wilson line. So another, easier way of expressing them is:

$$i\nabla^a_{\boldsymbol{x}}U_{\boldsymbol{y}} = \delta^{(2)}_{\boldsymbol{x},\boldsymbol{y}}U_{\boldsymbol{y}}t^a, \qquad i\overline{\nabla}^a_{\boldsymbol{x}}U_{\boldsymbol{y}} = -\delta^{(2)}_{\boldsymbol{x},\boldsymbol{y}}t^a U_{\boldsymbol{y}}, \tag{2.18}$$

where $\delta^{(2)}_{\boldsymbol{x},\boldsymbol{y}}$ is the two-dimensional Dirac-delta function. One can then find the way in which these left- and right-invariant vector fields act on $U^\dagger_{\boldsymbol{y}}$ by using the unitarity of Wilson lines as elements of SU(N) and the product rule, since these left- and right-invariant vector fields are derivative operators. This is done below:

$$\begin{aligned}
&U^\dagger_{\boldsymbol{y}}U_{\boldsymbol{y}} = \mathbb{1}\\
&\implies i\overline{\nabla}^a_{\boldsymbol{x}}\left(U^\dagger_{\boldsymbol{y}}U_{\boldsymbol{y}}\right) = 0\\
&\implies U^\dagger_{\boldsymbol{y}}\underbrace{\left(i\overline{\nabla}^a_{\boldsymbol{x}}U_{\boldsymbol{y}}\right)}_{-\delta^{(2)}_{\boldsymbol{x},\boldsymbol{y}}t^aU_{\boldsymbol{y}}} + \left(i\overline{\nabla}^a_{\boldsymbol{x}}U^\dagger_{\boldsymbol{y}}\right)U_{\boldsymbol{y}} = 0\\
&\implies \left(i\overline{\nabla}^a_{\boldsymbol{x}}U^\dagger_{\boldsymbol{y}}\right)U_{\boldsymbol{y}} = \delta^{(2)}_{\boldsymbol{x},\boldsymbol{y}}U^\dagger_{\boldsymbol{y}}t^aU_{\boldsymbol{y}}\\
&\implies i\overline{\nabla}^a_{\boldsymbol{x}}U^\dagger_{\boldsymbol{y}} = \delta^{(2)}_{\boldsymbol{x},\boldsymbol{y}}U^\dagger_{\boldsymbol{y}}t^a.
\end{aligned} \tag{2.19}$$

And similarly:

$$i\nabla^a_{\boldsymbol{x}}U^\dagger_{\boldsymbol{y}} = -\delta^{(2)}_{\boldsymbol{x},\boldsymbol{y}}t^aU^\dagger_{\boldsymbol{y}}. \tag{2.20}$$

Collecting all these together:

$$i\nabla^a_{\boldsymbol{x}}U_{\boldsymbol{y}} = \delta^{(2)}_{\boldsymbol{x},\boldsymbol{y}}U_{\boldsymbol{y}}t^a, \qquad i\overline{\nabla}^a_{\boldsymbol{x}}U_{\boldsymbol{y}} = -\delta^{(2)}_{\boldsymbol{x},\boldsymbol{y}}t^aU_{\boldsymbol{y}}, \tag{2.21a}$$

$$i\nabla^a_{\boldsymbol{x}}U^\dagger_{\boldsymbol{y}} = -\delta^{(2)}_{\boldsymbol{x},\boldsymbol{y}}t^aU^\dagger_{\boldsymbol{y}}, \qquad i\overline{\nabla}^a_{\boldsymbol{x}}U^\dagger_{\boldsymbol{y}} = \delta^{(2)}_{\boldsymbol{x},\boldsymbol{y}}U^\dagger_{\boldsymbol{y}}t^a. \tag{2.21b}$$

These left and right vector fields satisfy the Lie algebra commutation relations as they are

[3] These definitions actually hold for Wilson lines in any representation [17]

isomorphic to the tangent space at the identity for SU(N), which is the Lie algebra [27]. For convenience of reference, the commutation relations are as follows:

$$\begin{aligned}
[i\overline{\mathbb{V}}^a_{\boldsymbol{x}}, i\overline{\mathbb{V}}^b_{\boldsymbol{y}}] &= if^{abc} i\overline{\mathbb{V}}^c_{\boldsymbol{x}} \delta^{(2)}(\boldsymbol{x}-\boldsymbol{y}), \\
0 &= [i\overline{\mathbb{V}}^a_{\boldsymbol{x}}, \mathbb{V}^b_{\boldsymbol{y}}], \\
[i\mathbb{V}^a_{\boldsymbol{x}}, i\mathbb{V}^b_{\boldsymbol{y}}] &= if^{abc} i\mathbb{V}^c_{\boldsymbol{x}} \delta^{(2)}(\boldsymbol{x}-\boldsymbol{y}).
\end{aligned} \tag{2.22}$$

Equation 2.14 tells us that the JIMWLK equation gives the rapidity evolution of observables that depend on Wilson lines in the CGC. To illustrate this point in a clearer way, consider an operator $\widehat{O}[U]$, which depends on Wilson lines U, in the CGC regime. From Eq. 2.14, we get that:

$$\langle \widehat{O}[U] \rangle_Y = \int \mathcal{D}[U] \mathcal{O}[U] Z_Y[U]. \tag{2.23}$$

Differentiating both sides of Eq. 2.23 and noting that the only rapidity dependence on the RHS of Eq. 2.23 is in the functional weight, we get:

$$\begin{aligned}
\frac{d}{dY}\langle \widehat{O}[U] \rangle_Y &= \int \mathcal{D}[U]\, \mathcal{O}[U] \frac{dZ_Y[U]}{dY} \\
&= -\int \mathcal{D}[U]\, \mathcal{O}[U] H_{\text{JIMWLK}} Z_Y[U] \\
&\quad \text{(Where we have used Eq. 2.13 for } \frac{dZ_Y[U]}{dY} \text{ here)} \\
&= -\int \mathcal{D}[U]\, H(\mathcal{O}[U]) Z_Y[U].
\end{aligned} \tag{2.24}$$

where we have integrated by parts and assumed vanishing boundary terms here in the last line. Equation 2.24 can be written more compactly as:

$$\frac{d}{dY}\langle \widehat{O}[U] \rangle_Y = -\langle H_{\text{JIMWLK}} \widehat{O}[U] \rangle_Y. \tag{2.25}$$

We present an example for $\widehat{O}[U]$ to illustrate the mechanics of the JIMWLK equation. The exposition of this section closely follows Section 2.1.1 of [40]. When a photon splits into a $q\overline{q}$ pair and interacts with the target through eikonal gluon emissions and re-absorptions, the relevant operator is [17]

$$\frac{\text{tr}\left(U_{\boldsymbol{x}} U^\dagger_{\boldsymbol{y}}\right)}{N_c}.$$

This operator is commonly referred to as the dipole correlator. Hence, we encounter our first (and simplest) Wilson line correlator, which we will work with in this thesis. The JIMWLK evolution for this Wilson line correlator will be

$$\frac{d}{dY}\left\langle \frac{\mathrm{tr}(U_{\boldsymbol{x}}U_{\boldsymbol{y}}^{\dagger})}{N_c}\right\rangle_Y = -\left\langle H_{\mathrm{JIMWLK}}\frac{\mathrm{tr}(U_{\boldsymbol{x}}U_{\boldsymbol{y}}^{\dagger})}{N_c}\right\rangle_Y . \tag{2.26}$$

We compute the JIMWLK Hamiltonian for the $q\bar{q}$-dipole in two parts: first the term without the adjoint Wilson line, then the term with it. For the term without the adjoint Wilson line, we have that:

$$\begin{aligned}&\int_{\boldsymbol{uzv}} \mathcal{K}_{\boldsymbol{uzv}}\left(i\nabla^a_{\boldsymbol{u}}i\nabla^a_{\boldsymbol{v}} + i\overline{\nabla}^a_{\boldsymbol{u}}i\overline{\nabla}^a_{\boldsymbol{v}}\right)\mathrm{tr}\left(U_{\boldsymbol{x}}U_{\boldsymbol{y}}^{\dagger}\right)\\ &= \int_{\boldsymbol{uzv}} \mathcal{K}_{\boldsymbol{uzv}}\left(i\nabla^a_{\boldsymbol{u}}i\nabla^a_{\boldsymbol{v}}\mathrm{tr}\left(U_{\boldsymbol{x}}U_{\boldsymbol{y}}^{\dagger}\right) + i\overline{\nabla}^a_{\boldsymbol{u}}i\overline{\nabla}^a_{\boldsymbol{v}}\mathrm{tr}\left((U_{\boldsymbol{y}}U_{\boldsymbol{x}}^{\dagger})^{\dagger}\right)\right).\end{aligned} \tag{2.27}$$

Now, from Eqs. 2.21 and the fact that the trace commutes with derivatives, we can write Eq. 2.27 as

$$\begin{aligned}&\int_{\boldsymbol{uzv}} \mathcal{K}_{\boldsymbol{uzv}}\,\mathrm{tr}\left(i\nabla^a_{\boldsymbol{u}}i\nabla^a_{\boldsymbol{v}}(U_{\boldsymbol{x}}U_{\boldsymbol{y}}^{\dagger}) + (\boldsymbol{x}\leftrightarrow\boldsymbol{y})\right)\\ &= \int_{\boldsymbol{uzv}} \mathcal{K}_{\boldsymbol{uzv}}\,\mathrm{tr}\left(\left(i\nabla^a_{\boldsymbol{u}}i\nabla^a_{\boldsymbol{v}}U_{\boldsymbol{x}}\right)U_{\boldsymbol{y}}^{\dagger} + U_{\boldsymbol{x}}i\nabla^a_{\boldsymbol{v}}i\nabla^a_{\boldsymbol{u}}(U_{\boldsymbol{y}}^{\dagger}) + 2i\nabla^a_{\boldsymbol{u}}(U_{\boldsymbol{x}})i\nabla^a_{\boldsymbol{v}}(U_{\boldsymbol{y}}^{\dagger}) + (\boldsymbol{x}\leftrightarrow\boldsymbol{y})\right)\end{aligned}$$

(Applying the product rule here and using the fact that $\mathcal{K}_{\boldsymbol{uzv}}$ is symmetric about $\boldsymbol{u}$ and $\boldsymbol{v}$)

$$\begin{aligned}&= \int_{\boldsymbol{uzv}} \mathcal{K}_{\boldsymbol{uzv}}\,\mathrm{tr}\left(\delta^{(2)}_{\boldsymbol{v},\boldsymbol{x}}\delta^{(2)}_{\boldsymbol{u},\boldsymbol{x}}U_{\boldsymbol{x}}t^at^aU_{\boldsymbol{y}}^{\dagger} + \delta^{(2)}_{\boldsymbol{v},\boldsymbol{y}}\delta^{(2)}_{\boldsymbol{u},\boldsymbol{y}}U_{\boldsymbol{x}}t^at^aU_{\boldsymbol{y}}^{\dagger} - 2\delta^{(2)}_{\boldsymbol{u},\boldsymbol{x}}\delta^{(2)}_{\boldsymbol{v},\boldsymbol{y}}U_{\boldsymbol{x}}t^at^aU_{\boldsymbol{y}}^{\dagger} + (\boldsymbol{x}\leftrightarrow\boldsymbol{y}))\right)\\ &= C_F\int_{\boldsymbol{z}}\left(\mathcal{K}_{\boldsymbol{xzx}} + \mathcal{K}_{\boldsymbol{yzy}} - 2\mathcal{K}_{\boldsymbol{xzy}}\right)\left(\mathrm{tr}(U_{\boldsymbol{x}}U_{\boldsymbol{y}}^{\dagger}) + (\boldsymbol{x}\leftrightarrow\boldsymbol{y})\right)\end{aligned}$$

(Evaluating the integrals using the Dirac delta functions and using the fact that for the generators of SU(N), $t^at^a = C_F\mathbb{1} = \dfrac{N_c^2-1}{2Nc}\mathbb{1}$)

$$= 2C_F\int_{\boldsymbol{z}}\left(\mathcal{K}_{\boldsymbol{xzx}} + \mathcal{K}_{\boldsymbol{yzy}} - 2\mathcal{K}_{\boldsymbol{xzy}}\right)\left(\mathrm{tr}\left(U_{\boldsymbol{x}}U_{\boldsymbol{y}}^{\dagger}\right)\right), \tag{2.28}$$

where in the last line, we have leveraged the fact the $\mathcal{K}_{\boldsymbol{xzy}}$ is symmetric about an interchange of $\boldsymbol{x}$ and $\boldsymbol{y}$.

Now let us look at the term which has the adjoint Wilson line:

$$\int_{\boldsymbol{uzv}} \mathcal{K}_{\boldsymbol{uzv}}\,\widetilde{U}^{ab}_{\boldsymbol{z}}\left(i\overline{\nabla}^a_{\boldsymbol{x}}\nabla^b_{\boldsymbol{y}} + i\nabla^a_{\boldsymbol{x}}\overline{\nabla}^b_{\boldsymbol{y}}\right)\mathrm{tr}\left(U_{\boldsymbol{x}}U_{\boldsymbol{y}}^{\dagger}\right).$$

Because the left- and right-invariant vector fields commute with each other (Eq. 2.22), we have that:

$$\begin{aligned}
&\int_{\boldsymbol{uzv}} \mathcal{K}_{\boldsymbol{uzv}}\, \widetilde{U}^{ab}_{\boldsymbol{z}} \left(i\overline{\nabla}^a_{\boldsymbol{x}} \nabla^b_{\boldsymbol{y}} + i\nabla^a_{\boldsymbol{x}} \overline{\nabla}^b_{\boldsymbol{y}} \right) \mathrm{tr}\left(U_{\boldsymbol{x}} U^\dagger_{\boldsymbol{y}} \right) \\
&= \int_{\boldsymbol{uzv}} \mathcal{K}_{\boldsymbol{uzv}}\, \widetilde{U}^{ab}_{\boldsymbol{z}}\, \mathrm{tr}\left(i\overline{\nabla}^a_{\boldsymbol{u}} i\nabla^b_{\boldsymbol{v}} (U_{\boldsymbol{x}} U^\dagger_{\boldsymbol{y}}) + (a \leftrightarrow b, \boldsymbol{u} \leftrightarrow \boldsymbol{v}) \right) \\
&= \int_{\boldsymbol{uzv}} \mathcal{K}_{\boldsymbol{uzv}}\, \widetilde{U}^{ab}_{\boldsymbol{z}}\, \mathrm{tr}\left(\left(i\overline{\nabla}^a_{\boldsymbol{u}} i\nabla^b_{\boldsymbol{v}} U_{\boldsymbol{x}} \right) U^\dagger_{\boldsymbol{y}} + U_{\boldsymbol{x}} i\overline{\nabla}^a_{\boldsymbol{u}} i\nabla^b_{\boldsymbol{v}} \left(U^\dagger_{\boldsymbol{y}} \right) \right. \\
&\left. + i\overline{\nabla}^a_{\boldsymbol{u}} \left(U_{\boldsymbol{x}} \right) i\nabla^b_{\boldsymbol{v}} \left(U^\dagger_{\boldsymbol{y}} \right) + i\overline{\nabla}^b_{\boldsymbol{v}} \left(U_{\boldsymbol{x}} \right) i\nabla^a_{\boldsymbol{u}} \left(U^\dagger_{\boldsymbol{y}} \right) + (a \leftrightarrow b, \boldsymbol{u} \leftrightarrow \boldsymbol{v}) \right) \\
&= -\int_{\boldsymbol{z}} \left(\mathcal{K}_{\boldsymbol{xzx}} + \mathcal{K}_{\boldsymbol{yzy}} - 2\mathcal{K}_{\boldsymbol{xzy}} \right) \widetilde{U}^{ab}_{\boldsymbol{z}} \mathrm{tr}\left(t^a U_{\boldsymbol{x}} t^b U^\dagger_{\boldsymbol{y}} \right),
\end{aligned} \tag{2.29}$$

where we used the product rule, exploited the symmetry of $\mathcal{K}_{\boldsymbol{xzy}}$ under swapping its $\boldsymbol{x}$ and $\boldsymbol{y}$ coordinates, and applied the cyclicity of the trace to reach Eq. 2.29. Putting everything together, we finally get that for the dipole correlator, the JIMWLK evolution equation is:

$$\frac{d}{dY} \left\langle \frac{\mathrm{tr}(U_{\boldsymbol{x}} U^\dagger_{\boldsymbol{y}})}{N_c} \right\rangle_Y = \frac{\alpha_s}{\pi^2} \left(-C_F \left\langle \int_{\boldsymbol{z}} \widetilde{\mathcal{K}}_{\boldsymbol{xzy}} \frac{\mathrm{tr}(U_{\boldsymbol{x}} U^\dagger_{\boldsymbol{y}})}{N_c} \right\rangle_Y + \left\langle \int_{\boldsymbol{z}} \widetilde{\mathcal{K}}_{\boldsymbol{xzy}} \widetilde{U}^{ab}_{\boldsymbol{z}} \frac{\mathrm{tr}(t^a U_{\boldsymbol{x}} t^b U^\dagger_{\boldsymbol{y}})}{N_c} \right\rangle_Y \right), \tag{2.30}$$

where we have defined

$$\widetilde{\mathcal{K}}_{\boldsymbol{xzy}} := -\mathcal{K}_{\boldsymbol{xzx}} - \mathcal{K}_{\boldsymbol{yzy}} + 2\mathcal{K}_{\boldsymbol{xzy}}. \tag{2.31}$$

Equation 2.30 shows that the rapidity evolution of the dipole correlator depends on itself and the 3-point Wilson line correlator

$$\widetilde{U}^{ab}_{\boldsymbol{z}} \frac{\mathrm{tr}(t^a U_{\boldsymbol{x}} t^b U^\dagger_{\boldsymbol{y}})}{N_c},$$

which is known as the $q\bar{q}g$-correlator (the g indicating a gluon). The JIMWLK evolution of the 3-point Wilson line correlator $\widetilde{U}^{ab}_{\boldsymbol{z}} \frac{\mathrm{tr}(t^a U_{\boldsymbol{x}} t^b U^\dagger_{\boldsymbol{y}})}{N_c}$ also depends on itself and several 4-point correlators. This pattern continues indefinitely, resulting in an infinite hierarchy of coupled integro-differential equations known as the Balitsky hierarchy [13]. Hence, JIMWLK is challenging to work with as such a hierarchy cannot be solved numerically or analytically.

To address this challenge, let us closely examine the correlators $q\bar{q}$ and $q\bar{q}g$. We can write the $q\bar{q}$-dipole correlator as:

$$\frac{\mathrm{tr}\left(U_{\boldsymbol{x}} U^\dagger_{\boldsymbol{y}} \right)}{N_c} = \frac{1}{N_c} \delta^l{}_i \left[U_{\boldsymbol{x}} \right]^i{}_j \left[U^\dagger_{\boldsymbol{y}} \right]^j{}_m \delta^m{}_l, \tag{2.32}$$

and the $q\bar{q}g$ correlator can be written as:

$$\widetilde{U}^{ab}_{\boldsymbol{z}}\frac{\mathrm{tr}(t^a U_{\boldsymbol{x}} t^b U^\dagger_{\boldsymbol{y}})}{N_c} = \widetilde{U}^{ab}_{\boldsymbol{z}}\,[t^a]^i{}_j\,[U_{\boldsymbol{x}}]^j{}_l\left[t^b\right]^l{}_m\left[U^\dagger_{\boldsymbol{y}}\right]^m{}_i. \tag{2.33}$$

In Eq. 2.32, the $\delta^l{}_i$ and $\delta^m{}_l$ terms are colour singlet states. Similarly, in Eq. 2.33, the $[t^a]^i{}_j$ and $\left[t^b\right]^l{}_m$ terms, along with $\widetilde{U}^{ab}_{\boldsymbol{z}}$, form a gluon singlet state. We can express Eqs. 2.32 and 2.33 as an inner product with the colour singlet states. We denote the color singlet states corresponding to the Kronecker δ's as $\langle 1|$ and $|1\rangle$ and the generators as $\langle t^a|$ and $|t^b\rangle$. Then we will have that:

$$\frac{\mathrm{tr}\left(U_{\boldsymbol{x}}U^\dagger_{\boldsymbol{y}}\right)}{N_c} = \frac{1}{N_c}\delta^l{}_i\,[U_{\boldsymbol{x}}]^i{}_j\left[U^\dagger_{\boldsymbol{y}}\right]^j{}_m\,\delta^m{}_l = \frac{1}{N_c}\langle 1|U_{\boldsymbol{x}}\otimes U^\dagger_{\boldsymbol{y}}|1\rangle, \tag{2.34}$$

and

$$\widetilde{U}^{ab}_{\boldsymbol{z}}\frac{\mathrm{tr}(t^a U_{\boldsymbol{x}} t^b U^\dagger_{\boldsymbol{y}})}{N_c} = \widetilde{U}^{ab}_{\boldsymbol{z}}\,[t^a]^i{}_j\,[U_{\boldsymbol{x}}]^j{}_l\left[t^b\right]^l{}_m\left[U^\dagger_{\boldsymbol{y}}\right]^m{}_i = \frac{1}{N_c}\widetilde{U}^{ab}_{\boldsymbol{z}}\langle t^a|U_{\boldsymbol{x}}\otimes U^\dagger_{\boldsymbol{y}}|t^b\rangle. \tag{2.35}$$

This notation for color singlets and "sandwiching" Wilson lines in-between them is what we shall use for the remainder of this thesis. The observation that Wilson lines must be expressed with color singlets is consistent; Wilson line correlators in the CGC framework must be color-neutral, and thus be expressed as color singlet states.

For indeed, Wilson lines carry singlets into singlets which is a result of colour conservation at each vertex in the underlying Feynman diagrams.[4] Thus, when one wants to properly encapsulate the JIMWLK evolution of Wilson line correlators corresponding to more than one $q\bar{q}$-dipole, one would need to consider a matrix of Wilson line correlators instead of a single Wilson line correlator. This is because a singlet state can be mapped to another by an eikonal interaction, i.e., by a Wilson line [17]. In DIS, the only singlet states that are possible are when there are an equal number of quarks and anti-quarks [13, 17]. Furthermore, even if there are m quarks and $\overline{m}$ anti-quarks where $m \neq \overline{m}$, one can show that there will be singlet states in such a configuration if and only if there exist positive integers $a, b \in \mathbb{N}^+$. These integers must satisfy $m - aN = \overline{m} - bN =: k$. In this case, such singlet states can be mapped onto an equivalent colour singlet state, which corresponds to an equal number of quarks and anti-quarks [50]. Thus, we shall restrict our attention to cases where there are only an equal number of quarks and anti-quarks as it is much easier to compute singlet states and work with Wilson line correlators for such configurations. Hence, we will need all singlet states of $\mathrm{SU}(N)$ over $V^{\otimes m}\otimes(V^*)^{\otimes m}$, where V has the fundamental representation of $\mathrm{SU}(N)$ (quark) and V^* has the anti-fundamental representation of $\mathrm{SU}(N)$ (anti-quark) [23] and the Wilson line correlator matrix in question will take the form of $\langle\mathcal{A}\rangle(Y)$ where the entry in the i-th

[4] This comes from the Feynman rules of QCD [2, 4, 34].

row and j-th column, $\langle \mathcal{A} \rangle_{ij}(Y)$, will be [23]:

$$\langle \mathcal{A} \rangle_{ij}(Y) = \langle j \left| \mathbf{U}^m_{\boldsymbol{x},\boldsymbol{y}} \right| i \rangle, \tag{2.36}$$

where $\mathbf{U}^m_{\boldsymbol{x},\boldsymbol{y}} := U_{\boldsymbol{x_1}} \otimes U^\dagger_{\boldsymbol{y_1}} \otimes U_{\boldsymbol{x_2}} \otimes U^\dagger_{\boldsymbol{y_2}} \otimes U_{\boldsymbol{x_3}} \otimes U^\dagger_{\boldsymbol{y_3}} \otimes \ldots \otimes U_{\boldsymbol{x_m}} \otimes U^\dagger_{\boldsymbol{y_m}}$, with $\boldsymbol{x}_i$ and $\boldsymbol{y}_i$ as transverse coordinates, and the states $|i\rangle, |j\rangle$ are global singlet states of SU(N):

$$\begin{gathered} \mathbf{U}^m_{\boldsymbol{x},\boldsymbol{y}} \begin{Bmatrix} |i\rangle \\ |j\rangle \end{Bmatrix} = \begin{Bmatrix} |i\rangle \\ |j\rangle \end{Bmatrix} \\ \text{and} \\ \begin{Bmatrix} \langle i| \\ \langle j| \end{Bmatrix} \left(\mathbf{U}^m_{\boldsymbol{x},\boldsymbol{y}}\right)^\dagger = \begin{Bmatrix} \langle i| \\ \langle j| \end{Bmatrix} \\ \text{if} \\ \boldsymbol{x}_1 = \boldsymbol{x}_2 = \ldots = \boldsymbol{x}_m = \boldsymbol{y}_1 = \boldsymbol{y}_2 = \ldots = \boldsymbol{y}_m. \end{gathered} \tag{2.37}$$

In Chapter 3.2, we will detail the construction of Wilson line correlator matrices and analyze how different singlet state bases fit various coincidence limits. This requires birdtrack notation, which simplifies complex expressions intuitively, introduced in Chapter 3 as well. For now, we state the JIMWLK evolution equation for $\langle \mathcal{A} \rangle_{ij}(Y)$ as it will be needed later. The JIMWLK evolution for is given by:

$$\frac{d}{dY} \langle \mathcal{A}_{ij} \rangle (Y) = \left\langle \frac{\alpha_s}{2\pi^2} \int\limits_{\boldsymbol{uvz}} \mathcal{K}_{\boldsymbol{uvz}} \left[i\nabla^a_{\boldsymbol{u}} i\nabla^a_{\boldsymbol{v}} + i\overline{\nabla}^a_{\boldsymbol{u}} i\overline{\nabla}^a_{\boldsymbol{v}} + 2\widetilde{U}^{ab}_{\boldsymbol{z}} i\overline{\nabla}^a_{\boldsymbol{u}} i\nabla^b_{\boldsymbol{v}} \right] \mathcal{A}_{ij} \right\rangle (Y). \tag{2.38}$$

Efforts to find approximate solutions to the JIMWLK equation include numerical methods by recasting it as a Fokker-Planck or Langevin diffusion equation ([27]), and analytical solutions using the large N_c limit, leading to the BK equation ([28–32]). Each method has its limitations, discussed in [17, 38] for the large N_c-limit. This highlights the need for a more robust analytical approach at finite N_c, such as gauge-invariant, symmetry-preserving truncations developed by R. Moerman and H. Weigert in [33]. So far, there have been promising results for these truncations as discussed in [33, 37]. This thesis aims to extend truncations to 4-point, seeking to fully capture the physics of rapidity evolution in 4-point Wilson line correlators. The machinery and truncations are discussed in Chapters 3 and 4.

Chapter 3

Wilson Line Correlators

3.1 Birdtracks: It's all Kronecker δ's

3.1.1 API $(\mathbf{SU}(N), V^{\otimes m})$

We first consider the permutation group S_n and its group algebra over real numbers $\mathbb{R}[S_n]$[1]. Birdtracks visualize elements of the group algebra $\mathbb{R}[S_n]$, simplifying calculations, and illustrating concepts. This section summarizes key points from the lecture notes by J. Alcock-Zeilinger [51]. Additional resources on birdtracks and SU(N) representation theory are [44, 52]. Familiarity with elementary group theory, including permutation groups and their basics (cycle notation, even and odd permutations, cyclic permutations, etc.), is assumed. For a refresher, consult any number of group theory textbooks. We provide only the briefest of introductions here.

Recall that an element of S_n permutes n ordered objects in a specific way. As a basic example, consider the element (123) (written in cycle notation) of the permutation group S_3 acting on the ordered set $\{1, 2, 3\}$. This element acting on the ordered set yields

$$(123) : \{1, 2, 3\} \mapsto \{2, 3, 1\}.$$

Of course, one can do this similarly for all the other elements of S_3 (and S_n in general). Birdtracks now come-in in that they are a visual and natural way of representing elements of S_n. In order to write a birdtrack for $\rho \in S_n$, we write the two columns $(1, 2, 3, ..., n)^t$ and $(\rho(1), \rho(2), \rho(3), ..., \rho(n))^t$ next to each other with the latter column on the left and then connect the entry i of the right column to the value of $\rho(i)$ in the left column, marking each line with an arrow from the right to the left. The numbers are then deleted from the diagram,

[1] One can also consider the group algebra of S_n over the complex numbers, $\mathbb{C}[S_n]$. However, throughout this thesis, complex coefficients never appear and therefore, it is sufficient to consider the group algebra over the real numbers.

leaving only the lines. Let us illustrate with an example, say $\rho = (134)(25) \in S_5$:

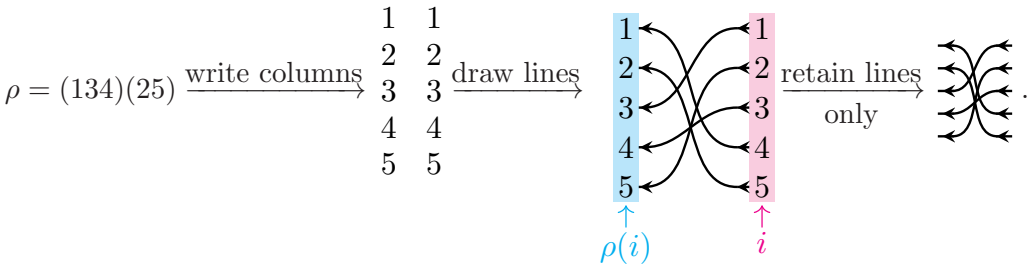

(3.1)

Birdtracks are useful as visual representations of linear maps on $\{1, 2, 3, ..., n\}$: write numbers $\{1, 2, 3, ..., n\}$ in order on the right, then follow the arrows to map them. For completeness, we provide birdtracks for all elements of the group S_3 to illustrate their utility:

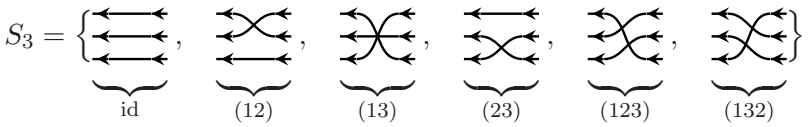

(3.2)

The group operation of multiplication on the group S_n can also easily be done via birdtracks: you simply connect lines and "straighten them out". Illustrating via another example, consider the product of $(123) \in S_3$ and $(13) \in S_3$.

In birdtracks, this is looks like:

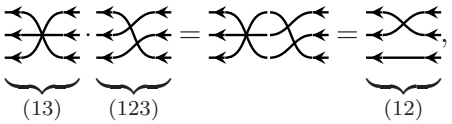

(3.3)

and thus, we can once again see their use as visual tools to carry out computations regarding the permutation group, S_n. To compute the inverse of an element of S_n using birdtracks, traverse the lines of $\rho \in S_n$ in reverse to obtain the birdtrack of ρ^{-1}. For example,

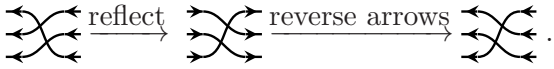

(3.4)

We can make the notion of elements of S_n acting on ordered sets a bit more precise by considering an important example of what they can act on. Elements of the permutation group, S_n, can act on a tensor $\mathbf{v} := v^{a_1 a_2 ... a_n} \in V^{\otimes n}$, where V is some vector space by permuting the indices of $\mathbf{v}$ as follows:

$$[\rho \circ \mathbf{v}]^{a_1 a_2 ... a_n} := [\rho\,(\mathbf{v})]^{a_1 a_2 ... a_n} := v^{a_{\rho(1)} a_{\rho(2)} ... a_{\rho(n)}} \quad \text{for every } \rho \in S_n. \tag{3.5}$$

We have introduced the notation of $\circ$ to denote an element of S_n acting on a tensor which is

somewhat unconventional. However, the ∘ notation shall be employed throughout this thesis as it will drastically reduce the number of brackets in the coming calculations.

Thus, by considering elements of S_n as linear maps on $V^{\otimes n}$, we can write every $\rho \in S_n$ as a product of Kronecker δ's. The permutation, $(123) \in S_3$, can be thought of as a linear map on $V^{\otimes 3}$ for example and can be expressed in-terms of Kronecker δ's as:

$$[(123)]^{b_1 b_2 b_3}{}_{a_1 a_2 a_3} = \delta^{b_2}{}_{a_1} \delta^{b_3}{}_{a_2} \delta^{b_1}{}_{a_3}. \tag{3.6}$$

Therefore, every line of a birdtrack can be thought of as representing a Kronecker δ, i.e.

$$\delta^{b_{\rho(i)}}{}_{a_i} = b_{\rho(i)} \longleftarrow a_i, \tag{3.7}$$

and thus

$$[(123)]^{b_1 b_2 b_3}{}_{a_1 a_2 a_3} = \delta^{b_2}{}_{a_1} \delta^{b_3}{}_{a_2} \delta^{b_1}{}_{a_3} = \tag{3.8}$$

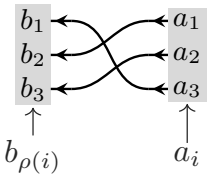

The multiplication of elements in S_n can be expressed using Kronecker δ's. Let ρ and σ be two elements in S_n represented as:

$$[\rho]^{b_1 b_2 \ldots b_n}{}_{a_1 a_2 \ldots a_n} = \delta^{b_{\rho(n)}}{}_{a_n} \ldots \delta^{b_{\rho(3)}}{}_{a_3} \delta^{b_{\rho(2)}}{}_{a_2} \delta^{b_{\rho(1)}}{}_{a_1}, \tag{3.9}$$

and similarly for σ. The product $\rho \cdot \sigma$ is given by:

$$\begin{aligned} [\rho \cdot \sigma]^{c_1 c_2 \ldots c_n}{}_{a_1 a_2 \ldots a_n} &= \delta^{c_{\rho(n)}}{}_{b_n} \ldots \delta^{c_{\rho(3)}}{}_{b_3} \delta^{c_{\rho(2)}}{}_{b_2} \delta^{c_{\rho(1)}}{}_{b_1} \delta^{b_{\sigma(n)}}{}_{a_n} \ldots \delta^{b_{\sigma(3)}}{}_{a_3} \delta^{b_{\sigma(2)}}{}_{a_2} \delta^{b_{\sigma(1)}}{}_{a_1} \\ &= \delta^{c_{\rho\cdot\sigma(n)}}{}_{a_n} \ldots \delta^{c_{\rho\cdot\sigma(3)}}{}_{a_3} \delta^{c_{\rho\cdot\sigma(2)}}{}_{a_2} \delta^{c_{\rho\cdot\sigma(1)}}{}_{a_1}. \end{aligned} \tag{3.10}$$

Birdtracks boil down to products of Kronecker δ's, which one should remember when working with or stuck on computations involving birdtracks[2].

So far, we have only looked at birdtracks for elements of S_n. However, it is entirely possible and valid to look at birdtracks for elements of the group algebra $\mathbb{R}[S_n]$ over S_n, which is slightly more general and what we shall be mainly encountering for the majority of this thesis. In general, a group algebra over a finite group[3] is defined as [53]:

Definition 3.1.1 (Finite Group Algebra)**.** Let G be a finite group equipped with the group

[2] This is actually how computations involving birdtracks are done on a computer in programs such as *Mathematica*. Birdtracks are a way to intuitively visualize what is happening

[3] One can also define a group algebra for Lie groups but this is significantly more complicated to deal with.

operation, $\cdot$, and $\mathbb{F}$ be a field. A finite group algebra, $\mathbb{F}[G]$, is the set of all linear combinations of the elements of G with coefficients in $\mathbb{F}$ and hence all elements of the form

$$\sum_{g\in G} \lambda_g g, \quad \text{with } \lambda_g \in \mathbb{F} \text{ and } g \in G, \tag{3.11}$$

equipped with the group operation $\cdot$.

A finite group algebra, $\mathbb{F}[G]$, is an algebra over G with respect to addition defined as

$$\sum_{g\in G} \lambda_g g + \sum_{g\in G} \kappa_g g = \sum_{g\in G} (\lambda_g + \kappa_g)\, g, \tag{3.12}$$

multiplication by a scalar defined as

$$\lambda \sum_{g\in G} \lambda_g g = \sum_{g\in G} (\lambda\lambda_g)\, g, \tag{3.13}$$

and multiplication of two finite group algebra elements defined as

$$\left(\sum_{g\in G} \lambda_g g\right)\left(\sum_{h\in G} \kappa_h h\right) = \sum_{g,h\in G} (\lambda_g \kappa_h)\, g\cdot h, \tag{3.14}$$

and also note that a finite group algebra is also a vector space [53]. We will restrict ourselves to the finite group algebras, specifically the finite group algebra $\mathbb{R}[S_n]$, throughout this thesis as this is all that we will need.

Elements of $\mathbb{R}[S_n]$ can be defined to act on a tensor $v^{a_1a_2\ldots a_n} \in V^{\otimes n}$, where V is a vector space, as follows:

$$g \circ v^{a_1a_2\ldots a_n} = \sum_{\rho\in S_n} \lambda_\rho\, v^{a_{\rho(1)}a_{\rho(2)}\ldots a_{\rho(n)}}, \tag{3.15}$$

where $g = \sum\limits_{\rho\in S_n} \lambda_\rho\rho \in \mathbb{R}[S_n]$ and $\lambda_\rho \in \mathbb{R}$ are scalar coefficients.

Thus, we can write a group algebra element, $\mathrm{g} = \sum_{\rho\in S_n} \lambda_\rho\rho \in \mathbb{R}[S_n]$ where $\lambda_\rho \in \mathbb{R} \forall \rho \in S_n$ and $\forall\rho \in S_n$, as product of Kronecker δ's when they act on tensors:

$$[\mathrm{g}]^{b_1b_2\ldots b_n}{}_{a_1a_2\ldots a_n} = \sum_{\rho\in S_n} \lambda_\rho\, [\rho]^{b_1b_2\ldots b_n}{}_{a_1a_2\ldots a_n} = \sum_{\rho\in S_n} \lambda_\rho \delta^{b_{\rho(n)}}{}_{a_n} \ldots \delta^{b_{\rho(3)}}{}_{a_3} \delta^{b_{\rho(2)}}{}_{a_2} \delta^{b_{\rho(1)}}{}_{a_1}. \tag{3.16}$$

Elements of $\mathbb{R}[S_n]$ acting on tensors can therefore be considered as linear maps on $V^{\otimes n}$ where V is some vector space. So naturally, we can define an inner product on $\mathbb{R}[S_n]$ which comes from how inner products are defined on linear maps from a vector space to itself [54]. Such an inner product is defined as:

Definition 3.1.2 (Inner product on $\mathrm{Lin}(V)$)**.** Let V be a vector space and A and B be a linear map from V to itself, i.e. $A, B \in \mathrm{Lin}(V)$. The inner product between A and B $\langle\cdot|\cdot\rangle$ is defined as

$$\langle A|B\rangle := \mathrm{tr}\left(A^\dagger B\right), \tag{3.17}$$

where $A^\dagger$ denotes the Hermitian conjugate, i.e. complex conjugate transpose, of A.

If $A, B \in \mathrm{Lin}(V^{\otimes n})$, then A and B can be represented as tensors with n upper indices and n lower indices

$$A^{i_1 i_2 i_3 \ldots i_n}{}_{j_1 j_2 j_3 \ldots j_n},$$

and similarly for B. We will not do so here, but it can fairly easily be shown[4] [25, 44] that the Hermitian conjugate of A, $A^\dagger$, can be represented as a tensor as:

$$A^\dagger = \left(A^{i_1 i_2 i_3 \ldots i_n}{}_{j_1 j_2 j_3 \ldots j_n}\right)^* =: A_{i_1 i_2 i_3 \ldots i_n}{}^{j_1 j_2 j_3 \ldots j_n}{}^{5}. \tag{3.18}$$

In birdtracks, what this means is that the Hermitian conjugate of a birdtrack operator, A, with respect to the inner product given by Eq. 3.17 (and the hence the inner product to be defined in Eq. 3.22) is obtained by flipping the birdtrack about its vertical axis and reversing the arrows [25, 44, 51]:

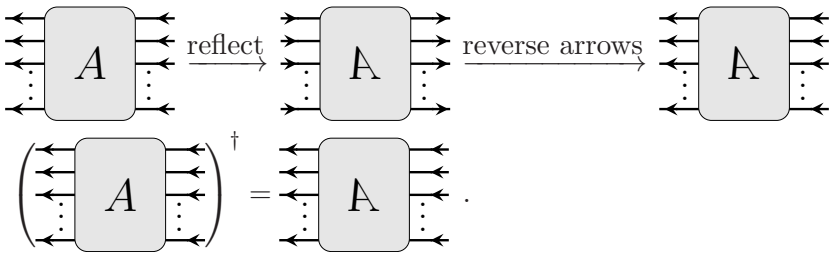

(3.19)

The contents of box A are vertically reflected and their arrows reversed, as indicated by $\mathbb{A}$ in Eq. 3.19. Here, we have introduced an additional birdtrack notation where a box with a label A, is shorthand for a group algebra element $\mathbb{R}[S_n]$. This way, we do not have to write out group algebra elements as arbitrary sums whenever we want to write them out as birdtracks. An immediate consequence of Eq. 3.19 is that for $\rho \in S_n$, its Hermitian conjugate is also its inverse, i.e. every single element of S_n is unitary:

$$\rho^{-1} = \rho^\dagger, \quad \text{for all } \rho \in S_n. \tag{3.20}$$

[4] One simply considers the definition of the Hermitian conjugate of an operator on a vector space, $\langle w, Pu\rangle_W \stackrel{!}{=} \langle P^\dagger w, u\rangle_U$, where $w \in W$ and $u \in U$ and W and U are vector spaces with $P : U \to W$ and $P^\dagger : W \to U$ and goes from there.

[5] Keep in-mind that this raising and lowering of indices will induce a complex conjugation of the tensor components [25].

The trace of $A \in \mathrm{Lin}\,(V^{\otimes n})$ is given by:

$$\mathrm{tr}\,(A) = A^{i_1 i_2 i_3 \ldots i_n} \qquad _{i_1 i_2 i_3 \ldots i_n} = \quad , \tag{3.21}$$

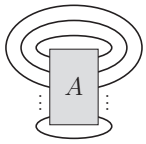

where the birdtracks representation of a trace means "connecting index lines on the same level". Equations 3.18 and 3.21 therefore allow us to compute the inner product between two elements of $\mathrm{Lin}\,(V^{\otimes n})$ via Eq. 3.17.

Thus, the inner product on $\mathbb{R}[S_n]$, when considering its elements to be linear maps on $V^{\otimes n}$ where V is some vector space, will be defined as follows:

Definition 3.1.3 (Inner product on $\mathbb{R}\,(S_n)$)**.** Let $\mathrm{g} \in \mathbb{R}[S_n]$ and $\mathrm{h} \in \mathbb{R}[S_n]$. Then, we have that:

$$[\mathrm{g}]^{b_1 b_2 \ldots b_n} \qquad _{a_1 a_2 \ldots a_n} = \sum_{\rho \in S_n} \lambda_\rho \, [\rho]^{b_1 b_2 \ldots b_n} \qquad _{a_1 a_2 \ldots a_n} = \sum_{\rho \in S_n} \lambda_\rho \delta^{b_{\rho(n)}} \, _{a_n} \ldots \delta^{b_{\rho(3)}} \, _{a_3} \delta^{b_{\rho(2)}} \, _{a_2} \delta^{b_{\rho(1)}} \, _{a_1},$$

where $\lambda_\rho \in \mathbb{R}$ and similarly for h. The inner product on $\mathbb{R}[S_n]$ will be given by Eq. 3.17 and thus, the inner product between g and h will be:

$$\begin{aligned}
\langle \mathrm{g} | \mathrm{h} \rangle &= \mathrm{tr}\left(\mathrm{g}^\dagger \mathrm{h}\right) \\
&= \left(\sum_{\rho \in S_n} \lambda_\rho \delta^{b_{\rho(n)}} \, _{a_n} \ldots \delta^{b_{\rho(3)}} \, _{a_3} \delta^{b_{\rho(2)}} \, _{a_2} \delta^{b_{\rho(1)}} \, _{a_1} \right)^\dagger \\
&\times \left(\sum_{\sigma \in S_n} \kappa_\sigma \delta^{b_{\sigma(n)}} \, _{a_n} \ldots \delta^{b_{\sigma(3)}} \, _{a_3} \delta^{b_{\sigma(2)}} \, _{a_2} \delta^{b_{\sigma(1)}} \, _{a_1} \right) \\
&= \left(\sum_{\rho \in S_n} \lambda_\rho \delta_{b_{\rho(n)}} \, ^{a_n} \ldots \delta_{b_{\rho(3)}} \, ^{a_3} \delta_{b_{\rho(2)}} \, ^{a_2} \delta_{b_{\rho(1)}} \, ^{a_1} \right)^* \\
&\times \left(\sum_{\sigma \in S_n} \kappa_\sigma \delta^{b_{\sigma(n)}} \, _{a_n} \ldots \delta^{b_{\sigma(3)}} \, _{a_3} \delta^{b_{\sigma(2)}} \, _{a_2} \delta^{b_{\sigma(1)}} \, _{a_1} \right) \\
&= \left(\sum_{\rho \in S_n} \lambda_\rho \delta_{b_{\rho(n)}} \, ^{a_n} \ldots \delta_{b_{\rho(3)}} \, ^{a_3} \delta_{b_{\rho(2)}} \, ^{a_2} \delta_{b_{\rho(1)}} \, ^{a_1} \right) \\
&\times \left(\sum_{\sigma \in S_n} \kappa_\sigma \delta^{b_{\sigma(n)}} \, _{a_n} \ldots \delta^{b_{\sigma(3)}} \, _{a_3} \delta^{b_{\sigma(2)}} \, _{a_2} \delta^{b_{\sigma(1)}} \, _{a_1} \right),
\end{aligned} \tag{3.22}$$

using the fact that the Kronecker δ's, λ_ρ, and κ_σ are real to get to the result on the last line.

In the case of $\mathbb{R}[S_n]$, we have that each Kronecker δ is a linear map from V to V, i.e. ${\delta^b}_a : V \to V$. If V has dimension N, then we have that:

$$\mathrm{tr}\left({\delta^b}_a\right) = {\delta^a}_a = \dim(V) = N. \tag{3.23}$$

Equations 3.22 and 3.23 then give us all the necessary tools required to compute inner products on $\mathbb{R}[S_n]$. Of course, this now begs the question: how does one compute inner products on $\mathbb{R}[S_n]$ using birdtracks? To answer this, consider the trace of $[\mathrm{g}]^{b_1 b_2 \ldots b_n}{}_{a_1 a_2 \ldots a_n} = \sum_{\rho \in S_n} \lambda_\rho {\delta^{b_{\rho(n)}}}_{a_n} \ldots {\delta^{b_{\rho(3)}}}_{a_3} {\delta^{b_{\rho(2)}}}_{a_2} {\delta^{b_{\rho(1)}}}_{a_1} \in \mathbb{R}[S_n]$. This is given by:

$$\begin{aligned}\mathrm{tr}\,(\mathrm{g}) &= \mathrm{tr}\left(\sum_{\rho \in S_n} \lambda_\rho {\delta^{b_{\rho(n)}}}_{a_n} \ldots {\delta^{b_{\rho(3)}}}_{a_3} {\delta^{b_{\rho(2)}}}_{a_2} {\delta^{b_{\rho(1)}}}_{a_1}\right) \\ &= \sum_{\rho \in S_n} \lambda_\rho {\delta^{b_{\rho(n)}}}_{b_n} \ldots {\delta^{b_{\rho(3)}}}_{b_3} {\delta^{b_{\rho(2)}}}_{b_2} {\delta^{b_{\rho(1)}}}_{b_1}.\end{aligned} \tag{3.24}$$

However, another way in which one can contract the indices in Eq. 3.24 is by multiplying each Kronecker δ in g such that:

$$\begin{aligned}&\mathrm{tr}\left(\sum_{\rho \in S_n} \lambda_\rho {\delta^{b_{\rho(n)}}}_{a_n} \ldots {\delta^{b_{\rho(3)}}}_{a_3} {\delta^{b_{\rho(2)}}}_{a_2} {\delta^{b_{\rho(1)}}}_{a_1}\right) \\ &= \sum_{\rho \in S_n} \lambda_\rho {\delta^{b_{\rho(n)}}}_{a_n} {\delta^{a_n}}_{b_{\rho(n)}} \ldots {\delta^{b_{\rho(3)}}}_{a_3} {\delta^{a_3}}_{b_{\rho(3)}} {\delta^{b_{\rho(2)}}}_{a_2} {\delta^{a_2}}_{b_{\rho(2)}} {\delta^{b_{\rho(1)}}}_{a_1} {\delta^{a_1}}_{b_{\rho(1)}} \\ &= \sum_{\rho \in S_n} \lambda_\rho {\delta^{b_{\rho(n)}}}_{b_n} \ldots {\delta^{b_{\rho(3)}}}_{b_3} {\delta^{b_{\rho(2)}}}_{b_2} {\delta^{b_{\rho(1)}}}_{b_1}.\end{aligned} \tag{3.25}$$

But recall that each line in a birdtrack represents a Kronecker δ. Therefore, Eq. 3.25 indicates that to find the trace of a birdtrack operator in $\mathbb{R}[S_n]$, connect index lines at the same level as shown in Eq. 3.21. Each closed loop is replaced by a factor of $\dim(V) = N$, according to Eq. 3.23, acknowledging potential self-intersection of loops.

Thus, to compute the inner product between two elements of $\mathrm{g}, \mathrm{h} \in \mathbb{R}[S_n]$ in the birdtrack formalism, take the Hermitian conjugate of the birdtrack of g as per Eq. 3.19, multiply it with the birdtrack of h following the multiplication rules, and use Eq. 3.21 to compute the inner product.

It will also prove to be imperative later to briefly introduce symmetrisers and antisymmetrisers.

Definition 3.1.4 (Symmetrisers and Antisymmetrisers)**.** Consider the group algebra $\mathbb{R}[S_n]$ and let $\{a_1, a_2, \ldots, a_k\}$ be a subset of $\{1, 2, \ldots, n\}$. The symmetriser over $\{a_1, a_2, \ldots, a_k\}$ is the sum of all permutations, σ, over the elements in $\{a_1, a_2, \ldots, a_k\}$ with a global prefactor

$\frac{1}{k!}$

$$\boldsymbol{S}_{a_1a_2\ldots a_k} := \frac{1}{k!} \sum_{\sigma \text{ permutes } \{a_1,a_2,\ldots,a_k\}} \sigma. \tag{3.26}$$

The antisymmetriser over the set $\{a_1, a_2, \ldots, a_k\}$ is defined similarly, but each permutation in the sum is multiplied by its signature $\text{sign}(\sigma)$:

$$\boldsymbol{A}_{a_1a_2\ldots a_k} := \frac{1}{k!} \sum_{\sigma \text{ permutes } \{a_1,a_2,\ldots,a_k\}} \text{sign}(\sigma)\sigma. \tag{3.27}$$

In birdtracks, a symmetriser $\boldsymbol{S}_{a_1a_2\ldots a_k}$ is indicated by a white box over the index lines $a_1, a_2, \ldots, a_k$ of the corresponding birdtrack. An antisymmetriser, $\boldsymbol{A}_{a_1a_2\ldots a_k}$, will be denoted with a black box over the said index lines, and the birdtrack notation will already includes the prefactor $\frac{1}{k!}$.

Consider the following examples to illustrate our point: $\boldsymbol{S}_{1234}$, $\boldsymbol{S}_{124}$ and $\boldsymbol{A}_{123}$ all in the group algebra $\mathbb{R}[S_4]$ (we have omitted the arrows here to reduce clutter):

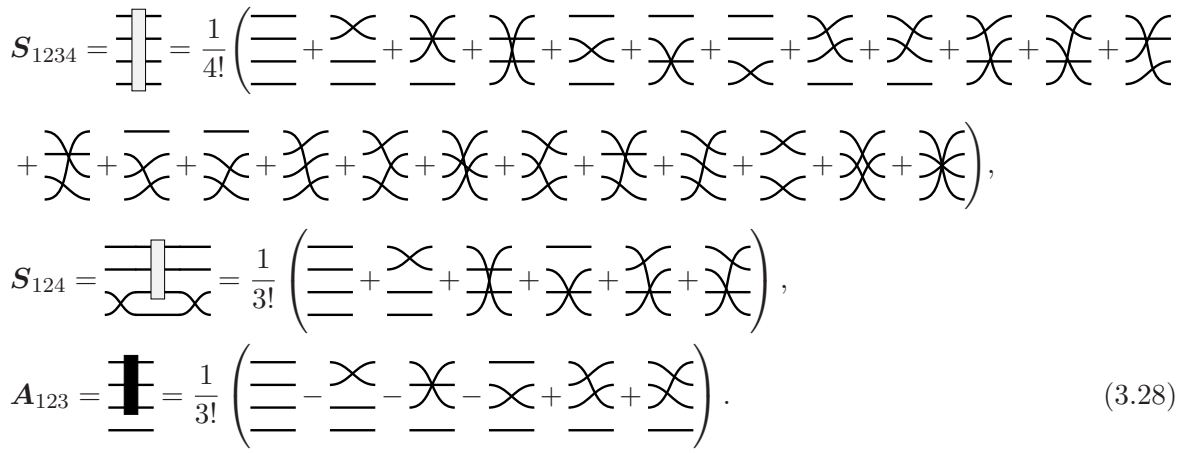

Thus, the birdtrack notation introduced for symmetrisers and antisymmetrisers makes the corresponding expressions for symmetrisers and antisymmetrisers much more compact as one can see in Eq. 3.28.

Symmetrisers and antisymmetrisers have the convenient property that they are idempotent which means that [44]

$$\begin{aligned} \boldsymbol{S}_{a_1a_2\ldots a_k} \cdot \boldsymbol{S}_{a_1a_2\ldots a_k} &= \boldsymbol{S}_{a_1a_2\ldots a_k}, \\ \boldsymbol{A}_{a_1a_2\ldots a_k} \cdot \boldsymbol{A}_{a_1a_2\ldots a_k} &= \boldsymbol{A}_{a_1a_2\ldots a_k}. \end{aligned} \tag{3.29}$$

A proof of Eq. 3.29 is available in [44, 51]; however, the validity of Eq. 3.29 should be relatively intuitive, as applying a symmetriser to a tensor that is already symmetric over the pertinent indices will yield the same tensor with symmetric indices. The same rationale applies to the

antisymmetriser. Also note that multiplying a symmetriser with an antisymmetriser over the same indices yields 0 (and vice versa) [44] i.e.

$$\begin{aligned} \boldsymbol{S}_{a_1a_2\ldots a_k} \cdot \boldsymbol{A}_{a_1a_2\ldots a_k} &= 0, \\ \boldsymbol{A}_{a_1a_2\ldots a_k} \cdot \boldsymbol{S}_{a_1a_2\ldots a_k} &= 0. \end{aligned} \tag{3.30}$$

A proof of Eq. 3.30 is provided in [44]; this should also be relatively intuitive, as applying an antisymmetriser to a tensor that is already symmetric over the pertinent indices will result in zero (and the converse holds true as well). Lastly, symmetrisers and antisymmetrisers are Hermitian which is relatively easy to prove in birdtrack notation from Eq. 3.19 (see for example, [44] for a formal proof):

$$\begin{aligned} \boldsymbol{S}^{\dagger}_{a_1a_2\ldots a_k} &= \boldsymbol{S}_{a_1a_2\ldots a_k}, \\ \boldsymbol{A}^{\dagger}_{a_1a_2\ldots a_k} &= \boldsymbol{A}_{a_1a_2\ldots a_k}. \end{aligned} \tag{3.31}$$

The aforementioned symmetrisers and antisymmetrisers serve as the fundamental components of the Hermitian Young Projection Operators and transition operators, which are integral to this thesis. The ensuing discussion will elaborate on these elements.

What we want to emphasise to the potentially intimidated reader at the end of the day is this:

> Birdtracks and elements of $\mathbb{R}[S_n]$ always boil down to Kronecker δ's at the end of the day and Kronecker δ's are easy to work with. So if you are ever struggling or in-doubt, rewrite birdtracks and/or elements of $\mathbb{R}[S_n]$ as Kronecker δ's and take it from there.

We are mainly interested in the group algebra $\mathbb{R}[S_n]$ in how it relates to a product representation of $\mathrm{SU}(N)$ constructed from its fundamental representation on a vector space, V, with $\dim(V) = N$.

Consider a product representation of $\mathrm{SU}(N)$ constructed from its fundamental representation on a vector space, V, with $\dim(V) = N$. The action of $U \in \mathrm{SU}(N)$ on $v \in V$ is given by $v \mapsto Uv$. In index notation, this becomes $v^i \mapsto U^i{}_j\, v^j$. Therefore, we immediately get a product representation of $\mathrm{SU}(N)$ acting on $V^{\otimes m}$ which takes the form:

$$\mathbf{U} \circ \mathbf{v} = \mathbf{U} \circ v^{j_1\ldots j_m} := \underbrace{U^{i_1}{}_{j_1} \ldots U^{i_m}{}_{j_m}}_{=:\mathbf{U}}\, v^{j_1\ldots j_m}. \tag{3.32}$$

where we have again employed the unconventional $\circ$ notation to denote an element of a product representation of $\mathrm{SU}(N)$ acting on an element of $V^{\otimes m}$. All factors of $V^{\otimes m}$ are identical, so permuting them for $v^{i_1i_2\ldots i_m}$ yields the same result, i.e.

$$v^{i_1 i_2 \ldots i_m} = v^{i_{\rho(1)} i_{\rho(2)} \cdots i_{\rho(m)}} \quad \forall \rho \in S_m. \tag{3.33}$$

Thus, Eqs. 3.32 and 3.33 immediately tell us that $\rho \in S_m$ and $\mathbf{U} \in \mathrm{SU}(N)$ commute as linear maps on $V^{\otimes m}$:

$$\mathbf{U} \cdot \rho \circ \mathbf{v} = \rho \cdot \mathbf{U} \circ \mathbf{v}. \tag{3.34}$$

Equation 3.34 implies that any permutation as a linear map is an invariant of $\mathrm{SU}(N)$ (abusing notation slightly)[6]:

$$\mathbf{U} \cdot \rho \cdot \mathbf{U}^{-1} = \rho. \tag{3.35}$$

Thus, we have that permutations as linear maps are invariants of $\mathrm{SU}(N)$ and [44] shows that permutations in-fact span the space of all linear invariants of $\mathrm{SU}(N)$ over $V^{\otimes m}$. Hence, permutations are considered to be the primitive invariants of $\mathrm{SU}(N)$ due to their isomorphism with $\mathrm{SU}(N)$'s primitive invariants:

$$S_m \cong \mathrm{PI}\left(\mathrm{SU}(N), V^{\otimes m}\right). \tag{3.36}$$

The full space of linear invariants is given by:

$$\mathrm{API}\left(\mathrm{SU}(N), V^{\otimes m}\right) := \left\{ \sum_{\sigma \in S_m} \alpha_\sigma \sigma \middle| \alpha_\sigma \in \mathbb{R}, \sigma \in S_m \right\} \subset \mathrm{Lin}\left(V^{\otimes m}\right), \tag{3.37}$$

where API stands for the Algebra of Primitive Invariants. We see that $\mathrm{API}\left(\mathrm{SU}(N), V^{\otimes m}\right)$ is in-fact isomorphic to the group algebra $\mathbb{R}[S_m]$. Thus, we can now of course express any primitive invariant of $\mathrm{SU}(N)$ over $V^{\otimes m}$ as a linear combination of products of Kronecker δ's[7].

3.1.2 API $\left(\mathbf{SU}(N), V^{\otimes m} \otimes (V^*)^{\otimes n}\right)$

One can generalise from the product representations of $\mathrm{SU}(N)$ on $V^{\otimes m}$, with V carrying the fundamental representation of $\mathrm{SU}(N)$. This generalization leads to the product representations of $\mathrm{SU}(N)$ on $V^{\otimes m} \otimes (V^*)^{\otimes m}$, where V^* carries the antifundamental representation of $\mathrm{SU}(N)$. The next step will then be to proceed to find singlets of $\mathrm{SU}(N)$ on $V^{\otimes m} \otimes (V^*)^{\otimes m}$ which is done in Chapter 3.2.2.

As such this will require new birdtrack notation for elements of $S_{m,n}$ which are isomorphic to the primitive invariants of $\mathrm{SU}(N)$ over $V^{\otimes m} \otimes (V^*)^{\otimes n}$:

$$S_{m,n} \cong \mathrm{PI}\left(\mathrm{SU}(N), V^{\otimes m} \otimes (V^*)^{\otimes n}\right). \tag{3.38}$$

[6] In-fact, this holds true for any Lie group G acting on V [25].

[7] Remember, when in-doubt, always rewrite as Kronecker δ's and take it from there.

Notice that so far, birdtracks always go from right to left and are defined as fundamental lines: each right-to-left line is an element of $\mathrm{Lin}(V)$ where V carries the fundamental representation of $\mathrm{SU}(N)$. Hence, it is natural to define a left-to-right line as an element of $\mathrm{Lin}\,(V^*)$, making it an antifundamental line. This is summarised in Eq. 3.39 below[8]:

$$\begin{aligned} \delta_i{}^j &= i \longrightarrow j \in \mathrm{Lin}\,(V^*)\,, \\ \delta^i{}_j &= i \longleftarrow j \in \mathrm{Lin}\,(V)\,. \end{aligned} \tag{3.39}$$

One can therefore obtain the primitive invariants, $S_{m,n}$, from S_{m+n} by swapping fundamental lines for antifundamental lines [44]. This is done graphically by swapping the left and right end points of a birdtrack corresponding to a specific V in $V^{\otimes(m+n)}$ to be converted to its dual space V^*. To illustrate via an example, consider the primitive invariants, $S_3 \cong \mathrm{PI}\left(\mathrm{SU}(N), V^{\otimes 3}\right)$ and how they map onto $S_{2,1} \cong \mathrm{PI}\left(\mathrm{SU}(N), V^{\otimes 2} \otimes (V^*)^{\otimes 1}\right)$:

S_3 : 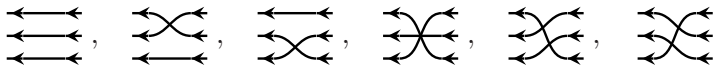 (3.40a)

$S_{2,1}$:  (3.40b)

For the sake of completeness, let us write one of the elements of $S_{2,1}$ in terms of Kronecker δ's. Take for example, the birdtrack,  $\in \mathrm{Lin}\left(V^{\otimes 2} \otimes (V^*)^{\otimes 1}\right)$. Written in-terms of Kronecker δ's, this birdtrack is:

 $= \delta^{b_2 a_3}\, \delta_{b_3 a_2}\, \delta^{b_1}{}_{a_1}\,.$ (3.41)

Note how the relevant indices get lowered or raised since this birdtrack now acts on $\mathbf{v} := v^{a_1 a_2}{}_{a_3} \in V^{\otimes 2} \otimes (V^*)^{\otimes 1}$.

The birdtrack multiplication rule for connecting and following lines applies to elements of $S_{m,n}$ [44]. However, $S_{m,n}$ is not generally a group, as not all its elements have inverses since index contraction is not an inverse operation. Consequently, the multiplication tables of the algebras $\mathrm{API}\left(\mathrm{SU}(N), V^{\otimes(m+n)}\right)$ and $\mathrm{API}\left(\mathrm{SU}(N), V^{\otimes m} \otimes (V^*)^{\otimes n}\right)$ will differ greatly.

The inner product on $\mathrm{Lin}\left(V^{\otimes m} \otimes (V^*)^{\otimes n}\right)$ for two elements $A, B \in \mathrm{Lin}\left(V^{\otimes m} \otimes (V^*)^{\otimes n}\right)$ is defined by contracting the indices of $A^\dagger$ with B or by taking the trace:

$$\langle A|B\rangle = \mathrm{tr}(|A\rangle\langle B|) = \mathrm{tr}(A^\dagger B) \quad \forall A, B \in \mathrm{Lin}\left(V^{\otimes m} \otimes (V^*)^{\otimes n}\right). \tag{3.42}$$

[8] Note that the relation between index placement (upper/lower) differs from the commonly used convention; for example [44]. We employ this convention to indicate the direction in which the corresponding birdtrack arrow points and because it aligns with the way subsequent equations are displayed.

3.1.3 Wilson Lines, Singlet States and Generators

In order to construct Wilson Line correlator matrices, we will need to introduce further birdtrack notation for Wilson lines in the fundamental representation, $U_{\boldsymbol{x}}$, and the anti-fundamental representation, $U^\dagger_{\boldsymbol{y}}$ ($\boldsymbol{x}$ and $\boldsymbol{y}$ here are the transverse coordinates of the Wilson lines). A Wilson line in the fundamental and anti-fundamental representations are denoted in birdtracks by:

$$U_{\boldsymbol{x}} :=$$ 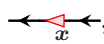 $$, \quad [U_{\boldsymbol{x}}]^i{}_j :=$$ $$, \tag{3.43}$$

$$U^\dagger_{\boldsymbol{y}} :=$$ 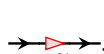 $$, \quad [U^\dagger_{\boldsymbol{y}}]_i{}^j :=$$ $$. \tag{3.44}$$

When Wilson lines do not have or do not need a transverse coordinate, they are given in birdtracks by:

$$U :=$$ 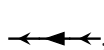 $$, \quad [U]^i{}_j :=$$ $$, \tag{3.45}$$

$$U^\dagger :=$$ $$, \quad [U^\dagger]_i{}^j :=$$ $$. \tag{3.46}$$

To minimize clutter, we will omit coordinate labels on Wilson lines unless explicitly needed for clarity. As a simple example, note that the dipole we encountered in Eq. 2.30 can be written in birdtracks as:

$$\frac{\mathrm{tr}\left(U_{\boldsymbol{x}}U^\dagger_{\boldsymbol{y}}\right)}{N_c} = \frac{1}{N_c} \underbrace{\delta^l{}_i}_{\in (V\otimes V^*)^* \text{ and is the Hermitian conjugate of a singlet state}} [U_{\boldsymbol{x}}]^i{}_j [U^\dagger_{\boldsymbol{y}}]^k{}_l$$

$$\times \underbrace{\delta^j{}_k}_{\in V\otimes V^* \text{ and is a singlet state}}$$

$$=$$ 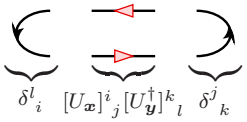

$$=$$ 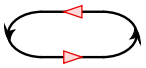 $$. \tag{3.47}$$

Thus, we see that the $q\bar{q}$-dipole we encountered previously is a Wilson line correlator of the form as in Eq. 2.36. For the case of the $q\bar{q}$-dipole, there are only 1 possible singlet states (which we will explain in the following sections), and therefore the Wilson correlator matrix for a $q\bar{q}$-dipole is just a number[9].

[9] Note that in birdtracks, a closed loop will always correspond to a trace as seen for the examples in Eq. 3.47 and 3.25

A tensor product of Wilson lines is represented in birdtracks by stacking them on top of each other, e.g.:

$$(U_{\boldsymbol{x}_1} \otimes U^\dagger_{\boldsymbol{y}_1}) \otimes \cdots \otimes (U_{\boldsymbol{x}_m} \otimes U^\dagger_{\boldsymbol{y}_m}) =:$$

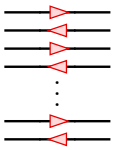

m-pairs . (3.48)

The birdtrack notation for a tensor product of Wilson lines that all have the same transverse coordinate is given by:

$$(U_{\boldsymbol{x}} \otimes U^\dagger_{\boldsymbol{x}}) \otimes \cdots \otimes (U_{\boldsymbol{x}} \otimes U^\dagger_{\boldsymbol{x}}) =:$$

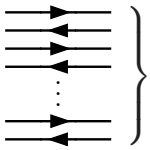

m-pairs . (3.49)

We will also find it necessary to define the birdtrack for an arbitrary singlet state $|m; s\rangle$ in $V^{\otimes m} \otimes (V^*)^{\otimes m}$. There are two ways in which one can display an arbitrary singlet state in birdtrack notation which depends on how one organises the fundamental and anti-fundamental lines. One can arrange fundamental lines above anti-fundamental lines:

$$|m; s\rangle =: m\text{-pairs}$$

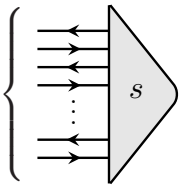

. (3.50)

Or stack all fundamental lines together and all anti-fundamental lines together:

$$|m; s\rangle =: m\text{-pairs}$$

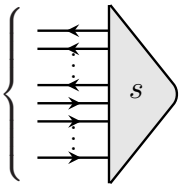

. (3.51)

Both are equivalent ways of representing states in $V^{\otimes m} \otimes (V^*)^{\otimes m}$ since we have that $V^{\otimes m} \otimes (V^*)^{\otimes m}$ is canonically isomorphic to $(V \otimes V^*)^{\otimes m}$:

$$V^{\otimes m} \otimes (V^*)^{\otimes m} \cong (V \otimes V^*)^{\otimes m} . \tag{3.52}$$

Singlet states from the basis constructed frm Hermitian Young Projection Operators and transition operators which we will discuss later on are conveniently expressed by Eq. 3.50. However, Eq. 3.51 will prove more convenient in the Fierz basis as we shall see shortly.

We will define birdtrack notation for SU(N) generators, t^a, elements of $A^{\otimes m}$ where A

is a real vector space with SU(N)'s adjoint representation, and Clebsch-Gordan operators mapping (anti-)fundamental indices to or from an adjoint vertex.

- Generators of SU(N) in the fundamental representation are written in birdtracks as

$$\sqrt{2}t^a := \quad , \quad \sqrt{2}\,[t^a]^i{}_j := i \quad j \ , \tag{3.53}$$

  where dotted lines are now used to indicate colour indices and the $\sqrt{2}$ is a chosen normalization convention such that we obtain Eq. 3.57 below.

- If A is a real vector space carrying the adjoint representation of SU(N), then an element $\mathbf{C}^{(s)} := \mathcal{C}^{(s)a_1a_2a_3\ldots a_m} \in A^{\otimes m}$ (where the a_i's are colour indices now) is written in birdtracks as:

$$\mathcal{C}^{(s)a_1a_2a_3\ldots a_m} = \quad . \tag{3.54}$$

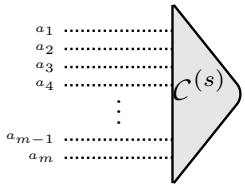

  Note the dotted lines indicating the colour indices of $\mathcal{C}^{(s)a_1a_2a_3\ldots a_m}$.

- Clebsch-Gordan operators are written in birdtracks as:

$$\sqrt{2}|t^b\rangle =: \quad b \quad , \quad \sqrt{2}\langle t^a| =: \ a \quad . \tag{3.55}$$

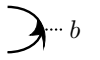

Let us work through a two important examples to illustrate to the reader how these birdtracks work.

First, let us look at a Wilson line in the adjoint representation, $\widetilde{U}^{ab}_{\boldsymbol{z}}$, which can be expressed in terms of fundamental and anti-fundamental Wilson lines as [19, 55]:

$$[\widetilde{U}_{\boldsymbol{z}}]^{ab} := 2\,\mathrm{tr}\left(t^a U_z t^b U_z^\dagger\right) = 2\langle t^a|U_z \otimes U_z^\dagger|t^b\rangle = a \quad \boldsymbol{z} \quad b\,. \tag{3.56}$$

Now let us look at the trace of two generators of SU(N). This is given in birdtracks by:

$$2\,\mathrm{tr}\left(t^a t^b\right) = a \quad b = \delta^l{}_i [t^a]^i{}_j [t^b]^k{}_l \delta^j{}_k = \delta^{ab} =: a \quad b\,. \tag{3.57}$$

Thus, we have the birdtrack for an adjoint line.

The $q\overline{q}g$-correlator that we dealt with in the previous chapter in Eq. 2.35 can then be expressed in birdtracks as:

$$\widetilde{U}^{ab}_{\boldsymbol{z}}\frac{\mathrm{tr}(t^aU_{\boldsymbol{x}}t^bU^\dagger_{\boldsymbol{y}})}{N_c} =$$

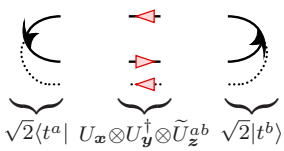

$$=$$

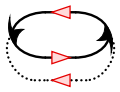

. (3.58)

3.2 Constructing Correlator Matrices

3.2.1 $q^2\overline{q}^2$ correlator matrices

Taking (anti)-quark/(anti)-quark coincidence limits

Now let us construct a more complicated correlator matrix, namely a $q^2\overline{q}^2$ correlator matrix: As discussed in Chapter 2.3, we construct the Wilson line correlator matrix for $q^2\overline{q}^2$ by finding a set of singlet states for $V^{\otimes 2}\otimes(V^*)^{\otimes 2}$ and "sandwich" the Wilson line tensor product $U_{\boldsymbol{x}_1}\otimes U_{\boldsymbol{x}_2}\otimes U^\dagger_{\boldsymbol{y}_1}\otimes U^\dagger_{\boldsymbol{y}_2}$ between each pair of singlet states as per Eq. 2.36.

The singlet states in $V^{\otimes m}\otimes(V^*)^{\otimes m}$ are obtained by "bending" elements in $\mathrm{API}\left(\mathrm{SU}(N),V^{\otimes m}\right)$ since they are primitive invariants of $\mathrm{SU}(N)$ [23, 50]. For a singlet in $V^{\otimes 1}\otimes(V^*)^{\otimes 1}$ to construct the $q\overline{q}$-correlator, "bend" the sole basis element of $\mathrm{API}\left(\mathrm{SU}(N),V^{\otimes 1}\right)$:

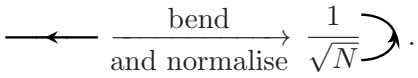

. (3.59)

Now we can obviously use the elements of S_2 and reshape them to obtain a valid set of singlet states for $V^{\otimes 2}\otimes(V^*)^{\otimes 2}$. But this set of singlet states will not be convenient for our uses due to the major issue that it lacks orthogonality as one can easily verify and this will not hold in general for S_n. We therefore need a more suitable basis for the space of singlet states of $V^{\otimes 2}\otimes(V^*)^{\otimes 2}$, ideally an orthogonal one.

For singlet states in $V^{\otimes 2}\otimes(V^*)^{\otimes 2}$, we can form one such basis by considering symmetrisers and anti-symmetrisers in $\mathrm{API}\left(\mathrm{SU}(N),V^{\otimes 2}\right)$ and using the fact that symmetrisers and anti-symmetrisers are orthogonal to one another in this algebra over the same set of legs via Eq.

3.30. Thus, one such set of singlet states of $V^{\otimes 2} \otimes (V^*)^{\otimes 2}$ that is orthonormal is given by:

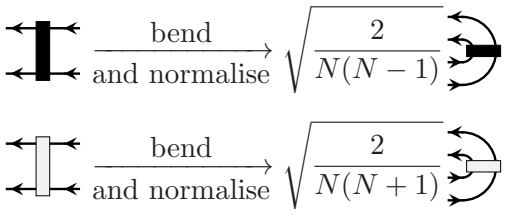

(3.60)

The symmetrisers and anti-symmetrisers which we "bent" to form these singlet states are in-fact the Hermitian Young Projection operators which form an orthogonal basis for API(SU(N), $V^{\otimes 2}$) and project onto the irreducible representations of SU(N) over $V^{\otimes 2}$. We will briefly elaborate more on Hermitian Young Projection Operators in the following sections.

These singlet states are in the form of Eq. 3.51. While they can be reordered as in Eq. 3.50, it's more convenient to keep them in the current basis as we will see shortly. The correlator matrix $\mathcal{A}(Y)$, which is inherently dependent on rapidity Y, is given by

$$\mathcal{A}(Y) = \left(\begin{array}{cc} \frac{2}{N(N+1)} & \frac{2}{N\sqrt{N^2-1}} \\ \frac{2}{N\sqrt{N^2-1}} & \frac{2}{N(N-1)} \end{array} \right)(Y) \,, \tag{3.61}$$

with coordinate dependence omitted for brevity.

Now let us take what is called a coincidence limit, which is when we set two or more coordinates for the Wilson lines equal to one another. For the correlator matrix in Eq. 3.61, we will take what is called a quark-quark coincidence limit where we set the coordinates of the Wilson lines in the fundamental representation equal to each other. Alternatively, one can also take an anti-quark/anti-quark coincidence limit, which is where we set the coordinates of the Wilson lines in the anti-fundamental representation equal to each other, and obtain very similar results. Taking a quark-quark coincidence limit in Eq. 3.61 where $\boldsymbol{x}_2 \to \boldsymbol{x}_1$, we see that for the off-diagonal elements in Eq. 3.61, the fundamental lines that connect the symmetriser to the anti-symmetriser are now the same and hence, by Eq. 3.30, these off-diagonal terms in the matrix will be 0

$$\left(\begin{array}{cc} \frac{2}{N(N+1)} & \frac{2}{N\sqrt{N^2-1}} \\ \frac{2}{N\sqrt{N^2-1}} & \frac{2}{N(N-1)} \end{array} \right)(Y)$$

$$\xrightarrow[\text{or } \boldsymbol{x}_1\to\boldsymbol{x}_2]{\boldsymbol{y}_1\to\boldsymbol{y}_2} \begin{pmatrix} \frac{2}{N(N+1)} & 0 \\ 0 & \frac{2}{N(N-1)} \end{pmatrix} (Y) \ . \tag{3.62}$$

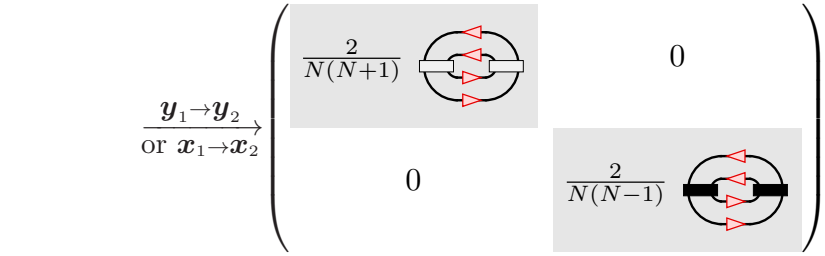

Thus, we see that taking a (anti)-quark/(anti)-quark coincidence limit yields great simplification in the Wilson line correlator matrix. This outcome is expected since the singlet states used in forming the correlator matrix in Eq. 3.61 are orthogonal. Hence, applying successive coincidence limits increasingly simplifies the Wilson line correlator matrix, eventually making it unity in a global coincidence limit, as shown in Eq. 2.37.

In general, Wilson lines corresponding to the quarks and anti-quarks that interact with the target will all have different transverse coordinates which describe the location at which the parton's wordline pierces the $x^- = 0$ plane [17, 23]. In some cases, such as when the distance between two partons is very small relative to the target size, quarks and anti-quarks interacting with the target may have the same transverse coordinates [17, 23]. Thus, it is in our interests to investigate various different coincidence limits. As we saw in Eq. 3.62, taking a (anti)-quark/(anti)-quark coincidence limit yielded great simplification in the correlator matrix when working in the basis constructed in Eq. 3.61.

However, this basis is not well-suited for taking quark/anti-quark coincidence limits. Taking a quark/anti-quark coincidence limit for the correlator matrix in Eq. 3.62 will not yield a result that is block diagonal and immediately simpler to work with. Therefore, we need a singlet basis that simplifies the correlator matrix significantly when a quark/anti-quark coincidence limit is taken, with this simplification clearly represented in birdtrack notation.

Taking quark/anti-quark coincidence limits

To that end, consider that each pair $V \otimes V^*$ contains a singlet and adjoint representation as its irreducible components

$$\delta_{\overline{p}q}\delta_{pq} = \delta^{ab}[t^a]_{\overline{q}q}[t^b]_{\overline{p}p} + \frac{1}{N}\delta_{\overline{q}q}\delta_{\overline{p}p} \tag{3.63a}$$

$$= \underbrace{\qquad}_{\text{adjoint projector}} + \underbrace{\qquad}_{\text{singlet projector}} \ ; \tag{3.63b}$$

Equation 3.63 is known as the Fierz identity.

By "bending" the adjoint and singlet projectors in Eq. 3.63b, we obtain a set of singlet states that span the space of singlets in $(V \otimes V^*)^{\otimes 2}$. Since we have that $(V \otimes V^*)^{\otimes 2}$ is

canonically isomorphic to $V^{\otimes 2} \otimes (V^*)^{\otimes 2}$ via Eq. 3.52, we also obtain a valid set of states that span the singlet states of $V^{\otimes 2} \otimes (V^*)^{\otimes 2}$. Thus, these singlet states are given by:

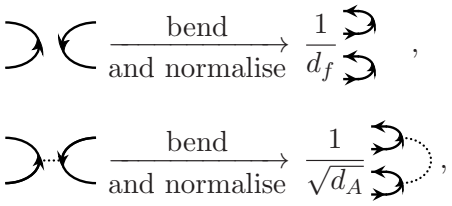

(3.64)

where $d_f = N$ and $d_A = N^2 - 1$. The basis of colour singlet states in Eq. 3.64 is known as the Fierz basis [17]. The Fierz basis and the basis given in Eq. 3.60 span the same space and as such, they can be related via a change of basis of which is computed in chapter 1.6.2 in [23].

Note that we have expressed the singlet states in the Fierz basis in the form of Eq. 3.50 where each fundamental line is on top of an anti-fundamental line. The correlator matrix in this basis will therefore be:

$$\mathcal{A}(Y) = \left(\begin{array}{cc} \frac{1}{\mathrm{d}_f^2} & \frac{1}{\mathrm{d}_f\sqrt{\mathrm{d}_A}} \\ \frac{1}{\mathrm{d}_f\sqrt{\mathrm{d}_A}} & \frac{1}{\mathrm{d}_A} \end{array} \right) (Y) \ . \tag{3.65}$$

We rearranged the Wilson lines to pair those in fundamental and anti-fundamental representations, enabling the construction of the correlator matrix in the singlet states' form as in Eq. 3.64. We will see why it is convenient to do it this way now.

Taking a quark/anti-quark coincidence limit where $\boldsymbol{x}_2 \to \boldsymbol{y}_2$, (similar results will hold if take $\boldsymbol{x}_1 \to \boldsymbol{y}_1$)[10] we see that the off-diagonal term, $\mathcal{A}_{21}(Y)$, becomes:

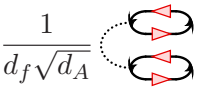

$$\begin{aligned} &= \frac{1}{d_f\sqrt{d_A}} \operatorname{tr}\left(U_{\boldsymbol{x}_1} t^a U^\dagger_{\boldsymbol{y}_1}\right) \operatorname{tr}\left(U_{\boldsymbol{x}_2} t^a U^\dagger_{\boldsymbol{y}_2}\right) \\ &\overset{\boldsymbol{x}_2 \to \boldsymbol{y}_2}{=} \frac{1}{d_f\sqrt{d_A}} \operatorname{tr}\left(U_{\boldsymbol{x}_1} t^a U^\dagger_{\boldsymbol{y}_1}\right) \operatorname{tr}\left(U_{\boldsymbol{x}_2} t^a U^\dagger_{\boldsymbol{x}_2}\right) \\ &= \frac{1}{d_f\sqrt{d_A}} \operatorname{tr}\left(U_{\boldsymbol{x}_1} t^a U_{\boldsymbol{y}_1}\right) \operatorname{tr}\left(U_{\boldsymbol{x}_2} U^\dagger_{\boldsymbol{x}_2} t^a\right) \quad \text{(Using the cyclicity of the trace)} \\ &= \frac{1}{d_f\sqrt{d_A}} \operatorname{tr}\left(U_{\boldsymbol{x}_1} t^a U_{\boldsymbol{y}_1}\right) \operatorname{tr}\left(t^a\right) \end{aligned}$$

[10] The choice on whether we take $\boldsymbol{x}_2 \to \boldsymbol{y}_2$ or $\boldsymbol{x}_1 \to \boldsymbol{y}_1$ is somewhat arbitrary as it depends on how we order the basis elements for the singlet states when constructing the matrix of correlators. One can take coincidence limits in whichever order and way they want without loss of generality.

$$= 0 \quad \text{(Since the trace of a generator is 0).} \tag{3.66}$$

Similarly, we find $\mathcal{A}_{21}(Y) \to 0$ as $\boldsymbol{x}_2 \to \boldsymbol{y}_2$. The diagonal terms $\mathcal{A}_{11}(Y)$ and $\mathcal{A}_{22}(Y)$ also simplify greatly in this coincidence limit. We see that:

$$\mathcal{A}_{11}(Y) = \frac{1}{d_f^2}$$

$$\underset{=}{\boldsymbol{x}_2 \to \boldsymbol{y}_2} \frac{1}{d_f}$$

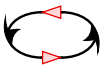

(As we obtain a factor of  $= d_f$ when taking a coincidence limit of the bottom pair of quark and anti-quark)

$$= \frac{1}{d_f} \operatorname{tr}\left(U_{\boldsymbol{x}_1} U^{\dagger}_{\boldsymbol{y}_1}\right). \tag{3.67}$$

Thus, we see that $\mathcal{A}_{11}(Y)$ simplifies to the $q\overline{q}$-dipole correlator that we encountered previously in the quark/anti-quark coincidence limit. One can easily compute $\mathcal{A}_{22}(Y)$ in the quark/anti-quark coincidence limit as well and find that it reduces to the $q\overline{q}g$-correlator that we have also encountered previously. Thus, the matrix of correlators for $q^2\overline{q}^2$ in the Fierz basis reduces to, in the quark/anti-quark coincidence limit:

$$\begin{pmatrix} \frac{1}{\mathrm{d}_f^2} & \frac{1}{\mathrm{d}_f\sqrt{\mathrm{d}_A}} \\ \frac{1}{\mathrm{d}_f\sqrt{\mathrm{d}_A}} & \frac{1}{\mathrm{d}_A} \end{pmatrix} (Y) \xrightarrow{\boldsymbol{x}_2 \to \boldsymbol{y}_2} \begin{pmatrix} \frac{1}{\mathrm{d}_f} & 0 \\ 0 & \frac{1}{\mathrm{d}_A} \end{pmatrix} (Y)\,. \tag{3.68}$$

The Fierz basis is therefore useful for quark/anti-quark coincidence limits and is orthogonal up to at least $m = 3$ as we will see shortly.

Observe that the Wilson line correlator matrix in Eq. 3.68 contains the $q\overline{q}$-dipole correlator and the $q\overline{q}g$-correlator which both appear in the JIMWLK evolution equation for the $q\overline{q}$-dipole correlator. The JIMWLK evolution of the $q\overline{q}$ -dipole is embedded in a sense within the greater Wilson line correlator matrix for $q^2\overline{q}^2$ before coincidence limits are taken. Also, note that the

Wilson line correlator matrix in Eq. 3.68 is block diagonal. These are important observations that we will come back to later.

A brief comment on arranging fundamental and anti-fundamental index lines in correlator matrices: For quark/anti-quark coincidence limits, arranging each fundamental line on top of an anti-fundamental line (as in Eq. 3.50) simplifies the correlator matrices in bird-track notation. Similarly, for (anti)-quark/(anti)-quark coincidence limits, it is better to first group all fundamental lines together, then all anti-fundamental lines (as in Eq. 3.51). Both arrangements are valid and depends on convenience.

3.2.2 Singlet States

Orthogonal bases for singlet states in $V^{\otimes 3} \otimes (V^*)^{\otimes 3}$ are needed to construct $q^3\overline{q}^3$-correlator matrices that simplify in various coincidence limits. H. Weigert and J. Alcock-Zeileinger showed in [23, 50] that one can construct an orthogonal basis for the space of singlet states of $\mathrm{SU}(N)$ over $V^{\otimes 3} \otimes (V^*)^{\otimes 3}$ by "bending" orthogonal basis elements of $\mathrm{API}\,(\mathrm{SU}(N), V^{\otimes m})$[11] to obtain normalised global colour singlet states

$$\frac{|i\rangle}{\sqrt{\langle i|i\rangle}},$$

which are orthogonal. Thus, there will be exactly $m!$ singlet states in $V^{\otimes m} \otimes (V^*)^{\otimes m}$, which is why there is only 1 singlet state for the case of the $q\overline{q}$ dipole in Eq. 3.47 and $(2!\ =)2$ singlet states for the $q^2\overline{q}^2$-correlator. The proof of this fact can be found in [23]. We also see examples in Eqs. 3.47 and 3.60 of "bending" basis elements in $\mathrm{API}\left(\mathrm{SU}(N), V^{\otimes 1}\right)$ and $\mathrm{API}\left(\mathrm{SU}(N), V^{\otimes 2}\right)$ to obtain singlet states:

A detailed proof of this theorem can be found in chapter 5 of [23]. To construct various $q^3\overline{q}^3$ correlators now suited for various combinations of coincidence limits, we now need to consider various bases for the space of singlet states of $V^{\otimes 3} \otimes (V^*)^{\otimes 3}$.

3.2.3 $q^3\overline{q}^3$ correlator matrices

Taking (anti)-quark/(anti)-quark coincidence limits

Let us now construct the correlator matrices for $q^3\overline{q}^3$. In order to construct the $q^3\overline{q}^3$ correlator matrix in a basis so that we can take (anti)-quark/(anti)-quark coincidence limits, we need to use Hermitian Young Projection Operators and their corresponding transition operators. We briefly summarize the key properties of Hermitian Young Projection Operators and transition

[11] One can also find global colour singlet states for the more general $\mathrm{API}\left(\mathrm{SU}(N), V^{\otimes m} \otimes (V^*)^{\otimes n}\right)$ involving ϵ tensors but this will not be necessary for our purposes as we will only need to be dealing with the case when $m = n$. See Chapter 2.3 and [23, 50] for why this is the case.

operators necessary for this thesis, with more details provided in Appendix D, serving as a short review of the subject. Hermitan Young Projection Operators and transition operators are the subject of extensive study, research and discussion in [23–26, 50].

A Hermitian Young Projection Operator (HYPO) is an element of $\mathrm{API}(\mathrm{SU}(N), V^{\otimes m})$ which projects onto the irreducible representations of $\mathrm{SU}(N)$ over $V^{\otimes m}$ where V is a vector space of dimension N. Hermitian Young Projection Operators are in a one-to-one correspondence to Young tableaux that have m boxes through the fact that the Young tableaux themselves are in a direct one-to-one correspondence with the irreducible representations of $\mathrm{SU}(N)$ over $V^{\otimes m}$. As the name implies, HYPOs are Hermitian along with the fact that they are idempotent, orthogonal and sum to unity. However, HYPOs by themselves do not form a complete basis for $\mathrm{API}(\mathrm{SU}(N), V^{\otimes m})$ as the number of HYPOs for any given m is strictly less than $m!$ for $m > 2$. In order to obtain a complete basis for $\mathrm{API}(\mathrm{SU}(N), V^{\otimes m})$, we also need transition operators which are operators that map between the equivalent irreducible representations of $\mathrm{SU}(N)$ over $V^{\otimes m}$. All Young tableaux that have the same underlying Young diagrams correspond to equivalent representations of $\mathrm{SU}(N)$ over $V^{\otimes m}$. Therefore, it is oftentimes convenient to label HYPOs by the Young tableau which is in correspondence to the irreducible representation which the HYPO projects onto and the transition operators by the two Young tableaux between which the transition operator "transitions" between equivalent irreducible representations which is how this is done in Figure 3.1. Figure 3.1 lists all the HYPOs and their corresponding transition operators up to $m = 4$.

Let us have a closer look at the properties of the HYPOs and transition operators. For $m = 3$, notice that some of the transition operators between the irreducible representations are not shown. For example, $T_{\begin{smallmatrix}1&2\\3\end{smallmatrix}\,\begin{smallmatrix}1&3\\2\end{smallmatrix}}$ is shown but not $T_{\begin{smallmatrix}1&3\\2\end{smallmatrix}\,\begin{smallmatrix}1&2\\3\end{smallmatrix}}$. The reason is that knowing a transition operator between two irreducible representations allows one to obtain the reverse transition operator by taking the Hermitian conjugate of the original operator [24]. So in the case of $T_{\begin{smallmatrix}1&2\\3\end{smallmatrix}\,\begin{smallmatrix}1&3\\2\end{smallmatrix}}$, we have that:

$$T_{\begin{smallmatrix}1&3\\2\end{smallmatrix}\,\begin{smallmatrix}1&2\\3\end{smallmatrix}} = \left(T_{\begin{smallmatrix}1&2\\3\end{smallmatrix}\,\begin{smallmatrix}1&3\\2\end{smallmatrix}}\right)^{\dagger}. \tag{3.69}$$

Transition operators between irreducible representations that are *not* equivalent are not shown because they are always zero [24]. All HYPOs and transition operators corresponding to the same Young diagram form a closed subalgebra, orthogonal to others. This can be verified easily from the birdtrack diagrams for $m = 3, 4$ in Figure 3.1 and it holds in-general [24].

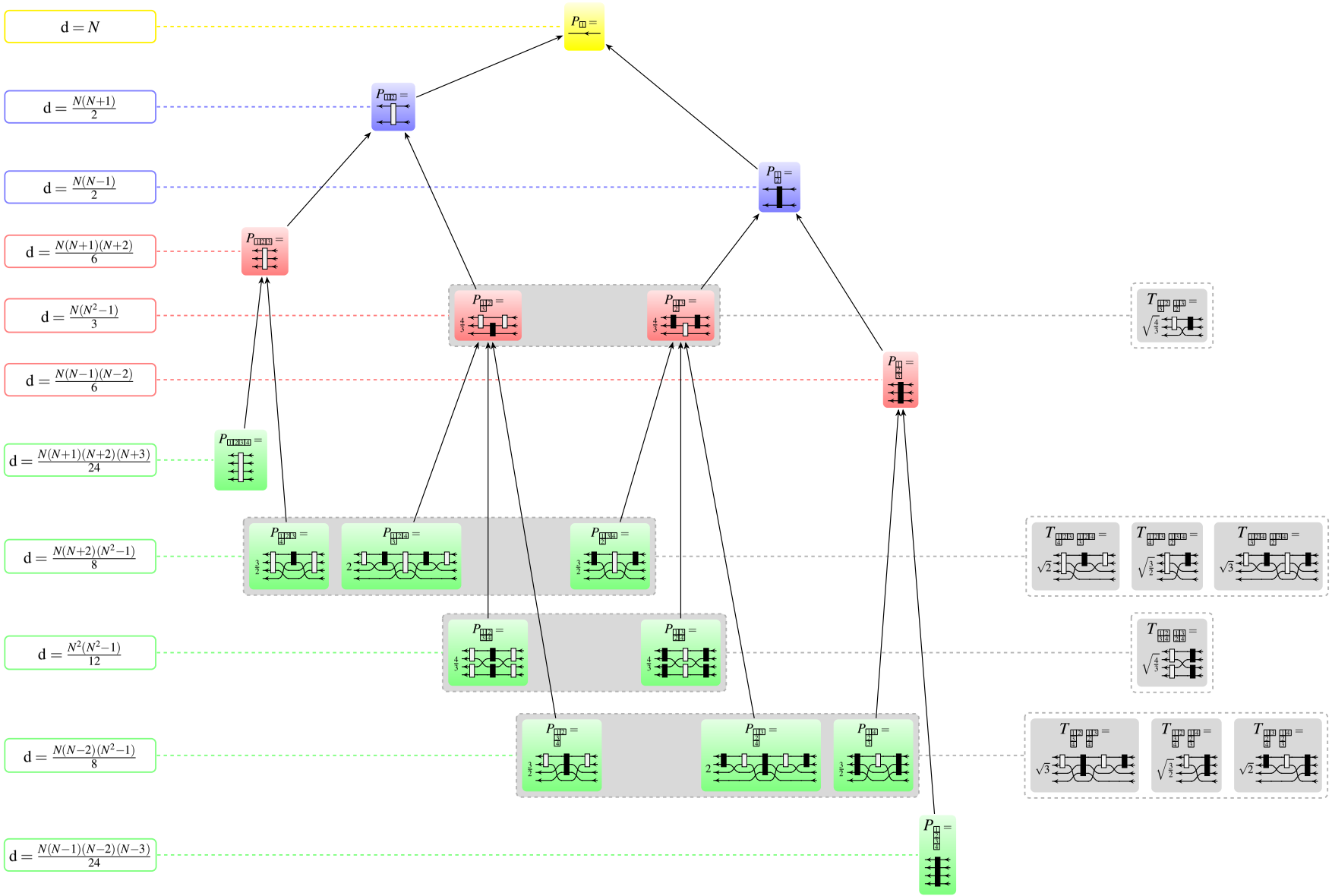

FIGURE 3.1: The complete set of Hermitian Young Projection Operators (HYPOs) and their corresponding transition operators over $V^{\otimes m}$ for $m = 1, 2, 3, 4$, along with the dimensions of the irreducible representations the HYPOs project onto. Arrows indicate the hierarchy derived from the Young tableaux, as discussed in [23, 24]. The HYPOs and transition operators are labelled by the Young tableau corresponding to the irreducible representation they project onto and transition operators between and whilst this notation is convenient, for our purposes we will find it more prudent to use the notation defined in Eq. 3.70. This figure is reproduced from [24].

For this thesis, we will exploit these properties and label the basis of HYPOs and their transition operators by

$$T_{\Theta ij}, \tag{3.70}$$

for a specific m. The operator $T_{\Theta ij}$ transitions from the irreducible representation projected out by the HYPO corresponding to the Young tableau j to that for i in case of $i \neq j$. It acts as the HYPO corresponding to the Young tableau i for $i = j$. The term Θ represents the Young diagram for the tableaux i and j. If the Young tableaux i and j differ in shape, then Θ is not defined and thus, no such operator exists and in those cases we define

$$T_{\Theta ij} = 0.$$

As an example, consider the transition operator expressed in-terms of Young tableaux from Figure 3.1:

$$T_{\begin{array}{|c|c|}\hline 1&2\\\hline 3\\\cline{1-1}\end{array}\ \begin{array}{|c|c|}\hline 1&3\\\hline 2\\\cline{1-1}\end{array}}\ .$$

In our notation, for transition operators $T_{\Theta ij}$, Θ will refer to the Young diagram $\begin{array}{|c|c|}\hline \ &\ \\\hline \ \\\cline{1-1}\end{array}$, i will refer to the Young tableau $\begin{array}{|c|c|}\hline 1&2\\\hline 3\\\cline{1-1}\end{array}$ and j will refer to the Young tableau, $\begin{array}{|c|c|}\hline 1&3\\\hline 2\\\cline{1-1}\end{array}$:

$$T_{\Theta ij} = \overbrace{T_{\underbrace{\begin{array}{|c|c|}\hline 1&2\\\hline 3\\\cline{1-1}\end{array}}_{i}\ \underbrace{\begin{array}{|c|c|}\hline 1&3\\\hline 2\\\cline{1-1}\end{array}}_{j}}}^{\begin{array}{|c|c|}\hline \ &\ \\\hline \ \\\cline{1-1}\end{array}\ \rightarrow \Theta} = T_{\begin{array}{|c|c|}\hline \ &\ \\\hline \ \\\cline{1-1}\end{array}\ \begin{array}{|c|c|}\hline 1&2\\\hline 3\\\cline{1-1}\end{array}\ \begin{array}{|c|c|}\hline 1&3\\\hline 2\\\cline{1-1}\end{array}}\ . \tag{3.71}$$

As another example, consider the projection operator,

$$P_{\begin{array}{|c|c|}\hline 1&2\\\hline 3\\\cline{1-1}\end{array}}\ .$$

It is implicitly implied here that

$$P_{\begin{array}{|c|c|}\hline 1&2\\\hline 3\\\cline{1-1}\end{array}} = T_{\begin{array}{|c|c|}\hline 1&2\\\hline 3\\\cline{1-1}\end{array}\ \begin{array}{|c|c|}\hline 1&2\\\hline 3\\\cline{1-1}\end{array}}\ .$$

Therefore, in our notation for $T_{\Theta ij}$, $i = j$ which will both refer to the Young tableau $\begin{array}{|c|c|}\hline 1&2\\\hline 3\\\cline{1-1}\end{array}$ and Θ will refer to the Young diagram $\begin{array}{|c|c|}\hline \ &\ \\\hline \ \\\cline{1-1}\end{array}$:

$$T_{\Theta ij} = \overbrace{P_{\underbrace{\begin{array}{|c|c|}\hline 1&2\\\hline 3\\\cline{1-1}\end{array}}_{i=j}}}^{\begin{array}{|c|c|}\hline \ &\ \\\hline \ \\\cline{1-1}\end{array}\ \rightarrow \Theta} = T_{\Theta ii} = T_{\begin{array}{|c|c|}\hline \ &\ \\\hline \ \\\cline{1-1}\end{array}\ \begin{array}{|c|c|}\hline 1&2\\\hline 3\\\cline{1-1}\end{array}\ \begin{array}{|c|c|}\hline 1&2\\\hline 3\\\cline{1-1}\end{array}}\ . \tag{3.72}$$

Finally, if we have a transition operator between two Young tableuax of different shapes, for example:

$$T_{\begin{array}{|c|c|c|c|c|}\hline 1&2&3&1&3\\\hline\end{array}\atop\begin{array}{|c|}\hline 2\\\hline\end{array}}\,.$$

Then $T_{\Theta ij} = 0$ as $T_{\begin{array}{|c|c|c|c|c|}\hline 1&2&3&1&3\\\hline\end{array}\atop\begin{array}{|c|}\hline 2\\\hline\end{array}} = 0$.

This notation becomes cluttered when a specific $T_{\Theta ij}$ requires a Young diagram and two tableaux as subscripts for the Θ, i and j indices. To simplify, we assign arbitrary numerical values to the Young diagrams and tableaux, which slightly diminishes the immediate physical interpretation of a specific $T_{\Theta ij}$. However, this reduces expression size, which is the aim of this thesis. The choice to use numerical values or the original Young diagrams and tableaux is left to individual discretion. We provide a list mapping Young tableaux and diagrams to numerical values, included here and in Appendix A, as well as wherever we feel worth repeating to assist readers in following our calculations. The numerical assignment is as follows:

For Young diagrams with 2 boxes:

- $\begin{array}{|c|c|}\hline\ &\ \\\hline\end{array} \to 1$
  - $\begin{array}{|c|c|}\hline 1&2\\\hline\end{array} \to 1$
- $\begin{array}{|c|}\hline\ \\\hline\ \\\hline\end{array} \to 2$
  - $\begin{array}{|c|}\hline 1\\\hline 2\\\hline\end{array} \to 2$

The two projection operators associated with these two Young tableaux will therefore be (in our notation):

$$P_{\begin{array}{|c|c|}\hline 1&2\\\hline\end{array}} = T_{111} \tag{3.73a}$$

$$P_{\begin{array}{|c|}\hline 1\\\hline 2\\\hline\end{array}} = T_{222} \tag{3.73b}$$

For Young diagrams with 3 boxes:

- $\begin{array}{|c|c|c|}\hline\ &\ &\ \\\hline\end{array} \to 1$
  - $\begin{array}{|c|c|c|}\hline 1&2&3\\\hline\end{array} \to 1$
- $\begin{array}{|c|c|}\hline\ &\ \\\hline\ \\\cline{1-1}\end{array} \to 2$
  - $\begin{array}{|c|c|}\hline 1&3\\\hline 2\\\cline{1-1}\end{array} \to 1$

  - $\begin{array}{|c|c|}\hline 1 & 2 \\ \hline 3 \\ \cline{1-1}\end{array} \rightarrow 2$

- $\begin{array}{|c|}\hline \\ \hline \\ \hline \\ \cline{1-1}\end{array} \rightarrow 3$

  - $\begin{array}{|c|}\hline 1 \\ \hline 2 \\ \hline 3 \\ \cline{1-1}\end{array} \rightarrow 1$

Consider the following two examples which may add clarity:

$$T_{\begin{array}{|c|c|}\hline 1 & 2 \\ \hline 3 \\ \cline{1-1}\end{array}\ \begin{array}{|c|c|}\hline 1 & 3 \\ \hline 2 \\ \cline{1-1}\end{array}} = T_{212} \tag{3.74a}$$

$$P_{\begin{array}{|c|c|}\hline 1 & 2 \\ \hline 3 \\ \cline{1-1}\end{array}} = T_{211} \tag{3.74b}$$

For Young diagrams with 4 boxes:

- $\begin{array}{|c|c|c|c|}\hline \\ \hline\end{array} \rightarrow 1$

  - $\begin{array}{|c|c|c|c|}\hline 1 & 2 & 3 & 4 \\ \hline\end{array} \rightarrow 1$

- $\begin{array}{|c|c|c|}\hline \\ \hline \\ \cline{1-1}\end{array} \rightarrow 2$

  - $\begin{array}{|c|c|c|}\hline 1 & 3 & 4 \\ \hline 2 \\ \cline{1-1}\end{array} \rightarrow 3$
  - $\begin{array}{|c|c|c|}\hline 1 & 2 & 4 \\ \hline 3 \\ \cline{1-1}\end{array} \rightarrow 2$
  - $\begin{array}{|c|c|c|}\hline 1 & 2 & 3 \\ \hline 4 \\ \cline{1-1}\end{array} \rightarrow 1$

- $\begin{array}{|c|c|}\hline \\ \hline \\ \hline\end{array} \rightarrow 3$

  - $\begin{array}{|c|c|}\hline 1 & 3 \\ \hline 2 & 4 \\ \hline\end{array} \rightarrow 2$
  - $\begin{array}{|c|c|}\hline 1 & 2 \\ \hline 3 & 4 \\ \hline\end{array} \rightarrow 1$

- $\begin{array}{|c|c|}\hline \\ \hline \\ \hline \\ \cline{1-1}\end{array} \rightarrow 4$

  - $\begin{array}{|c|c|}\hline 1 & 4 \\ \hline 2 \\ \hline 3 \\ \cline{1-1}\end{array} \rightarrow 3$
  - $\begin{array}{|c|c|}\hline 1 & 3 \\ \hline 2 \\ \hline 4 \\ \cline{1-1}\end{array} \rightarrow 2$
  - $\begin{array}{|c|c|}\hline 1 & 2 \\ \hline 3 \\ \hline 4 \\ \cline{1-1}\end{array} \rightarrow 1$

- $\begin{array}{|c|}\hline\ \\\hline\ \\\hline\ \\\hline\ \\\hline\end{array} \to 5$

  - $\begin{array}{|c|}\hline 1\\\hline 2\\\hline 3\\\hline 4\\\hline\end{array} \to 1$

Consider the following two examples which may add clarity:

$$T_{\begin{array}{|c|c|}\hline 1&2\\\hline 3&4\\\hline\end{array}\begin{array}{|c|c|}\hline 1&3\\\hline 2&4\\\hline\end{array}} = T_{321} \tag{3.75a}$$

$$P_{\begin{array}{|c|}\hline 1\\\hline 2\\\hline 3\\\hline 4\\\hline\end{array}} = T_{511} \tag{3.75b}$$

Our notation easily highlights the relation regarding the Hermitian conjugate of the transition operators and HYPOs in one line [26]:

$$\boxed{(T_{\Theta ij})^\dagger = T_{\Theta ji}}. \tag{3.76}$$

The key advantage of this notation for HYPOs and transition operators is the straightforward expression of their multiplication table:

$$T_{\Theta ij} \cdot T_{\Phi lm} = \delta_{\Theta\Phi}\delta_{jl}T_{\Theta im}. \tag{3.77}$$

The multiplication table in Eq. 3.77 unveils the subalgebra structure which we have mentioned: HYPOs and transition operators linked to the same Young diagram form distinct subalgebras, orthogonal to those tied to different diagrams. Our notation groups all $T_{\Theta ij}$ with the same Θ (Young diagram), as the Θ index pertains to a specific subalgebra. This efficiently highlights that all HYPOs and transition operators sharing a Young diagram are easily grouped. See Appendix D in Eq. D.10 for illustration.

The drawback of this notation is the need for specific values for Θ, i, and j to refer to a HYPO or transition operator. In this thesis, we use numerical values for Θ, i, and j, with Appendix A providing the relevant values of Θij used. This approach minimizes clutter and streamlines calculations. We shall make use of this multiplication table extensively in the coming sections. Hermitian Young Projection Operators and transition operators thus form a complete orthogonal basis for $\mathrm{API}\left(\mathrm{SU}(N), V^{\otimes m}\right)$ and we shall refer to the set of all HYPOs and transition operators for a specific m in $\mathrm{API}\left(\mathrm{SU}(N), V^{\otimes m}\right)$ as $\mathfrak{G}_m$.

The singlet states corresponding to the $\mathfrak{G}_3$ basis is given by

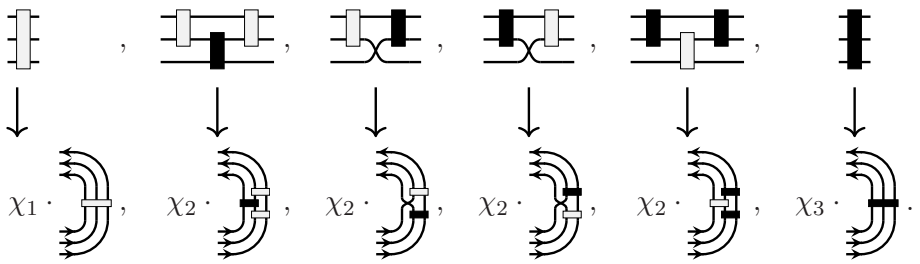

(3.78a)

(3.78b)

The normalization constants χ_i are given by

$$\chi_1 = \frac{6}{(N+2)(N+1)N}\,, \quad \chi_2 = \frac{3\cdot\theta_{N>1}}{N(N^2-1)} \quad \text{and} \quad \chi_3 = \frac{6\cdot\theta_{N>2}}{(N-2)(N-1)N}\,, \tag{3.79}$$

where the function $\theta_{N>p}$ is defined as

$$\theta_{N>p} := \begin{cases} 1 & \text{if } N > p \\ 0 & \text{if } N \leq p \end{cases}, \quad p \in \mathbb{N} \tag{3.80}$$

tells us which of the singlet states are dimensionally zero for specific values of N and the χ_i are the relevant normalisation factors. For SU(3), none of the 6 states are dimensionally zero and all of them will contribute.

Using the singlet states in Eq. 3.78b, we get the following correlator matrix:

$$\mathcal{A}(Y) = \left(\right.$$

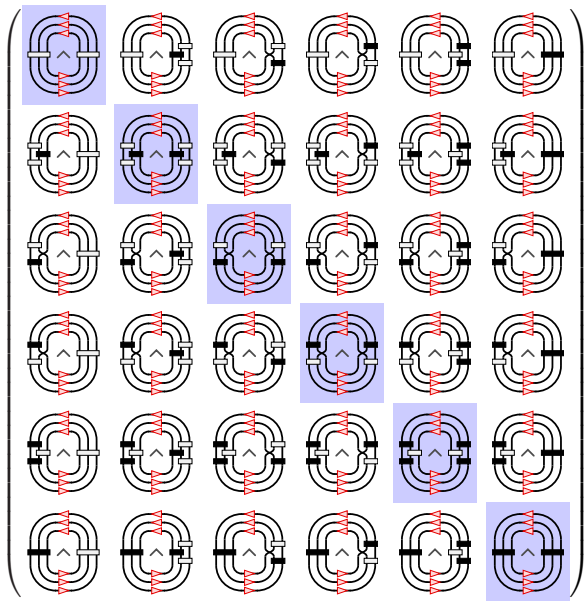

$$\left.\right)(Y)\ . \tag{3.81}$$

where the scheme for assigning indices (1,2,3) to $\boldsymbol{x}$- and $\mathbf{y}$- is increasing from top to bottom for the $\boldsymbol{x}$-coordinates, i.e. Wilson lines in the fundamental representation and decreasing from top to bottom for the $\boldsymbol{y}$-coordinates, i.e. Wilson lines in the anti-fundamental representation.

The hat symbol in the correlator matrix denotes that the states are properly normalized, simplifying the notation. Taking a coincidence limit between the top two Wilson lines and then the bottom two Wilson lines yields the following simplification:

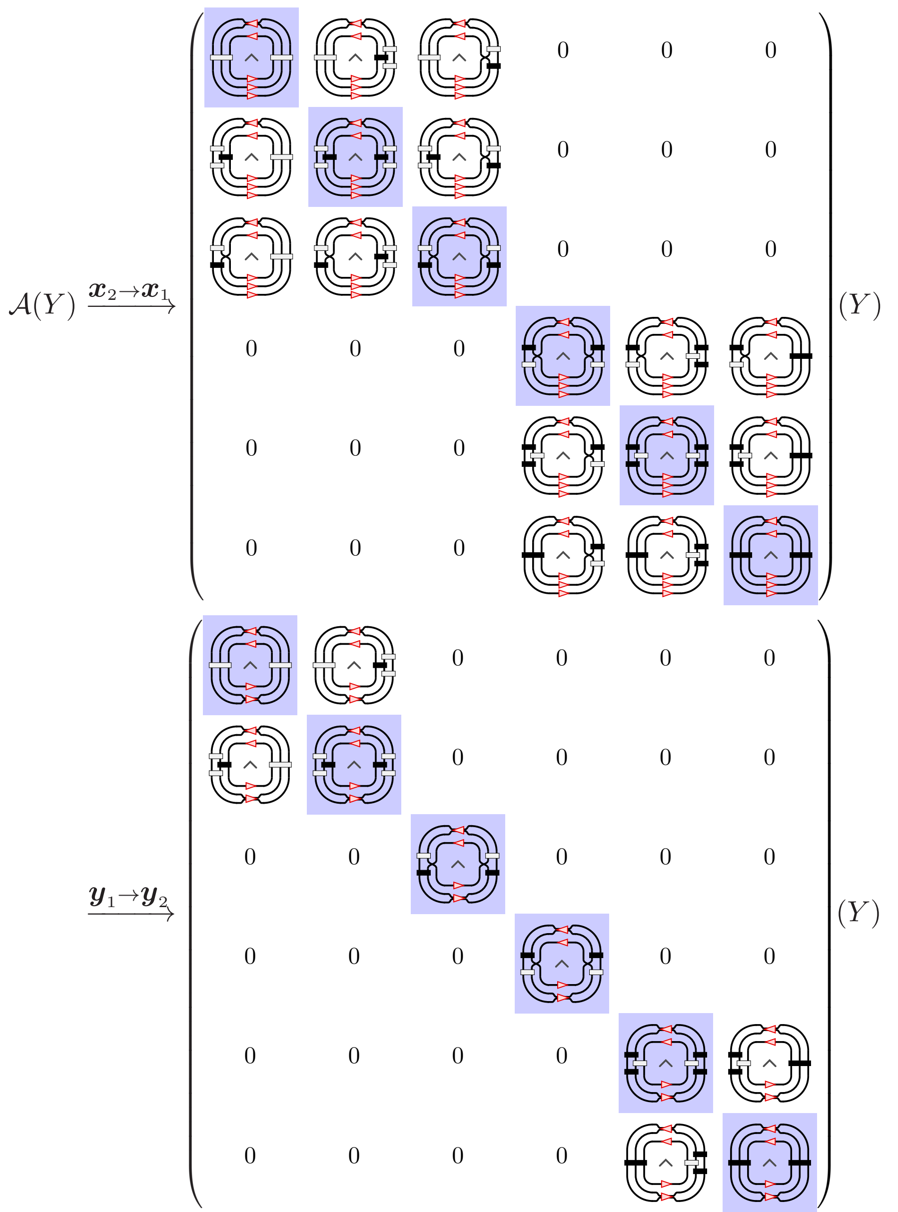

(3.82)

Again, taking (anti)-quark/(anti)-quark coincidence limits in the basis from $\mathfrak{G}_3$ simplifies the Wilson line correlator matrices, making them block-diagonal. This happens because symmetrisers multiply with anti-symmetrisers for some matrix elements, resulting in 0 via Eq. 3.30.

Taking quark/anti-quark coincidence limits

Constructing the Fierz basis for singlet states that is suited for quark/anti-quark coincidence limits is unfortunately not as straightforward as constructing a basis suited for (anti)-quark/(anti)-quark coincidence limits. One cannot simply "bend" adjoint and singlet projectors as was done in Eq. 3.64. An algorithm for constructing the Fierz basis exists up to $m = 3$, which is sufficient for our case, despite its dependence on N_c and insensitivity to dimensional zeros. However, it will suffice to build our Wilson line correlator matrix suited for quark/(anti)-quark coincidence limits.

The Fierz basis is constructed from the trace basis for $A^{\otimes m}$ by multiplying each element by $\sqrt{2^m}|t^{a_1}\rangle \otimes \cdots \otimes |t^{a_m}\rangle$ [33]. This basis simplifies the Wilson line correlator matrix quark/anti-quark coincidence limits, making the adjoint representation, corresponding to gluons, more manifest. Details of constructing the Fierz basis can be found in [33, 50].

In order to construct the Fierz basis however, we first need the trace basis which is another basis for the space of singlet states of $V^{\otimes m} \otimes (V^*)^{\otimes m}$. The trace basis is not immediately orthogonal and one obtains the Fierz basis from the trace basis by orthogonalizing in a suitable way (see [33] for more details on this). We need an algorithm to construct and orthogonalize the trace basis in the case of $m = 3$, which will suffice for our aims.

The following description of the algorithm for constructing the trace basis is reproduced verbatim from [50].

Trace basis algorithm:

1. Write any $\rho \in S_m$ in its disjoint cycle form, and also explicitly display the conventionally omitted 1-cycles:
$$\rho = \sigma_k \sigma_{k-1} \dots \sigma_1 \ ; \tag{3.83}$$

2. Replace every cycle σ (in the permutation ρ) of length > 1 containing elements i_j, with the trace
$$\mathrm{tr}\left(t^{a_{i_{\sigma(1)}}} t^{a_{i_{\sigma(2)}}} \dots t^{a_{i_{\sigma(|\sigma|)}}}\right) \ , \tag{3.84a}$$
and multiply this trace with the tensor product
$$[t^{a_{i_1}}]_{\bar{q}_{i_1} q_{i_1}} \otimes [t^{a_{i_2}}]_{\bar{q}_{i_2} q_{i_2}} \otimes \cdots \otimes [t^{a_{i_{|\sigma|}}}]_{\bar{q}_{i_{|\sigma|}} q_{i_{|\sigma|}}} \ . \tag{3.84b}$$
using a summation convention for all repeated indices a_k.

3. Replace every 1-cycle (j), with the Kronecker δ $\delta_{\bar{q}_j q_j}$.

The resulting object is a singlet state $|i\rangle \in V^{\otimes m} \otimes (V^*)^{\otimes m}$, presented in index notation. The $q_1, \dots q_m$ refer to the V factors, the $\overline{q}_1, \dots \overline{q}_m$ refer to the V^* factors in $V^{\otimes m} \otimes (V^*)^{\otimes m}$. The procedure creates a unique state for each permutation $\rho \in S_m$, since the disjoint cycle decomposition of ρ is unique and therefore produces a basis for the space of singlet states in $V^{\otimes m} \otimes (V^*)^{\otimes m}$.

The trace basis also lends itself easily to depiction via birdtracks.

Now we construct the Wilson line correlator matrix using the Fierz basis. The trace basis algorithm for $m = 3$ yields:

$$\mathrm{id} = (1)(2)(3) \longrightarrow \delta_{\overline{q}_1 q_1} \otimes \delta_{\overline{q}_2 q_2} \otimes \delta_{\overline{q}_3 q_3} = \tag{3.85a}$$

$$(12)(3) \longrightarrow \mathrm{tr}\,(t^{a_1} t^{a_2})\, [t^{a_1}]_{\overline{q}_1 q_1} \otimes [t^{a_2}]_{\overline{q}_2 q_2} \otimes \delta_{\overline{q}_3 q_3} = \tag{3.85b}$$

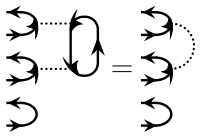

$$(13)(2) \longrightarrow \mathrm{tr}\,(t^{a_1} t^{a_3})\, [t^{a_1}]_{\overline{q}_1 q_1} \otimes \delta_{\overline{q}_2 q_2} \otimes [t^{a_3}]_{\overline{q}_3 q_3} = \tag{3.85c}$$

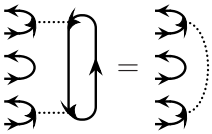

$$(23)(1) \longrightarrow \mathrm{tr}\,(t^{a_2} t^{a_3})\, \delta_{\overline{q}_1 q_1} \otimes [t^{a_2}]_{\overline{q}_2 q_2} \otimes [t^{a_3}]_{\overline{q}_3 q_3} = \tag{3.85d}$$

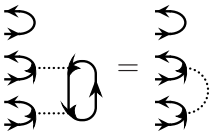

$$(123) \longrightarrow \mathrm{tr}\,(t^{a_1} t^{a_2} t^{a_3})\, [t^{a_1}]_{\overline{q}_1 q_1} \otimes [t^{a_2}]_{\overline{q}_2 q_2} \otimes [t^{a_3}]_{\overline{q}_3 q_3} = \tag{3.85e}$$

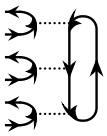

$$(132) \longrightarrow \mathrm{tr}\,(t^{a_1} t^{a_3} t^{a_2})\, [t^{a_1}]_{\overline{q}_1 q_1} \otimes [t^{a_2}]_{\overline{q}_2 q_2} \otimes [t^{a_3}]_{\overline{q}_3 q_3} = . \tag{3.85f}$$

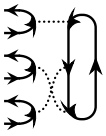

One can check that the states in Eqs. 3.85e and 3.85f are not orthogonal to each other. However, we can still orthogonalise this basis fairly easily by forming the symmetric and anti-symmetric linear combinations

$$:= \frac{1}{2} \left(+ \right) \quad \text{and} \quad := \frac{1}{2} \left(- \right) , \tag{3.86}$$

where we follow the notation in [44] where a black dot represents the antisymmetric structure, constant of the Lie algebra of SU(N), f^{abc},

$$f^{abc} := \frac{2}{i}\,\mathrm{tr}\left(\left[t^a, t^b\right] t^c\right) = \quad , \tag{3.87}$$

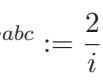

and an open dot represents the symmetric structure constant, d^{abc}, of the Lie algebra of SU(N)

$$d^{abc} := 2\,\mathrm{tr}\left(\left\{t^a, t^b\right\} t^c\right) = \quad . \tag{3.88}$$

Orthogonalizing the basis in this way is useful due to the fact that the basis we have now constructed is sensitive to dimensional zeroes as the symmetric structure constant d^{abc} vanishes for $N < 3$ whilst the anti-symmetric structure constant is non-zero for all $N > 1$. The singlet states in the Fierz basis for $m = 3$ is therefore given by:

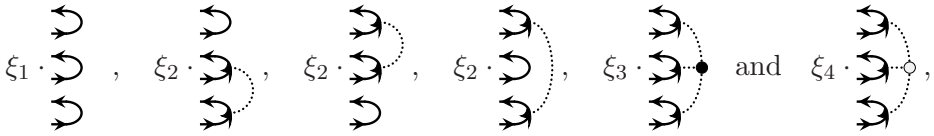

(3.89a)

with normalization constants ξ_i given by

$$\xi_1 = \frac{1}{\sqrt{N^3}}\,, \quad \xi_2 = \frac{\theta_{N>1}}{\sqrt{N(N^2-1)}}\,, \quad \xi_3 = \frac{\theta_{N>1}}{\sqrt{2N(N^2-1)}} \text{ and } \xi_4 = \sqrt{\frac{\theta_{N>2}\cdot N}{2(N^2-4)(N^2-1)}}. \tag{3.89b}$$

The correlator matrix in this basis will then be:

$$\mathcal{A}(Y) = \begin{pmatrix} A^{(3)}_{11}\cdot & A^{(3)}_{12}\cdot & A^{(3)}_{13}\cdot & A^{(3)}_{14}\cdot & A^{(3)}_{15}\cdot & A^{(3)}_{16}\cdot \\ A^{(3)}_{21}\cdot & A^{(3)}_{22}\cdot & A^{(3)}_{23}\cdot & A^{(3)}_{24}\cdot & A^{(3)}_{25}\cdot & A^{(3)}_{26}\cdot \\ A^{(3)}_{31}\cdot & A^{(3)}_{32}\cdot & A^{(3)}_{33}\cdot & A^{(3)}_{34}\cdot & A^{(3)}_{35}\cdot & A^{(3)}_{36}\cdot \\ A^{(3)}_{41}\cdot & A^{(3)}_{42}\cdot & A^{(3)}_{43}\cdot & A^{(3)}_{44}\cdot & A^{(3)}_{45}\cdot & A^{(3)}_{46}\cdot \\ A^{(3)}_{51}\cdot & A^{(3)}_{52}\cdot & A^{(3)}_{53}\cdot & A^{(3)}_{54}\cdot & A^{(3)}_{55}\cdot & A^{(3)}_{56}\cdot \\ A^{(3)}_{61}\cdot & A^{(3)}_{62}\cdot & A^{(3)}_{63}\cdot & A^{(3)}_{64}\cdot & A^{(3)}_{65}\cdot & A^{(3)}_{66}\cdot \end{pmatrix} (Y)\,, \tag{3.90}$$

where $A^{(3)}_{ij}$ are the appropriate normalisation factors. The scheme for assigning indices (1,2,3) to the $\boldsymbol{x}$- and $\boldsymbol{y}$-coordinates here is increasing from top to bottom for both the $\boldsymbol{x}$- and $\boldsymbol{y}$-coordinates. Taking two quark/anti-quark coincidence limits gives the following simplification:

$$\mathcal{A}(Y) \xrightarrow{\boldsymbol{x}_1\to\boldsymbol{y}_1} \begin{pmatrix} A^{(3)}_{11}\cdot & A^{(3)}_{12}\cdot & 0 & 0 & 0 & 0 \\ A^{(3)}_{21}\cdot & A^{(3)}_{22}\cdot & 0 & 0 & 0 & 0 \\ 0 & 0 & A^{(3)}_{33}\cdot & A^{(3)}_{34}\cdot & A^{(3)}_{35}\cdot & A^{(3)}_{36}\cdot \\ 0 & 0 & A^{(3)}_{43}\cdot & A^{(3)}_{44}\cdot & A^{(3)}_{45}\cdot & A^{(3)}_{46}\cdot \\ 0 & 0 & A^{(3)}_{53}\cdot & A^{(3)}_{54}\cdot & A^{(3)}_{55}\cdot & A^{(3)}_{56}\cdot \\ 0 & 0 & A^{(3)}_{63}\cdot & A^{(3)}_{64}\cdot & A^{(3)}_{65}\cdot & A^{(3)}_{66}\cdot \end{pmatrix} (Y)$$

$$\xrightarrow{\boldsymbol{x}_2 \to \boldsymbol{y}_2} \begin{pmatrix} A^{(3)}_{11} \cdot & 0 & 0 & 0 & 0 & 0 \\ 0 & A^{(3)}_{22} \cdot & 0 & 0 & 0 & 0 \\ 0 & 0 & A^{(3)}_{33} \cdot & 0 & 0 & 0 \\ 0 & 0 & 0 & A^{(3)}_{44} \cdot & A^{(3)}_{45} \cdot & A^{(3)}_{46} \cdot \\ 0 & 0 & 0 & A^{(3)}_{54} \cdot & A^{(3)}_{55} \cdot & A^{(3)}_{56} \cdot \\ 0 & 0 & 0 & A^{(3)}_{64} \cdot & A^{(3)}_{65} \cdot & A^{(3)}_{66} \cdot \end{pmatrix} (Y) \,. \tag{3.91}$$

Thus, the $q^3\overline{q}^3$ correlator matrix block-diagonalizes with the first coincidence limit in Eq. 3.91, and further with the second. The upper left block after the first limit is the $q^2\overline{q}^2$ correlator matrix, while the bottom right block is the $q^2\overline{q}^2 g$ correlator matrix. This is purely analogous to what we saw happen in Eq. 3.68 where the $q\overline{q}$ and $q\overline{q}g$ correlator is embedded within a $q^2\overline{q}^2$ with respect to a coincidence limit. One can therefore make a guess that the lower 4-by-4 block in Eq. 3.91 (after the first coincidence limit has been taken) drives the JIMWLK evolution of the $q^2\overline{q}^2$ correlator matrix similar to how the $q\overline{q}g$ correlator drives the evolution of the $q\overline{q}$ correlator. Indeed, this is the case [17] and R. Moerman and H. Weigert showed in [33] that in-general, the JIMWLK evolution of the $q^m\overline{q}^m$ correlator is driven by the $q^m\overline{q}^m g$ correlator, creating an evolution hierarchy within the matrix of correlators. In other words, the JIMWLK equation couples the disjoint blocks of the $q^{m+1}\overline{q}^{m+1}$ correlator matrix constructed with the Fierz basis of singlet states after a quark/anti-quark coincidence limit has been taken [33]. We will elaborate more on this important result and how one can leverage it in the coming sections.

Taking a combination of (anti)-quark/(anti)-quark and quark/anti-quark coincidence limits

There is also another basis that we can construct that is suited for taking a *combination* of quark/anti-quark and (anti)-quark/(anti)-quark coincidence limits as opposed to just quark/anti-quark or (anti)-quark/(anti)-quark coincidence limits and we give a construction

of this basis and the corresponding Wilson line correlator matrix. To our knowledge, this basis is new and has not been found in the literature before. We find this basis by decomposing unity into three parts for

$$\mathbb{1}_{V^{\otimes 2}\otimes(V\otimes V^*)\otimes(V^*)^{\otimes 2}} =$$ 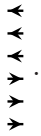 . (3.92)

- For the first two fundamental lines in Eq. 3.92, we have:

$$\mathbb{1}_{V^{\otimes 2}} =$$ 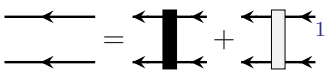 . (3.93)

- For the central fundamental and anti-fundamental lines in Eq. 3.92, we have:

$$\mathbb{1}_{V\otimes V^*} =$$ 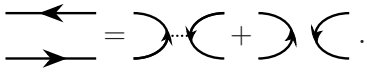 . (3.94)

- For the lower two anti-fundamental lines corresponding to $(V^*)^{\otimes 2}$, we have simply have Eq. 3.93 but with the arrows flipped around.

We then multiply out this decomposition of unity to obtain 8 projection operators which we then act on our 6 basis states in Eq. 3.78b with the hope that we will obtain a new basis that is suitable for taking the aforementioned coincidence limits. We have good reason to hope for such an outcome because we perform a decomposition of unity on a pair of fundamental and anti-fundamental lines. This may project onto a basis where taking a quark/anti-quark limit is made manifest. Additionally, a decomposition of unity on a pair of fundamental lines and a pair of anti-fundamental lines may make (anti)-quark/(anti)-quark coincidence limits manifest as well.

Thus, we get that:

$$\mathbb{1}_{V^{\otimes 2}\otimes(V\otimes V^*)\otimes(V^*)^{\otimes 2}} =$$ 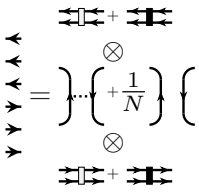

$$=$$ 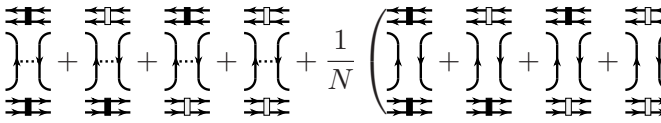 . (3.95)

[12] For the decomposition of unity for a pair of anti-fundamental lines, simply flip the direction of the arrows

And hence, our 8 projection operators which sum up to unity are:

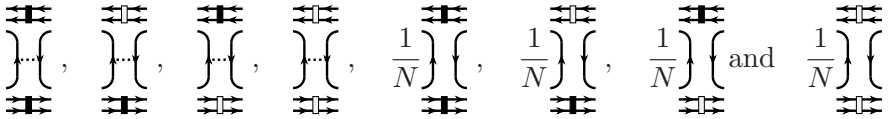

(3.96)

Applying the 8 projection operators to the 6 basis states in Eq. 3.78b might not give states that fully span the singlet space of $V^{\otimes 3} \otimes (V^*)^{\otimes 3}$. Even if they do, the resulting spanning set will have $(8 \times 6 =)42$ elements that will include linearly dependent elements that must be removed. This basis may not be orthogonal, necessitating the use of Gram-Schmidt orthogonalization, or the like to achieve an orthogonal basis. Nevertheless, let us proceed with acting these 8 projection operators on the basis states to see if we obtain an orthogonal basis from the outset.

Many results from applying these projection operators to the states will immediately be 0. One such instance of this is

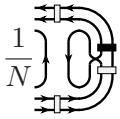

(3.97)

due to the presence of the anti-symmetriser in the middle of two symmetrisers over the same legs which gives 0 via Eq. 3.30. Thus, because of a symmetriser hitting an anti-symmetriser or vice versa over the same legs, we will get that most of the 42 states from the 8 projection operators acting on the 6 basis elements will be 0. In order to simplify the non-zero elements further, we make use of Eq. 3.94 (the Fierz identity) in order to simplify projection operators with the adjoint projector acting on one of the 6 states. As an example:

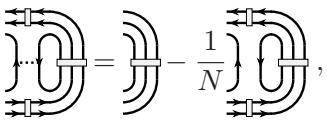

(3.98)

making use of Eq. 3.29 regarding symmetrisers to simplify to the first term on the LHS.

To simplify Eq. 3.98, we expand the contraction of a symmetriser leg in the second term on the RHS of Eq. 3.98 using primitive invariants, then compute the results. The result of this is[13]:

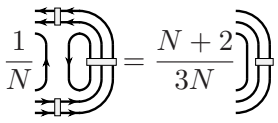

(3.99)

[13]This is an example of a more general case of contracting $p - k$ legs of a symmetriser or anti-symmetriser over k legs. See equations 6.12 and 6.23 of [44].

One can perform a similar calculation for the contraction of a leg of anti-symmetriser to obtain:

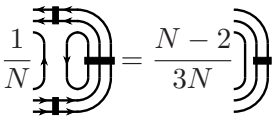

(3.100)

However, we shall retain the adjoint line for compactness and clearer physical interpretation in quark/anti-quark coincidence limits.

By simplifying the non-zero elements and removing those that are linearly dependent (which were simply scalar multiples of others), we, somewhat surprisingly, obtain 6 orthogonal states:

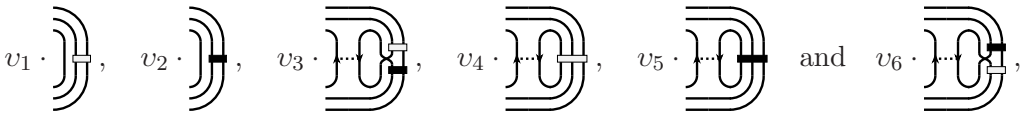

(3.101)

where the normalization constants are given by

$$\upsilon_1 = \frac{18}{(N+1)(N+2)^2}\ , \quad \upsilon_2 = \frac{18\cdot\theta_{N>1}}{(N-2)^2(N-1)}\ , \quad \upsilon_3 = \upsilon_6 = \frac{3\cdot\theta_{N>1}}{N(N^2-1)}\ ,$$
$$\upsilon_4 = \frac{9}{N^3+2N^2-N-2} \text{ and } \quad \upsilon_5 = \frac{9\cdot\theta_{N>2}}{N^3-2N^2-N+2}\ , \tag{3.102}$$

and where the function $\theta_{N>p}$ is defined as in Eq. 3.80. Note that for two of the basis elements in Eq. 3.101, we have that:

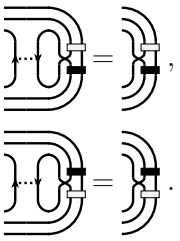

(3.103)

Again, we will choose to keep the adjoint line as this will prove to be more convenient when taking quark/anti-quark coincidence limits but one should always keep in-mind Eq. 3.103 when working with these basis states. Thus, we have found another basis for the space of singlet states of $V^{\otimes 3}\otimes(V^*)^{\otimes 3}$ which may be suitable for taking a combination of (anti)-quark/(anti)-quark and quark/anti-quark coincidence limits.

The correlator matrix in this basis will then be:

$$\mathcal{A}(Y) = \left(\right)(Y) \, .$$

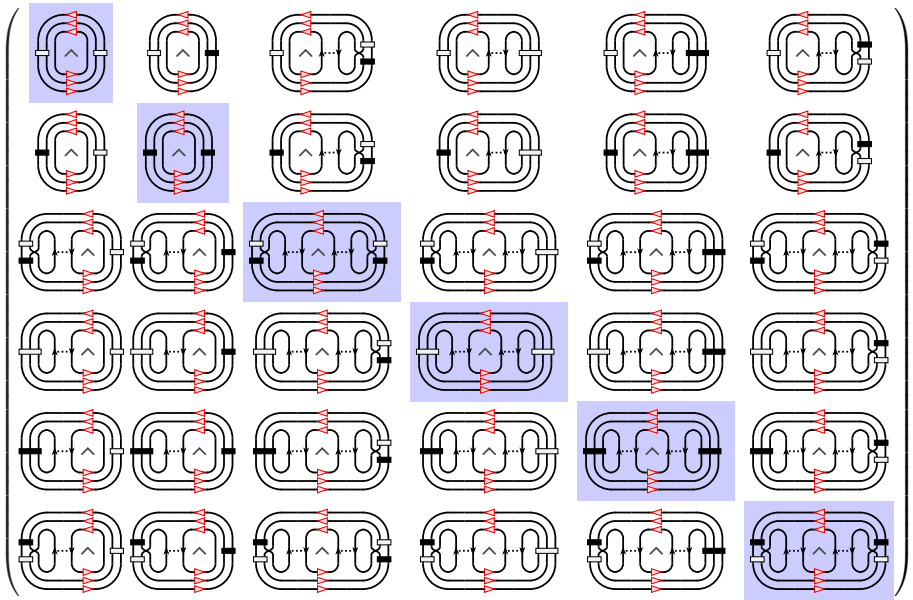

(3.104)

where we have followed the same scheme for index labelling of the $\boldsymbol{x}$- and $\boldsymbol{y}$-coordinates as Eq. 3.81. Taking a quark/anti-quark coincidence limit, then a quark/quark coincidence limit and finally an anti-quark/anti-quark coincidence limit gives the following simplifications:

$$\mathcal{A}(Y) \xrightarrow{\boldsymbol{x}_3 \to \boldsymbol{y}_3} \left(\right)(Y)$$

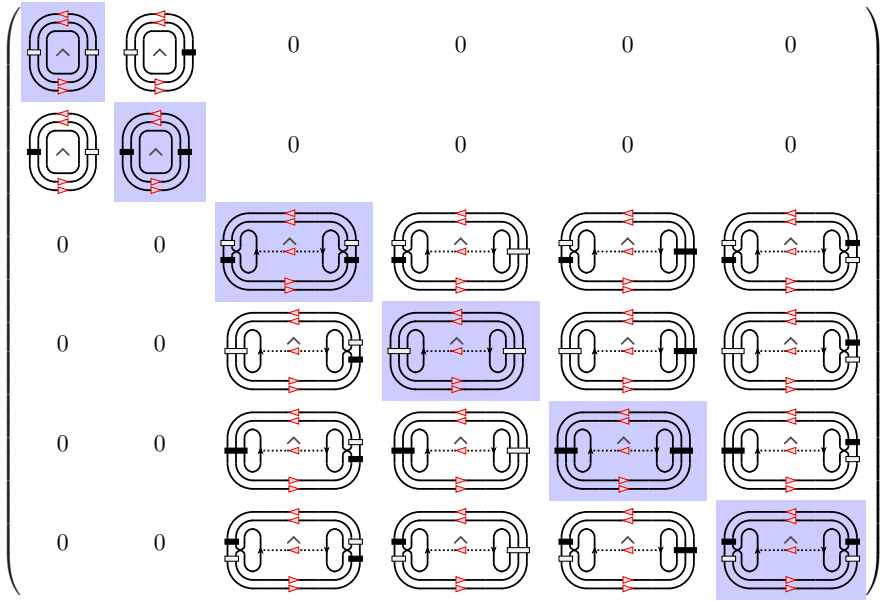

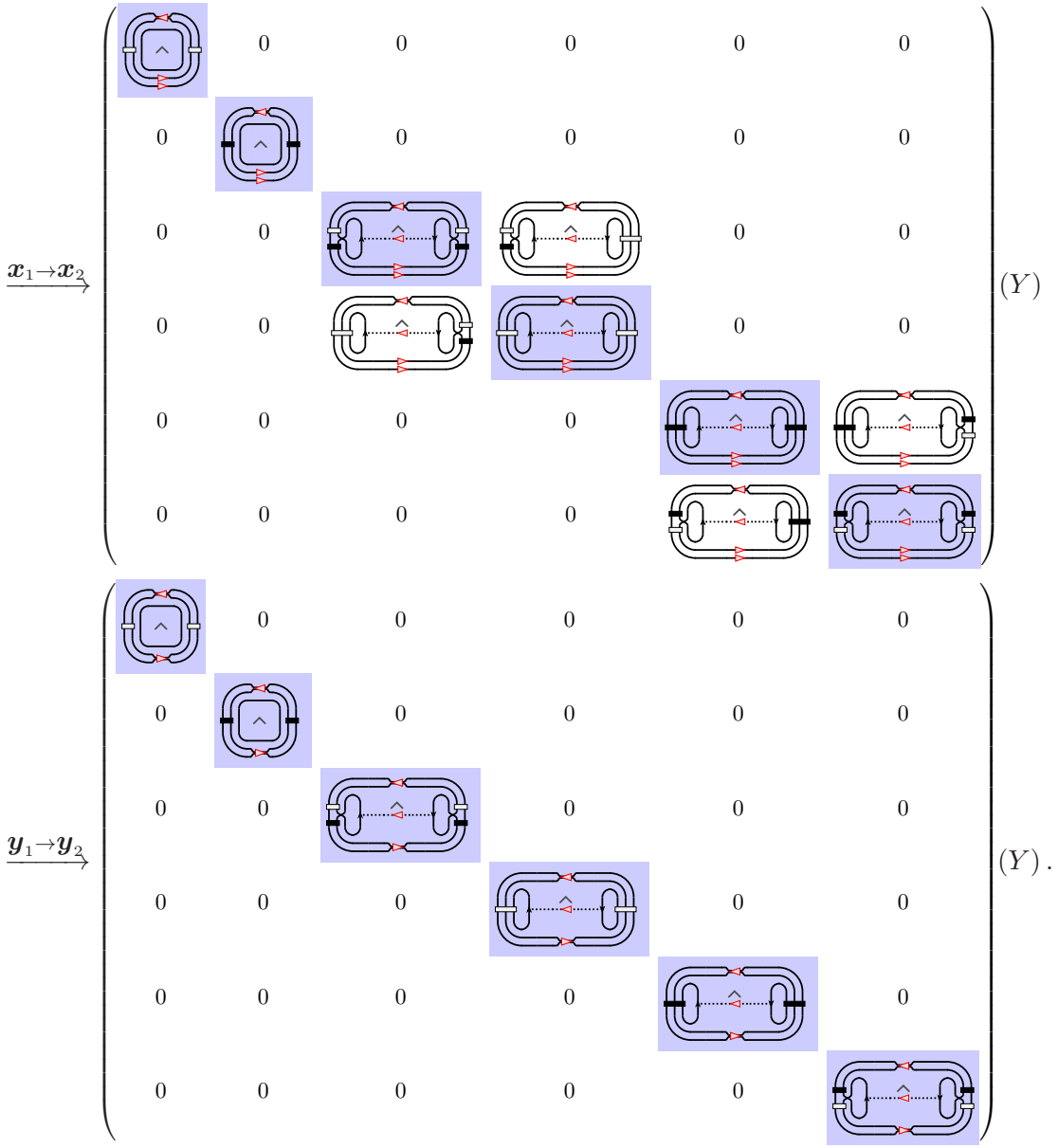

(3.105)

The $q^3\overline{q}^3$ correlator matrix block-diagonalizes in this basis by when taking *combined* quark/anti-quark and (anti)-quark coincide limits, demonstrating the usefulness of the basis in Eq. 3.101. In the final coincidence limit in Eq. 3.105, the $q^3\overline{q}^3$ correlator matrix becomes fully diagonal. This may simplify solving a differential equation for the $q^3\overline{q}^3$ correlator matrix in this basis, as diagonal matrices make this process much easier than non-block diagonal ones.

Notice from Eqs. 3.101 and 3.103 that two of the basis elements of this mixed Fierz/HYPO basis are the same as the basis elements corresponding to $\mathfrak{G}_3$. This means that if we were to take a quark/quark coincidence limit in Eq. 3.105 and reorder the basis elements to construct

our Wilson line correlator matrix as follows

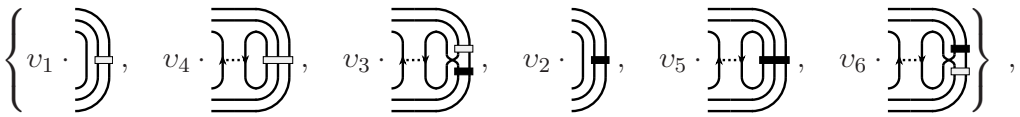

(3.106)

then our Wilson line correlator matrix would block diagonalise in a quark/quark coincidence limit with the same block diagonal structure as when a quark/quark coincidence limit was taken in Eq. 3.82.

Since the Fierz basis, the basis from $\mathfrak{G}_3$ and the mixed Fierz/(anti)-symmetrizer basis both form a basis for the colour singlet states of SU(N) over $V^{\otimes 3} \otimes (V^*)^{\otimes 3}$, they can be related by a change of basis. Thus, the correlator matrices in these bases are also related via a change of basis. These matrices, which we show in Appendix B, are straightforward to compute due to the orthogonality of these bases.

In conclusion, further coincidence limits in Eqs. 3.82, 3.91, and 3.105 could align more coordinates, simplifying the Wilson line correlator matrix even more [33] and emphasizing the value of adapted limit singlet state bases. However, detailing these is unnecessary for this thesis, so they are not illustrated.

Chapter 4

Gauge-Invariant, Symmetry Preserving Truncations of JIMWLK

4.1 A Novel Parameterization of JIMWLK

Since the JIMWLK equation leads to an infinite hierarchy of coupled integro-differential equations that cannot be solved exactly, there is a need for a more robust analytical approach to solving the JIMWLK evolution equation. As mentioned previously, R. Moerman and H. Weigert have devised a parameterization scheme [33] which has the following properties [33]:

- **Valid for any finite value of N_c.** Obtaining a parameterization for the JIMWLK evolution equation that holds for finite N_c is desirable as there are limitations to the large N_c limit [17, 38].
- **Keeping N_c as an explicit parameter.** This is so that one can compare with the large N_c limit at any time.
- **Independent evolution of the symmetric and anti-symmetric parts of any Wilson line correlator matrix.** The JIMWLK Hamiltonian acts component wise on the Wilson line correlator matrix in the JIMWLK evolution equation and hence evolves the symmetric and anti-symmetric parts of the matrix of correlators independently. Therefore, we want any parameterization of the JIMWLK equation to do the same and preserve the symmetry of JIMWLK evolution.
- **Obeys the coincidence limits of the Wilson line correlator matrix.** Chapter 3.2 shows that taking coincidence limits simplifies the Wilson line correlator matrix. A $q^m\overline{q}^m$ correlator matrix can embed into a higher dimensional $q^{m+1}\overline{q}^{m+1}$ correlator matrix, which includes the $q^m\overline{q}^m g$ correlator matrix and drives the $q^m\overline{q}^m$ correlator matrix's JIMWLK evolution, as demonstrated by R. Moerman and H. Weigert. Thus, it is reasonable to require that any valid parameterisation preserve these coincidence

limits since these coincidence limits carry important information about the JIMWLK evolution of correlators. Wilson line correlator simplification in coincidence limits arises from gauge-invariance [33]. Thus, it is in this sense, adhering to these coincidence limit properties, that our parameterisation must be gauge-invariant.

A full derivation of such a parameterisation can be found in [33]. We give a brief outline of the derivation here. The parameterisation equation takes the form [33, 37]:

$$\frac{d}{dY}\langle\mathcal{A}\rangle_Y = \frac{1}{2}\underbrace{\left(\frac{d}{dY}\langle\mathcal{A}\rangle\right)_Y\langle\mathcal{A}\rangle_Y^{-1}}_{:=-\mathcal{M}_Y}\langle\mathcal{A}\rangle_Y + \langle\mathcal{A}\rangle_Y\underbrace{\frac{1}{2}\langle\mathcal{A}\rangle_Y^{-1}\left(\frac{d}{dY}\langle\mathcal{A}\rangle\right)_Y}_{:=-\mathcal{M}_Y^T}$$

$$\implies \frac{d}{dY}\langle\mathcal{A}\rangle_Y = -\mathcal{M}_Y\langle\mathcal{A}\rangle_Y + \langle\mathcal{A}\rangle_Y\left(-\mathcal{M}_Y^T\right). \tag{4.1}$$

What we have simply done here is multiply $\frac{d}{dY}\langle\mathcal{A}\rangle_Y$ on both the left- and right-hand side with factors of $\mathbb{1} = \langle\mathcal{A}\rangle_Y^{-1}\langle\mathcal{A}\rangle_Y$ [1]. The parameterisation in Eq. 4.1 ensures that the symmetric and anti-symmetric parts of $\langle\mathcal{A}\rangle_Y$ evolve independently regardless of the structure of $\mathcal{M}_Y$. Equation 4.1 has an exponential solution

$$\langle\mathcal{A}\rangle_Y = \mathcal{P}\exp\left[-\int_{Y_0}^{Y} dY'\,\mathcal{M}(Y')\right]\langle\mathcal{A}\rangle_{Y_0}\left(\mathcal{P}\exp\left[-\int_{Y_0}^{Y} dY'\,\mathcal{M}(Y')\right]\right)^T, \tag{4.2}$$

, with,

$$\left(\mathcal{P}\exp\left[-\int_{Y_0}^{Y} dY'\,\mathcal{M}(Y')\right]\right)^T = \overline{\mathcal{P}}\exp\left[-\int_{Y_0}^{Y} dY'\,\mathcal{M}^T(Y')\right], \tag{4.3}$$

where $\overline{\mathcal{P}}$ is the anti-path ordering operator and $\langle\mathcal{A}\rangle_{Y_0}$ is a set of initial conditions of the Wilson line correlator matrix. Now we need an explicit expression for $\mathcal{M}_Y$.

Since we have essentially shifted the rapidity evolution of $\langle\mathcal{A}\rangle_Y$ onto $\mathcal{M}_Y$, we need to have the $\mathcal{M}_Y$ matrix obeys the coincidence limits of the Wilson line correlator matrix. We can define this $\mathcal{M}_Y$ matrix through the operators $\widehat{L}(Y)$ and $\widehat{R}(Y)$ such that it will satisfy the coincidence limits:

$$\langle\widehat{L}(Y)\,A\rangle_Y := \mathcal{M}_Y\langle A\rangle_Y, \tag{4.4}$$

$$\langle\widehat{R}(Y)\,A\rangle_Y := \langle A\rangle_Y\mathcal{M}_Y^t. \tag{4.5}$$

The only operators that are capable of extracting information of the Wilson line correlator matrix, $\mathcal{A}$, are the left- and right-invariant vector fields defined in Eq. 2.18. R. Moerman and

[1] We assume that $\langle\mathcal{A}\rangle_Y^{-1}$ exists because $\langle\mathcal{A}\rangle_Y^{-1}$ exists if none of $\langle\mathcal{A}\rangle_Y$'s eigenvalues are 0. If any of $\langle\mathcal{A}\rangle_Y$'s eigenvalues were 0, $\langle\mathcal{A}\rangle_Y^{-1}$ and thus $\mathcal{M}_Y$ would have infinite eigenvalues. However, $\mathcal{M}_Y$ can only have infinite eigenvalues if JIMWLK diverges, since $\mathcal{M}_Y$ parameterises JIMWLK. Although JIMWLK convergence for colour singlets is unresolved, we make the reasonable assumption it converges, so $\langle\mathcal{A}\rangle_Y^{-1}$ must exist.

H. Weigert showed in [33], that constructing the most general form of the operators in Eqs. 4.4 and 4.5 such that it satisfies coincidence limits takes the form of an infinite sum which involves the left- and right-invariant vector fields in Eqs. 2.18:

$$\widehat{L}\left(Y\right) := \sum_{k=1}^{\infty} \widehat{L}^{k}\left(Y\right),$$

where

$$\widehat{L}^{k}\left(Y\right) := (-1)^{k} \sum_{m} \int_{\boldsymbol{u}_1 \boldsymbol{u}_2 \ldots \boldsymbol{u}_k} G^{(k;m)}_{\boldsymbol{u}_1 \boldsymbol{u}_2 \ldots \boldsymbol{u}_k}\left(Y\right) \mathcal{C}_m^{a_1 a_2 \ldots a_k} i\overline{\nabla}^{a_1}_{\boldsymbol{u}_1} i\overline{\nabla}^{a_2}_{\boldsymbol{u}_2} \ldots i\overline{\nabla}^{a_k}_{\boldsymbol{u}_k} \tag{4.6}$$

and

$$\widehat{R}\left(Y\right) := \sum_{k=1}^{\infty} \widehat{R}^{k}\left(Y\right),$$

where

$$\widehat{R}^{k}\left(Y\right) := \sum_{m} \int_{\boldsymbol{u}_1 \boldsymbol{u}_2 \ldots \boldsymbol{u}_k} G^{(k;m)}_{\boldsymbol{u}_1 \boldsymbol{u}_2 \ldots \boldsymbol{u}_k}\left(Y\right) \left(\mathcal{C}_m^{a_1 a_2 \ldots a_k}\right) i\nabla^{a_1}_{\boldsymbol{u}_1} i\nabla^{a_2}_{\boldsymbol{u}_2} \ldots i\nabla^{a_k}_{\boldsymbol{u}_k}. \tag{4.7}$$

Here, k is the desired truncation order, summing over the m basis elements that span the colour singlet states of $A^{\otimes k}$, $\mathfrak{C}\left(A^{\otimes k}\right)$, where A carries the adjoint representation of SU(N). An element $\mathcal{C}^{a_1 a_2 \ldots a_k} \in \mathfrak{C}\left(A^{\otimes k}\right)$ therefore satisfies:

$$\mathcal{C}^{a_1 a_2 \ldots a_k} \widetilde{U}^{a_1 b_1} \widetilde{U}^{a_2 b_2} \ldots \widetilde{U}^{a_k b_k} = \mathcal{C}^{b_1 b_2 \ldots b_k} \quad \forall \mathcal{C}^{a_1 a_2 \ldots a_k} \in \mathfrak{C}\left(A^{\otimes k}\right), \tag{4.8}$$

where $\widetilde{U}^{a_i b_i}$ are elements of SU(N) in the adjoint representation. $\mathcal{C}_m^{a_1 a_2 \ldots a_k}$ is the m-th basis element that spans $\mathfrak{C}\left(A^{\otimes k}\right)$. The adjoint colour structures must be singlets to maintain colour neutrality, as left- and right-vector fields add generators—and thus gluons—next to the Wilson line. Adjoint singlet states are essential to keep the configuration neutral.

The $G^{(k;m)}_{\boldsymbol{u}_1 \boldsymbol{u}_2 \ldots \boldsymbol{u}_k}\left(Y\right)$ is an undetermined function called colour structure functions. A colour structure function typically exists for each m of the $\mathcal{C}_m^{a_1 a_2 \ldots a_k}$'s for a specific k, as their symmetry features are defined by the colour adjoint singlet states, which we will discuss in Chapter 4.3. The rapidity dependence of the Wilson line correlators is now fully in the colour structure functions. Determining these functions is crucial for solving the JIMWLK equation, and they are the focus of this thesis. We will also refer to the $\mathcal{C}_m^{a_1 a_2 \ldots a_k}$'s as adjoint colour singlet states and we will discuss these further in Chapter 4.2.

It is fruitful now to view this parameterisation from a birdtracks angle. Consider how left- and right-invariant vector fields appear in birdtracks. The left(right)-vector field acts by inserting a generator on the left(right) of a fundamental Wilson line with a minus sign, or on the right(left) of an anti-fundamental Wilson line, along with a Dirac δ function as per Eq.

2.18. In birdtracks, this looks like:

$$i\overline{\nabla}^a_{\boldsymbol{x}} \; \boldsymbol{y} = -\delta^{(2)}_{\boldsymbol{xy}} \; \boldsymbol{y} \;, \; a \tag{4.9a}$$

$$i\overline{\nabla}^a_{\boldsymbol{x}} \; \boldsymbol{y} = \delta^{(2)}_{\boldsymbol{xy}} \; \boldsymbol{y} \;, \; a \tag{4.9b}$$

$$i\nabla^a_{\boldsymbol{x}} \; \boldsymbol{y} = \delta^{(2)}_{\boldsymbol{xy}} \; \boldsymbol{y} \;, \; a \tag{4.9c}$$

$$i\nabla^a_{\boldsymbol{x}} \; \boldsymbol{y} = -\delta^{(2)}_{\boldsymbol{xy}} \; \boldsymbol{y} \;. \; a \tag{4.9d}$$

Therefore, the action of a left-invariant vector field acting on a tensor product of fundamental and anti-fundamental Wilson lines

$$(U_{\boldsymbol{x}_1} \otimes U^\dagger_{\boldsymbol{y}_1}) \otimes \cdots \otimes (U_{\boldsymbol{x}_m} \otimes U^\dagger_{\boldsymbol{y}_m}) =$$

is given by[2]

$$i\overline{\nabla}^a_{\boldsymbol{z}} = -\left(\delta^{(2)}_{\boldsymbol{z}\boldsymbol{x}_1} + \cdots + \delta^{(2)}_{\boldsymbol{z}\boldsymbol{x}_m} - \delta^{(2)}_{\boldsymbol{z}\boldsymbol{y}_1} - \cdots - \delta^{(2)}_{\boldsymbol{z}\boldsymbol{y}_m} \right) \; a, \boldsymbol{z}$$

$$=: \; a, \boldsymbol{z} \;, \tag{4.10}$$

where we have introduced new birdtrack notation in the last line which simply represents the previous line. One similarly finds for the right-invariant vector fields that:

$$i\nabla^a_{\boldsymbol{z}} =: \; a, \boldsymbol{z} \;. \tag{4.11}$$

Now we calculate the action of the operator $\widehat{L}(Y)$ on the Wilson line correlator matrix, $\mathcal{A}$.

[2] This discussion of left- and right-invariant vector fields acting on Wilson lines is related to the discussion of the "invariance condition" in Sec. 4.4 of [44]. Specifically, Eq. 4.10 is closely related to Eqs. 4.35 - 4.35 in [44] in the limit that all Wilson lines are constant.

Recall that an element of a Wilson line correlator matrix is constructed from a basis of singlet states as in Eq. 2.36. In birdtracks, this looks like:

$$[\mathcal{A}]^{i}{}_{j}(Y) =: \quad . \tag{4.12}$$

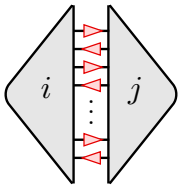

Therefore, the action of $\widehat{L}(Y)$ on $[\mathcal{A}]^{i}{}_{j}(Y)$ in birdtracks is given by (temporarily omitting rapidity dependence of the amplitude matrix for brevity):

$$\widehat{L}(Y)\,[\mathcal{A}]^{i}{}_{j} = \sum_{k=1}^{\infty}\sum_{m}(-1)^{k}\int_{\boldsymbol{u}_1\ldots\boldsymbol{u}_k} G^{(k;m)}_{\boldsymbol{u}_1\boldsymbol{u}_2\ldots\boldsymbol{u}_k}(Y)\,\mathcal{C}_m^{a_1a_2\ldots a_k} i\overline{\nabla}^{a_1}_{\boldsymbol{u}_1}\ldots i\overline{\nabla}^{a_k}_{\boldsymbol{u}_k}$$

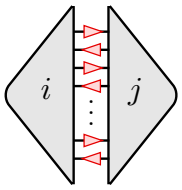

$$= \sum_{k=1}^{\infty}\sum_{m}\int_{\boldsymbol{u}_1\ldots\boldsymbol{u}_k} G^{(k;m)}_{\boldsymbol{u}_1\boldsymbol{u}_2\ldots\boldsymbol{u}_k}(Y)\,\mathcal{C}_m^{a_1a_2\ldots a_k}$$

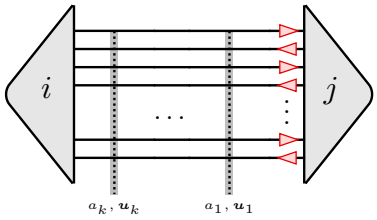

$$= \sum_{s}\underbrace{\sum_{k=1}^{\infty}\sum_{m}\int_{\boldsymbol{u}_1\ldots\boldsymbol{u}_k} G^{(k;m)}_{\boldsymbol{u}_1\boldsymbol{u}_2\ldots\boldsymbol{u}_k}(Y)\,\mathcal{C}_m^{a_1a_2\ldots a_k}}_{=:[\mathcal{M}(Y)]^{i}{}_{s}}$$

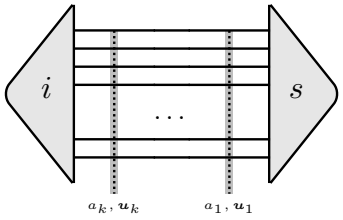

$$\times$$

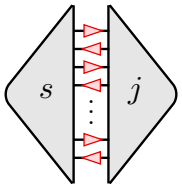

$$= [\mathcal{M}(Y)]^{i}{}_{s}\,[\mathcal{A}]^{s}{}_{j}\ , \tag{4.13}$$

where in the second to last line, we have inserted a factor of one,

$$\mathbb{1}_{\text{Singlet States}} = \sum_{s}$$

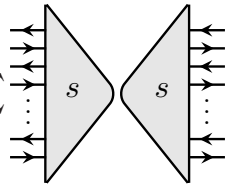

$$,$$

to get to the last line. The reason why we are allowed to do this is because the state

$$\mathcal{C}_m^{a_1 a_2 \ldots a_k}$$ 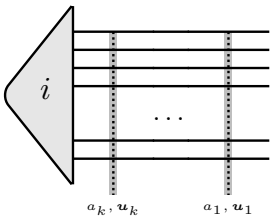

, (4.14)

is a colour singlet state since it is invariant under a global SU(N) action. To show this note that:

$$\widetilde{U}^{ab} \, [U]^{i_1}{}_{i_2} \left[t^b\right]^{i_2}{}_{j_1} = [t^a]^{i_1}{}_{j_2} \, [U]^{j_2}{}_{j_1} \ , \qquad \widetilde{U}^{ab}$$ 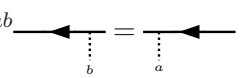

$$= \ ,$$ (4.15a)

$$\widetilde{U}^{ab} \left[t^b\right]^{i_1}{}_{j_2} \left[U^\dagger\right]^{j_2}{}_{j_1} = \left[U^\dagger\right]^{i_1}{}_{i_2} [t^a]^{i_2}{}_{j_1} \ , \qquad \widetilde{U}^{ab}$$ 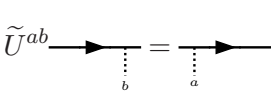

$$= \ ,$$ (4.15b)

which follows from the Fierz identity. Therefore, we will have that:

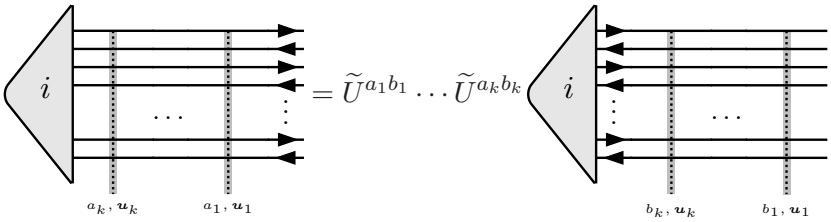

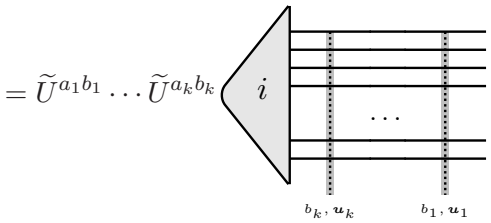

(Since 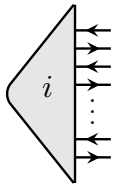 is a colour singlet state)

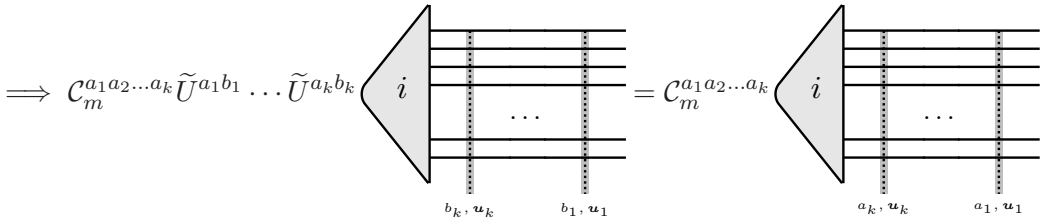

, (4.16)

where in the last line we have used Eq. 4.8 and relabelled indices. Thus, we can insert a complete set of singlet states in the second to last line of Eq. 4.13, demonstrating why the adjoint color structures in the parameterization ansatz in Eqs. 4.6 and 4.7 must also be color

singlets. Otherwise, the physics requirement for color neutrality and the form of Eq. 4.8 prevent an ansatz permitting an exponential solution.

The birdtrack calculation for $\widehat{R}(Y)$ on $\mathcal{A}_{ij}$ follows in exactly the same fashion to yield:

$$\widehat{R}(Y)\,\mathcal{A}^{i}{}_{j} = \mathcal{A}^{i}{}_{l}\left[\left(\mathcal{M}(Y)\right)^{t}\right]^{l}{}_{j}\ . \tag{4.17}$$

Thus, we see from Eqs. 4.13 and 4.17 that the $\mathcal{M}_Y$-matrices has no Wilson lines in it and, therefore, to compute the matrix elements of $\mathcal{M}_Y$ (and thus $\mathcal{M}_Y^t$) in Eq. 4.1, one must act the $\widehat{L}(Y)$ operators on the Wilson line correlator of interest element-by-element and then simply set all the Wilson lines to unity.

Since $\widehat{L}(Y)$ and $\widehat{R}(Y)$ are infinite sums, we cannot compute their action fully on $\mathcal{A}$. We must truncate the sum at some order p to obtain $\widehat{L}_p(Y)$ and $\widehat{R}_p(Y)$, as given by:

$$\begin{aligned}\widehat{L}_p(Y) &:= \sum_{k=1}^{p}\widehat{L}^k(Y)\,,\\ \widehat{R}_p(Y) &:= \sum_{k=1}^{p}\widehat{L}^k(Y)\,.\end{aligned} \tag{4.18}$$

Applying $\widehat{L}_p(Y)$ and $\widehat{R}_p(Y)$ to a correlator matrix $\mathcal{A}$ is called the p-point truncation of JIMWLK. The 2-point truncation, known as the Gaussian truncation, and the 3-point truncation of the JIMWLK equation have been extensively studied, as mentioned in [13, 17, 33, 37, 39]. This thesis will focus on extending the existing 2- and 3-point truncations up to 4-point truncations where we shall obtain a parameterisation equation for JIMWLK evolution up to 4-point level. We need a viable basis for $\mathfrak{C}\left(A^{\otimes 4}\right)$ due to the adjoint color singlet states in the truncation, which we elaborate on in the next section.

4.2 Adjoint Colour Singlet States

The set $\mathfrak{C}\left(A^{\otimes k}\right)$ is defined as the set of all colour singlet states in $A^{\otimes k}$ where A is a real vector space carrying the adjoint representation of SU(N). The inner product on $\mathfrak{C}\left(A^{\otimes k}\right)$ is defined as

$$\langle A^{a_1\cdots a_k}, B^{a_1\cdots a_k}\rangle := \sum_{a_1,\ldots,a_k}\overline{A_{a_1\cdots a_k}}B^{a_1\cdots a_k} \quad \text{where } A^{a_1\cdots a_k}, B^{a_1\cdots a_k} \in \mathfrak{C}\left(A^{\otimes k}\right)\,, \tag{4.19}$$

where the overline denotes complex conjugation The definition in Eq. 4.8 is analogous to the defintion of colour singlet states in Eq. 2.37 where in Eq. 2.37, they are defined in-terms of fundamental and anti-fundamental representations. We aim to find an orthogonal basis for $\mathfrak{C}\left(A^{\otimes k}\right)$ with clear interpretations. It would be convenient if we could use the properties

of HYPOs and transition operators to project onto the irreducible representations of SU(N) over $A^{\otimes m}$ and construct the singlet states from there as discussed in Chapter 3.2. However, one can already see that such methods will not work here, as now we are dealing with a vector space, A, that carries the adjoint representation of SU(N) as opposed to vector spaces which carry the fundamental and anti-fundamental representation.

J. Rayner and H. Weigert developed a suitable basis for $\mathfrak{C}(A^{\otimes m})$ for the m-point truncation of JIMWLK [40]. They constructed a basis for $\mathfrak{C}(A^{\otimes m})$ that, while not completely orthogonal, is "mostly" orthogonal and interpretable through HYPOs. Other orthogonal bases for $\mathfrak{C}(A^{\otimes m})$ do exist and they are commonly referred to as multiplet bases. One such orthogonal basis and its construction in birdtracks can be found in Sec. 9.12 in [44]. It consists of seven projection operators (six for $N = 3$, seven for for $N > 3$), projecting to the irreducible representations within $A \otimes A$, and of two transition operators, mapping two copies of the adjoint representation onto each other [44, 52, 56, 57]. These multiplet bases are constructed using various different methodologies and are each suited for its own unique purpose. For the purposes of this thesis, we require a basis for $\mathfrak{C}(A^{\otimes m})$ that is interpretable through HYPOs and orthogonal as we suspect that such may facilitate the solving of JIMWLK evolution better. Hence, we proceed with the basis constructed in [40]. We now present the method for constructing this basis, clarify what we mean by "mostly" orthogonal, and refer readers to [40] for derivation details.

To construct a basis for $\mathfrak{C}(A^{\otimes m})$, we first start with the trace basis for $\mathfrak{C}(A^{\otimes m})$: a basis for $\mathfrak{C}(A^{\otimes m})$ that is constructed from all possible m-index products of traces of products of $\mathfrak{su}(N)$ generators [56]. The "trace basis" for $N < m$ is not linearly independent and shrinks to a smaller set if subjected to orthogonalisation as mentioned above. So one would need to eliminate elements that are linearly dependent in a somewhat ad-hoc procedure for sufficiently small N. This trace basis mirrors Chapter 3.2.3's, but excludes states with a Kronecker δ and omits Clebsch-Gordan operators from the rest, retaining only the gluonic parts. Consequently, the size of this basis is reduced, making it less than $m!$. As a few examples, we give the trace basis for $m = 2, 3, 4$:

$$m = 2 : \{\mathrm{tr}(t^{a_1}t^{a_2})\}\,, \tag{4.20}$$

$$m = 3 : \{\mathrm{tr}(t^{a_1}t^{a_2}t^{a_3}),\ \mathrm{tr}(t^{a_1}t^{a_3}t^{a_2})\}\,, \tag{4.21}$$

$$\begin{aligned} m = 4 : \{&\mathrm{tr}(t^{a_1}t^{a_2}t^{a_3}t^{a_4}), \mathrm{tr}(t^{a_1}t^{a_3}t^{a_2}t^{a_4}), \mathrm{tr}(t^{a_1}t^{a_2}t^{a_4}t^{a_3}),\\ &\mathrm{tr}(t^{a_1}t^{a_3}t^{a_4}t^{a_2}), \mathrm{tr}(t^{a_1}t^{a_4}t^{a_2}t^{a_3}), \mathrm{tr}(t^{a_1}t^{a_4}t^{a_3}t^{a_2}),\\ &\mathrm{tr}(t^{a_1}t^{a_2})\mathrm{tr}(t^{a_3}t^{a_4}), \mathrm{tr}(t^{a_1}t^{a_3})\mathrm{tr}(t^{a_2}t^{a_4}), \mathrm{tr}(t^{a_1}t^{a_4})\mathrm{tr}(t^{a_2}t^{a_3})\}\,. \end{aligned} \tag{4.22}$$

The trace basis gives us a practical formula for computing the dimension of $\mathfrak{C}(A^{\otimes m})$ for sufficiently large N but not in-general for small N ($N < m$). Notice that we can put the trace of a product of generators in a direct 1-1 correspondence with the elements of S_m that

have no fixed point[3]. A few examples to illustrate this are given below:

$$\begin{aligned} \mathrm{tr}(t^{a_1}t^{a_2}t^{a_3}) &\iff (123), \\ \mathrm{tr}(t^{a_1}t^{a_3}t^{a_2}) &\iff (132), \\ \mathrm{tr}(t^{a_1}t^{a_2}t^{a_3}t^{a_4}) &\iff (1234), \\ \mathrm{tr}(t^{a_1}t^{a_2})\,\mathrm{tr}(t^{a_3}t^{a_4}) &\iff (12)(34)\,. \end{aligned} \tag{4.23}$$

Not all elements of S_m are included in this 1-1 correspondence because an element of S_m with a fixed point creates a 0, corresponding to the trace of a single generator, and the generators of $\mathfrak{su}(N)$ are traceless. These correspond to the elements in the original trace basis which contain a Kronecker δ. The elements of S_m that have no fixed point are known as derangements and the number of derangements in S_m is given by the subfactorial of m, denoted by $!\,m$. The subfactorial, in-turn, is given by [58, 59]:

$$!\,m = m!\sum_{i=0}^{m}\frac{(-1)^i}{i!}\,. \tag{4.24}$$

The trace basis is a first step towards systematically constructing a basis for $\mathfrak{C}\,(A^{\otimes m})$. However, there are two major issues with the trace basis:

- It is not orthogonal.
- It is not sensitive to dimensional zeroes. A basis for $\mathfrak{C}\,(A^{\otimes m})$ is said to be sensitive to dimensional zeroes if for $N < m$, certain basis elements automatically drop/become zero such that the remaining basis elements are still linearly independent and still span $\mathfrak{C}\,(A^{\otimes m})$[4].

To fix the latter issue and "mostly" fix the former issue, J. Rayner and H. Weigert used HYPOs acting on an arbitrary element of $\mathfrak{C}\,(A^{\otimes m})$ and showed that they project out onto orthogonal subspaces of $\mathfrak{C}\,(A^{\otimes m})$[5] [40]. These orthogonal subspaces are not necessarily one-dimensional, and the basis elements for such subspaces are the ones that may not be orthogonal (since there is more than one of them needed to span the subspace). However, since the subspaces projected out by these HYPOs are orthogonal, we see that the inner product between elements of these different subspaces will always be 0. This is what we mean when we say that a basis constructed this way is "mostly" orthogonal.

[3] Elements of S_m that have no fixed point are elements that have no disjoint 1-cycles.

[4] Recall our discussion earlier when $d^{abc} = 0$ when $N = 2$

[5] HYPOs act on elements of $A^{\otimes m}$, and hence $\mathfrak{C}\left(A^{\otimes m}\right)$ as defined in Eq. 3.15 as the definition in Eq. 3.15 was for any arbitrary vector space V, not just a vector space that carries the fundamental representation of SU(N).

To illustrate, let us put this method into practice. The case of $k = 2$ is somewhat trivial as there is only one trace basis element when $k = 2$ and hence, all elements of $\mathfrak{C}\left(A^{\otimes 2}\right)$ are scalar multiples of $\mathrm{tr}\left(t^{a_1}t^{a_2}\right) = \delta^{a_1a_2}$. The case of $k = 3$ is more interesting.

As a reminder, the numerical assignment for the Young diagrams and tableaux for $m = 3$ is given below:

For Young diagrams with 3 boxes:

- $\ydiagram{3} \to 1$
  - $\begin{ytableau} 1 & 2 & 3 \end{ytableau} \to 1$
- $\ydiagram{2,1} \to 2$
  - $\begin{ytableau} 1 & 3 \\ 2 \end{ytableau} \to 1$
  - $\begin{ytableau} 1 & 2 \\ 3 \end{ytableau} \to 2$
- $\ydiagram{1,1,1} \to 3$
  - $\begin{ytableau} 1 \\ 2 \\ 3 \end{ytableau} \to 1$

We will also find it to be more convenient to define a group algebra element $g = \sum_{\sigma \in S_k} \alpha_\sigma \sigma \in \mathbb{R}[S_k]$ acting on an element $\mathcal{C}^{a_1a_2\ldots a_k} \in A^{\otimes k}$ where A carries the adjoint representation of $\mathrm{SU}(N)$. The notation is as follows:

$$(g \circ \mathcal{C})^{a_1a_2\ldots a_k} := \sum_{\sigma \in S_k} \alpha_\sigma \mathcal{C}^{a_{\sigma(1)}a_{\sigma(2)}\ldots a_{\sigma(k)}} \,. \tag{4.25}$$

When $k = 3$, an arbitrary element of $\mathfrak{C}\left(A^{\otimes 3}\right)$, $v^{a_1a_2a_3}$, will be given in-terms of the trace basis as

$$v^{a_1a_2a_3} = c_1\,\mathrm{tr}(t^{a_1}t^{a_2}t^{a_3}) + c_2\,\mathrm{tr}(t^{a_2}t^{a_1}t^{a_3}),$$

where $c_1, c_2 \in \mathbb{R}$. The result of projecting on v with the HYPOs will be[6]:

$$\begin{aligned}(T_{111} \circ v)^{a_1a_2a_3} &= \left(\frac{c_1 + c_2}{2}\right)\left(\mathrm{tr}(t^{a_1}t^{a_2}t^{a_3}) + \mathrm{tr}(t^{a_2}t^{a_1}t^{a_3})\right) \\ &= \left(\frac{c_1 + c_2}{4}\right) d^{a_1a_2a_3}\,,\end{aligned} \tag{4.26}$$

[6] We simplify the results using the cyclicity of the trace.

$$(T_{211} \circ v)^{a_1a_2a_3} = 0, \quad (T_{222} \circ v)^{a_1a_2a_3} = 0\,, \tag{4.27}$$

$$\begin{aligned}(T_{311} \circ v)^{a_1a_2a_3} &= \left(\frac{c_1 - c_2}{2}\right)(\mathrm{tr}(t^{a_1}t^{a_2}t^{a_3}) - \mathrm{tr}(t^{a_2}t^{a_1}t^{a_3})) \\ &= \left(\frac{c_1 - c_2}{4}\right) if^{a_1a_2a_3}\,. \end{aligned} \tag{4.28}$$

Since c_1 and c_2 are arbitrary constants, we can always redefine $\left(\frac{c_1+c_2}{4}\right)$ and $\left(\frac{c_1-c_2}{4}\right)$ as one constant. Thus, we have a basis for $\mathfrak{C}\left(A^{\otimes 3}\right)$

$$\mathcal{C}_1^{a_1a_2a_3} := d^{a_1a_2a_3}, \quad \mathcal{C}_2^{a_1a_2a_3} := if^{a_1a_2a_3}\,, \tag{4.29}$$

where it is easy to see that $\mathcal{C}_1^{a_1a_2a_3}$ and $\mathcal{C}_2^{a_1a_2a_3}$ each span its own subspace that is orthogonal to each other. Furthermore, we see that dimensional zeroes are made manifest in this basis as $d^{a_1a_2a_3} = 0$ when $N = 2$. J. Rayner and H. Weigert showed in [40] that a basis constructed this way will make dimensional zeroes manifest.

As a reminder, the numerical assignment for the Young diagrams and tableaux for $m = 4$ is given below:

For Young diagrams with 4 boxes:

- $\ydiagram{4} \to 1$
  - $\begin{array}{|c|c|c|c|}\hline 1&2&3&4\\\hline\end{array} \to 1$
- $\ydiagram{3,1} \to 2$
  - $\begin{array}{|c|c|c|}\hline 1&3&4\\\hline 2\\\cline{1-1}\end{array} \to 3$
  - $\begin{array}{|c|c|c|}\hline 1&2&4\\\hline 3\\\cline{1-1}\end{array} \to 2$
  - $\begin{array}{|c|c|c|}\hline 1&2&3\\\hline 4\\\cline{1-1}\end{array} \to 1$
- $\ydiagram{2,2} \to 3$
  - $\begin{array}{|c|c|}\hline 1&3\\\hline 2&4\\\hline\end{array} \to 2$
  - $\begin{array}{|c|c|}\hline 1&2\\\hline 3&4\\\hline\end{array} \to 1$
- $\ydiagram{2,1,1} \to 4$
  - $\begin{array}{|c|c|}\hline 1&4\\\hline 2\\\cline{1-1}3\\\cline{1-1}\end{array} \to 3$

- $\begin{array}{|c|c|}\hline 1 & 3 \\ \hline 2 \\ \cline{1-1} 4 \\ \cline{1-1}\end{array} \to 2$
- $\begin{array}{|c|c|}\hline 1 & 2 \\ \hline 3 \\ \cline{1-1} 4 \\ \cline{1-1}\end{array} \to 1$

• $\begin{array}{|c|}\hline \\ \hline \\ \hline \\ \hline \\ \hline\end{array} \to 5$

- $\begin{array}{|c|}\hline 1 \\ \hline 2 \\ \hline 3 \\ \hline 4 \\ \hline\end{array} \to 1$

The new basis for $\mathfrak{C}\left(A^{\otimes 4}\right)$ using this methodology is given in Eq. A.4 in Appendix A where we use the trace basis to express an element $v^{a_1a_2a_3a_4} \in \left(A^{\otimes 4}\right)$ as $v^{a_1a_2a_3a_4} = \sum_i c_i v_i^{a_1a_2a_3a_4} \in \mathfrak{C}\left(A^{\otimes 4}\right)$ where $v_i^{a_1a_2a_3a_4}$ is an element of the trace basis. The important point is that:

- The HYPOs T_{211}, T_{222}, T_{233} and T_{511} all project onto 0-dimensional subspaces.
- The HYPOs T_{411}, T_{422} and T_{433} all project onto 1-dimensional subspaces.
- The HYPOs T_{111}, T_{311} and T_{322} all project onto 2-dimensional subspaces

Most of these basis elements in Eq. A.4 are already orthogonal except the ones that are in the 2-dimensional subspaces:

$$\langle \mathcal{C}_1^{a_1a_2a_3a_4}, \mathcal{C}_2^{a_1a_2a_3a_4} \rangle \neq 0, \quad \langle \mathcal{C}_3^{a_1a_2a_3a_4}, \mathcal{C}_4^{a_1a_2a_3a_4} \rangle \neq 0, \quad \langle \mathcal{C}_5^{a_1a_2a_3a_4}, \mathcal{C}_6^{a_1a_2a_3a_4} \rangle \neq 0\,. \tag{4.30}$$

These pairs of basis elements span a two-dimensional subspace, so they aren't expected to automatically be orthogonal from the method we used to find them, as seen in Eq. 4.30. The dimensional zeroes in this basis is also manifest for $N < 4$ which is discussed in [40] (it will not be necessary for our purposes here).

We therefore have a useful basis for $\mathfrak{C}\left(A^{\otimes 4}\right)$ that serves as a starting point for computing the 4-point truncation of the JIMWLK equation. We shall refer to a basis constructed using the method above as a HYPO basis. Later on, we will make adjustments to this basis that makes it fully orthogonal in a useful way and exploit some of its symmetry properties regarding the operators in $\mathfrak{G}_4$ that was not discussed in [40] and to our knowledge, is new.

4.3 Putting Everything Together

We demonstrate obtaining parameterisation equations for the p-point truncation of JIMWLK and using them to solve the JIMWLK equation. To solve the JIMWLK equation for a $q^m\overline{q}^m$

correlator matrix up to p-point truncation, we follow these steps:

1. Construct the $q^{m+1}\overline{q}^{m+1}$ correlator matrix, which we will call $\mathcal{A}^{(m+1)}_{\vec{\boldsymbol{x}};\vec{\boldsymbol{y}}}(Y)$. Use an appropriate basis for colour singlet states of SU(N) over $V^{\otimes m+1}\otimes(V^*)^{\otimes m+1}$. Here, V carries the fundamental representation of SU(N), and V^* carries the anti-fundamental representation of SU(N). Here we have introduced the notation

$$\begin{aligned}\left\langle m;i\left|(U_{\boldsymbol{x}_1}\otimes U^\dagger_{\boldsymbol{y}_1})\otimes\cdots\otimes(U_{\boldsymbol{x}_m}\otimes U^\dagger_{\boldsymbol{y}_m})\right|m;j\right\rangle &:= \left[\mathcal{A}^{(m)}_{\boldsymbol{x}_1\cdots\boldsymbol{x}_m;\boldsymbol{y}_1\cdots\boldsymbol{y}_m}\right]_{ij}\\ &=: \left[\mathcal{A}^{(m)}_{\vec{\boldsymbol{x}};\vec{\boldsymbol{y}}}\right]_{ij},\end{aligned}$$

   to include the transverse coordinates of the Wilson lines. The reason for doing this is because one can obtain the $q^m\overline{q}^m$ and $q^m\overline{q}^m g$ correlator matrices after taking a quark/anti-quark coincidence limit and we saw in Chapter 3.2 that the $q^m\overline{q}^m g$ correlator matrix drives the JIMWLK evolution of the $q^m\overline{q}^m$ correlator. Thus, it is better to start by constructing the $q^{m+1}\overline{q}^{m+1}$ correlator matrix first and take coincidence limits at the end (more on this below).

2. Apply the p-point truncation to the $q^{m+1}\overline{q}^{m+1}$ correlator matrix to obtain the $\mathcal{M}_Y$ matrices that parameterise the JIMWLK evolution of the $q^{m+1}\overline{q}^{m+1}$ correlator matrix, i.e. apply the operators defined in Eq. 4.18[7] to the $q^{m+1}\overline{q}^{m+1}$ correlator matrix and then set all Wilson lines to unity to obtain the $\mathcal{M}_Y$ matrices. We will denote the $\mathcal{M}$-matrices that parameterise the $q^{m+1}\overline{q}^{m+1}$ correlator matrix by $\mathcal{M}^{(m+1)}_Y$

3. The $\mathcal{M}$ matrices will have the same coincidence limit structure as $\mathcal{A}^{(m+1)}_{\vec{\boldsymbol{x}};\vec{\boldsymbol{y}}}(Y)$ since this is how the parameterisation is constructed. Thus, we now take a quark/anti-quark coincidence limit to then obtain the $\mathcal{M}^{(m)}_Y$ and $\mathcal{M}^{(m;g)}_Y$ matrices which parameterise the $q^m\overline{q}^m$ and $q^m\overline{q}^m g$ correlator matrices respectively.

4. Obtain solutions to the parameterisation equations for the $q^m\overline{q}^m$ and $q^m\overline{q}^m g$ correlator matrices, $\left\langle\mathcal{A}^{(m)}_{\vec{\boldsymbol{x}};\vec{\boldsymbol{y}}}(Y)\right\rangle$ and $\left\langle\mathcal{A}^{(m;g)}_{\vec{\boldsymbol{x}};\vec{\boldsymbol{y}};\boldsymbol{z}}(Y)\right\rangle$, by using Eqs. 4.2 and 4.3 along with a set of initial conditions for the $\left\langle\mathcal{A}^{(m)}_{\vec{\boldsymbol{x}};\vec{\boldsymbol{y}}}(Y)\right\rangle$ and $\left\langle\mathcal{A}^{(m;g)}_{\vec{\boldsymbol{x}};\vec{\boldsymbol{y}};\boldsymbol{z}}(Y)\right\rangle$ matrices that we choose. We have introduced additional notation here for when we take a quark/anti-quark coincidence limit of $\mathcal{A}^{(m+1)}_{\vec{\boldsymbol{x}};\vec{\boldsymbol{y}}}(Y)$:

$$\mathcal{A}^{(m+1)}_{\vec{\boldsymbol{x}};\vec{\boldsymbol{y}}}(Y)\xrightarrow[\text{Block diagonal which corresponds to } q\bar{q}g\text{-correlator}]{\boldsymbol{x}_m\to\boldsymbol{y}_m:=\boldsymbol{z}}\mathcal{A}^{(m;g)}_{\vec{\boldsymbol{x}};\vec{\boldsymbol{y}};\boldsymbol{z}}(Y)\,. \tag{4.31}$$

   Note that taking a path-ordered exponential will mix the elements in each block diagonal correlator matrix, $\mathcal{M}^{(m)}_Y$ and $\mathcal{M}^{(m;g)}_Y$. This gives another reason why it is essential to

[7] In-principle, one would only need to apply the p-point truncation with left-invariant vector fields, $\widehat{L}_p(Y)$, to $\mathcal{A}^{(m+1)}_{\vec{\boldsymbol{x}};\vec{\boldsymbol{y}}}(Y)$. Using the right-invariant truncation on $\mathcal{A}^{(m+1)}_{\vec{\boldsymbol{x}};\vec{\boldsymbol{y}}}(Y)$ results in the transpose of the $\mathcal{M}_Y$ matrix found via its left analogue, as shown in Eqs. 4.13 and 4.17.

consider a matrix of correlators when looking at JIMWLK evolution as opposed to a single correlator.

5. Now consider the JIMWLK evolution equation for $\mathcal{A}^{(m)}_{\vec{\boldsymbol{x}};\vec{\boldsymbol{y}}}(Y)$ as given by Eq. 2.38. R. Moerman and H. Weigert showed in [33] that applying the JIMWLK Hamiltonian in Eq. 2.38, leads to the simplified JIMWLK equation for the $\mathcal{A}^{(m)}_{\vec{\boldsymbol{x}};\vec{\boldsymbol{y}}}(Y)$ correlator matrix:

$$\frac{d}{dY}\left\langle \mathcal{A}^{(m)}_{\vec{\boldsymbol{x}};\vec{\boldsymbol{y}}} \right\rangle (Y) = \frac{\alpha_s}{4\pi^2} \sum_{h=1}^{2} \int_{\boldsymbol{z}} \left(P^{(1)h}_{\vec{\boldsymbol{x}};\vec{\boldsymbol{y}};\boldsymbol{z}} \cdot \left\langle \begin{bmatrix} \mathcal{A}^{(m)}_{\vec{\boldsymbol{x}};\vec{\boldsymbol{y}}} & 0 \\ 0 & \mathcal{A}^{(m;g)}_{\vec{\boldsymbol{x}};\vec{\boldsymbol{y}};\boldsymbol{z}} \end{bmatrix} \right\rangle (Y) \cdot \left(P^{(2)h}_{\vec{\boldsymbol{x}};\vec{\boldsymbol{y}};\boldsymbol{z}} \right)^t + P^{(2)h}_{\vec{\boldsymbol{x}};\vec{\boldsymbol{y}};\boldsymbol{z}} \cdot \left\langle \begin{bmatrix} \mathcal{A}^{(m)}_{\vec{\boldsymbol{x}};\vec{\boldsymbol{y}}} & 0 \\ 0 & \mathcal{A}^{(m;g)}_{\vec{\boldsymbol{x}};\vec{\boldsymbol{y}};\boldsymbol{z}} \end{bmatrix} \right\rangle (Y) \cdot \left(P^{(1)h}_{\vec{\boldsymbol{x}};\vec{\boldsymbol{y}};\boldsymbol{z}} \right)^t \right), \tag{4.32}$$

where $P^{(1)h}_{\vec{\boldsymbol{x}};\vec{\boldsymbol{y}};\boldsymbol{z}}$ and $P^{(2)h}_{\vec{\boldsymbol{x}};\vec{\boldsymbol{y}};\boldsymbol{z}}$ are the non-square $m! \times (m+1)!$ matrices

$$P^{(1)h}_{\vec{\boldsymbol{x}};\vec{\boldsymbol{y}};\boldsymbol{z}} := \left[-\mathcal{K}^{(L)h}_{\vec{\boldsymbol{x}};\vec{\boldsymbol{y}};\boldsymbol{z}} \cdot \left(\mathcal{K}^{(L)h}_{\vec{\boldsymbol{x}};\vec{\boldsymbol{y}};\boldsymbol{z}} \right)^t \;\; \mathcal{K}^{(L)h}_{\vec{\boldsymbol{x}};\vec{\boldsymbol{y}};\boldsymbol{z}} \right], \quad P^{(2)h}_{\vec{\boldsymbol{x}};\vec{\boldsymbol{y}};\boldsymbol{z}} := \left[\mathbb{1}_{m!\times m!} \;\; \mathcal{K}^{(L)h}_{\vec{\boldsymbol{x}};\vec{\boldsymbol{y}};\boldsymbol{z}} \right], \tag{4.33}$$

and $\left[\mathcal{K}^{(L)h}_{\vec{\boldsymbol{x}};\vec{\boldsymbol{y}};\boldsymbol{z}}\right]_{ik}$ is given in birdtracks as[a]:

$$\left[\mathcal{K}^{(L)h}_{\vec{\boldsymbol{x}};\vec{\boldsymbol{y}};\boldsymbol{z}}\right]_{ik} := \int_{\boldsymbol{u}} \mathcal{K}^{h}_{\boldsymbol{u}\boldsymbol{z}}$$

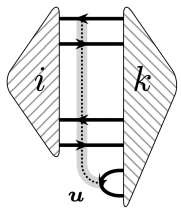

, (4.34)

which is an $m! \times m \cdot m!$ matrix. The kernel $\mathcal{K}^{h}_{\boldsymbol{u}\boldsymbol{z}}$ is given by:

$$\mathcal{K}^{h}_{\boldsymbol{u}\boldsymbol{z}} := \frac{(\boldsymbol{u}-\boldsymbol{z})^h}{(\boldsymbol{u}-\boldsymbol{z})^2}\,. \tag{4.35}$$

[a] Here i are the are basis elements that span the space of colour singlet states of SU(N) over $V^{\otimes m} \otimes (V^*)^{\otimes m}$ and k are the basis elements that span the space of colour singlet states of SU(N) over $V^{\otimes (m+1)} \otimes (V^*)^{\otimes (m+1)}$.

We therefore explicitly see in Eq. 4.32 how the $\mathcal{A}^{(m;g)}_{\vec{\boldsymbol{x}};\vec{\boldsymbol{y}};\boldsymbol{z}}(Y)$ matrix drives the evolution of $\mathcal{A}^{(m)}_{\vec{\boldsymbol{x}};\vec{\boldsymbol{y}}}(Y)$ and why it is needed. Thus, in-order to solve the JIMWLK equation for the $\mathcal{A}^{(m)}_{\vec{\boldsymbol{x}};\vec{\boldsymbol{y}}}(Y)$ correlator matrix, we plug in the solutions to the parameterisation equations found in the previous step into Eq. 4.32. This, in-turn, gives us a set of coupled integro-differential equations for the colour structure functions, which we shall now refer to as the G's, along with the initial conditions for the correlator matrices which we must set pre-emptively.

6. Select valid initial conditions for the correlator matrices, then solve the integro-differential equations for the G's to obtain the JIMWLK evolution for the $\mathcal{A}^{(m)}_{\vec{\boldsymbol{x}};\vec{\boldsymbol{y}}}(Y)$ correlator matrix[8].

The steps outlined above should, in theory, lead one to obtaining solutions to the JIMWLK equation for any Wilson line correlator matrix. We have already discussed Step 1 above on how to obtain the $\mathcal{A}^{(m+1)}_{\vec{\boldsymbol{x}};\vec{\boldsymbol{y}}}(Y)$ correlator matrix in different bases suitable for different coincidence limits in Chapter 3.2. Let us now discuss step 2 in the procedure we have outlined above.

While applying the p-point truncation from Eq. 4.18 can yield the $\mathcal{M}_Y$ matrices, it often results in complex and unwieldy $\mathcal{M}_Y$ matrices. We need a method to simplify these $\mathcal{M}_Y$ matrices to effectively solve the JIMWLK equation for $\mathcal{A}^{(m)}_{\vec{\boldsymbol{x}};\vec{\boldsymbol{y}}}(Y)$. R. Moerman and H. Weigert in [33] found a way of doing this that involves how the symmetries of the HYPO basis for $\mathfrak{C}\left(A^{\otimes m}\right)$ imprint themselves onto the G' s. We present the argument here to demonstrate this.

The general idea comes from looking at $\widehat{L}^k(Y)$ defined in Eq. 4.6 and symmetrizing over all the integration variables $\boldsymbol{u}_1, \boldsymbol{u}_2, \cdots, \boldsymbol{u}_k$ and leveraging the fact that the order of integration is irrelevant[9]. Making this more concrete

$$\begin{aligned}\widehat{L}^k\left(Y\right) &:= (-1)^k \sum_m \int_{\boldsymbol{u}_1\boldsymbol{u}_2\ldots\boldsymbol{u}_k} G^{(k;m)}_{\boldsymbol{u}_1\boldsymbol{u}_2\ldots\boldsymbol{u}_k}\left(Y\right) \mathcal{C}_m^{a_1a_2\ldots a_k}\, i\overline{\nabla}^{a_1}_{\boldsymbol{u}_1}\, i\overline{\nabla}^{a_2}_{\boldsymbol{u}_2}\ldots i\overline{\nabla}^{a_k}_{\boldsymbol{u}_k} \\ &= (-1)^k \sum_m \frac{1}{k!} \int_{\boldsymbol{u}_1\boldsymbol{u}_2\ldots\boldsymbol{u}_k} \sum_{\sigma\in S_k} \left(\sigma \circ G^{(k;m)}\right)_{\boldsymbol{u}_1\boldsymbol{u}_2\ldots\boldsymbol{u}_k}\left(Y\right) \mathcal{C}_m^{a_1a_2\ldots a_k}\, i\overline{\nabla}^{a_1}_{\boldsymbol{u}_{\sigma(1)}}\, i\overline{\nabla}^{a_2}_{\boldsymbol{u}_{\sigma(2)}}\ldots i\overline{\nabla}^{a_k}_{\boldsymbol{u}_{\sigma(k)}},\end{aligned} \tag{4.36}$$

where we have introduced the more convenient notation for a group algebra element $g = \sum_{\sigma\in S_K} \alpha_\sigma\sigma \in \mathbb{R}[S_k]$ acting on a function with transverse coordinates $\boldsymbol{u}_1, \boldsymbol{u}_2, \ldots, \boldsymbol{u}_k$ as:

$$\left(g \circ F\right)_{\boldsymbol{u}_1\boldsymbol{u}_2\ldots\boldsymbol{u}_k} := \sum_{\sigma\in S_k} \alpha_\sigma F_{\boldsymbol{u}_{\sigma(1)}\boldsymbol{u}_{\sigma(2)}\ldots\boldsymbol{u}_{\sigma(k)}}\,. \tag{4.37}$$

Going back to Eq. 4.36, one proceeds from here by rearranging all the left-invariant vector fields such that the transverse coordinates appear in the original ascending order and then relabel the indices on these vector fields so that they are also in the original ascending order. Doing all this incurs a permutation on the order of the adjoint indices in $\mathcal{C}_m^{a_1a_2\ldots a_k}$ as well as commutator terms that arise from rearranging the left-invariant vector fields. We ignore the commutator terms since they can either be subsumed into lower order terms in the left-

[8] When we say solution, it should always be kept in-mind that these are not the most general solutions since we had an infinite sum in Eqs. 4.6 and 4.7 that we truncated at some point p.

[9] Assuming the functions are sufficiently "nice" (the usual physicist assumption).

invariant vector fields or are 0 [33]. Thus, we get for Eq. 4.36

$$\begin{aligned}\widehat{L}^k(Y) &= (-1)^k \sum_m \frac{1}{k!} \int_{\boldsymbol{u}_1\ldots\boldsymbol{u}_k} \sum_{\sigma\in S_k} \left(\sigma\circ G^{(k;m)}\right)_{\boldsymbol{u}_1\ldots\boldsymbol{u}_k}(Y)\, \mathcal{C}_m^{a_1\ldots a_k}\, i\overline{\nabla}^{a_1}_{\boldsymbol{u}_{\sigma(1)}}\ldots i\overline{\nabla}^{a_k}_{\boldsymbol{u}_{\sigma(k)}} \\ &= (-1)^k \sum_m \frac{1}{k!} \int_{\boldsymbol{u}_1\ldots\boldsymbol{u}_k} \sum_{\sigma\in S_k} \left(\sigma\circ G^{(k;m)}\right)_{\boldsymbol{u}_1\ldots\boldsymbol{u}_k}(Y)\, (\sigma\circ\mathcal{C}_m)^{a_1\ldots a_k}\, i\overline{\nabla}^{a_1}_{\boldsymbol{u}_1} i\ldots i\overline{\nabla}^{a_k}_{\boldsymbol{u}_k}, \quad (4.38)\end{aligned}$$

where we have dropped the commutator terms since they have no bearing. Since each σ in Eq. 4.38 is a group algebra element, or rather an element of API $\left(\mathrm{SU}(N), V^{\otimes k}\right)$, we can express the σ's in Eq. 4.38 in-terms of HYPOs and their corresponding transition operators, i.e. the elements of $\mathfrak{G}_k$. Recall that the multiplication table for HYPOs and transition operators is given by:

$$T_{\Theta ij}\cdot T_{\Phi lm} = \delta_{\Theta\Phi}\delta_{jl} T_{\Theta im}\,. \quad (4.39)$$

Going back again to Eq. 4.38 and performing a change of basis, we get

$$\begin{aligned}\widehat{L}^k(Y) &= (-1)^k \sum_m \frac{1}{k!} \int_{\boldsymbol{u}_1\boldsymbol{u}_2\ldots\boldsymbol{u}_k} \sum_{\sigma\in S_k} \left(\sigma\circ G^{(k;m)}\right)_{\boldsymbol{u}_1\boldsymbol{u}_2\ldots\boldsymbol{u}_k}(Y)\, (\sigma\circ\mathcal{C}_m)^{a_1a_2\ldots a_k} \\ &\quad\times i\overline{\nabla}^{a_1}_{\boldsymbol{u}_1} i\overline{\nabla}^{a_2}_{\boldsymbol{u}_2}\ldots i\overline{\nabla}^{a_k}_{\boldsymbol{u}_k} \\ &= (-1)^k \sum_m \int_{\boldsymbol{u}_1\boldsymbol{u}_2\ldots\boldsymbol{u}_k} \left(\frac{1}{k!}\sum_{\sigma,(\Theta ij),(\Theta' i'j')} \left(M^{(\Theta ij)}{}_{\sigma} T_{\Theta ij}\circ G^{(k;m)}\right)_{\boldsymbol{u}_1\boldsymbol{u}_2\ldots\boldsymbol{u}_k} \right. \\ &\quad\left.\times \left(M^{(\Theta' i'j')}{}_{\sigma} T_{\Theta' i'j'}\circ\mathcal{C}_m\right)^{a_1a_2\ldots a_k}\right) \\ &\quad\times \overline{\nabla}^{a_1}_{\boldsymbol{u}_1}\overline{\nabla}^{a_2}_{\boldsymbol{u}_2}\ldots\overline{\nabla}^{a_k}_{\boldsymbol{u}_k} \\ &= (-1)^k \sum_m \int_{\boldsymbol{u}_1\boldsymbol{u}_2\ldots\boldsymbol{u}_k} \left(\frac{1}{k!}\sum_{\sigma,(\Theta ij),(\Theta' i'j')} \left(T_{\Theta ij}\circ G^{(k;m)}\right)_{\boldsymbol{u}_1\boldsymbol{u}_2\ldots\boldsymbol{u}_k} M^{(\Theta ij)}{}_{\sigma} M^{(\Theta' i'j')}{}_{\sigma} \right. \\ &\quad\left.\times \left(T_{\Theta' i'j'}\circ\mathcal{C}_m\right)^{a_1a_2\ldots a_k}\right)\overline{\nabla}^{a_1}_{\boldsymbol{u}_1}\overline{\nabla}^{a_2}_{\boldsymbol{u}_2}\ldots\overline{\nabla}^{a_k}_{\boldsymbol{u}_k} \\ &= (-1)^k \sum_m \int_{\boldsymbol{u}_1\boldsymbol{u}_2\ldots\boldsymbol{u}_k} \left(\frac{1}{k!}\sum_{(\Theta ij),(\Theta' i'j')} \left(T_{\Theta ij}\circ G^{(k;m)}\right)_{\boldsymbol{u}_1\boldsymbol{u}_2\ldots\boldsymbol{u}_k} \left(MM^t\right)^{(\Theta ij)(\Theta' i'j')} \right. \\ &\quad\left.\times \left(T_{\Theta' i'j'}\circ\mathcal{C}_m\right)^{a_1a_2\ldots a_k}\right)\overline{\nabla}^{a_1}_{\boldsymbol{u}_1}\overline{\nabla}^{a_2}_{\boldsymbol{u}_2}\ldots\overline{\nabla}^{a_k}_{\boldsymbol{u}_k} \\ &= (-1)^k \sum_m \int_{\boldsymbol{u}_1\boldsymbol{u}_2\ldots\boldsymbol{u}_k} \left(\frac{1}{k!}\sum_{(\Theta ij),(\Theta' i'j')} \left(T_{\Theta ij}\circ G^{(k;m)}\right)_{\boldsymbol{u}_1\boldsymbol{u}_2\ldots\boldsymbol{u}_k} \alpha_\Theta \delta^{(\Theta ij)(\Theta' i'j')} \right. \\ &\quad\left.\times \left(T_{\Theta' i'j'}\circ\mathcal{C}_m\right)^{a_1a_2\ldots a_k}\right)\overline{\nabla}^{a_1}_{\boldsymbol{u}_1}\overline{\nabla}^{a_2}_{\boldsymbol{u}_2}\ldots\overline{\nabla}^{a_k}_{\boldsymbol{u}_k} \\ &= (-1)^k \sum_m \frac{1}{k!} \int_{\boldsymbol{u}_1\boldsymbol{u}_2\ldots\boldsymbol{u}_k} \sum_{(\Theta ij)} \alpha_{\Theta ij}\left(T_{\Theta ij}\circ G^{(k;m)}\right)_{\boldsymbol{u}_1\boldsymbol{u}_2\ldots\boldsymbol{u}_k}(Y) \\ &\quad\times \left(T_{\Theta ij}\circ\mathcal{C}_m\right)^{a_1a_2\ldots a_k} i\overline{\nabla}^{a_1}_{\boldsymbol{u}_1} i\overline{\nabla}^{a_2}_{\boldsymbol{u}_2}\ldots i\overline{\nabla}^{a_k}_{\boldsymbol{u}_k}\,. \quad (4.40)\end{aligned}$$

In the second last line, we applied change of basis properties to derive the last line, absorbing the constant $\alpha_{\Theta ij}$ into G's. $\sum_{(\Theta ij)}$ denotes summation over all Θ, i, and j. Applying the same process to $\widehat{R}^k(Y)$ yields the same result with left-invariant vector fields replaced by right-invariant ones.

The p-point truncation in the form of the $\widehat{L}^k(Y)$ and $\widehat{R}^k(Y)$ operators from Eq. 4.40 can simplify results for the $\mathcal{M}_Y$ matrices in Gaussian and 3-point JIMWLK truncations [17, 33, 37–39]. If we use the HYPO basis for $\mathfrak{C}\left(A^{\otimes k}\right)$, then notice that the basis elements will be simultaneous eigenstates of the HYPOs with an eigenvalue of 1 or 0 up to normalization [40]. Thus, the $T_{\Theta ii}$, terms in Eq. 4.40 can lead to drastic simplification. As for the transition operators, the $T_{\Theta ij}$'s where $i \neq j$, we will soon show that they can be mapped onto the other basis elements in the HYPO basis for $\mathfrak{C}\left(A^{\otimes k}\right)$. We illustrate, through relatively simple examples for $k = 2, 3$, how Eq. 4.40 can lead to great simplification.

For k=2, we only have one basis element in $\mathfrak{C}\left(A^{\otimes 2}\right)$: $\delta^{a_1 a_2}$. Thus, the expression for $\widehat{L}^2(Y)$ is relatively simple as we only have 2 elements for the $T_{\Theta ij}$'s, the total symmetriser and the total anti-symmetriser. The total anti-symmetriser acting on $\delta^{a_1 a_2}$ gives 0 and thus we get[10]:

$$\widehat{L}^2(Y) = (-1)^2 \frac{1}{2!} \int_{\boldsymbol{u}_1 \boldsymbol{u}_2} \left(T_{111} \circ G^{(2;\delta)}\right)_{\boldsymbol{u}_1 \boldsymbol{u}_2}(Y) \delta^{a_1 a_2} i\overline{\nabla}^{a_1}_{\boldsymbol{u}_1} i\overline{\nabla}^{a_2}_{\boldsymbol{u}_2} . \tag{4.41}$$

Now notice that $\left(T_{111} \circ G^{(2;\delta)}\right)_{\boldsymbol{u}_1 \boldsymbol{u}_2}(Y)$ is symmetric about an interchange of $\boldsymbol{u}_1$ and $\boldsymbol{u}_2$. Thus, when acting $\widehat{L}^2(Y)$ on a Wilson line to obtain the $\mathcal{M}_Y$ matrices, we can apply it in the form of Eq. 4.41 and use the symmetric features of $\left(T_{111} \circ G^{(2;\delta)}\right)_{\boldsymbol{u}_1 \boldsymbol{u}_2}(Y)$ to simplify the results we get for the $\mathcal{M}_Y$ matrices. To illustrate how this simplification may occur, consider the simple linear combination of $\left(T_{111} \circ G^{(2;\delta)}\right)_{\boldsymbol{u}_1 \boldsymbol{u}_2}(Y)$'s:

$$\left(T_{111} \circ G^{(2;\delta)}\right)_{\boldsymbol{x}_1 \boldsymbol{y}_2}(Y) + \left(T_{111} \circ G^{(2;\delta)}\right)_{\boldsymbol{y}_2 \boldsymbol{x}_1}(Y) .$$

Since $\left(T_{111} \circ G^{(2;\delta)}\right)_{\boldsymbol{u}_1 \boldsymbol{u}_2}(Y)$ is totally symmetric about an interchange of its coordinates, the terms $\left(T_{111} \circ G^{(2;\delta)}\right)_{\boldsymbol{x}_1 \boldsymbol{y}_2}(Y)$ and $\left(T_{111} \circ G^{(2;\delta)}\right)_{\boldsymbol{y}_2 \boldsymbol{x}_1}(Y)$ are not independent of each other, in-fact, they are equal. Therefore, one can simplify the aforementioned linear combination

$$\left(T_{111} \circ G^{(2;\delta)}\right)_{\boldsymbol{x}_1 \boldsymbol{y}_2}(Y) + \left(T_{111} \circ G^{(2;\delta)}\right)_{\boldsymbol{y}_2 \boldsymbol{x}_1}(Y) = 2\left(T_{111} \circ G^{(2;\delta)}\right)_{\boldsymbol{x}_1 \boldsymbol{y}_2}(Y) . \tag{4.42}$$

Thus, instead of considering an individual $G^{(2;\delta)}_{\boldsymbol{u}_1 \boldsymbol{u}_2}(Y)$ in $\widehat{L}^2(Y)$, we use a linear combination of $G^{(2;\delta)}_{\boldsymbol{u}_1 \boldsymbol{u}_2}(Y)$'s to exploit their symmetry. Specifically, we use the linear combination of $G^{(2;\delta)}_{\boldsymbol{u}_1 \boldsymbol{u}_2}(Y)$'s given by $\left(T_{111} \circ G^{(2;\delta)}\right)_{\boldsymbol{u}_1 \boldsymbol{u}_2}(Y)$, symmetric under coordinate interchange. This

[10] Absorbing the unimportant $\alpha_{\Theta ij}$ scalar factor into the G.

approach in JIMWLK parameterization results in more manageable, compact expressions. We might as well consider $\left(T_{111} \circ G^{(2;\delta)}\right)_{\boldsymbol{u}_1\boldsymbol{u}_2}(Y)$ instead of $G^{(2;\delta)}_{\boldsymbol{u}_1\boldsymbol{u}_2}(Y)$ in subsequent calculations. So, let us redefine $G^{(2;\delta)}_{\boldsymbol{u}_1\boldsymbol{u}_2}(Y)$ as $\left(T_{111} \circ G^{(2;\delta)}\right)_{\boldsymbol{u}_1\boldsymbol{u}_2}(Y)$ so that from now on, the $G^{(2;\delta)}_{\boldsymbol{u}_1\boldsymbol{u}_2}(Y)$'s we deal with now have the property of symmetry under an interchange of its coordinates.

For k=3, we have two elements for the HYPO basis for $\mathfrak{C}\left(A^{\otimes 3}\right)$ as found in Chapter 4.2: $d^{a_1a_2a_3}$ and $if^{a_1a_2a_3}$. For $d^{a_1a_2a_3}$, only the total symmetriser contributes in the sum over Θ, i and j for the term that has $d^{a_1a_2a_3}$ in $\widehat{L}^3(Y)$, which we call $\widehat{L}^{(3;d)}(Y)$. Thus, we get (using the fact that $d^{a_1a_2a_3}$ is an eigenstate of the total symmetriser with eigenvalue 1):

$$\widehat{L}^{(3;d)}(Y) = (-1)^3 \frac{1}{3!} \int\limits_{\boldsymbol{u}_1\boldsymbol{u}_2\boldsymbol{u}_3} \left(T_{111} \circ G^{(3;d)}\right)_{\boldsymbol{u}_1\boldsymbol{u}_2\boldsymbol{u}_3}(Y) d^{a_1a_2a_3} i\overline{\mathbb{V}}^{a_1}_{\boldsymbol{u}_1} i\overline{\mathbb{V}}^{a_2}_{\boldsymbol{u}_2} i\overline{\mathbb{V}}^{a_3}_{\boldsymbol{u}_3} . \tag{4.43}$$

Similarly to $\delta^{a_1a_2}$ for $k=2$, we see that the linear combination of $G^{(3;d)}_{\boldsymbol{u}_1\boldsymbol{u}_2\boldsymbol{u}_3}(Y)$'s,

$$\left(T_{111} \circ G^{(3;d)}\right)_{\boldsymbol{u}_1\boldsymbol{u}_2\boldsymbol{u}_3}(Y) ,$$

is totally symmetric about any permutations of its transverse coordinates. Therefore, similarly to $\delta^{a_1a_2}$ for $k=2$, when we apply $\widehat{L}^{(3;d)}(Y)$ on a Wilson line correlator matrix, we apply it in the form of Eq. 4.43 and exploit the symmetric properties of $\left(T_{111} \circ G^{(3;d)}\right)_{\boldsymbol{u}_1\boldsymbol{u}_2\boldsymbol{u}_3}(Y)$ to simplify the results we get for our $\mathcal{M}_Y$ matrices. Hence, we might as well again redefine $G^{(3;d)}_{\boldsymbol{u}_1\boldsymbol{u}_2\boldsymbol{u}_3}(Y)$ to be $\left(T_{111} \circ G^{(3;d)}\right)_{\boldsymbol{u}_1\boldsymbol{u}_2\boldsymbol{u}_3}(Y)$ and take $G^{(3;d)}_{\boldsymbol{u}_1\boldsymbol{u}_2\boldsymbol{u}_3}(Y)$ from now on to have the property of being totally symmetric about any interchange of its transverse coordinates.

Performing a similar analysis for $if^{a_1a_2a_3}$, we find that now, only the total anti-symmetriser contributes in the sum over Θ, i and j in the $if^{a_1a_2a_3}$ term in $\widehat{L}^3(Y)$, which we will call $\widehat{L}^{(3;f)}(Y)$. We therefore get (once again using the fact that $if^{a_1a_2a_3}$ is an eigenstate of the total anti-symmetriser with eigenvalue 1):

$$\widehat{L}^{(3;f)}(Y) = (-1)^3 \frac{1}{3!} \int\limits_{\boldsymbol{u}_1\boldsymbol{u}_2\boldsymbol{u}_3} \left(T_{311} \circ G^{(3;f)}\right)_{\boldsymbol{u}_1\boldsymbol{u}_2\boldsymbol{u}_3}(Y) if^{a_1a_2a_3} i\overline{\mathbb{V}}^{a_1}_{\boldsymbol{u}_1} i\overline{\mathbb{V}}^{a_2}_{\boldsymbol{u}_2} i\overline{\mathbb{V}}^{a_3}_{\boldsymbol{u}_3} . \tag{4.44}$$

Now we find a linear combination of G's that is anti-symmetric in that permuting its transverse coordinates incurs a minus sign depending whether the permutation is odd or even. We can of course, still exploit this property when simplifying the $\mathcal{M}_Y$ matrices we get and thus, we redefine

$$G^{(3;f)}_{\boldsymbol{u}_1\boldsymbol{u}_2\boldsymbol{u}_3}(Y)$$

to be $\left(T_{311} \circ G^{(3;f)}\right)_{\boldsymbol{u}_1\boldsymbol{u}_2\boldsymbol{u}_3}(Y)$ and take $G^{(3;f)}_{\boldsymbol{u}_1\boldsymbol{u}_2\boldsymbol{u}_3}(Y)$ from now on to have the added property of anti-symmetry about a permutation of its transverse coordinates.

To illustrate again how such a simplification can occur, consider the linear combination of $G^{(3;f)}_{\boldsymbol{u}_1\boldsymbol{u}_2\boldsymbol{u}_3}$'s:

$$G^{(3;f)}_{\boldsymbol{x}_1\boldsymbol{x}_2\boldsymbol{x}_3} + G^{(3;f)}_{\boldsymbol{x}_2\boldsymbol{x}_1\boldsymbol{x}_3} + G^{(3;f)}_{\boldsymbol{x}_3\boldsymbol{x}_2\boldsymbol{x}_1} \,.$$

Since, $G^{(3;f)}_{\boldsymbol{u}_1\boldsymbol{u}_2\boldsymbol{u}_3}$ now has the property that it is totally anti-symmetric about an interchange of coordinates, we again have that each of the terms in the linear combination expressed above is not independent. Thus, we can simplify the above expression using the anti-symmetric property of $G^{(3;f)}_{\boldsymbol{u}_1\boldsymbol{u}_2\boldsymbol{u}_3}$ as follows:

$$G^{(3;f)}_{\boldsymbol{x}_1\boldsymbol{x}_2\boldsymbol{x}_3} + \underbrace{G^{(3;f)}_{\boldsymbol{x}_2\boldsymbol{x}_1\boldsymbol{x}_3}}_{=-G^{(3;f)}_{\boldsymbol{x}_1\boldsymbol{x}_2\boldsymbol{x}_3}} + \underbrace{G^{(3;f)}_{\boldsymbol{x}_3\boldsymbol{x}_2\boldsymbol{x}_1}}_{=-G^{(3;f)}_{\boldsymbol{x}_1\boldsymbol{x}_2\boldsymbol{x}_3}} = -G^{(3;f)}_{\boldsymbol{x}_1\boldsymbol{x}_2\boldsymbol{x}_3} \,. \tag{4.45}$$

Thus, when applying $\widehat{L}^3\left(Y\right) = \widehat{L}^{(3;f)}\left(Y\right) + \widehat{L}^{(3;d)}\left(Y\right)$ to a Wilson line correlator matrix, we exploit the symmetry properties of $G^{(3;f)}_{\boldsymbol{u}_1\boldsymbol{u}_2\boldsymbol{u}_3}(Y)$ and $G^{(3;d)}_{\boldsymbol{u}_1\boldsymbol{u}_2\boldsymbol{u}_3}(Y)$ in order to simplify the $\mathcal{M}_Y$ matrices to obtain more compact and readable expressions. This is why we label each colour structure function by the adjoint colour singlet states, as these states imprint their symmetry onto the functions, leading to independent linear combinations of G's, each representing a unique degree of freedom.

Working in the HYPO basis for $\mathfrak{C}\left(A^{\otimes k}\right)$ (at least for $k = 2, 3$) benefits us because the basis elements are eigenstates of the HYPOs with eigenvalues 1 or 0 (up to normalisation). This imprints the symmetries of these color structures on the G's via Eq. 4.40, greatly simplifying the $\mathcal{M}_Y$ matrices in the parameterization equation. Using this methodology in *step 2* of the method outlined above to solve the JIMWLK equation helps us to "tame" the results we get and we shall generalize this methodology when we investigate the 4-point truncation of JIMWLK in Chapter 5.

Chapter 5

The 4-Point Truncation of JIMWLK

5.1 Generalising the parameterisation

The parameterisation scheme from [33], discussed previously, is not the most general one usable for solving the JIMWLK evolution equation while satisfying all stated properties. Indeed, one can add an extra term to Eq. 4.1 such that we still have a valid parameterisation which is given by:

$$\begin{aligned}\left\langle \widehat{LR}\,(Y)\,A\right\rangle_Y &:= \sum_{k=2}^{\infty}\sum_{l=2}^{\infty}\left\langle \widehat{LR}^{(k;l)}\,(Y)\,A\right\rangle_Y \\ &= \sum_{k=2}^{\infty}\sum_{l=2}^{\infty}\int_{\boldsymbol{u}_1\boldsymbol{u}_2\ldots\boldsymbol{u}_k\boldsymbol{v}_1\boldsymbol{v}_2\ldots\boldsymbol{v}_l} G^{((\alpha,\beta);k;l)}_{\boldsymbol{u}_1\boldsymbol{u}_2\ldots\boldsymbol{u}_k\boldsymbol{v}_1\boldsymbol{v}_2\ldots\boldsymbol{v}_l}(Y)\,\widetilde{\mathcal{M}}^{(k)}_Y\,\langle A\rangle_Y\left(\widetilde{\mathcal{M}}^{(l)}_Y\right)^t, \end{aligned} \tag{5.1}$$

where the operator $\widehat{LR}^{(k;l)}\,(Y)$ is defined as

$$\begin{aligned}\widehat{LR}^{(k;l)}\,(Y)\,[A]^i{}_j &:= \sum_{\alpha,\beta}\int_{\boldsymbol{u}_1\boldsymbol{u}_2\ldots\boldsymbol{u}_k\boldsymbol{v}_1\boldsymbol{v}_2\ldots\boldsymbol{v}_l} G^{((\alpha,\beta);k;l)}_{\boldsymbol{u}_1\boldsymbol{u}_2\ldots\boldsymbol{u}_k\boldsymbol{v}_1\boldsymbol{v}_2\ldots\boldsymbol{v}_l}(Y)\,\mathcal{C}^{a_1a_2\ldots a_k}_{\alpha}\mathcal{C}^{b_1b_2\ldots b_l}_{\beta} \\ &\quad\times i\overline{\nabla}^{a_1}_{\boldsymbol{u}_1} i\overline{\nabla}^{a_2}_{\boldsymbol{u}_2}\ldots i\overline{\nabla}^{a_k}_{\boldsymbol{u}_k} i\nabla^{b_1}_{\boldsymbol{v}_1} i\nabla^{b_2}_{\boldsymbol{v}_2}\ldots i\nabla^{b_l}_{\boldsymbol{v}_l}\end{aligned}$$

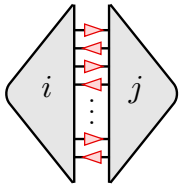

$$= \sum_{\alpha,\beta}\int_{\boldsymbol{u}_1\boldsymbol{u}_2\ldots\boldsymbol{u}_k\boldsymbol{v}_1\boldsymbol{v}_2\ldots\boldsymbol{v}_l} G^{((\alpha,\beta);k;l)}_{\boldsymbol{u}_1\boldsymbol{u}_2\ldots\boldsymbol{u}_k\boldsymbol{v}_1\boldsymbol{v}_2\ldots\boldsymbol{v}_l}(Y)\,\mathcal{C}^{a_1a_2\ldots a_k}_{\alpha}\mathcal{C}^{b_1b_2\ldots b_l}_{\beta}$$

$\times$ 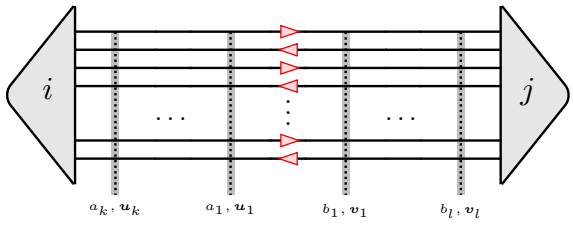

$$= \sum_{\alpha,\beta} \int_{\boldsymbol{u}_1\boldsymbol{u}_2\ldots\boldsymbol{u}_k\boldsymbol{v}_1\boldsymbol{v}_2\ldots\boldsymbol{v}_l} G^{((\alpha,\beta);k;l)}_{\boldsymbol{u}_1\boldsymbol{u}_2\ldots\boldsymbol{u}_k\boldsymbol{v}_1\boldsymbol{v}_2\ldots\boldsymbol{v}_l}(Y)\, \mathcal{C}^{a_1a_2\ldots a_k}_{\alpha} \mathcal{C}^{b_1b_2\ldots b_l}_{\beta}$$

$\times \sum_s \sum_m$ 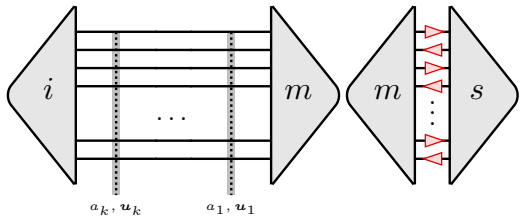

$\times$ 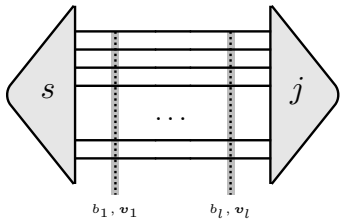

$$= \sum_{\alpha,\beta} \sum_s \sum_m \int_{\boldsymbol{u}_1\boldsymbol{u}_2\ldots\boldsymbol{u}_k\boldsymbol{v}_1\boldsymbol{v}_2\ldots\boldsymbol{v}_l} G^{((\alpha,\beta);k;l)}_{\boldsymbol{u}_1\boldsymbol{u}_2\ldots\boldsymbol{u}_k\boldsymbol{v}_1\boldsymbol{v}_2\ldots\boldsymbol{v}_l}(Y)$$

$\times\, \mathcal{C}^{a_1a_2\ldots a_k}_{\alpha}$ 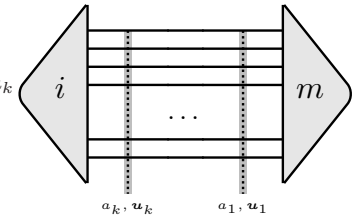

$=: \left[\widetilde{M}^{(k)}_Y\right]^i_{\ m}$

$\times$ 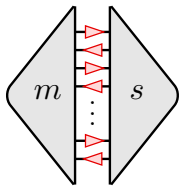

$\times\, \mathcal{C}^{b_1b_2\ldots b_l}_{\beta}$ 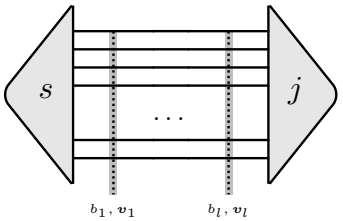

$=: \left[\left(\widetilde{M}^{(l)}_Y\right)^t\right]^s_{\ j}$

$$= \sum_{\alpha,\beta} \sum_{s} \sum_{m} \int_{\boldsymbol{u}_1\boldsymbol{u}_2\ldots\boldsymbol{u}_k\boldsymbol{v}_1\boldsymbol{v}_2\ldots\boldsymbol{v}_l} G^{((\alpha,\beta);k;l)}_{\boldsymbol{u}_1\boldsymbol{u}_2\ldots\boldsymbol{u}_k\boldsymbol{v}_1\boldsymbol{v}_2\ldots\boldsymbol{v}_l}(Y) \left[\widetilde{M}^{(k)}_Y\right]^i{}_m \left[\mathcal{A}\right]^m{}_s \times \left[\left(\widetilde{M}^{(l)}_Y\right)^t\right]^s{}_j , \tag{5.2}$$

where we have inserted a complete set of singlet states

$$\mathbb{1}_{\text{Singlet States}} = \sum_m$$

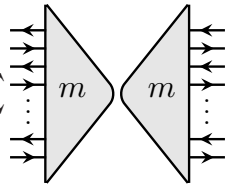

which we are allowed to do so if we choose the adjoint colour structures $\mathcal{C}^{a_1a_2\ldots a_k}_\alpha$ and $\mathcal{C}^{b_1b_2\ldots b_l}_\beta$ in our parameterisation ansatz for $\widehat{LR}(Y)$ to be colour singlet states (see the discussion in Chapter 4.1 regarding Eq. 4.16). Thus, we must have that $\mathcal{C}^{a_1a_2\ldots a_k}_\alpha \in \mathfrak{C}\left(A^{\otimes k}\right)$ and $\mathcal{C}^{b_1b_2\ldots b_l}_\beta \in \mathfrak{C}\left(A^{\otimes l}\right)$ for our definition of $\widehat{LR}^{(k;l)}(Y)$ and similarly to $\widehat{L}(Y)$ and $\widehat{R}(Y)$ in Eqs. 4.6 and 4.7, we have that the sums over α and β run over the basis elements of $\mathfrak{C}\left(A^{\otimes k}\right)$ and $\mathfrak{C}\left(A^{\otimes l}\right)$ respectively for some chosen bases. This is also a physics requirement of requiring the configuration to be colour neutral. And similarly to our definitions for $\widehat{L}(Y)$ and $\widehat{R}(Y)$, G is some yet-to-be determined colour structure function which now encodes the rapidity dependence of the Wilson line correlator.

Our new operator now has a "mixture" of left- and right-invariant vector fields as opposed to the operators in 4.6 and 4.7. Notice now that the G for these "mixed" terms is now not part of the defintion for $\widetilde{\mathcal{M}}^{(k)}_Y$ or $\widetilde{\mathcal{M}}^{(l)}_Y$.

The p-point truncation of $\widehat{LR}\,(Y)$ is defined as:

$$\widehat{LR}_p\,(Y) := \sum_{k=2}^{p} \sum_{l=2}^{p-k} \widehat{LR}^{(k;l)}\,(Y)\ . \tag{5.3}$$

The additional term in Eq. 5.1 fulfills JIMWLK parameterisation by independently evolving symmetric and anti-symmetric parts of any Wilson line correlator matrix. This is constructed in Eq. 5.1 and preserves the coincidence limit structure through left- and right-invariant vector fields. These fields are described in Eq. 2.18. All the above is achieved while keeping N_c as a parameter and maintaining validity for all finite N_c. This additional term will only appear in the 4-point truncation of the JIMWLK evolution equation since there exists no adjoint colour singlet states in $\mathfrak{C}\left(A^{\otimes 1}\right)$ and it will be given by:

$$\widehat{LR}_4\,(Y) := \sum_{k=2}^{4} \sum_{l=2}^{4-k} \widehat{LR}^{(k;l)}\,(Y)$$

$$= \widehat{LR}^{(2;2)}(Y) \quad (\text{Since } \widehat{LR}^{(1;3)}(Y) = \widehat{LR}^{(3;1)}(Y) = 0)$$
$$= \int_{\boldsymbol{u}_1\boldsymbol{u}_2\boldsymbol{v}_1\boldsymbol{v}_2} G^{((2,2);2;2)}_{\boldsymbol{u}_1\boldsymbol{u}_2\boldsymbol{v}_1\boldsymbol{v}_2}(Y)\, \delta^{a_1a_2}\delta^{b_1b_2} i\overline{\mathbb{V}}^{a_1}_{\boldsymbol{u}_1} i\overline{\mathbb{V}}^{a_2}_{\boldsymbol{u}_2} i\mathbb{V}^{b_1}_{\boldsymbol{v}_1} i\mathbb{V}^{b_2}_{\boldsymbol{v}_2}\,. \tag{5.4}$$

And therefore, the full parameterisation equation up to 4-point truncation will be:

$$\boxed{\frac{d}{dY}\langle\mathcal{A}\rangle_Y = -\underbrace{\mathcal{M}^{(4)}_Y\langle\mathcal{A}\rangle_Y}_{\langle\widehat{L}_4(Y)A\rangle_Y} + \underbrace{\langle\mathcal{A}\rangle_Y\left(-\mathcal{M}^{(4)}_Y\right)^T}_{\langle\widehat{R}_4(Y)A\rangle_Y} + \underbrace{\int_{\boldsymbol{u}_1\boldsymbol{u}_2\boldsymbol{v}_1\boldsymbol{v}_2} G^{((2,2);2;2)}_{\boldsymbol{u}_1\boldsymbol{u}_2\boldsymbol{v}_1\boldsymbol{v}_2}(Y)\,\widetilde{\mathcal{M}}^{(2)}_Y\langle A\rangle_Y\left(\widetilde{\mathcal{M}}^{(2)}_Y\right)^t}_{\langle\widehat{LR}^{(2;2)}(Y)A\rangle_Y}}. \tag{5.5}$$

However, we now have the added complication of solving this parameterisation equation as it no longer has an obvious exponential solution. To obtain an exponential solution, we need to employ a few linear algebra tools. We start by expressing the amplitude matrix in terms of a linear combination of some orthonormal basis[1] for the matrix space of $n \times n$-matrices that $\langle\mathcal{A}\rangle_Y$ lives in:

$$\begin{aligned}\frac{d}{dY}b_{(i)}\langle\mathcal{A}^i\rangle_Y &= -\mathcal{M}^{(4)}_Y b_{(i)}\langle\mathcal{A}^i\rangle_Y + b_{(i)}\langle\mathcal{A}^i\rangle_Y\left(-\mathcal{M}^{(4)}_Y\right)^T \\ &\quad + \int_{\boldsymbol{u}_1\boldsymbol{u}_2\boldsymbol{v}_1\boldsymbol{v}_2} G^{((2,2);2;2)}_{\boldsymbol{u}_1\boldsymbol{u}_2\boldsymbol{v}_1\boldsymbol{v}_2}(Y)\,\widetilde{\mathcal{M}}^{(2)}_Y b_{(i)}\langle A^i\rangle_Y\left(\widetilde{\mathcal{M}}^{(2)}_Y\right)^t \\ &= \Bigg(-\mathcal{M}^{(4)}_Y b_{(i)} + b_{(i)}\left(-\mathcal{M}^{(4)}_Y\right)^T \\ &\quad + \int_{\boldsymbol{u}_1\boldsymbol{u}_2\boldsymbol{v}_1\boldsymbol{v}_2} G^{((2,2);2;2)}_{\boldsymbol{u}_1\boldsymbol{u}_2\boldsymbol{v}_1\boldsymbol{v}_2}(Y)\,\widetilde{\mathcal{M}}^{(2)}_Y b_{(i)}\left(\widetilde{\mathcal{M}}^{(2)}_Y\right)^t\Bigg)\langle\mathcal{A}^i\rangle_Y\,,\end{aligned} \tag{5.6}$$

where the $b_{(i)}$'s form an orthonormal basis for the space of $n \times n$-matrices that $\langle\mathcal{A}\rangle_Y$ lives in. Multiplying both sides of Eq. 5.6 by $\left(b^{(j)}\right)^t$ where $b^{(j)}$ is some other basis element and taking the trace on both sides, we obtain an inner product on both sides:

$$\begin{aligned}&\frac{d}{dY}\langle b^{(j)}|b_{(i)}\rangle\langle\mathcal{A}^i\rangle_Y = \Bigg\langle b^{(j)}\Bigg|\Bigg(-\mathcal{M}^{(4)}_Y b_{(i)} + b_{(i)}\left(-\mathcal{M}^{(4)}_Y\right)^T \\ &\underbrace{+\int_{\boldsymbol{u}_1\boldsymbol{u}_2\boldsymbol{v}_1\boldsymbol{v}_2} G^{((2,2);2;2)}_{\boldsymbol{u}_1\boldsymbol{u}_2\boldsymbol{v}_1\boldsymbol{v}_2}(Y)\,\widetilde{\mathcal{M}}^{(2)}_Y b_{(i)}\left(\widetilde{\mathcal{M}}^{(2)}_Y\right)^t\Bigg)\Bigg\rangle}_{:=\varepsilon^{(j)}{}_{(i)}(Y)}\langle\mathcal{A}^i\rangle_Y \\ &\implies \frac{d}{dY}\delta^{(j)}{}_{(i)}\langle\mathcal{A}^i\rangle_Y = \varepsilon^{(j)}{}_{(i)}(Y)\langle\mathcal{A}^i\rangle_Y\end{aligned}$$

[1] Orthonormal with respect to the inner product on the vector space of $n \times n$ matrices. See Eq. 3.17 for a defintion.

$$\implies \boxed{\frac{d}{dY}\langle \mathcal{A}^j\rangle_Y = \varepsilon^{(j)}{}_{(i)}(Y)\langle \mathcal{A}^i\rangle_Y}. \tag{5.7}$$

Equation 5.7 now permits an exponential solution. Thus, in order to obtain a solution to the parameterisation equation for the 4-point truncation, one needs to choose an orthonormal basis for $\langle \mathcal{A}\rangle_Y$ in order to find the exponentiating matrix, $\varepsilon^{(j)}{}_{(i)}(Y)$. We should emphasise that Eq. 5.6 has an implicit solution in-terms of the colour structure functions, the G's, which then need to be determined via the JIMWLK evolution equation.

Since JIMWLK respects the symmetry of $\langle \mathcal{A}\rangle_Y$, if one were to choose the basis of symmetric and anti-symmetric matrices for $\langle \mathcal{A}\rangle_Y$, the exponentiating matrix $\varepsilon^{(j)}{}_{(i)}(Y)$ would end up being block diagonal. Such a basis may prove to be useful when trying to simplify the evolution equations such that it may be easier to solve (numerically).

5.2 Obtaining a useful basis for $\mathfrak{C}\left(A^{\otimes 4}\right)$

With the 4-point truncation, our focus is on new information from 4-point functions, the 4-point G's. The parameterisation equation will also feature other forms of 4-point functions. Matrix exponentiation results in the square of the Gaussian truncation in the Taylor series, introducing 4-point functions as products of 2-point functions. Already well-understood, the Gaussian truncation squared provides known information and it is reasonable to think it overlaps with the 4-point truncation due to the colour adjoint singlet state being an element of $\mathfrak{C}\left(A^{\otimes 4}\right)$. To illustrate this, let's compute the Gaussian truncation squared[2]:

$$\begin{aligned}
&\widehat{L}_2(Y)+\widehat{R}_2(Y) = \int\limits_{\boldsymbol{u}_1\boldsymbol{u}_2} G^{(2;\delta)}_{\boldsymbol{u}_1\boldsymbol{u}_2}(Y)\delta^{a_1a_2}\left(\nabla^{a_1}_{\boldsymbol{u}_1}\nabla^{a_2}_{\boldsymbol{u}_2}+\overline{\nabla}^{a_1}_{\boldsymbol{u}_1}\overline{\nabla}^{a_2}_{\boldsymbol{u}_2}\right)\\
&\implies \left(\widehat{L}_2(Y)+\widehat{R}_2(Y)\right)^2 = \left(\int\limits_{\boldsymbol{u}_1\boldsymbol{u}_2} G^{(2;\delta)}_{\boldsymbol{u}_1\boldsymbol{u}_2}(Y)\delta^{a_1a_2}\left(\nabla^{a_1}_{\boldsymbol{u}_1}\nabla^{a_2}_{\boldsymbol{u}_2}+\overline{\nabla}^{a_1}_{\boldsymbol{u}_1}\overline{\nabla}^{a_2}_{\boldsymbol{u}_2}\right)\right)^2\\
&\implies \left(\widehat{L}_2(Y)+\widehat{R}_2(Y)\right)^2 = \int\limits_{\boldsymbol{u}_1\boldsymbol{u}_2\boldsymbol{u}_3\boldsymbol{u}_4} G^{(2;\delta)}_{\boldsymbol{u}_1\boldsymbol{u}_2}(Y)G^{(2;\delta)}_{\boldsymbol{u}_3\boldsymbol{u}_4}(Y)\delta^{a_1a_2}\delta^{a_3a_4}\Big(\nabla^{a_1}_{\boldsymbol{u}_1}\nabla^{a_2}_{\boldsymbol{u}_2}\nabla^{a_3}_{\boldsymbol{u}_3}\nabla^{a_4}_{\boldsymbol{u}_4}\\
&+\nabla^{a_1}_{\boldsymbol{u}_1}\nabla^{a_2}_{\boldsymbol{u}_2}\overline{\nabla}^{a_3}_{\boldsymbol{u}_3}\overline{\nabla}^{a_4}_{\boldsymbol{u}_4}+\overline{\nabla}^{a_1}_{\boldsymbol{u}_1}\overline{\nabla}^{a_2}_{\boldsymbol{u}_2}\nabla^{a_3}_{\boldsymbol{u}_3}\nabla^{a_4}_{\boldsymbol{u}_4}+\overline{\nabla}^{a_1}_{\boldsymbol{u}_1}\overline{\nabla}^{a_2}_{\boldsymbol{u}_2}\overline{\nabla}^{a_3}_{\boldsymbol{u}_3}\overline{\nabla}^{a_4}_{\boldsymbol{u}_4}\Big).
\end{aligned} \tag{5.8}$$

The color adjoint singlet state of the Gaussian truncation squared is $\delta^{a_1a_2}\delta^{a_3a_4}$ within $\mathfrak{C}\left(A^{\otimes 4}\right)$. This suggests an overlap between the Gaussian truncation squared and the 4-point truncation, with the latter containing elements of the former. Given our understanding of

[2] We abuse notation slightly here by squaring and multiplying the operators defined in Eq. 4.18

the Gaussian truncation, we aim to subtract its known information from the 4-point truncation to uncover new insights in the 4-point functions. This is analogous to how disconnected diagrams are subtracted off in calculating a total cross section from a generating functional in quantum field theory. In that calculation, vacuum diagrams cancel out and do not contribute to the cross-section; see [4, 34, 49] and other quantum field theory textbooks for an exposition on this. To try and distinguish components of the 4-point truncation mapping to the Gaussian truncation squared, it is practical to build a basis for $\mathfrak{C}\left(A^{\otimes 4}\right)$ that clarifies this correspondence.

To that end, consider the HYPO basis for $\mathfrak{C}\left(A^{\otimes 4}\right)$ as given in Eq. A.4.A straightforward method to orthogonalise this basis is to apply the Gram-Schmidt procedure to each of the three 2-dimensional subspaces spanned by the non-orthogonal elements of the HYPO basis. Although this would be viable, we can do this in such a way that we construct this basis so that the parts that map to $\delta^{a_1a_2}\delta^{a_3a_4}$ from the squared Gaussian truncation are separated and isolated. Taking an inner product for $\delta^{a_1a_2}\delta^{a_3a_4}$ from the Gaussian truncation squared with all the basis elements in Eq. A.4, we get that there is a non-zero overlap with 4 of the nine basis elements in Eq. A.4, namely:

$$\begin{aligned}
\langle \delta^{a_1a_2}\delta^{a_3a_4} | \mathcal{C}_1^{a_1a_2a_3a_4} \rangle &= \frac{2N^4 - 5N^2 + 3}{8N} \\
\langle \delta^{a_1a_2}\delta^{a_3a_4} | \mathcal{C}_2^{a_1a_2a_3a_4} \rangle &= \frac{1}{16}\left(N^4 - 1\right) \\
\langle \delta^{a_1a_2}\delta^{a_3a_4} | \mathcal{C}_3^{a_1a_2a_3a_4} \rangle &= \frac{1}{4}N\left(N^2 - 1\right) \\
\langle \delta^{a_1a_2}\delta^{a_3a_4} | \mathcal{C}_4^{a_1a_2a_3a_4} \rangle &= \frac{1}{8}\left(-N^4 + 3N^2 - 2\right) \ .
\end{aligned} \tag{5.9}$$

Returning briefly to the original HYPO notation using Young tableaux, observe that $\mathcal{C}_1^{a_1a_2a_3a_4}$ and $\mathcal{C}_2^{a_1a_2a_3a_4}$ are in the 2-dimensional subspace projected out by $P_{\boxed{1}\boxed{2}\boxed{3}\boxed{4}}$ and $\mathcal{C}_3^{a_1a_2a_3a_4}$ and $\mathcal{C}_4^{a_1a_2a_3a_4}$ are in the 2-dimensional subspace projected out by $P_{\begin{smallmatrix}\boxed{1}\boxed{2}\\ \boxed{3}\boxed{4}\end{smallmatrix}}$.

For the sake of brevity, we shall refer to the subspaces projected out by the HYPOs by their Young tableau from now on, e.g. the subspace projected out by $P_{\boxed{1}\boxed{2}\boxed{3}\boxed{4}}$ will now be referred to as the $\boxed{1}\boxed{2}\boxed{3}\boxed{4}$ subspace. Thus, we have that $\delta^{a_1a_2}\delta^{a_3a_4}$ has a piece in both the $\boxed{1}\boxed{2}\boxed{3}\boxed{4}$ subspace and the $\begin{smallmatrix}\boxed{1}\boxed{2}\\ \boxed{3}\boxed{4}\end{smallmatrix}$ subspace. We can therefore consider the piece of $\delta^{a_1a_2}\delta^{a_3a_4}$ that live in the $\boxed{1}\boxed{2}\boxed{3}\boxed{4}$ subspace and the $\begin{smallmatrix}\boxed{1}\boxed{2}\\ \boxed{3}\boxed{4}\end{smallmatrix}$ subspace which will be given by the projections of $\delta^{a_1a_2}\delta^{a_3a_4}$ onto these subspaces

$$P_{\boxed{1}\boxed{2}\boxed{3}\boxed{4}} \circ \delta^{a_1a_2}\delta^{a_3a_4} = \frac{1}{3}\left(\mathrm{tr}\left(t^{a_1}t^{a_4}\right)\mathrm{tr}\left(t^{a_2}t^{a_3}\right) + \mathrm{tr}\left(t^{a_1}t^{a_3}\right)\mathrm{tr}\left(t^{a_2}t^{a_4}\right) + \mathrm{tr}\left(t^{a_1}t^{a_2}\right)\mathrm{tr}\left(t^{a_3}t^{a_4}\right)\right)$$

$$P_{\begin{array}{|c|c|}\hline 1&2\\\hline 3&4\\\hline\end{array}}\circ\delta^{a_1a_2}\delta^{a_3a_4}=\frac{1}{3}\left(-\mathrm{tr}\left(t^{a_1}t^{a_4}\right)\mathrm{tr}\left(t^{a_2}t^{a_3}\right)-\mathrm{tr}\left(t^{a_1}t^{a_3}\right)\mathrm{tr}\left(t^{a_2}t^{a_4}\right)+2\mathrm{tr}\left(t^{a_1}t^{a_2}\right)\mathrm{tr}\left(t^{a_3}t^{a_4}\right)\right). \tag{5.10}$$

and use these projections as a starting point for the Gram-Schmidt orthogonalization procedure for each of the 2 subspaces in question to form a basis where 2 of the elements linearly span $\delta^{a_1a_2}\delta^{a_3a_4}$ and the other 7 are orthogonal to $\delta^{a_1a_2}\delta^{a_3a_4}$. This new basis is given in Appendix A in Eq. A.5.

Using this basis for our 4-point truncation means that we have explicitly separated out the parts of the 4-point truncation that overlap with the Gaussian truncation squared and the parts that do not by orthogonality of the colour adjoint singlet states. The basis given in Eq. A.5 is still not fully orthogonal. Of course, one can again apply the Gram-Schmidt procedure for the $\begin{array}{|c|c|}\hline 1&3\\\hline 3&4\\\hline\end{array}$ subspace (the subspace that was not orthogonalized previously), and this would be viable since we have already separated and isolated the pieces that map onto $\delta^{a_1a_2}\delta^{a_3a_4}$. Although we can do better, and to do so, we employ the HYPOs and transition operators from $\mathfrak{G}_4$.

Recall the multiplication table for projection and transition operators in Eq. 3.77. If one were to act the transition operator, $T_{\begin{array}{|c|c|}\hline 1&3\\\hline 2&4\\\hline\end{array}\leftarrow\begin{array}{|c|c|}\hline 1&2\\\hline 3&4\\\hline\end{array}}$, on an element of $\mathfrak{C}\left(A^{\otimes 4}\right)$ living in the $\begin{array}{|c|c|}\hline 1&2\\\hline 3&4\\\hline\end{array}$ subspace, the result would be an element in the $\begin{array}{|c|c|}\hline 1&3\\\hline 2&4\\\hline\end{array}$ subspace and similarly for $T_{\begin{array}{|c|c|}\hline 1&2\\\hline 3&4\\\hline\end{array}\leftarrow\begin{array}{|c|c|}\hline 1&3\\\hline 2&4\\\hline\end{array}}$. For example, we get that:

$$T_{\begin{array}{|c|c|}\hline 1&2\\\hline 3&4\\\hline\end{array}\leftarrow\begin{array}{|c|c|}\hline 1&3\\\hline 2&4\\\hline\end{array}}\circ\underbrace{\mathcal{C}_5^{a_1a_2a_3a_4}}_{\text{Element of }\begin{array}{|c|c|}\hline 1&3\\\hline 2&4\\\hline\end{array}\text{ subspace}}=\underbrace{\mathcal{C}_3^{a_1a_2a_3a_4}}_{\text{Element of }\begin{array}{|c|c|}\hline 1&2\\\hline 3&4\\\hline\end{array}\text{ subspace}}, \tag{5.11}$$

where $\mathcal{C}_5^{a_1a_2a_3a_4}$ and $\mathcal{C}_3^{a_1a_2a_3a_4}$ are the basis elements given in Eq. A.4.

In general, acting $T_{\Theta ij}$ on $\mathcal{C}\in\mathfrak{C}\left(A^{\otimes 4}\right)$ yields an element $\mathcal{C}_{\Theta i}$, where $\mathcal{C}_{\Theta i}$ belongs to the i subspace (with Θ as the Young diagram of i), using the notation for HYPOs and transition operators in Eq. 3.70 for adjoint colour singlet states.

Thus, the transition operators between the $\begin{array}{|c|c|}\hline 1&2\\\hline 3&4\\\hline\end{array}$ and $\begin{array}{|c|c|}\hline 1&3\\\hline 2&4\\\hline\end{array}$ subspaces form a linear map between the two subspaces in a linear algebra sense. Recall that if we have two vector spaces V and W each with dimension n and m respectively and a basis given by $\mathcal{B}_V=\{v_1,v_2,...,v_n\}$ and $\mathcal{B}_W=\{w_1,w_2,...,w_m\}$, then the matrix of the linear map $L:V\to W$ with respect to the bases $\mathcal{B}_V$ and $\mathcal{B}_W$ is given by an $m\times n$ matrix where its columns are the coordinates of the vectors $L(v_1),L(v_2),...,L(v_n)$ with respect to the basis of W, $\mathcal{B}_W$. If $L_{\mathcal{B}_W}^{\mathcal{B}_V}$ denotes the

matrix of L relative to $\mathcal{B}_V$ and $\mathcal{B}_W$, then:

$$L^{\mathcal{B}_V}_{\mathcal{B}_W} = \left([L(v_1)]_{\mathcal{B}_W}, [L(v_2)]_{\mathcal{B}_W}, ..., [L(v_n)]_{\mathcal{B}_W} \right) . \tag{5.12}$$

Therefore, we want to design a basis for $\mathfrak{C}\left(A^{\otimes 4}\right)$ to map subspace elements using transition operators within the same subalgebra in this way. This basis, $\left\{ \left(\mathcal{C}^{(k)}_{\Theta i} \right)^{a_1 a_2 a_3 a_4} \right\}$, involves Θ as the Young diagram, i as the Young tableau, and (k) as an index for specific basis elements in the subspace projected by the HYPO, $T_{\Theta ii}$. The basis element $\left(\mathcal{C}^{(k)}_{\Theta i} \right)^{a_1 a_2 a_3 a_4}$ belongs to the i subspace, defined by Θ as the underlying Young diagram for i, and is a basis element of i. We follow the notation from Eq. 3.70 regarding HYPOs and transition operators for the new basis of adjoint color singlet states, aiming for the basis $\left\{ \left(\mathcal{C}^{(k)}_{\Theta i} \right)^{a_1 a_2 a_3 a_4} \right\}$ to meet the following property:

$$\boxed{\left(T_{\Xi lm} \circ \mathcal{C}^{(k)}_{\Theta i} \right)^{a_1 a_2 a_3 a_4} = \delta_{\Xi\Theta} \delta_{mi} \left(\mathcal{C}^{(k)}_{\Theta l} \right)^{a_1 a_2 a_3 a_4}} . \tag{5.13}$$

The explicit elements of this basis for $\mathfrak{C}\left(A^{\otimes 4}\right)$ is given by Eq. A.8 and one can check that this basis is fully orthonormal as well. We employ the basis in Eq. A.8 for the 4-point truncation, as the basis elements map onto each other nicely via transition operators; the elements that overlap with the Gaussian truncation squared are separated out which may make subtracting off the Gaussian truncation squared easier.

5.3 Taming the evolution equations

We now proceed with the derivation of the $\mathcal{M}^{(4)}_Y$ and $\widetilde{\mathcal{M}}^{(2)}_Y$ matrices in Eq. 5.5 in order to solve the parameterization equation in Eq. 5.5. Subsequently, this solution is substituted into the JIMWLK evolution equation in Eq. 4.32, facilitating the resolution of the various 4-point functions.

To start, notice that $\mathcal{M}^{(4)}_Y$ comes from the Gaussian and 3-point truncations as well as the 4-point truncation:

$$\begin{aligned} \mathcal{M}^{(4)}_Y \langle \mathcal{A} \rangle_Y &:= \left\langle \widehat{L}_4(Y) A \right\rangle_Y \\ &= \left\langle \widehat{L}^2(Y) A \right\rangle_Y + \left\langle \widehat{L}^3(Y) A \right\rangle_Y + \left\langle \widehat{L}^4(Y) A \right\rangle_Y \\ &= \mathcal{M}^{(\text{2-pt})}_Y \langle \mathcal{A} \rangle_Y + \mathcal{M}^{(\text{3-pt})}_Y \langle \mathcal{A} \rangle_Y + \mathcal{M}^{(\text{4-pt})}_Y \langle \mathcal{A} \rangle_Y , \end{aligned} \tag{5.14}$$

where we have introduced the new notation

$$\mathcal{M}^{(p\text{-pt})}_Y \langle \mathcal{A} \rangle_Y := \left\langle \widehat{L}^p(Y) A \right\rangle_Y . \tag{5.15}$$

In [39], it was shown that the contribution from the 3-point truncation, known as the Odderon term, is purely imaginary and parity odd in the transverse plane. As such, its contribution to the total cross sections in DIS, which averages over all directions in the transverse plane will be zero. Since these are the observables we are primarily interested in, we find it prudent to set the Odderon contribution to zero. However, it should be noted that one would need to account for the Odderon contribution for experiments that are sensitive to parity, such as measuring a spin asymmetry in STSA [39]. Our analysis will therefore simplify to focus only on the Gaussian and 4-point truncations. Equation 5.14 becomes:

$$\mathcal{M}_Y^{(4)}\langle\mathcal{A}\rangle_Y = \mathcal{M}_Y^{(2\text{-pt})}\langle\mathcal{A}\rangle_Y + \mathcal{M}_Y^{(4\text{-pt})}\langle\mathcal{A}\rangle_Y\,. \tag{5.16}$$

The $\mathcal{M}_Y^{(2\text{-pt})}\langle\mathcal{A}\rangle_Y$-matrix is obtained by acting the Gaussian truncation on the amplitude matrix $\langle\mathcal{A}\rangle_Y$

$$\mathcal{M}_Y^{(2\text{-pt})}\,\langle\mathcal{A}\rangle_Y = \left\langle \int\limits_{\boldsymbol{u}_1\boldsymbol{u}_2} i\overline{\mathbb{V}}^{a_1}_{\boldsymbol{u}_1}\overline{\mathbb{V}}^{a_2}_{\boldsymbol{u}_2}\delta^{a_1a_2}G^{(2;\delta)}_{\boldsymbol{u}_2\boldsymbol{u}_2}(Y)\mathcal{A}\right\rangle_Y\,, \tag{5.17}$$

and the $\mathcal{M}_Y^{(4\text{-pt})}\langle\mathcal{A}\rangle_Y$-matrix is obtained by

$$\begin{aligned}\mathcal{M}_Y^{(4\text{-pt})}\,\langle\mathcal{A}\rangle_Y = \Bigg\langle \int\limits_{\boldsymbol{u}_2\boldsymbol{u}_2\boldsymbol{u}_3\boldsymbol{u}_4} \sum_{\theta ik}\sum_{\Xi lm}\left(T_{\Xi lm}\circ\mathcal{C}^{(k)}_{\theta i}\right)^{a_1a_2a_3a_4}\left(T_{\Xi lm}\circ G^{\left(\mathcal{C}^{(k)}_{\theta i}\right)}\right)_{\boldsymbol{u}_2\boldsymbol{u}_2\boldsymbol{u}_3\boldsymbol{u}_4}(Y)\\ \times\overline{\mathbb{V}}^{a_1}_{\boldsymbol{u}_1}\overline{\mathbb{V}}^{a_2}_{\boldsymbol{u}_2}\overline{\mathbb{V}}^{a_3}_{\boldsymbol{u}_3}\overline{\mathbb{V}}^{a_4}_{\boldsymbol{u}_4}\mathcal{A}\Bigg\rangle_Y\,,\end{aligned} \tag{5.18}$$

where we have chosen the basis given in Eq. A.8 for $\mathfrak{C}\left(A^{\otimes 4}\right)$ in the 4-point truncation.

Our main goal now is this: **to obtain the JIMWLK evolution equation for the $\left\langle\mathcal{A}^{(2)}_{\vec{\boldsymbol{x}};\vec{\boldsymbol{y}}}\right\rangle(Y)$ correlator matrix up to 4-point truncation and then solve for the various G's**. To do so, we need employ the steps outlined in Chapter 4.3:

1. Construct the $\mathcal{A}^{(3)}_{\vec{\boldsymbol{x}};\vec{\boldsymbol{y}}}(Y)$ correlator matrix using a suitable basis.

2. Apply the 4-point truncation on the $\mathcal{A}^{(3)}_{\vec{\boldsymbol{x}};\vec{\boldsymbol{y}}}(Y)$ correlator matrix to obtain the $\mathcal{M}_Y$ and $\widetilde{\mathcal{M}}_Y$ matrices.

3. Take a quark/anti-quark coicindence limit to obtain the parameterisation equation for the $\left\langle\mathcal{A}^{(2;g)}_{\vec{\boldsymbol{x}};\vec{\boldsymbol{y}};\boldsymbol{z}}\right\rangle(Y)$ correlator matrix, as this matrix feeds the JIMWLK evolution of the $\left\langle\mathcal{A}^{(2)}_{\vec{\boldsymbol{x}};\vec{\boldsymbol{y}}}\right\rangle(Y)$ correlator matrix, and the parameterisation equation of the $\left\langle\mathcal{A}^{(2)}_{\vec{\boldsymbol{x}};\vec{\boldsymbol{y}}}\right\rangle(Y)$ correlator matrix.

4. Solve the parameterisation equations for these correlator matrices using Eq. 5.7 (as there is now an additional term introduced by the operator in Eq. 5.4).

5. Substitute these solutions into Eq. 4.32 to obtain the JIMWLK evolution equation for the $\left\langle \mathcal{A}^{(2)}_{\vec{\boldsymbol{x}};\vec{\boldsymbol{y}}} \right\rangle (Y)$ correlator matrix.
6. Select valid initial conditions for the correlator matrices and then solve the integro-differential equations for the G's, numerically or otherwise.

Since Eq. 4.32 only applies to correlator matrices constructed in the Fierz basis, it is most convenient to do *step 1* by constructing our amplitude matrix, $\mathcal{A}^{(3)}_{\vec{\boldsymbol{x}};\vec{\boldsymbol{y}}}(Y)$, in the Fierz basis, i.e., to use Eq. 3.90 for $\mathcal{A}^{(3)}_{\vec{\boldsymbol{x}};\vec{\boldsymbol{y}}}(Y)$. Performing *step 2* now, we apply the 4-point truncation to our $\mathcal{A}^{(3)}_{\vec{\boldsymbol{x}};\vec{\boldsymbol{y}}}(Y)$ matrix to obtain $\mathcal{M}^{(4)}_Y$ via Eqs. 5.17 and 5.18. Afterwards, we apply *step 3* and take a quark/anti-quark coincidence limit to obtain the parameterisation equations for $\left\langle \mathcal{A}^{(2;g)}_{\vec{\boldsymbol{x}};\vec{\boldsymbol{y}};\boldsymbol{z}} \right\rangle (Y)$ and $\left\langle \mathcal{A}^{(2)}_{\vec{\boldsymbol{x}};\vec{\boldsymbol{y}}} \right\rangle (Y)$. We then solve the parameterisation equations (*step 4*) and substitute them into Eq. 4.32 (*step 5*).

Solving for the G's in *step 6*, even numerically, is unwieldy due to repeated arguments in G's like $G^{\left(\mathcal{C}^{(1)}_{11}\right)}_{\boldsymbol{x}_1\boldsymbol{x}_1\boldsymbol{x}_1\boldsymbol{y}_2}$. This repetition of arguments hinders deriving an update equation for the JIMWLK evolution of G's, necessary for solving the G's numerically. Repeated arguments in G's thus further complicate the issue; one that needs to be overcome to have any hope of solving for the G's.

A significant problem arises when solving for the G's: for the 4-point truncation, there are 11 distinct G's to address,

- **Nine** from $\mathcal{M}^{(4\text{-pt})}_Y$ in Eq. 5.18 as there is a distinct G for each $\mathcal{C}^{(k)}_{\theta i}$ and there are nine $\mathcal{C}^{(k)}_{\theta i}$'s in total (since they are basis elements which span $\mathfrak{C}\left(A^{\otimes 4}\right)$).
- **One** from the Gaussian truncation: $G^{(2;\delta)}_{\boldsymbol{u}_1\boldsymbol{u}_2}(Y)$.
- **One** from $\widetilde{M}^{(2)}_Y$: $G^{((2,2);2;2)}_{\boldsymbol{u}_1\boldsymbol{u}_2\boldsymbol{v}_1\boldsymbol{v}_2}(Y)$.

The JIMWLK evolution equation for the $\left\langle \mathcal{A}^{(2)}_{\vec{\boldsymbol{x}};\vec{\boldsymbol{y}}} \right\rangle (Y)$ amplitude matrix results in 4 integro-differential equations (as $\left\langle \mathcal{A}^{(2)}_{\vec{\boldsymbol{x}};\vec{\boldsymbol{y}}} \right\rangle (Y)$ is a 2-by-2 matrix). Thus, it's impossible to resolve 11 degrees of freedom, the G's, with just 4 equations.
Furthermore, after conducting *step 5*, we found that certain G's remain unsolvable, even without the issue of excess degrees of freedom. This is because the LHS integro-differential equation (Eq. 4.32) yields a G with a maximum of 3 distinct coordinates, while the RHS yields a G with all 4 coordinates. This occurs with the G's related to the colour adjoint singlet states of the 1-dimensional subspaces, described by the Young diagram $\begin{array}{|c|c|}\hline \multicolumn{1}{|c}{} & \multicolumn{1}{c|}{} \\ \hline \multicolumn{1}{|c}{} \\ \cline{1-1} \multicolumn{1}{|c}{} \\ \cline{1-1} \end{array} = 4$. Therefore, the G's:,

- $G^{\left(\mathcal{C}^{(1)}_{41}\right)}_{\boldsymbol{u}_1\boldsymbol{u}_2\boldsymbol{u}_3\boldsymbol{u}_4}(Y)$

- $G^{\left(\mathcal{C}^{(1)}_{42}\right)}_{\boldsymbol{u}_1\boldsymbol{u}_2\boldsymbol{u}_3\boldsymbol{u}_4}(Y)$
- $G^{\left(\mathcal{C}^{(1)}_{43}\right)}_{\boldsymbol{u}_1\boldsymbol{u}_2\boldsymbol{u}_3\boldsymbol{u}_4}(Y)$

are unsolvable.
We need a larger Wilson line correlator matrix with more than three $q\overline{q}$-pairs to address the imbalance between degrees of freedom and integro-differential equations. Creating this matrix and applying the 4-point truncation to it requires more computing power than a standard laptop can provide, preventing us from proceeding further.

Nevertheless, let us simplify the 4-point truncation in a meaningful way to create a more accessible version before addressing the more complex problem. To that end, we focus now on the parts of the 4-point truncation that might align with the Gaussian truncation squared, as we believe they contain overlapping information and we want to develop an algorithm to subtract off the Gaussian truncation squared. Therefore, it is worthwhile to explore terms that have potential overlap with the Gaussian truncation squared and investigate whether one can precisely subtract off this repeated information in some meaningful way. To do so, we "turn off" terms in the 4-point truncation that don't map onto $\delta^{a_1a_2}\delta^{a_3a_4}$ from the Gaussian truncation squared. This means that in Eq. 5.18, terms that have a color adjoint singlet state in $\mathfrak{C}\left(A^{\otimes 4}\right)$ which have an inner product of 0 with $\delta^{a_1a_2}\delta^{a_3a_4}$ are set to 0. So for example, since

$$\left\langle \mathcal{C}^{(1)}_{41} | \delta^{a_1a_2}\delta^{a_3a_3} \right\rangle = 0\,, \tag{5.19}$$

we will discard the

$$\left(T_{\Xi lm}\circ\mathcal{C}^{(1)}_{41}\right)^{a_1a_2a_3a_4}\left(T_{\Xi lm}\circ G^{\left(\mathcal{C}^{(1)}_{41}\right)}\right)_{\boldsymbol{u}_2\boldsymbol{u}_2\boldsymbol{u}_3\boldsymbol{u}_4}(Y)$$

term in Eq. 5.18. As a reminder for numerical assignment for the Young diagrams and tableaux:

For Young diagrams with 4 boxes:

- $\square\square\square\square \to 1$
  - $\boxed{1}\boxed{2}\boxed{3}\boxed{4} \to 1$
- $\begin{array}{|c|c|c|}\hline &&\\\hline \\\cline{1-1}\end{array} \to 2$
  - $\begin{array}{|c|c|c|}\hline 1&3&4\\\hline 2\\\cline{1-1}\end{array} \to 3$
  - $\begin{array}{|c|c|c|}\hline 1&2&4\\\hline 3\\\cline{1-1}\end{array} \to 2$

- $\begin{array}{|c|c|c|}\hline 1&2&3\\\hline 4\\\cline{1-1}\end{array} \to 1$

- $\begin{array}{|c|c|}\hline \ &\ \\\hline \ &\ \\\hline\end{array} \to 3$
  - $\begin{array}{|c|c|}\hline 1&3\\\hline 2&4\\\hline\end{array} \to 2$
  - $\begin{array}{|c|c|}\hline 1&2\\\hline 3&4\\\hline\end{array} \to 1$

- $\begin{array}{|c|c|}\hline \ &\ \\\hline \ \\\cline{1-1} \ \\\cline{1-1}\end{array} \to 4$
  - $\begin{array}{|c|c|}\hline 1&4\\\hline 2\\\cline{1-1} 3\\\cline{1-1}\end{array} \to 3$
  - $\begin{array}{|c|c|}\hline 1&3\\\hline 2\\\cline{1-1} 4\\\cline{1-1}\end{array} \to 2$
  - $\begin{array}{|c|c|}\hline 1&2\\\hline 3\\\cline{1-1} 4\\\cline{1-1}\end{array} \to 1$

- $\begin{array}{|c|}\hline \ \\\hline \ \\\hline \ \\\hline \ \\\hline\end{array} \to 5$
  - $\begin{array}{|c|}\hline 1\\\hline 2\\\hline 3\\\hline 4\\\hline\end{array} \to 1$

This will only leave us with 2 terms in Eq. 5.18. Since $\delta^{a_1a_2}\delta^{a_3a_4}$ is a linear combination of $\mathcal{C}_{11}^{(1)}$ and $\mathcal{C}_{31}^{(1)}$ as shown in

$$\delta^{a_1a_2}\delta^{a_3a_4} = \alpha_1\mathcal{C}_{11}^{(1)} + \alpha_2\mathcal{C}_{31}^{(1)}\,, \tag{5.20}$$

with constants α_1 and α_2, we multiply the remaining two terms in the 4-point truncation by the scalars α_1 or α_2 to try and directly compare with the Gaussian truncation squared. We are allowed to do this since any such constants can always be absorbed into the G's. Thus, the 4-point truncation reduces to just two terms:

$$\begin{aligned}\mathcal{M}_Y^{(4\text{-pt})}\langle\mathcal{A}\rangle_Y = \Bigg\langle \int_{\boldsymbol{u}_2\boldsymbol{u}_2\boldsymbol{u}_3\boldsymbol{u}_4} \Bigg(&\sum_{\Xi lm}\left(T_{\Xi lm}\circ\mathcal{C}_{11}^{(1)}\right)^{a_1a_2a_3a_4}\left(T_{\Xi lm}\circ G^{\left(\mathcal{C}_{11}^{(1)}\right)}\right)_{\boldsymbol{u}_2\boldsymbol{u}_2\boldsymbol{u}_3\boldsymbol{u}_4}(Y)\\ &+\sum_{\Xi lm}\left(T_{\Xi lm}\circ\mathcal{C}_{31}^{(1)}\right)^{a_1a_2a_3a_4}\left(T_{\Xi lm}\circ G^{\left(\mathcal{C}_{31}^{(1)}\right)}\right)_{\boldsymbol{u}_2\boldsymbol{u}_2\boldsymbol{u}_3\boldsymbol{u}_4}(Y)\Bigg)\\ &\times\overline{\mathbb{V}}^{a_1}_{\boldsymbol{u}_1}\overline{\mathbb{V}}^{a_2}_{\boldsymbol{u}_2}\overline{\mathbb{V}}^{a_3}_{\boldsymbol{u}_3}\overline{\mathbb{V}}^{a_4}_{\boldsymbol{u}_4}\mathcal{A}\Bigg\rangle_Y .\end{aligned} \tag{5.21}$$

In-what follows, we shall relabel the distinct multiplet G's in the 4-point truncation, $G^{\left(\mathcal{C}_{11}^{(1)}\right)}_{\boldsymbol{u}_2\boldsymbol{u}_2\boldsymbol{u}_3\boldsymbol{u}_4}(Y)$ and $G^{\left(\mathcal{C}_{31}^{(1)}\right)}_{\boldsymbol{u}_2\boldsymbol{u}_2\boldsymbol{u}_3\boldsymbol{u}_4}(Y)$, to $G^{(11)}_{\boldsymbol{u}_2\boldsymbol{u}_2\boldsymbol{u}_3\boldsymbol{u}_4}(Y)$ and $G^{(31)}_{\boldsymbol{u}_2\boldsymbol{u}_2\boldsymbol{u}_3\boldsymbol{u}_4}(Y)$ respectively for the sake of notational brevity. It should also be noted that there is another term in the 4-point truncation that may map onto the Gaussian truncation squared and that is the $\widetilde{\mathcal{M}}_Y^{(2)}\langle A\rangle_Y\left(\widetilde{\mathcal{M}}_Y^{(2)}\right)^t$-term in Eq. 5.5.

Thus, we have 4 distinct multiplet G's to solve for from the JIMWLK evolution equation for the $\left\langle \mathcal{A}^{(2)}_{\vec{\boldsymbol{x}};\vec{\boldsymbol{y}}}\right\rangle(Y)$ amplitude matrix:

- $G^{(2;\delta)}_{\boldsymbol{u}_1\boldsymbol{u}_2}(Y)$ (from the Gaussian truncation in $\mathcal{M}_Y^{(2\text{-pt})}$)

  and

- $G^{(11)}_{\boldsymbol{u}_2\boldsymbol{u}_2\boldsymbol{u}_3\boldsymbol{u}_4}(Y)$,

- $G^{(31)}_{\boldsymbol{u}_2\boldsymbol{u}_2\boldsymbol{u}_3\boldsymbol{u}_4}(Y)$

  and

- $G^{((2;2);2;2)}_{\boldsymbol{u}_2\boldsymbol{u}_2\boldsymbol{v}_3\boldsymbol{v}_4}(Y)$ (from the 4-point truncation in $\mathcal{M}_Y^{(4\text{-pt})}$ and $\widetilde{M}_Y^{(2)}$)

The $\left\langle \mathcal{A}^{(2)}_{\vec{\boldsymbol{x}};\vec{\boldsymbol{y}}}\right\rangle(Y)$ amplitude matrix is 2×2 matrix, leading to 4 integro-differential equations with 4 distinct multiplet G's, which is promising so far.

5.3.1 Taming $\mathcal{M}_Y^{(2\text{-pt})}$

Now let us try to massage the $\mathcal{M}_Y$-matrices into an update equation that can be solved numerically. First, let us start with the simpler term of $\mathcal{M}_Y^{(2\text{-pt})}$ from the Gaussian truncation. We have already discussed how to tame the $\mathcal{M}_Y^{(2\text{-pt})}$ matrix in Chapter 4.3. Now consider the Gaussian truncation acting on a $q\bar{q}$-correlator, $\mathrm{tr}\left(U_{\boldsymbol{x}}U^\dagger_{\boldsymbol{y}}\right)$. The parameterisation equation from the Gaussian truncation acting on $\mathrm{tr}\left(U_{\boldsymbol{x}}U^\dagger_{\boldsymbol{y}}\right)$ will be [17, 37]:

$$\frac{d}{dY}\left\langle \mathrm{tr}\left(U_{\boldsymbol{x}}U^\dagger_{\boldsymbol{y}}\right)\right\rangle_Y = C_f\left(G^{(2;\delta)}_{\boldsymbol{x}\boldsymbol{y}}(Y)-\frac{1}{2}\left(G^{(2;\delta)}_{\boldsymbol{x}\boldsymbol{x}}(Y)+G^{(2;\delta)}_{\boldsymbol{y}\boldsymbol{y}}(Y)\right)\right)\left\langle \mathrm{tr}\left(U_{\boldsymbol{x}}U^\dagger_{\boldsymbol{y}}\right)\right\rangle_Y . \quad (5.22)$$

As we take the coincidence limit of $\boldsymbol{x}\to\boldsymbol{y}$ in Eq. 5.22, the G's will cancel and the coincidence limit is made manifest.

It is further made manifest in the parameterisation equation for the $q^2\bar{q}^2$ correlator matrix

$$\left\langle \mathcal{A}^{(2)}_{\vec{\boldsymbol{x}};\vec{\boldsymbol{y}}}\right\rangle(Y) = \mathcal{M}_Y^{(2\text{-pt};\ q^2\bar{q}^2)}\left\langle \mathcal{A}^{(2)}_{\vec{\boldsymbol{x}};\vec{\boldsymbol{y}}}\right\rangle(Y)\,, \quad (5.23a)$$

where $\mathcal{M}_Y^{(2\text{-pt};\, q^2\bar{q}^2)}$ is the matrix which parameterises the $q^2\bar{q}^2$ correlator with entries $m_{ij}(Y)$ given by

$$
\begin{aligned}
m_{11}(Y) &= \frac{\left(N^2-1\right)}{4N}\Big(-2G^{(2;\delta)}_{\boldsymbol{x}_1\boldsymbol{y}_1}(Y) - 2G^{(2;\delta)}_{\boldsymbol{x}_2\boldsymbol{y}_2}(Y) + G^{(2;\delta)}_{\boldsymbol{x}_1\boldsymbol{x}_1}(Y) + G^{(2;\delta)}_{\boldsymbol{x}_2\boldsymbol{x}_2}(Y) \\
&+ G^{(2;\delta)}_{\boldsymbol{y}_1\boldsymbol{y}_1}(Y) + G^{(2;\delta)}_{\boldsymbol{y}_2\boldsymbol{y}_2}(Y)\Big)\,, \\
m_{12}(Y) &= \frac{\left(N^2-1\right)}{2N\sqrt{N^2-1}}\Big(-G^{(2;\delta)}_{\boldsymbol{x}_1\boldsymbol{y}_2}(Y) - G^{(2;\delta)}_{\boldsymbol{x}_2\boldsymbol{y}_1}(Y) + G^{(2;\delta)}_{\boldsymbol{x}_1\boldsymbol{x}_2}(Y) + G^{(2;\delta)}_{\boldsymbol{y}_1\boldsymbol{y}_2}(Y)\Big) = m_{21}(Y)\,, \\
m_{22}(Y) &= \frac{\left(N^2-1\right)}{4N\left(N^2-1\right)}\Big(-2N^2G^{(2;\delta)}_{\boldsymbol{x}_1\boldsymbol{y}_2}(Y) - 2N^2G^{(2;\delta)}_{\boldsymbol{x}_2\boldsymbol{y}_1}(Y) + N^2G^{(2;\delta)}_{\boldsymbol{x}_2\boldsymbol{x}_2}(Y) \\
&+ \left(N^2-1\right)G^{(2;\delta)}_{\boldsymbol{x}_1\boldsymbol{x}_1}(Y) + N^2G^{(2;\delta)}_{\boldsymbol{y}_1\boldsymbol{y}_1}(Y) + N^2G^{(2;\delta)}_{\boldsymbol{y}_2\boldsymbol{y}_2}(Y) + 2G^{(2;\delta)}_{\boldsymbol{x}_1\boldsymbol{y}_1}(Y) + 4G^{(2;\delta)}_{\boldsymbol{x}_1\boldsymbol{y}_2}(Y) \\
&+ 4G^{(2;\delta)}_{\boldsymbol{x}_2\boldsymbol{y}_1}(Y) + 2G^{(2;\delta)}_{\boldsymbol{x}_2\boldsymbol{y}_2}(Y) - 4G^{(2;\delta)}_{\boldsymbol{x}_1\boldsymbol{x}_2}(Y) - G^{(2;\delta)}_{\boldsymbol{x}_2\boldsymbol{x}_2}(Y) - G^{(2;\delta)}_{\boldsymbol{y}_1\boldsymbol{y}_1}(Y) \\
&- 4G^{(2;\delta)}_{\boldsymbol{y}_1\boldsymbol{y}_2}(Y) - G^{(2;\delta)}_{\boldsymbol{y}_2\boldsymbol{y}_2}(Y)\Big)\,.
\end{aligned}
\tag{5.23b}
$$

Taking the quark/anti-quark coincidence limit in Eq. 5.23 where $\boldsymbol{x}_2 \to \boldsymbol{y}_2$, we easily see $m_{12}(Y) = m_{21}(Y) = 0$ in Eq. 5.23b[3]. This aligns with the parameterisation ansatz's design to satisfy the coincidence limit structure of the Wilson line correlator matrix. Thus, defining

$$
\boxed{G^{(2;\delta)}_{\boldsymbol{x}\boldsymbol{x}}(Y) = 0}\,,
\tag{5.24}
$$

is sensible as it doesn't affect the calculations and greatly simplifies the parameterisation equations in $\mathcal{M}_Y^{(2\text{-pt})}$ [37].

Now let us try to tame the significantly more complicated $\mathcal{M}_Y^{(4\text{-pt})}$.

5.3.2 Taming $\mathcal{M}_Y^{(4\text{-pt})}$

Based on Eq. A.8 for $\mathfrak{C}\left(A^{\otimes 4}\right)$ used in the 4-point truncation, which satisfies Eq. 5.13, certain linear combinations of $G^{(11)}_{\boldsymbol{u}_2\boldsymbol{u}_2\boldsymbol{u}_3\boldsymbol{u}_4}(Y)$ and $G^{(31)}_{\boldsymbol{u}_2\boldsymbol{u}_2\boldsymbol{u}_3\boldsymbol{u}_4}(Y)$ appear in our $\mathcal{M}_Y^{(4\text{-pt})}$-matrix when applying the truncation as per Eq. 5.21 to our correlator matrices. These linear combinations are given by:

- $\left(T_{111} \circ G^{(11)}\right)_{\boldsymbol{u}_1\boldsymbol{u}_2\boldsymbol{u}_3\boldsymbol{u}_4}(Y)$,
- $\left(T_{311} \circ G^{(31)}\right)_{\boldsymbol{u}_1\boldsymbol{u}_2\boldsymbol{u}_3\boldsymbol{u}_4}(Y)$,
- $\left(T_{321} \circ G^{(31)}\right)_{\boldsymbol{u}_1\boldsymbol{u}_2\boldsymbol{u}_3\boldsymbol{u}_4}(Y)$.

Using these linear combinations of G's instead of the individual ones is simpler due to their exploitable symmetry features which we discuss below.

[3] Note that we also exploit the symmetry properties of $G^{(2;\delta)}_{\boldsymbol{u}_1\boldsymbol{u}_2}(Y)$ as discussed in Chapter 4.3.

Permuting arguments to some standard order

Following the reasoning in Chapter 4.3, we can exploit the symmetries of the colour adjoint singlet states in the 4-point truncation to simplify the $\mathcal{M}_Y$-matrices. In-fact, consider the linear combination:

$$\left(T_{111} \circ G^{(11)}\right)_{\boldsymbol{u}_1\boldsymbol{u}_2\boldsymbol{u}_3\boldsymbol{u}_4}(Y).$$

This linear combination of G's is totally symmetric about an interchange of its coordinates. Thus, similarly to the case of $G^{(2;\delta)}_{\boldsymbol{u}_1\boldsymbol{u}_2}(Y)$ and $G^{(3;d)}_{\boldsymbol{u}_1\boldsymbol{u}_2\boldsymbol{u}_3}(Y)$, one can exploit this symmetry property to simplify the complex expressions we get in our $\mathcal{M}_Y^{(4\text{-pt})}$ matrix.

We can generalize to exploit the symmetry features of the more general $T_{\Xi lm}$'s acting on the G's by permuting the arguments of $\left(T_{\Xi lm} \circ G^{(\theta i)}\right)_{\boldsymbol{u}_1\boldsymbol{u}_2\boldsymbol{u}_3\boldsymbol{u}_4}(Y)$[4] to some standard order in the arguments as follows:

$$\begin{aligned}
\left(T_{\Xi lm} \circ G^{(\theta i)}\right)_{\boldsymbol{u}_1\boldsymbol{u}_2\boldsymbol{u}_3\boldsymbol{u}_4}(Y) &= \sigma^{-1} \cdot \left(T_{\Xi lm} \circ G^{(\theta i)}\right)_{\boldsymbol{u}_{\sigma(1)}\boldsymbol{u}_{\sigma(2)}\boldsymbol{u}_{\sigma(3)}\boldsymbol{u}_{\sigma(4)}}(Y) \\
&= N^{\sigma^{-1}}_{\Upsilon kj} T_{\Upsilon kj} \cdot \left(T_{\Xi lm} \circ G^{(\theta i)}\right)_{\boldsymbol{u}_{\sigma(1)}\boldsymbol{u}_{\sigma(2)}\boldsymbol{u}_{\sigma(3)}\boldsymbol{u}_{\sigma(4)}}(Y) \\
&= N^{\sigma^{-1}}_{\Upsilon kj} \delta_{\Upsilon\Xi}\delta_{jl} \left(T_{\Upsilon km} \circ G^{(\theta i)}\right)_{\boldsymbol{u}_{\sigma(1)}\boldsymbol{u}_{\sigma(2)}\boldsymbol{u}_{\sigma(3)}\boldsymbol{u}_{\sigma(4)}}(Y), \qquad (5.25)
\end{aligned}$$

where we have performed a change of basis of σ^{-1} into the basis of $\mathfrak{G}_4$ and used the multiplication table of the $T_{\Xi lm}$'s in Eq. 3.77 to allow simplification in the $\mathcal{M}_Y^{(4\text{-pt})}$-matrix. This is a generalization of what was done with the Gaussian and 3-point truncations where the symmetry of the colour adjoint singlet states imprinted itself onto the G's.

Now the question arises as to what kind of standard order we would want to sort the arguments of $\left(T_{\Xi lm} \circ G^{(\theta i)}\right)_{\boldsymbol{u}_1\boldsymbol{u}_2\boldsymbol{u}_3\boldsymbol{u}_4}(Y)$ into. In-order to choose a suitable standard order that will allow us to deal with repeated arguments, let us consider how the repeated arguments themselves may arise. In-general, we can have for $\left(T_{\Xi lm} \circ G^{(\theta i)}\right)_{\boldsymbol{u}_1\boldsymbol{u}_2\boldsymbol{u}_3\boldsymbol{u}_4}(Y)$:

1. All 4 arguments are different: $\left(T_{\Xi lm} \circ G^{(\theta i)}\right)_{\boldsymbol{xyzw}}(Y)$
2. Two repeated arguments with the other 2 arguments being different from each other; for example $\left(T_{\Xi lm} \circ G^{(\theta i)}\right)_{\boldsymbol{xxzw}}(Y)$
3. Two pairs of arguments that are the same; for example $\left(T_{\Xi lm} \circ G^{(\theta i)}\right)_{\boldsymbol{xxyy}}(Y)$
4. Three repeated arguments and one argument that is different from the 3 repeats; for example $\left(T_{\Xi lm} \circ G^{(\theta i)}\right)_{\boldsymbol{xxxy}}(Y)$
5. All 4 arguments are the same: $\left(T_{\Xi lm} \circ G^{(\theta i)}\right)_{\boldsymbol{xxxx}}(Y)$

[4] We express the general form of a transition operator acting on a multiplet G using our defined notation.

Case 3 is a specific example of case 2; so we will address these four cases. Let us begin with case 2. For terms of the form $\left(T_{\Xi lm} \circ G^{(\theta i)}\right)_{\boldsymbol{u_1 u_2 u_3 u_4}}(Y)$ with *two repeated arguments*, we permute the arguments using Eq. 5.25 so that the repeated arguments occupy the first two positions, and the remaining two arguments are ordered in the last 2 positions in a chosen standard form[5][6]. For instance, the arguments of $\left(T_{\Xi lm} \circ G^{(\theta i)}\right)_{\boldsymbol{xzxw}}(Y)$ and $\left(T_{\Xi lm} \circ G^{(\theta i)}\right)_{\boldsymbol{wxxz}}(Y)$ are reordered to the standard form $\left(T_{\Xi lm} \circ G^{(\theta i)}\right)_{\boldsymbol{xxzw}}(Y)$. Building on the approach for two repeated arguments, let us now consider the case where $\left(T_{\Xi lm} \circ G^{(\theta i)}\right)_{\boldsymbol{u_1 u_2 u_3 u_4}}(Y)$ contains *three repeated arguments*. Here, we permute the arguments using Eq. 5.25 such that the three repeated arguments occupy the first three positions, and the remaining argument is placed last. For instance, a term like $\left(T_{\Xi lm} \circ G^{(\theta i)}\right)_{\boldsymbol{yxxx}}(Y)$ or $\left(T_{\Xi lm} \circ G^{(\theta i)}\right)_{\boldsymbol{xyxx}}(Y)$ would be permuted into the form $\left(T_{\Xi lm} \circ G^{(\theta i)}\right)_{\boldsymbol{xxxy}}(Y)$. Next, consider the case where all four arguments are distinct. In this scenario, we simply permute the arguments into a standard order. The exact choice of standard order depends on the specific context or computational tool used (e.g., *Mathematica*'s *Sort* function [60]). For example, the term $\left(T_{\Xi lm} \circ G^{(\theta i)}\right)_{\boldsymbol{xzyw}}(Y)$ would be permuted into a form like $\left(T_{\Xi lm} \circ G^{(\theta i)}\right)_{\boldsymbol{xyzw}}(Y)$, depending on the imposed standard ordering. Finally, if all four arguments are identical, i.e., $\left(T_{\Xi lm} \circ G^{(\theta i)}\right)_{\boldsymbol{xxxx}}(Y)$, we do not need to perform any permutation since the arguments are already in the desired form. In such cases, no further action is required.

After doing all this, we now have in our $\mathcal{M}_Y^{(4\text{-pt})}$-matrix the following variations of linear combinations of G's:

- $\left(T_{\Xi lm} \circ G^{(\theta i)}\right)_{\boldsymbol{xyzw}}(Y)$; all 4 arguments different
- $\left(T_{\Xi lm} \circ G^{(\theta i)}\right)_{\boldsymbol{xxyz}}(Y)$; 2 arguments equal
- $\left(T_{\Xi lm} \circ G^{(\theta i)}\right)_{\boldsymbol{xxxy}}(Y)$; 3 arguments equal
- $\left(T_{\Xi lm} \circ G^{(\theta i)}\right)_{\boldsymbol{xxxx}}(Y)$; all 4 arguments equal

Certain Repeats of Arguments of $\left(T_{\Xi lm} \circ G^{(\theta i)}\right)_{\boldsymbol{u_1 u_2 u_3 u_4}}(Y)$ vanishing

Consider now $\left(T_{311} \circ G^{(31)}\right)_{\boldsymbol{xxxy}}(Y)$ and $\left(T_{321} \circ G^{(31)}\right)_{\boldsymbol{xxxy}}(Y)$ with 3 arguments equal. We have that:

$$T_{311} = \frac{4}{3}$$ 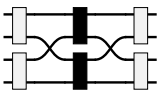

[5] Throughout this thesis, the standard form will be determined by *Mathematica*'s *Sort* function [60].

[6] In general, there may be multiple permutations satisfying this criterion; we will choose the first one identified, either through *Mathematica*'s *Sort* function [60] or other means.

$$T_{321} = \sqrt{\frac{4}{3}}$$ 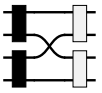 . (5.26)

Due to the anti-symmetrizer over at least two arguments in T_{311} and T_{321} (Eq. 5.26), both T_{311} and T_{321} will vanish when acting on any function with three repeated arguments[7]:

$$\boxed{\left(T_{311} \circ G^{(31)}\right)_{\boldsymbol{xxxy}}(Y) = \left(T_{321} \circ G^{(31)}\right)_{\boldsymbol{xxxy}}(Y) = 0} \,. \tag{5.27}$$

This also extends to functions with four identical arguments, as the former case generalizes the latter.

Furthermore, due to the anti-symmetrizer acting on the first and last two legs of T_{321}, the operator T_{321} will be anti-symmetric with respect to its first two and last two arguments (indices) when acting on any function (vector):

$$\boxed{\begin{aligned} \left(T_{321} \circ G^{(31)}\right)_{\boldsymbol{xyzw}} &= -\left(T_{321} \circ G^{(31)}\right)_{\boldsymbol{yxzw}} \\ \left(T_{321} \circ G^{(31)}\right)_{\boldsymbol{xyzw}} &= -\left(T_{321} \circ G^{(31)}\right)_{\boldsymbol{xywz}} \\ \implies \left(T_{321} \circ G^{(31)}\right)_{\boldsymbol{xxzw}} &= 0 \quad \text{and} \quad \left(T_{321} \circ G^{(31)}\right)_{\boldsymbol{yzxx}} = 0\,. \end{aligned}} \tag{5.28}$$

Now if one were to take the coincidence limit of setting all the coordinates equal to one another, i.e.

$$\boldsymbol{x}_1 = \boldsymbol{x}_2 = \boldsymbol{x}_3 = \boldsymbol{y}_1 = \boldsymbol{y}_2 = \boldsymbol{y}_3$$

then the amplitude matrices $\mathcal{A}^{(2;g)}_{\vec{\boldsymbol{x}};\vec{\boldsymbol{y}};\boldsymbol{z}}(Y)$ and $\mathcal{A}^{(2)}_{\vec{\boldsymbol{x}};\vec{\boldsymbol{y}}}(Y)$ will simply become unity. JIMWLK evolution leaves a unity matrix unchanged [13, 17]. This necessitates initial conditions allowing this, which means that $\mathcal{M}_Y = 0$ and $\widetilde{\mathcal{M}}^{(k)}_Y = 0$ (for all k) in the parameterisation equations for $\left\langle \mathcal{A}^{(2;g)}_{\vec{\boldsymbol{x}};\vec{\boldsymbol{y}};\boldsymbol{z}} \right\rangle (Y)$ and $\left\langle \mathcal{A}^{(2)}_{\vec{\boldsymbol{x}};\vec{\boldsymbol{y}}} \right\rangle (Y)$ in such a coincidence limit. Thus, to ensure the $\mathcal{M}_Y$ matrices yield physical results when all limits coincide, the G's with identical arguments must be set to zero, ensuring suitable physical behavior for our $\mathcal{M}_Y$ matrices. This therefore means that we can set

$$\boxed{G^{(11)}_{\boldsymbol{xxxx}}(Y) = 0} \,. \tag{5.29}$$

We have variations of linear combinations of multiplet G with repeated arguments in $\mathcal{M}^{(4\text{-pt})}_Y$ that vanish, simplifying $\mathcal{M}^{(4\text{-pt})}_Y$ and moving us closer to an update equation.

[7] Or an object with three repeated indices.

A list of all such linear combinations of multiplet G's which vanish is given below:

- $\left(T_{111} \circ G^{(11)}\right)_{\boldsymbol{xxxx}}(Y) = 0$; all 4 arguments equal
- $\left(T_{311} \circ G^{(31)}\right)_{\boldsymbol{xxxx}}(Y) = 0$; all 4 arguments equal
- $\left(T_{321} \circ G^{(31)}\right)_{\boldsymbol{xxxx}}(Y) = 0$; all 4 arguments equal
- $\left(T_{311} \circ G^{(31)}\right)_{\boldsymbol{xxxy}}(Y) = 0$; 3 arguments equal
- $\left(T_{321} \circ G^{(31)}\right)_{\boldsymbol{xxxy}}(Y) = 0$; 3 arguments equal
- $\left(T_{321} \circ G^{(31)}\right)_{\boldsymbol{xxyz}}(Y) = 0$; 2 arguments equal

The remaining linear combinations of G's in $\mathcal{M}_Y^{(4\text{-pt})}$ are now:

- $\left(T_{111} \circ G^{(11)}\right)_{\boldsymbol{xyzw}}(Y)$; all 4 arguments different
- $\left(T_{111} \circ G^{(11)}\right)_{\boldsymbol{xxyz}}(Y)$; 2 arguments equal
- $\left(T_{111} \circ G^{(11)}\right)_{\boldsymbol{xxxy}}(Y)$; 3 arguments equal
- $\left(T_{311} \circ G^{(31)}\right)_{\boldsymbol{xyzw}}(Y)$; all 4 arguments different
- $\left(T_{311} \circ G^{(11)}\right)_{\boldsymbol{xxyz}}(Y)$; 2 arguments equal
- $\left(T_{321} \circ G^{(11)}\right)_{\boldsymbol{xyzw}}(Y)$; all 4 arguments different

After simplifying $\mathcal{M}_Y^{(4\text{-pt})}$ and $\mathcal{M}_Y^{(2\text{-pt})}$ with the methods discussed, we apply the two quark/anti-quark coincidence limits, $\boldsymbol{x}_3 \to \boldsymbol{y}_3$ and then $\boldsymbol{x}_2 \to \boldsymbol{y}_2$ and reapplying the methods after each coincidence limit to address repeated arguments in G that may vanish. Figure 5.3 displays the matrix plots of $\mathcal{M}_Y^{(4)} = \mathcal{M}_Y^{(4\text{-pt})} + \mathcal{M}_Y^{(2\text{-pt})}$ after the procedure of taking two quark/anti-quark coincidence limits:

The $\mathcal{M}_Y^{(4)}$ block diagonalizes just like the Wilson line correlator matrix in the Fierz basis after the quark/anti-quark coincidence limits. This supports our parameterization ansatz condition for the $\mathcal{M}_Y$ to match the coincidence limit structure of the Wilson correlator matrix it is obtained from, affirming the accuracy of our calculations.

Breaking up G's with repeated arguments

We can more systematically simplify the $\left(T_{\Xi lm} \circ G^{(\theta i)}\right)$'s with repeated arguments by defining them as functions of 2 or 3 arguments rather than 4, then applying Eq. D.5's decomposition of unity.

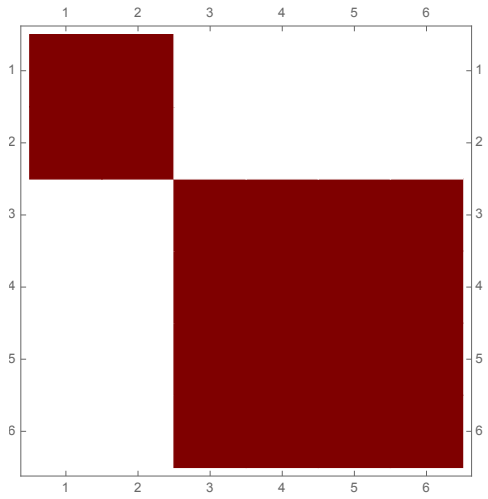

FIGURE 5.1: After one quark/anti-quark coincidence limit

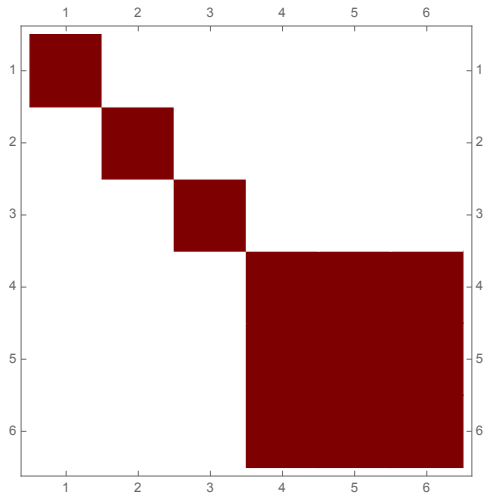

FIGURE 5.2: After two quark/anti-quark coincidence limits

FIGURE 5.3: Matrix plots of $\mathcal{M}_Y^{(4)} = \mathcal{M}_Y^{(4\text{-pt})} + \mathcal{M}_Y^{(2\text{-pt})}$ after applying two quark/anti-quark coincidence limit and the simplification methods from Chapter 5.3. Constructed in the same basis as the Wilson line correlator matrix in Eq. 3.90, $\mathcal{M}_Y^{(4)}$ exhibits the same block diagonalization as seen in Eq. 3.91 for the Wilson line correlator matrix in the Fierz basis.

We define:

$$\left(T_{\theta ii} \circ G^{(\theta i)}\right)_{\boldsymbol{xxyz}} := K^{(\theta i)}_{\boldsymbol{xyz}}\,, \tag{5.30}$$

and

$$\left(T_{\theta 11} \circ G^{(11)}\right)_{\boldsymbol{xxxy}} := K^{(11)}_{\boldsymbol{xy}}\,, \tag{5.31}$$

and perform a decomposition of unity

$$\begin{aligned} K^{(\theta i)}_{\boldsymbol{xyz}} &= \underbrace{\sum_{\Xi i} T_{\Xi ii}}_{\mathbb{1}} \circ K^{(\theta ji)}_{\boldsymbol{xyz}} \\ &= (T_{111} + T_{211} + T_{222} + T_{311}) \circ K^{(\theta i)}_{\boldsymbol{xyz}}\,. \end{aligned} \tag{5.32}$$

We recognize a potential ambiguity with our current notation regarding whether the $T_{\Theta ij}$'s belong to $\mathfrak{G}_3$ or $\mathfrak{G}_4$. However, the context should clarify this, and we will specify explicitly when necessary.

We then simplify $\mathcal{M}_Y^{(4\text{-pt})}$ by applying the same steps as above for functions with four arguments. Specifically, we permute the arguments of $T_{\theta ii} \circ K^{(\theta i)}$ into a standard order: repeated arguments are placed in the first two positions, while terms with all distinct arguments are permuted into a chosen standard order (using *Mathematica*'s *Sort* function [60] or otherwise). We then check if certain repeated-argument terms vanish and compile the remaining

$T_{\theta ij} \circ K^{(\theta i)}$ terms.

Before we do so, we note the relation:

$$\boxed{\left(\underbrace{T_{311}}_{\text{anti-symmetriser birdtrack}} \circ K^{(11)}\right)_{\boldsymbol{xyz}} = \left(\underbrace{T_{311}}_{\text{anti-symmetriser birdtrack}} \circ K^{(31)}\right)_{\boldsymbol{xyz}} = 0}\,. \tag{5.33}$$

This arises due to the properties of $K^{(11)}_{\boldsymbol{xyz}}$ and $K^{(31)}_{\boldsymbol{xyz}}$ themselves as when we act an anti-symmetriser on $K^{(11)}_{\boldsymbol{xyz}}$ and $K^{(31)}_{\boldsymbol{xyz}}$, we get pairs of terms that end up cancelling due to the symmetries of $K^{(11)}_{\boldsymbol{xyz}}$ and $K^{(31)}_{\boldsymbol{xyz}}$. For example, an anti-symmetriser acting on $K^{(11)}_{\boldsymbol{xyz}}$ gives the following pair of terms (amongst 2 other pairs which cancel similarly):

$$\begin{aligned} K^{(11)}_{\boldsymbol{xyz}} - K^{(11)}_{\boldsymbol{xzy}} &= \left(T_{111} \circ G^{(11)}\right)_{\boldsymbol{xxyz}} - \left(T_{111} \circ G^{(11)}\right)_{\boldsymbol{xxzy}} \\ &= 0\,, \end{aligned} \tag{5.34}$$

where we have used the fact that $\left(T_{111} \circ G^{(11)}\right)_{\boldsymbol{xxzy}} = \left(T_{111} \circ G^{(11)}\right)_{\boldsymbol{xxyz}}$ due to the fact that $\left(T_{111} \circ G^{(11)}\right)_{\boldsymbol{xyzw}}$ is totally symmetric about any interchange of its coordinates.

This will hold for $K^{(31)}_{\boldsymbol{xyz}}$ since $\left(T_{311} \circ G^{(31)}\right)_{\boldsymbol{xyzw}}$ is separately symmetric about an interchange of its first 2 and last arguments

$$\boxed{\begin{aligned} \left(T_{311} \circ G^{(31)}\right)_{\boldsymbol{xyzw}} &= \left(T_{311} \circ G^{(31)}\right)_{\boldsymbol{yxzw}} \\ \left(T_{311} \circ G^{(31)}\right)_{\boldsymbol{xyzw}} &= \left(T_{311} \circ G^{(31)}\right)_{\boldsymbol{xywz}} \end{aligned}}\,, \tag{5.35}$$

which will also result in pairs of terms canceling to give an overall result of 0. Therefore, any term of the form $T_{311} \circ K^{(\theta i)}$ is automatically killed off.

Terms of the form $\left(T_{211} \circ K^{(\theta i)}\right)_{\boldsymbol{xxy}}$ and $\left(T_{212} \circ K^{(\theta i)}\right)_{\boldsymbol{xxy}}$ will also vanish due to the presence of the anti-symmetriser over the first two legs of T_{211} and T_{212}. To see this, note that the birdtrack visualization of T_{211} and T_{212} is given by

$$\begin{aligned} T_{211} &= \frac{4}{3}\,, \\ T_{212} &= \sqrt{\frac{4}{3}}\,. \end{aligned} \tag{5.36}$$

Therefore, we have that:

$$\boxed{\begin{aligned} \left(T_{211}\circ K^{(\theta i)}\right)_{\boldsymbol{xyz}} &= -\left(T_{211}\circ K^{(\theta i)}\right)_{\boldsymbol{yxz}} \\ \left(T_{212}\circ K^{(\theta i)}\right)_{\boldsymbol{xyz}} &= -\left(T_{212}\circ K^{(\theta i)}\right)_{\boldsymbol{yxz}} \\ \implies \left(T_{211}\circ K^{(\theta i)}\right)_{\boldsymbol{xxz}} &= 0 \quad \text{and} \quad \left(T_{212}\circ K^{(\theta i)}\right)_{\boldsymbol{xxz}} = 0\ . \end{aligned}} \tag{5.37}$$

Again, this is similar to how $\left(T_{321}\circ G^{(31)}\right)_{\boldsymbol{xxyz}}(Y)=0$ in Eq. 5.28.

We therefore get the following non-vanishing linear combinations of K's in $\mathcal{M}_Y^{(4\text{-pt})}$:

- $\left(T_{111}\circ K^{(\theta i)}\right)_{\boldsymbol{xyz}}$; 3 distinct arguments
- $\left(T_{111}\circ K^{(\theta i)}\right)_{\boldsymbol{xxy}}$; 2 distinct arguments
- $\left(T_{211}\circ K^{(\theta i)}\right)_{\boldsymbol{xyz}}$; 3 distinct arguments
- $\left(T_{212}\circ K^{(\theta i)}\right)_{\boldsymbol{xyz}}$; 3 distinct arguments
- $\left(T_{222}\circ K^{(\theta i)}\right)_{\boldsymbol{xyz}}$; 3 distinct arguments
- $\left(T_{222}\circ K^{(\theta i)}\right)_{\boldsymbol{xxy}}$; 2 distinct arguments
- $\left(T_{221}\circ K^{(\theta i)}\right)_{\boldsymbol{xyz}}$; 3 distinct arguments
- $\left(T_{221}\circ K^{(\theta i)}\right)_{\boldsymbol{xxy}}$; 2 distinct arguments
- $\left(T_{11}\circ K^{(11)}\right)_{\boldsymbol{xy}}$; 2 distinct arguments
- $\left(T_{21}\circ K^{(11)}\right)_{\boldsymbol{xy}}$; 2 distinct arguments

Note that K's that have all 3 arguments equal will be 0.

The above list along with the list of linear combination of G's where all 4 arguments are different now gives a comprehensive list of all the various 4-point, 3-point and 2-point functions in $\mathcal{M}_Y^{(4\text{-pt})}$. Whilst we have made strides in simplifying $\mathcal{M}_Y^{(4\text{-pt})}$ greatly, the presence of functions that have repeated arguments (the 3- and 2-point functions which we have listed above) still complicates matters greatly and we are yet able to obtain an update equation to solve numerically. One would need to devise more ways to simplify or re-express the $\mathcal{M}_Y^{(4\text{-pt})}$ matrix in a form that permits an update equation.

Chapter 6

Conclusions and Outlook

6.1 Thesis summary

This thesis set out to investigate the 4-point truncation of the JIMWLK evolution equation within the context of high-energy QCD. The primary motivation was to develop a deeper understanding of the Color Glass Condensate (CGC) and the rapidity evolution of Wilson line correlators and their role in the total cross-section.

In **Chapter 2**, we laid the groundwork by discussing the high-energy physics that leads to the JIMWLK evolution equation. Starting with deep inelastic scattering (DIS) experiments, we described how the CGC emerges in the Regge-Gribov kinematic limit. We also introduced Wilson lines as elements of SU(N), highlighting their role in JIMWLK evolution and the Balitsky-Kovchegov hierarchy.

Chapter 3 focused on constructing Wilson line correlator matrices, a crucial tool for studying the rapidity evolution of observables in the CGC. Using birdtracks, Hermitian Young Projection Operators (HYPOs), and the Fierz basis, we built a basis for colour singlet states and sandwiched Wilson lines to obtain correlator matrices that simplify significantly in various coincidence limits. This chapter drew heavily on the work of J. Alcock-Zeilinger, particularly in constructing these matrices. Additionally, we presented a novel basis for colour singlet states specifically designed for correlator matrices that exhibit substantial simplifications under *combined* quark/anti-quark coincidence limits.

In **Chapter 4**, we explored gauge-invariant and symmetry-preserving truncations introduced by R. Moerman and H. Weigert. We provided a summary of J. Rayner's construction of adjoint colour singlet states, which formed the foundation for implementing the 4-point truncation.

Chapter 5 presented the main results of this thesis: the 4-point truncation of the JIMWLK evolution equation. We extended the parameterization used in previous truncations and refined the basis for adjoint colour singlet states to try to compare with and sub-

tract the Gaussian truncation squared. Applying the 4-point truncation, we obtained an integro-differential equation for the evolution of Wilson line correlator matrices. We then highlighted the methods we took to try to reduce this integro-differential equation into an update equation which can be solved for numerically.

Specifically in Chapter 5, where the main original results of this thesis are presented, to simplify the integro-differential equation, we exploited the symmetry properties of the Hermitian Young Projection Operators and their corresponding transition operators. By systematically defining the color structure functions, G's, with repeated arguments as functions of 2-point and 3-point coordinates, essentially reducing them to 2-point and 3-point functions, and employing a decomposition of unity of the HYPOs, we attempted to disentangle these functions. Following steps similar to those used for symmetry exploitation of the HYPOs and their transition operators, we further tamed the integro-differential equation.

Although we have made significant progress in investigating and understanding the properties of the 4-point truncation, there are still several major issues. The most crucial of which is that the integro-differential equation from the 4-point truncation is still very complex and unwieldy in the form we have massaged it into. We want to solve for the 4-point colour structure functions, the 4-point G's, as this will adequately capture the physics of 4-point Wilson line correlators. The integro-differential equation we have obtained is in-theory for the color structure functions, which can be solved. However, in practice, one cannot numerically solve for the G's from the form it is in now; at least to the knowledge of the authors of this thesis, there does not exist any numerical method in the literature for solving such a complex integro-differential equation. There is still much work to be done in this regard, and as such, the most pressing issue that needs to be resolved is a way of massaging the integro-differential equation we have into an update equation that can be solved numerically in a fairly straightforward way.

A key limitation of this study is that we investigated the 4-point truncation by effectively "turning off" terms expected to have no overlap with the Gaussian truncation squared. However, these terms are essential for obtaining the most general parameterisation of the JIMWLK evolution equation at the 4-point level. Notably, for the JIMWLK evolution of the $\left\langle \mathcal{A}^{(2)}_{\vec{\boldsymbol{x}};\vec{\boldsymbol{y}}} \right\rangle (Y)$ amplitude matrix, we found more degrees of freedom than solvable equations, with some degrees of freedom proving irrecoverable. This suggests the need for larger amplitude matrices, where applying the 4-point truncation could, in principle, yield a fully solvable JIMWLK equation for all multiplet G's. However, constructing and computing such matrices is highly resource-intensive and exceeds the computational capabilities available to the author at the time of writing.

These challenges present significant obstacles to solving the 4-point colour structure functions. Overcoming them requires more advanced computational resources and innovative ap-

proaches to deriving the 4-point colour structure functions while managing the complexity of larger amplitude matrices. In the next section, we discuss potential solutions and open questions that could guide future research in this direction.

6.2 Outlook and open questions

The JIMWLK evolution equation remains one of the primary frameworks for studying the CGC. Although it initially led to an infinite hierarchy of coupled integro-differential equations with no exact solution, significant progress has been made, particularly through gauge-invariant, symmetry-preserving truncations. These truncations maintain the symmetries and group-theoretic constraints of JIMWLK evolution while remaining valid for all N_c. Central to these truncations are the n-point colour structure functions, which encode the rapidity evolution of Wilson line correlators and directly contribute to various total cross-sections in DIS. Moreover, they interface closely with ongoing work in Soft Collinear Effective Theory and parton shower Monte Carlo codes. Understanding these colour structure functions is therefore essential for deepening our knowledge of the CGC and, by extension, fundamental aspects of QCD.

While 2-point and 3-point colour structure functions have been extensively studied, extending JIMWLK truncations to the 4-point level is necessary to fully describe the physics of 4-point Wilson line correlators. This thesis aimed to develop such a framework, yet much remains to be done in solving for all 4-point colour structure functions and understanding their properties.

One potential strategy for managing the resulting integro-differential equations is to construct specific linear combinations of the G's, introducing new functions that simplify the evolution equations and potentially enable an update equation. To illustrate this, consider a hypothetical case where the following linear combination of 4-point functions appears in the $\mathcal{M}_Y$ matrices:

$$\begin{aligned}\mathcal{M}_Y^{(\text{hypothetical})} &= G_{\boldsymbol{x}_1\boldsymbol{x}_2\boldsymbol{y}_1\boldsymbol{y}_2} + G_{\boldsymbol{x}_1\boldsymbol{x}_1\boldsymbol{y}_1\boldsymbol{y}_2} + G_{\boldsymbol{y}_3\boldsymbol{y}_2\boldsymbol{y}_1\boldsymbol{x}_1} + G_{\boldsymbol{y}_3\boldsymbol{y}_3\boldsymbol{y}_1\boldsymbol{y}_2} \\ &\quad + G_{\boldsymbol{x}_1\boldsymbol{x}_1\boldsymbol{y}_1\boldsymbol{y}_1} + G_{\boldsymbol{x}_1\boldsymbol{x}_1\boldsymbol{y}_1\boldsymbol{y}_2} + G_{\boldsymbol{y}_3\boldsymbol{y}_3\boldsymbol{y}_1\boldsymbol{y}_1} + G_{\boldsymbol{y}_3\boldsymbol{y}_3\boldsymbol{y}_1\boldsymbol{x}_2}. \end{aligned} \tag{6.1}$$

By defining new functions,

$$\begin{aligned} H_{\boldsymbol{u}_1\boldsymbol{u}_2\boldsymbol{u}_3\boldsymbol{u}_4} &:= G_{\boldsymbol{u}_1\boldsymbol{u}_2\boldsymbol{u}_3\boldsymbol{u}_4} + G_{\boldsymbol{u}_1\boldsymbol{u}_1\boldsymbol{u}_3\boldsymbol{u}_4}, \\ J_{\boldsymbol{u}_1\boldsymbol{u}_2\boldsymbol{u}_3} &:= G_{\boldsymbol{u}_1\boldsymbol{u}_1\boldsymbol{u}_2\boldsymbol{u}_2} + G_{\boldsymbol{u}_1\boldsymbol{u}_1\boldsymbol{u}_2\boldsymbol{u}_3}, \end{aligned} \tag{6.2}$$

Equation 6.1 simplifies to

$$\mathcal{M}_Y^{(\text{hypothetical})} = H_{\boldsymbol{x}_1\boldsymbol{x}_2\boldsymbol{y}_1\boldsymbol{y}_2} + H_{\boldsymbol{y}_3\boldsymbol{y}_2\boldsymbol{y}_1\boldsymbol{x}_1} + J_{\boldsymbol{x}_1\boldsymbol{y}_1\boldsymbol{y}_2} + J_{\boldsymbol{y}_3\boldsymbol{y}_1\boldsymbol{x}_2}. \tag{6.3}$$

This form is noticeably simpler, suggesting that solving for the newly defined H's and J's may facilitate the derivation of an update equation. While our methods in Chapter 5.3 did not yield a general update equation, this does not preclude the possibility of such a formulation. A notable example where this approach has been successful is the odderon, which has been studied extensively in [33, 39].

Indeed, there is currently no systematic approach for identifying such linear combinations, and the best available method is to simply "stare at the equation" and hope to recognize useful patterns. A possible systematic approach, however, could involve stepping back from the integro-differential equations and examining the derivative operators acting on Wilson lines at the parameterization level. It may be that these fourth-order derivatives, when acting on a tensor product of Wilson lines, naturally lead to specific linear combinations of G's that are unique up to permutations of their transverse coordinates. If so, one could study the combinatorial structure of these derivatives to identify patterns that might simplify the equations.

A simpler example that motivates this approach is the Gaussian truncation acting on a $q\bar{q}$-correlator, which we reiterate below:

$$\frac{d}{dY}\left\langle \operatorname{tr}\left(U_{\boldsymbol{x}}U_{\boldsymbol{y}}^\dagger\right)\right\rangle = C_f\left(G_{\boldsymbol{xy}}^{(2;\delta)}(Y) - \frac{1}{2}\left(G_{\boldsymbol{xx}}^{(2;\delta)}(Y) + G_{\boldsymbol{yy}}^{(2;\delta)}(Y)\right)\right)\left\langle \operatorname{tr}\left(U_{\boldsymbol{x}}U_{\boldsymbol{y}}^\dagger\right)\right\rangle. \tag{6.4}$$

As seen in Eq. 6.4, the terms $G_{\boldsymbol{xx}}^{(2;\delta)}(Y)$ and $G_{\boldsymbol{yy}}^{(2;\delta)}(Y)$ appear with a relative sign and a factor of $\frac{1}{2}$ compared to $G_{\boldsymbol{xy}}^{(2;\delta)}(Y)$. This structure arises from the way the differential operator $\nabla_{\boldsymbol{u}_1}^{a_1}\nabla_{\boldsymbol{u}_2}^{a_2}$ acts on $\operatorname{tr}\left(U_{\boldsymbol{x}}U_{\boldsymbol{y}}^\dagger\right)$. Specifically, the $G_{\boldsymbol{xy}}^{(2;\delta)}(Y)$-term comes from the derivative operators acting on both the fundamental and anti-fundamental Wilson lines. Due to the product rule, this operation happens twice, introducing an overall minus sign and a factor of 2. In contrast, the terms $G_{\boldsymbol{xx}}^{(2;\delta)}(Y)$ and $G_{\boldsymbol{yy}}^{(2;\delta)}(Y)$ arise from derivatives acting on the same (anti)-fundamental Wilson line, avoiding the additional factor of 2 and sign change.

If similar structures exist in the 4-point truncation, it raises the question: Can the entire integro-differential equation be rewritten in terms of such linear combinations to yield an update equation?

Another potential approach to bypass the complexity of integro-differential equations is to reconsider the parameterization itself. Rather than assigning a distinct multiplet G to each basis element of $\mathfrak{C}\left(A^{\otimes 4}\right)$, it may be possible to reduce the number of independent G's required while still maintaining a valid solution to the JIMWLK equation. The key question is

whether a more economical parameterization—one that employs fewer than nine independent G's—can be found without losing essential information about the evolution.

At the level of 4-point truncation, colour adjoint singlet states can belong to 2-dimensional subspaces projected out by HYPOs (as we saw in Chapter 4.2), unlike the purely 1-dimensional subspaces encountered in the 2- and 3-point cases. As a result, the corresponding multiplet G's inherit the same symmetry properties from these two adjoint singlet states. This raises a fundamental question: Do we need two independent multiplet G's for each of these 2-dimensional subspaces, or would a single G suffice? Since both states share identical symmetry constraints, it is unclear whether distinguishing them is necessary. Ultimately, must we introduce a separate G for each basis element of $\mathfrak{C}\left(A^{\otimes 4}\right)$, or can a more economical parameterization be found?

Finally, Appendix C presents a digression on the symmetry groups arising from the colour structures in the Gaussian truncation squared, which may suggest an alternative way of exploiting the symmetries of the colour adjoint singlet states in the 4-point truncation. Rather than relying solely on HYPOs and their transition operators, as in Eq. 5.25, could we instead consider the symmetry group of each colour structure in $\mathfrak{C}\left(A^{\otimes 4}\right)$ and imprint these symmetries directly onto the multiplet G's?

This digression serves to explore how these symmetry groups might connect to HYPOs and transition operators, and whether such a connection could aid in solving for the 4-point colour structure functions. To investigate this further, one would need to compute the symmetry groups of each colour structure in $\mathfrak{C}\left(A^{\otimes 4}\right)$ and express their summed elements in terms of the HYPO basis and transition operators, as a starting point for tackling this question.

Other open questions outside the scope of this thesis include the error term associated with truncating the JIMWLK equation and whether we can find an algorithm to obtain a fully orthogonal basis for $\mathfrak{C}\left(A^{\otimes 4}\right)$ from the outset. Regarding the former, truncating the parameterization ansatz at a certain order suggests the potential for an error term in the truncation, but it is not yet clear how to derive this error or determine the level of truncation needed to achieve a desired accuracy for Wilson line correlators' rapidity evolution.

On the latter point, a more robust algorithm for constructing a basis for $\mathfrak{C}\left(A^{\otimes 4}\right)$ would avoid the need for the Gram-Schmidt orthogonalization procedure, which relies on arbitrary starting vectors. A potential approach to this is discussed in [40].

Addressing these questions is crucial for solving the 4-point colour structure functions and gaining a deeper understanding of the JIMWLK equation. The work presented in this thesis, building on previous research, highlights the significant challenges that remain in understanding the high-energy asymptotic behavior of QCD. Gaining insight into this high-energy regime is essential for advancing our understanding of the Standard Model. We leave

the resolution of these open issues for future research, with the hope that they will lead to breakthroughs in high-energy physics and enhance our comprehension of the universe.

Appendix A

New Notation and Bases in $\mathfrak{C}\left(A^{\otimes 4}\right)$

A.1 Hermitian Young Projection Operators and Transition Operators in new Notation

We include a list mapping the Young tableaux and diagrams used in this thesis to numerical values for easy reference.

For Young diagrams with 2 boxes:

- $\ydiagram{2} \to 1$
  - $\ytableaushort{12} \to 1$
- $\ydiagram{1,1} \to 2$
  - $\ytableaushort{1,2} \to 2$

The two projection operators for associated with these two Young tableaux will therefore be (in our notation):

$$P_{\ytableaushort{12}} = T_{111} \tag{A.1a}$$

$$P_{\ytableaushort{1,2}} = T_{222} \tag{A.1b}$$

For Young diagrams with 3 boxes:

- $\ydiagram{3} \to 1$
  - $\ytableaushort{123} \to 1$
- $\ydiagram{2,1} \to 2$

  - $\begin{array}{|c|c|}\hline 1 & 3 \\ \hline 2 \\ \cline{1-1}\end{array} \to 1$
  - $\begin{array}{|c|c|}\hline 1 & 2 \\ \hline 3 \\ \cline{1-1}\end{array} \to 2$
- $\begin{array}{|c|}\hline \\ \hline \\ \hline \\ \cline{1-1}\end{array} \to 3$
  - $\begin{array}{|c|}\hline 1 \\ \hline 2 \\ \hline 3 \\ \cline{1-1}\end{array} \to 1$

Consider the following two examples which may add clarity:

$$T_{\begin{array}{|c|c|}\hline 1 & 2 \\ \hline 3 \\ \cline{1-1}\end{array}\ \begin{array}{|c|c|}\hline 1 & 3 \\ \hline 2 \\ \cline{1-1}\end{array}} = T_{212} \tag{A.2a}$$

$$P_{\begin{array}{|c|c|}\hline 1 & 2 \\ \hline 3 \\ \cline{1-1}\end{array}} = T_{211} \tag{A.2b}$$

For Young diagrams with 4 boxes:

- $\begin{array}{|c|c|c|c|}\hline \\ \hline\end{array} \to 1$
  - $\begin{array}{|c|c|c|c|}\hline 1 & 2 & 3 & 4 \\ \hline\end{array} \to 1$
- $\begin{array}{|c|c|c|}\hline \\ \hline \\ \cline{1-1}\end{array} \to 2$
  - $\begin{array}{|c|c|c|}\hline 1 & 3 & 4 \\ \hline 2 \\ \cline{1-1}\end{array} \to 3$
  - $\begin{array}{|c|c|c|}\hline 1 & 2 & 4 \\ \hline 3 \\ \cline{1-1}\end{array} \to 2$
  - $\begin{array}{|c|c|c|}\hline 1 & 2 & 3 \\ \hline 4 \\ \cline{1-1}\end{array} \to 1$
- $\begin{array}{|c|c|}\hline \\ \hline \\ \cline{1-2}\end{array} \to 3$
  - $\begin{array}{|c|c|}\hline 1 & 3 \\ \hline 2 & 4 \\ \cline{1-2}\end{array} \to 2$
  - $\begin{array}{|c|c|}\hline 1 & 2 \\ \hline 3 & 4 \\ \cline{1-2}\end{array} \to 1$
- $\begin{array}{|c|c|}\hline \\ \hline \\ \hline \\ \cline{1-1}\end{array} \to 4$
  - $\begin{array}{|c|c|}\hline 1 & 4 \\ \hline 2 \\ \hline 3 \\ \cline{1-1}\end{array} \to 3$
  - $\begin{array}{|c|c|}\hline 1 & 3 \\ \hline 2 \\ \hline 4 \\ \cline{1-1}\end{array} \to 2$

- $\begin{array}{|c|c|}\hline 1&2\\\hline 3\\\cline{1-1}4\\\cline{1-1}\end{array} \to 1$

- $\begin{array}{|c|}\hline \ \\\hline \ \\\hline \ \\\hline \ \\\hline\end{array} \to 5$

- $\begin{array}{|c|}\hline 1\\\hline 2\\\hline 3\\\hline 4\\\hline\end{array} \to 1$

Consider the following two examples which may add clarity:

$$T_{\begin{array}{|c|c|}\hline 1&2\\\hline 3&4\\\hline\end{array}\begin{array}{|c|c|}\hline 1&3\\\hline 2&4\\\hline\end{array}} = T_{312} \tag{A.3a}$$

$$P_{\begin{array}{|c|}\hline 1\\\hline 2\\\hline 3\\\hline 4\\\hline\end{array}} = T_{511} \tag{A.3b}$$

A.2 Different Bases for $\mathfrak{C}\left(A^{\otimes 4}\right)$

Using the trace basis to express an element $v^{a_1a_2a_3a_4} \in \left(A^{\otimes 4}\right)$ as $v^{a_1a_2a_3a_4} = \sum_i c_i \left(v_i\right)^{a_1a_2a_3a_4} \in \mathfrak{C}\left(A^{\otimes 4}\right)$ where $\left(v_i\right)^{a_1a_2a_3a_4}$ is an element of the trace basis, we act the HYPOs on $v^{a_1a_2a_3a_4}$ to obtain a "mostly" orthogonal basis for $\mathfrak{C}\left(A^{\otimes 4}\right)$. Doing do yields [40]:

$$\begin{aligned}
T_{111} \circ v^{a_1a_2a_3a_4} &= \frac{c_1'}{6}\Bigg(\operatorname{tr}(t^{a_1}t^{a_2}t^{a_3}t^{a_4}) + \operatorname{tr}(t^{a_1}t^{a_2}t^{a_4}t^{a_3}) + \operatorname{tr}(t^{a_1}t^{a_3}t^{a_2}t^{a_4}) \\
&\quad \underbrace{+ \operatorname{tr}(t^{a_1}t^{a_3}t^{a_4}t^{a_2}) + \operatorname{tr}(t^{a_1}t^{a_4}t^{a_2}t^{a_3}) + \operatorname{tr}(t^{a_1}t^{a_4}t^{a_3}t^{a_2})\Bigg)}_{=:\mathcal{C}_1^{a_1a_2a_3a_4}} \\
&\quad + \frac{c_2'}{3}\Bigg(\underbrace{\operatorname{tr}(t^{a_1}t^{a_4})\operatorname{tr}(t^{a_2}t^{a_3}) + \operatorname{tr}(t^{a_1}t^{a_3})\operatorname{tr}(t^{a_2}t^{a_4}) + \operatorname{tr}(t^{a_1}t^{a_2})\operatorname{tr}(t^{a_3}t^{a_4})}_{=:\mathcal{C}_2^{a_1a_2a_3a_4}}\Bigg) \\
T_{211} \circ v^{a_1a_2a_3a_4} &= 0, \quad T_{222} \circ v^{a_1a_2a_3a_4} = 0, \quad T_{233} \circ v^{a_1a_2a_3a_4} = 0 \\
T_{311} \circ v^{a_1a_2a_3a_4} &= \frac{c_3'}{12}\Bigg(\operatorname{tr}(t^{a_1}t^{a_2}t^{a_3}t^{a_4}) + \operatorname{tr}(t^{a_1}t^{a_2}t^{a_4}t^{a_3}) - 2\operatorname{tr}(t^{a_1}t^{a_3}t^{a_2}t^{a_4}) \\
&\quad \underbrace{+ \operatorname{tr}(t^{a_1}t^{a_3}t^{a_4}t^{a_2}) - 2\operatorname{tr}(t^{a_1}t^{a_4}t^{a_2}t^{a_3}) + \operatorname{tr}(t^{a_1}t^{a_4}t^{a_3}t^{a_2})}_{=:\mathcal{C}_3^{a_1a_2a_3a_4}}\Bigg) \\
&\quad - \frac{c_4'}{6}\Bigg(\underbrace{\operatorname{tr}(t^{a_1}t^{a_4})\operatorname{tr}(t^{a_2}t^{a_3}) + \operatorname{tr}(t^{a_1}t^{a_3})\operatorname{tr}(t^{a_2}t^{a_4}) - 2\operatorname{tr}(t^{a_1}t^{a_2})\operatorname{tr}(t^{a_3}t^{a_4})}_{=:\mathcal{C}_4^{a_1a_2a_3a_4}}\Bigg)
\end{aligned}$$

$$
\begin{aligned}
T_{322} \circ v^{a_1a_2a_3a_4} &= \frac{c_5'}{4}\Bigg(\operatorname{tr}(t^{a_1}t^{a_2}t^{a_3}t^{a_4}) - \operatorname{tr}(t^{a_1}t^{a_2}t^{a_4}t^{a_3}) - \operatorname{tr}(t^{a_1}t^{a_3}t^{a_4}t^{a_2}) \\
&\quad \underbrace{+ \operatorname{tr}(t^{a_1}t^{a_4}t^{a_3}t^{a_2})\Bigg)}_{=:\mathcal{C}_5^{a_1a_2a_3a_4}} \\
&\quad + \frac{c_6'}{2}\Bigg(\underbrace{\operatorname{tr}(t^{a_1}t^{a_4})\operatorname{tr}(t^{a_2}t^{a_3}) - \operatorname{tr}(t^{a_1}t^{a_3})\operatorname{tr}(t^{a_2}t^{a_4})}_{=:\mathcal{C}_6^{a_1a_2a_3a_4}}\Bigg) \\
T_{411} \circ v^{a_1a_2a_3a_4} &= \frac{c_7'}{4}\Bigg(\operatorname{tr}(t^{a_1}t^{a_2}t^{a_3}t^{a_4}) - \operatorname{tr}(t^{a_1}t^{a_2}t^{a_4}t^{a_3}) + \operatorname{tr}(t^{a_1}t^{a_3}t^{a_4}t^{a_2}) \\
&\quad \underbrace{- \operatorname{tr}(t^{a_1}t^{a_4}t^{a_3}t^{a_2})}_{=:\mathcal{C}_7^{a_1a_2a_3a_4}}\Bigg) \\
T_{422} \circ v^{a_1a_2a_3a_4} &= \frac{c_8'}{12}\Bigg(\operatorname{tr}(t^{a_1}t^{a_2}t^{a_3}t^{a_4}) + \operatorname{tr}(t^{a_1}t^{a_2}t^{a_4}t^{a_3}) + 2\operatorname{tr}(t^{a_1}t^{a_3}t^{a_2}t^{a_4}) \\
&\quad \underbrace{- \operatorname{tr}(t^{a_1}t^{a_3}t^{a_4}t^{a_2}) - 2\operatorname{tr}(t^{a_1}t^{a_4}t^{a_2}t^{a_3}) - \operatorname{tr}(t^{a_1}t^{a_4}t^{a_3}t^{a_2})}_{=:\mathcal{C}_8^{a_1a_2a_3a_4}}\Bigg) \\
T_{433} \circ v^{a_1a_2a_3a_4} &= \frac{c_9'}{6}\Bigg(\operatorname{tr}(t^{a_1}t^{a_2}t^{a_3}t^{a_4}) + \operatorname{tr}(t^{a_1}t^{a_2}t^{a_4}t^{a_3}) - \operatorname{tr}(t^{a_1}t^{a_3}t^{a_2}t^{a_4}) \\
&\quad \underbrace{- \operatorname{tr}(t^{a_1}t^{a_3}t^{a_4}t^{a_2}) + \operatorname{tr}(t^{a_1}t^{a_4}t^{a_2}t^{a_3}) - \operatorname{tr}(t^{a_1}t^{a_4}t^{a_3}t^{a_2})}_{=:\mathcal{C}_9^{a_1a_2a_3a_4}}\Bigg) \\
T_{511} \circ v^{a_1a_2a_3a_4} &= 0
\end{aligned}
\tag{A.4a}
$$

where

$$
\begin{aligned}
c_1' &:= c_1 + c_2 + c_3 + c_4 + c_5 + c_6 \\
c_2' &:= c_7 + c_8 + c_9 \\
c_3' &:= c_1 - 2c_2 + c_3 + c_4 - 2c_5 + c_6 \\
c_4' &:= 2c_7 - c_8 - c_9 \\
c_5' &:= c_1 - c_3 - c_4 + c_6 \\
c_6' &:= c_8 - c_9 \\
c_7' &:= c_1 - c_3 + c_4 - c_6 \\
c_8' &:= c_1 + 2c_2 + c_3 - c_4 - 2c_5 - c_6 \\
c_9' &:= c_1 - c_2 + c_3 - c_4 + c_5 - c_6
\end{aligned}
\tag{A.4b}
$$

As discussed in Chapter 5.2, we act the projection operators, T_{111} and T_{322} on $\delta^{a_1a_2}\delta^{a_3a_4}$ to obtain the pieces of $\delta^{a_1a_2}\delta^{a_3a_4}$ in the $\boxed{1}\boxed{2}\boxed{3}\boxed{4}$ and the $\begin{array}{|c|c|}\hline 1&2\\\hline 3&4\\\hline\end{array}$ subspaces respectively. We then

use these projections as the starting point for the Gram-Schmidt orthogonalization procedure for each of the 2 subspaces to form a basis where 2 of the elements linearly span $\delta^{a_1a_2}\delta^{a_3a_4}$ and the other 7 are orthogonal to $\delta^{a_1a_2}\delta^{a_3a_4}$. This new basis will be given by:

$$
\begin{aligned}
\widetilde{\mathcal{C}}_1^{a_1a_2a_3a_4} &:= \underbrace{\operatorname{tr}\left(t^{a_1}t^{a_2}\right)\operatorname{tr}\left(t^{a_3}t^{a_4}\right)+\operatorname{tr}\left(t^{a_1}t^{a_3}\right)\operatorname{tr}\left(t^{a_2}t^{a_4}\right)+\operatorname{tr}\left(t^{a_1}t^{a_4}\right)\operatorname{tr}\left(t^{a_2}t^{a_3}\right)}_{\text{Piece of } \delta^{a_1a_2}\delta^{a_3a_4} \text{ from the } \boxed{1}\boxed{2}\boxed{3}\boxed{4} \text{ subspace}} \\
\widetilde{\mathcal{C}}_2^{a_1a_2a_3a_4} &:= -\frac{2\left(2N^2-3\right)}{N^3+N}\left(\operatorname{tr}\left(t^{a_1}t^{a_2}\right)\operatorname{tr}\left(t^{a_3}t^{a_4}\right)+\operatorname{tr}\left(t^{a_1}t^{a_3}\right)\operatorname{tr}\left(t^{a_2}t^{a_4}\right)+\operatorname{tr}\left(t^{a_1}t^{a_4}\right)\operatorname{tr}\left(t^{a_2}t^{a_3}\right)\right) \\
&\quad+\left(\operatorname{tr}\left(t^{a_1}t^{a_2}t^{a_3}t^{a_4}\right)+\operatorname{tr}\left(t^{a_1}t^{a_2}t^{a_4}t^{a_3}\right)+\operatorname{tr}\left(t^{a_1}t^{a_3}t^{a_2}t^{a_4}\right)\right. \\
&\quad\left.+\operatorname{tr}\left(t^{a_1}t^{a_3}t^{a_4}t^{a_2}\right)+\operatorname{tr}\left(t^{a_1}t^{a_4}t^{a_2}t^{a_3}\right)+\operatorname{tr}\left(t^{a_1}t^{a_4}t^{a_3}t^{a_2}\right)\right) \\
\widetilde{\mathcal{C}}_3^{a_1a_2a_3a_4} &:= \underbrace{-2\operatorname{tr}\left(t^{a_1}t^{a_2}\right)\operatorname{tr}\left(t^{a_3}t^{a_4}\right)+\operatorname{tr}\left(t^{a_1}t^{a_3}\right)\operatorname{tr}\left(t^{a_2}t^{a_4}\right)+\operatorname{tr}\left(t^{a_1}t^{a_4}\right)\operatorname{tr}\left(t^{a_2}t^{a_3}\right)}_{\text{Piece of } \delta^{a_1a_2}\delta^{a_3a_4} \text{ from the } \begin{smallmatrix}\boxed{1}\boxed{2}\\ \boxed{3}\boxed{4}\end{smallmatrix} \text{ subspace}} \\
\widetilde{\mathcal{C}}_4^{a_1a_2a_3a_4} &:= \frac{2N}{N^2-2}\left(-2\operatorname{tr}\left(t^{a_1}t^{a_2}\right)\operatorname{tr}\left(t^{a_3}t^{a_4}\right)+\operatorname{tr}\left(t^{a_1}t^{a_3}\right)\operatorname{tr}\left(t^{a_2}t^{a_4}\right)+\operatorname{tr}\left(t^{a_1}t^{a_4}\right)\operatorname{tr}\left(t^{a_2}t^{a_3}\right)\right)+ \\
&\quad\left(\operatorname{tr}\left(t^{a_1}t^{a_2}t^{a_3}t^{a_4}\right)+\operatorname{tr}\left(t^{a_1}t^{a_2}t^{a_4}t^{a_3}\right)-2\operatorname{tr}\left(t^{a_1}t^{a_3}t^{a_2}t^{a_4}\right)\right. \\
&\quad\left.+\operatorname{tr}\left(t^{a_1}t^{a_3}t^{a_4}t^{a_2}\right)-2\operatorname{tr}\left(t^{a_1}t^{a_4}t^{a_2}t^{a_3}\right)+\operatorname{tr}\left(t^{a_1}t^{a_4}t^{a_3}t^{a_2}\right)\right) \\
\mathcal{C}_5^{a_1a_2a_3a_4} &= \operatorname{tr}(t^{a_1}t^{a_2}t^{a_3}t^{a_4})-\operatorname{tr}(t^{a_1}t^{a_2}t^{a_4}t^{a_3})-\operatorname{tr}(t^{a_1}t^{a_3}t^{a_4}t^{a_2})+\operatorname{tr}(t^{a_1}t^{a_4}t^{a_3}t^{a_2}) \\
\mathcal{C}_6^{a_1a_2a_3a_4} &= \operatorname{tr}(t^{a_1}t^{a_4})\operatorname{tr}(t^{a_2}t^{a_3})-\operatorname{tr}(t^{a_1}t^{a_3})\operatorname{tr}(t^{a_2}t^{a_4}) \\
\mathcal{C}_7^{a_1a_2a_3a_4} &= \operatorname{tr}(t^{a_1}t^{a_2}t^{a_3}t^{a_4})-\operatorname{tr}(t^{a_1}t^{a_2}t^{a_4}t^{a_3})+\operatorname{tr}(t^{a_1}t^{a_3}t^{a_4}t^{a_2})-\operatorname{tr}(t^{a_1}t^{a_4}t^{a_3}t^{a_2}) \\
\mathcal{C}_8^{a_1a_2a_3a_4} &= \operatorname{tr}(t^{a_1}t^{a_2}t^{a_3}t^{a_4})+\operatorname{tr}(t^{a_1}t^{a_2}t^{a_4}t^{a_3})+2\operatorname{tr}(t^{a_1}t^{a_3}t^{a_2}t^{a_4})-\operatorname{tr}(t^{a_1}t^{a_3}t^{a_4}t^{a_2}) \\
&\quad-2\operatorname{tr}(t^{a_1}t^{a_4}t^{a_2}t^{a_3})-\operatorname{tr}(t^{a_1}t^{a_4}t^{a_3}t^{a_2}) \\
\mathcal{C}_9^{a_1a_2a_3a_4} &= \operatorname{tr}(t^{a_1}t^{a_2}t^{a_3}t^{a_4})+\operatorname{tr}(t^{a_1}t^{a_2}t^{a_4}t^{a_3})-\operatorname{tr}(t^{a_1}t^{a_3}t^{a_2}t^{a_4})-\operatorname{tr}(t^{a_1}t^{a_3}t^{a_4}t^{a_2}) \\
&\quad+\operatorname{tr}(t^{a_1}t^{a_4}t^{a_2}t^{a_3})-\operatorname{tr}(t^{a_1}t^{a_4}t^{a_3}t^{a_2})
\end{aligned}
\tag{A.5a}
$$

where, in case we wish to normalise, the norms of these objects are given by

$$
\begin{aligned}
\|\widetilde{\mathcal{C}}_1^{a_1a_2a_3a_4}\|^2 &= \frac{3}{16}\left(N^4-1\right) \\
\|\widetilde{\mathcal{C}}_2^{a_1a_2a_3a_4}\|^2 &= \frac{3\left(N^2\left(N^2-7\right)^2-36\right)}{8\left(N^2+1\right)} \\
\|\widetilde{\mathcal{C}}_3^{a_1a_2a_3a_4}\|^2 &= \frac{3}{8}\left(N^4-3N^2+2\right) \\
\|\widetilde{\mathcal{C}}_4^{a_1a_2a_3a_4}\|^2 &= \frac{3N^2\left(N^4-5N^2+4\right)}{4\left(N^2-2\right)} \\
\|\mathcal{C}_5^{a_1a_2a_3a_4}\|^2 &= \frac{1}{4}N^2\left(N^2-1\right) \\
\|\mathcal{C}_6^{a_1a_2a_3a_4}\|^2 &= \frac{1}{8}\left(N^4-3N^2+2\right) \\
\|\mathcal{C}_7^{a_1a_2a_3a_4}\|^2 &= \frac{1}{4}\left(N^4-5N^2+4\right)
\end{aligned}
$$

$$\|\mathcal{C}_8^{a_1a_2a_3a_4}\|^2 = \frac{3}{4}\left(N^4 - 5N^2 + 4\right)$$
$$\|\mathcal{C}_9^{a_1a_2a_3a_4}\|^2 = \frac{3}{8}\left(N^4 - 5N^2 + 4\right) \tag{A.5b}$$

In this new basis, the basis elements for the $\boxed{1}\boxed{2}\boxed{3}\boxed{4}$ and $\begin{array}{|c|c|}\hline 1&2\\\hline 3&4\\\hline\end{array}$ are orthogonal, with one element from each basis overlapping with $\delta^{a_1a_2}\delta^{a_3a_4}$:

$$\left\langle \widetilde{\mathcal{C}}_1^{a_1a_2a_3a_4} | \widetilde{\mathcal{C}}_2^{a_1a_2a_3a_4} \right\rangle = 0$$
$$\left\langle \widetilde{\mathcal{C}}_3^{a_1a_2a_3a_4} | \widetilde{\mathcal{C}}_4^{a_1a_2a_3a_4} \right\rangle = 0 \tag{A.6}$$

Based on Chapter 5.2's new notation for adjoint colour singlet states, the basis for $\mathfrak{C}\left(A^{\otimes}\right)$ meets the property of

$$\left(T_{\Xi lm} \circ \mathcal{C}_{\Theta i}^{(k)}\right)^{a_1a_2a_3a_4} = \delta_{\Xi\Theta}\delta_{mi}\left(\mathcal{C}_{\Theta l}^{(k)}\right)^{a_1a_2a_3a_4} \tag{A.7}$$

with $\delta^{a_1a_2}\delta^{a_3a_4}$'s segments separated in the $\boxed{1}\boxed{2}\boxed{3}\boxed{4}$ and $\begin{array}{|c|c|}\hline 1&2\\\hline 3&4\\\hline\end{array}$ subspaces, orthogonal to other basis elements, following Appendix A.1's numbering for Young diagrams and tableaux:

$$\left(\mathcal{C}_{11}^{(1)}\right)^{a_1a_2a_3a_4} := \underbrace{\frac{4\left(\mathrm{tr}\left(t^{a_1}t^{a_4}\right)\mathrm{tr}\left(t^{a_2}t^{a_3}\right) + \mathrm{tr}\left(t^{a_1}t^{a_3}\right)\mathrm{tr}\left(t^{a_2}t^{a_4}\right) + \mathrm{tr}\left(t^{a_1}t^{a_2}\right)\mathrm{tr}\left(t^{a_3}t^{a_4}\right)\right)}{\sqrt{3}\sqrt{N^4-1}}}_{\text{Piece of } \delta^{a_1a_2}\delta^{a_3a_4} \text{ in the } \boxed{1}\boxed{2}\boxed{3}\boxed{4} \text{ subspace}}$$

$$\begin{aligned}\left(\mathcal{C}_{11}^{(2)}\right)^{a_1a_2a_3a_4} :=\ & \frac{2\sqrt{\frac{2}{3}}}{N\sqrt{N^8 - 13N^6 + 35N^4 + 13N^2 - 36}}\Bigg(2\left(3-2N^2\right)\mathrm{tr}\left(t^{a_1}t^{a_4}\right)\mathrm{tr}\left(t^{a_2}t^{a_3}\right)\\ & + 2\left(3-2N^2\right)\mathrm{tr}\left(t^{a_1}t^{a_3}\right)\mathrm{tr}\left(t^{a_2}t^{a_4}\right) + N\Bigg(\left(N^2+1\right)\Bigg(\mathrm{tr}\left(t^{a_1}t^{a_2}t^{a_3}t^{a_4}\right)\\ & + \mathrm{tr}\left(t^{a_1}t^{a_2}t^{a_4}t^{a_3}\right) + \mathrm{tr}\left(t^{a_1}t^{a_3}t^{a_2}t^{a_4}\right) + \mathrm{tr}\left(t^{a_1}t^{a_3}t^{a_4}t^{a_2}\right) + \mathrm{tr}\left(t^{a_1}t^{a_4}t^{a_2}t^{a_3}\right)\\ & + \mathrm{tr}\left(t^{a_1}t^{a_4}t^{a_3}t^{a_2}\right)\Bigg) - 4N\mathrm{tr}\left(t^{a_1}t^{a_2}\right)\mathrm{tr}\left(t^{a_3}t^{a_4}\right)\Bigg) + 6\mathrm{tr}\left(t^{a_1}t^{a_2}\right)\mathrm{tr}\left(t^{a_3}t^{a_4}\right)\Bigg)\end{aligned}$$

$$\left(\mathcal{C}_{31}^{(1)}\right)^{a_1a_2a_3a_4} := \underbrace{-\frac{2\sqrt{\frac{2}{3}}\left(\mathrm{tr}\left(t^{a_1}t^{a_4}\right)\mathrm{tr}\left(t^{a_2}t^{a_3}\right) + \mathrm{tr}\left(t^{a_1}t^{a_3}\right)\mathrm{tr}\left(t^{a_2}t^{a_4}\right) - 2\mathrm{tr}\left(t^{a_1}t^{a_2}\right)\mathrm{tr}\left(t^{a_3}t^{a_4}\right)\right)}{\sqrt{N^4-3N^2+2}}}_{\text{Piece of } \delta^{a_1a_2}\delta^{a_3a_4} \text{ in the } \begin{array}{|c|c|}\hline 1&2\\\hline 3&4\\\hline\end{array} \text{ subspace}}$$

$$\begin{aligned}\left(\mathcal{C}_{31}^{(2)}\right)^{a_1a_2a_3a_4} :=\ & \frac{2}{\sqrt{3}\sqrt{\frac{N^2(N^4-5N^2+4)}{N^2-2}}}\Bigg(\frac{2N}{N^2-2}\Bigg(\mathrm{tr}\left(t^{a_1}t^{a_4}\right)\mathrm{tr}\left(t^{a_2}t^{a_3}\right) + \mathrm{tr}\left(t^{a_1}t^{a_3}\right)\mathrm{tr}\left(t^{a_2}t^{a_4}\right)\\ & - 2\mathrm{tr}\left(t^{a_1}t^{a_2}\right)\mathrm{tr}\left(t^{a_3}t^{a_4}\right)\Bigg) + \mathrm{tr}\left(t^{a_1}t^{a_2}t^{a_3}t^{a_4}\right) + \mathrm{tr}\left(t^{a_1}t^{a_2}t^{a_4}t^{a_3}\right)\\ & - 2\mathrm{tr}\left(t^{a_1}t^{a_3}t^{a_2}t^{a_4}\right) + \mathrm{tr}\left(t^{a_1}t^{a_3}t^{a_4}t^{a_2}\right) - 2\mathrm{tr}\left(t^{a_1}t^{a_4}t^{a_2}t^{a_3}\right) + \mathrm{tr}\left(t^{a_1}t^{a_4}t^{a_3}t^{a_2}\right)\Bigg)\end{aligned}$$

$$\left(\mathcal{C}_{32}^{(1)}\right)^{a_1a_2a_3a_4} := \frac{2\sqrt{2}\left(\mathrm{tr}\left(t^{a_1}t^{a_3}\right)\mathrm{tr}\left(t^{a_2}t^{a_4}\right) - \mathrm{tr}\left(t^{a_1}t^{a_4}\right)\mathrm{tr}\left(t^{a_2}t^{a_3}\right)\right)}{\sqrt{N^4-3N^2+2}}$$

$$
\begin{aligned}
\left(\mathcal{C}_{32}^{(2)}\right)^{a_1a_2a_3a_4} &:= \frac{1}{(N^2-2)\sqrt{\frac{N^2(N^4-5N^2+4)}{N^2-2}}}\Big(-2\left(N^2-2\right)\Big(\operatorname{tr}\left(t^{a_1}t^{a_2}t^{a_3}t^{a_4}\right)-\operatorname{tr}\left(t^{a_1}t^{a_2}t^{a_4}t^{a_3}\right)\\
&\quad -\operatorname{tr}\left(t^{a_1}t^{a_3}t^{a_4}t^{a_2}\right)+\operatorname{tr}\left(t^{a_1}t^{a_4}t^{a_3}t^{a_2}\right)\Big)+4N\Big(\operatorname{tr}\left(t^{a_1}t^{a_4}\right)\operatorname{tr}\left(t^{a_2}t^{a_3}\right)\\
&\quad -\operatorname{tr}\left(t^{a_1}t^{a_3}\right)\operatorname{tr}\left(t^{a_2}t^{a_4}\right)\Big)\Big)\\
\left(\mathcal{C}_{41}^{(1)}\right)^{a_1a_2a_3a_4} &:= \frac{2}{\sqrt{4-5N^2+N^4}}\,\mathcal{C}_7^{a_1a_2a_3a_4}\\
&= \frac{2}{\sqrt{4-5N^2+N^4}}\Big(\operatorname{tr}(t^{a_1}t^{a_2}t^{a_3}t^{a_4})-\operatorname{tr}(t^{a_1}t^{a_2}t^{a_4}t^{a_3})\\
&\quad +\operatorname{tr}(t^{a_1}t^{a_3}t^{a_4}t^{a_2})-\operatorname{tr}(t^{a_1}t^{a_4}t^{a_3}t^{a_2})\Big)\\
\left(\mathcal{C}_{42}^{(1)}\right)^{a_1a_2a_3a_4} &:= \frac{2}{\sqrt{3}\sqrt{4-5N^2+N^4}}\mathcal{C}_8^{a_1a_2a_3a_4}\\
&= \frac{2}{\sqrt{3}\sqrt{4-5N^2+N^4}}\Big(\operatorname{tr}(t^{a_1}t^{a_2}t^{a_3}t^{a_4})+\operatorname{tr}(t^{a_1}t^{a_2}t^{a_4}t^{a_3})\\
&\quad +2\operatorname{tr}(t^{a_1}t^{a_3}t^{a_2}t^{a_4})-\operatorname{tr}(t^{a_1}t^{a_3}t^{a_4}t^{a_2})-2\operatorname{tr}(t^{a_1}t^{a_4}t^{a_2}t^{a_3})-\operatorname{tr}(t^{a_1}t^{a_4}t^{a_3}t^{a_2})\Big)\\
\left(\mathcal{C}_{43}^{(1)}\right)^{a_1a_2a_3a_4} &:= \frac{2\sqrt{2}}{\sqrt{3}\sqrt{4-5N^2+N^4}}\mathcal{C}_9^{a_1a_2a_3a_4}\\
&= \frac{2\sqrt{2}}{\sqrt{3}\sqrt{4-5N^2+N^4}}\Big(\operatorname{tr}(t^{a_1}t^{a_2}t^{a_3}t^{a_4})+\operatorname{tr}(t^{a_1}t^{a_2}t^{a_4}t^{a_3})-\operatorname{tr}(t^{a_1}t^{a_3}t^{a_2}t^{a_4})\\
&\quad -\operatorname{tr}(t^{a_1}t^{a_3}t^{a_4}t^{a_2})+\operatorname{tr}(t^{a_1}t^{a_4}t^{a_2}t^{a_3})-\operatorname{tr}(t^{a_1}t^{a_4}t^{a_3}t^{a_2})\Big)
\end{aligned}
\tag{A.8}
$$

It is tedious but straightforward to verify that this basis is orthonormal.

Appendix B

Change of Basis Matrices between the Different Bases of Colour Singlet States

Since the bases in Eqs. 3.78b, 3.89, and 3.105 span the same vector space, one can determine the change-of-basis matrices between them. Given that these bases are orthogonal, standard linear algebra techniques can be applied to compute these matrices. It's important to reorder the fundamental and anti-fundamental lines of the basis states appropriately to facilitate the computation of inner products when determining the change-of-basis matrices. For convenience in future reference, these matrices are provided here.

The change of basis from the Fierz basis to the basis corresponding to $\mathfrak{G}_3$ is given by:

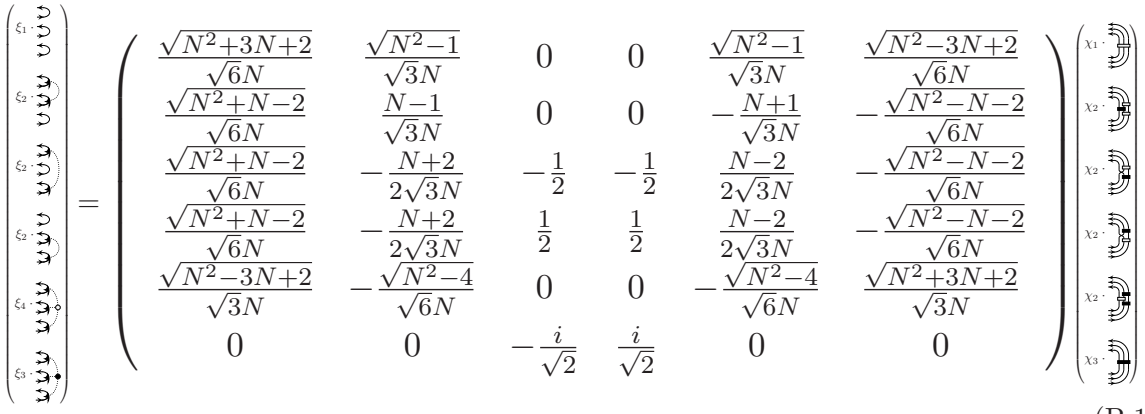

$$\begin{pmatrix}
\frac{\sqrt{N^2+3N+2}}{\sqrt{6}N} & \frac{\sqrt{N^2-1}}{\sqrt{3}N} & 0 & 0 & \frac{\sqrt{N^2-1}}{\sqrt{3}N} & \frac{\sqrt{N^2-3N+2}}{\sqrt{6}N} \\
\frac{\sqrt{N^2+N-2}}{\sqrt{6}N} & \frac{N-1}{\sqrt{3}N} & 0 & 0 & -\frac{N+1}{\sqrt{3}N} & -\frac{\sqrt{N^2-N-2}}{\sqrt{6}N} \\
\frac{\sqrt{N^2+N-2}}{\sqrt{6}N} & -\frac{N+2}{2\sqrt{3}N} & -\frac{1}{2} & -\frac{1}{2} & \frac{N-2}{2\sqrt{3}N} & -\frac{\sqrt{N^2-N-2}}{\sqrt{6}N} \\
\frac{\sqrt{N^2+N-2}}{\sqrt{6}N} & -\frac{N+2}{2\sqrt{3}N} & \frac{1}{2} & \frac{1}{2} & \frac{N-2}{2\sqrt{3}N} & -\frac{\sqrt{N^2-N-2}}{\sqrt{6}N} \\
\frac{\sqrt{N^2-3N+2}}{\sqrt{3}N} & -\frac{\sqrt{N^2-4}}{\sqrt{6}N} & 0 & 0 & -\frac{\sqrt{N^2-4}}{\sqrt{6}N} & \frac{\sqrt{N^2+3N+2}}{\sqrt{3}N} \\
0 & 0 & -\frac{i}{\sqrt{2}} & \frac{i}{\sqrt{2}} & 0 & 0
\end{pmatrix} \tag{B.1}$$

The change of basis from the Fierz basis to the mixed Fierz/HYPO basis in Eq. 3.101 is given by:

$$\begin{pmatrix} \xi_1 \cdot \\ \xi_2 \cdot \\ \xi_2 \cdot \\ \xi_2 \cdot \\ \xi_4 \cdot \\ \xi_3 \cdot \end{pmatrix} = \begin{pmatrix} \frac{\sqrt{\frac{1}{N}+1}}{\sqrt{2}} & \frac{\sqrt{\frac{N-1}{N}}}{\sqrt{2}} & 0 & 0 & 0 & 0 \\ \frac{\sqrt{\frac{N-1}{N}}}{\sqrt{2}} & -\frac{\sqrt{\frac{1}{N}+1}}{\sqrt{2}} & 0 & 0 & 0 & 0 \\ 0 & 0 & -\frac{1}{2} & \frac{1}{2}\sqrt{\frac{N+2}{N}} & -\frac{1}{2}\sqrt{\frac{N-2}{N}} & -\frac{1}{2} \\ 0 & 0 & \frac{1}{2} & \frac{1}{2}\sqrt{\frac{N+2}{N}} & -\frac{1}{2}\sqrt{\frac{N-2}{N}} & \frac{1}{2} \\ 0 & 0 & 0 & \frac{\sqrt{\frac{N-2}{N}}}{\sqrt{2}} & \frac{\sqrt{\frac{N+2}{N}}}{\sqrt{2}} & 0 \\ 0 & 0 & -\frac{i}{\sqrt{2}} & 0 & 0 & \frac{i}{\sqrt{2}} \end{pmatrix} \begin{pmatrix} v_1 \cdot \\ v_2 \cdot \\ v_3 \cdot \\ v_4 \cdot \\ v_5 \cdot \\ v_6 \cdot \end{pmatrix} \tag{B.2}$$

Here, ξ_i, v_i and χ_i are the appropriate normalization factors given in Eqs. 3.79, 3.89b and 3.102.

These change-of-basis matrices provide a straightforward method to compute the amplitude matrices—denoted as $\mathcal{M}_Y$ in Eq. 4.1 and $\widetilde{M}_Y$ in Eq. 5.1—across different bases, given that these matrices are known in one basis. Specifically, if $\mathfrak{M}^{S_1}$ represents such a matrix in the singlet state basis S_1, then to determine $\mathfrak{M}^{S_2}$ in another singlet state basis S_2, one can utilize the change-of-basis matrix from S_1 to S_2, denoted as $\mathfrak{C}_{S_2 \leftarrow S_1}$, and compute:

$$\mathfrak{M}^{S_2} = \mathfrak{C}_{S_2 \leftarrow S_1}\, \mathfrak{M}^{S_1}\, \mathfrak{C}^{\dagger}_{S_2 \leftarrow S_1} \tag{B.3}$$

Applying Eq. B.3 allows for the efficient computation of the amplitude matrices $\mathcal{M}_Y$ and $\widetilde{\mathcal{M}}_Y$ in different bases, thereby reducing computational resources when these matrices have been previously determined in a particular basis.

Appendix C

The Symmetry Group from the Gaussian Truncation Squared

A discussion on the symmetry groups that may arise from the colour structures in the truncation in Eq. 4.18 is in order. To start, recall the Gaussian truncation squared:

$$\left(\widehat{L}_2(Y)+\widehat{R}_2(Y)\right)^2 = \int\limits_{\boldsymbol{u}_1\boldsymbol{u}_2\boldsymbol{u}_3\boldsymbol{u}_4} G^{(2;\delta)}_{\boldsymbol{u}_1\boldsymbol{u}_2}(Y)G^{(2;\delta)}_{\boldsymbol{u}_3\boldsymbol{u}_4}(Y)\delta^{a_1a_2}\delta^{a_3a_4}\Big(\nabla^{a_1}_{\boldsymbol{u}_1}\nabla^{a_2}_{\boldsymbol{u}_2}\nabla^{a_3}_{\boldsymbol{u}_3}\nabla^{a_4}_{\boldsymbol{u}_4} + \nabla^{a_1}_{\boldsymbol{u}_1}\nabla^{a_2}_{\boldsymbol{u}_2}\overline{\nabla}^{a_3}_{\boldsymbol{u}_3}\overline{\nabla}^{a_4}_{\boldsymbol{u}_4} + \overline{\nabla}^{a_1}_{\boldsymbol{u}_1}\overline{\nabla}^{a_2}_{\boldsymbol{u}_2}\nabla^{a_3}_{\boldsymbol{u}_3}\nabla^{a_4}_{\boldsymbol{u}_4} + \overline{\nabla}^{a_1}_{\boldsymbol{u}_1}\overline{\nabla}^{a_2}_{\boldsymbol{u}_2}\overline{\nabla}^{a_3}_{\boldsymbol{u}_3}\overline{\nabla}^{a_4}_{\boldsymbol{u}_4}\Big) \tag{C.1}$$

As we can see, the square of the Gaussian truncation has 4 terms that will each need to be investigated with regards to the $\delta^{a_1a_2}\delta^{a_3a_4}$ colour structure that appears in order to see how the symmetry features of this colour structure imprint themselves onto the colour structure function. Suppressing rapidity dependence, let us generalize a bit and instead of looking specifically at the case where we have $G^{(2;\delta)}_{\boldsymbol{u}_1\boldsymbol{u}_2}G^{(2;\delta)}_{\boldsymbol{u}_3\boldsymbol{u}_4}$ in Eq. C.1 (the colour structure functions corresponding to the Gaussian truncation), let's look at a more general 4-point colour structure function, $G^{(\delta)}_{\boldsymbol{u}_1\boldsymbol{u}_2\boldsymbol{u}_3\boldsymbol{u}_4}$, with the $\delta^{a_1a_2}\delta^{a_3a_4}$ colour structure, i.e

$$\int\limits_{\boldsymbol{u}_1\boldsymbol{u}_2\boldsymbol{u}_3\boldsymbol{u}_4} G^{(\delta)}_{\boldsymbol{u}_1\boldsymbol{u}_2\boldsymbol{u}_3\boldsymbol{u}_4}\delta^{a_1a_2}\delta^{a_3a_4}\Big(\nabla^{a_1}_{\boldsymbol{u}_1}\nabla^{a_2}_{\boldsymbol{u}_2}\nabla^{a_3}_{\boldsymbol{u}_3}\nabla^{a_4}_{\boldsymbol{u}_4} + \nabla^{a_1}_{\boldsymbol{u}_1}\nabla^{a_2}_{\boldsymbol{u}_2}\overline{\nabla}^{a_3}_{\boldsymbol{u}_3}\overline{\nabla}^{a_4}_{\boldsymbol{u}_4} + \overline{\nabla}^{a_1}_{\boldsymbol{u}_1}\overline{\nabla}^{a_2}_{\boldsymbol{u}_2}\nabla^{a_3}_{\boldsymbol{u}_3}\nabla^{a_4}_{\boldsymbol{u}_4} + \overline{\nabla}^{a_1}_{\boldsymbol{u}_1}\overline{\nabla}^{a_2}_{\boldsymbol{u}_2}\overline{\nabla}^{a_3}_{\boldsymbol{u}_3}\overline{\nabla}^{a_4}_{\boldsymbol{u}_4}\Big) \tag{C.2}$$

We see that in Eq. C.2, the 4-terms each have a unique structure with regards to the left- and right-invariant vector fields that appear. The first- and fourth-terms each have only left- and right-invariant vector fields respectively whereas the middle 2 terms have a mix of left- and right-invariant vector fields. The middle 2 terms will be slightly more difficult to deal with so we set it aside for now and look at the first and fourth terms. Following the

discussion in [33], we symmetrise the first and fourth terms as follows:

$$\int\limits_{\boldsymbol{u}_1\boldsymbol{u}_2\boldsymbol{u}_3\boldsymbol{u}_4} G^{(\delta)}_{\boldsymbol{u}_1\boldsymbol{u}_2\boldsymbol{u}_3\boldsymbol{u}_4}\delta^{a_1a_2}\delta^{a_3a_4}\left(\nabla^{a_1}_{\boldsymbol{u}_1}\nabla^{a_2}_{\boldsymbol{u}_2}\nabla^{a_3}_{\boldsymbol{u}_3}\nabla^{a_4}_{\boldsymbol{u}_4}+\overline{\nabla}^{a_1}_{\boldsymbol{u}_1}\overline{\nabla}^{a_2}_{\boldsymbol{u}_2}\overline{\nabla}^{a_3}_{\boldsymbol{u}_3}\overline{\nabla}^{a_4}_{\boldsymbol{u}_4}\right)$$

$$=\frac{1}{4!}\sum_{\sigma\in S_4}\int\limits_{\boldsymbol{u}_1\boldsymbol{u}_2\boldsymbol{u}_3\boldsymbol{u}_4} G^{(\delta)}_{\boldsymbol{u}_{\sigma(1)}\boldsymbol{u}_{\sigma(2)}\boldsymbol{u}_{\sigma(3)}\boldsymbol{u}_{\sigma(4)}}\delta^{a_1a_2}\delta^{a_3a_4}\Bigg(\nabla^{a_1}_{\boldsymbol{u}_{\sigma(1)}}\nabla^{a_2}_{\boldsymbol{u}_{\sigma(2)}}\nabla^{a_3}_{\boldsymbol{u}_{\sigma(3)}}\nabla^{a_4}_{\boldsymbol{u}_{\sigma(4)}}$$

$$+\overline{\nabla}^{a_1}_{\boldsymbol{u}_{\sigma(1)}}\overline{\nabla}^{a_2}_{\boldsymbol{u}_{\sigma(2)}}\overline{\nabla}^{a_3}_{\boldsymbol{u}_{\sigma(3)}}\overline{\nabla}^{a_4}_{\boldsymbol{u}_{\sigma(4)}}\Bigg)$$

(Using the fact that the integration measure is invariant under permutations of coordinates)

$$=\frac{1}{4!}\sum_{\sigma\in S_4}\int\limits_{\boldsymbol{u}_1\boldsymbol{u}_2\boldsymbol{u}_3\boldsymbol{u}_4} G^{(\delta)}_{\boldsymbol{u}_{\sigma(1)}\boldsymbol{u}_{\sigma(2)}\boldsymbol{u}_{\sigma(3)}\boldsymbol{u}_{\sigma(4)}}\delta^{a_1a_2}\delta^{a_3a_4}\Bigg(\nabla^{a_{\sigma^{-1}(1)}}_{\boldsymbol{u}_1}\nabla^{a_{\sigma^{-1}(2)}}_{\boldsymbol{u}_2}\nabla^{a_{\sigma^{-1}(3)}}_{\boldsymbol{u}_3}\nabla^{a_{\sigma^{-1}(4)}}_{\boldsymbol{u}_4}$$

$$+\overline{\nabla}^{a_{\sigma^{-1}(1)}}_{\boldsymbol{u}_1}\overline{\nabla}^{a_{\sigma^{-1}(2)}}_{\boldsymbol{u}_2}\overline{\nabla}^{a_{\sigma^{-1}(3)}}_{\boldsymbol{u}_3}\overline{\nabla}^{a_{\sigma^{-1}41)}}_{\boldsymbol{u}_4}\Bigg)+\text{commutator terms}$$

(Commuting all the $\nabla^{a_i}_{\boldsymbol{u}_j}$'s and $\overline{\nabla}^{a_i}_{\boldsymbol{u}_j}$'s until the coordinate labels are in ascending order in all terms)

$$=\frac{1}{4!}\sum_{\sigma\in S_4}\int\limits_{\boldsymbol{u}_1\boldsymbol{u}_2\boldsymbol{u}_3\boldsymbol{u}_4} G^{(\delta)}_{\boldsymbol{u}_{\sigma(1)}\boldsymbol{u}_{\sigma(2)}\boldsymbol{u}_{\sigma(3)}\boldsymbol{u}_{\sigma(4)}}\delta^{a_{\sigma(1)}a_{\sigma(2)}}\delta^{a_{\sigma(3)}a_{\sigma(4)}}\left(\nabla^{a_1}_{\boldsymbol{u}_1}\nabla^{a_2}_{\boldsymbol{u}_2}\nabla^{a_3}_{\boldsymbol{u}_3}\nabla^{a_4}_{\boldsymbol{u}_4}+\overline{\nabla}^{a_1}_{\boldsymbol{u}_1}\overline{\nabla}^{a_2}_{\boldsymbol{u}_2}\overline{\nabla}^{a_3}_{\boldsymbol{u}_3}\overline{\nabla}^{a_4}_{\boldsymbol{u}_4}\right)$$

(By a relabelling of indices)

$$=\int\limits_{\boldsymbol{u}_1\boldsymbol{u}_2\boldsymbol{u}_3\boldsymbol{u}_4}\left(\frac{1}{4!}\sum_{\sigma\in S_4} G^{(\delta)}_{\boldsymbol{u}_{\sigma(1)}\boldsymbol{u}_{\sigma(2)}\boldsymbol{u}_{\sigma(3)}\boldsymbol{u}_{\sigma(4)}}\delta^{a_{\sigma(1)}a_{\sigma(2)}}\delta^{a_{\sigma(3)}a_{\sigma(4)}}\right)\Bigg(\nabla^{a_1}_{\boldsymbol{u}_1}\nabla^{a_2}_{\boldsymbol{u}_2}\nabla^{a_3}_{\boldsymbol{u}_3}\nabla^{a_4}_{\boldsymbol{u}_4}$$

$$+\overline{\nabla}^{a_1}_{\boldsymbol{u}_1}\overline{\nabla}^{a_2}_{\boldsymbol{u}_2}\overline{\nabla}^{a_3}_{\boldsymbol{u}_3}\overline{\nabla}^{a_4}_{\boldsymbol{u}_4}\Bigg)$$

$$=\int\limits_{\boldsymbol{u}_1\boldsymbol{u}_2\boldsymbol{u}_3\boldsymbol{u}_4}\left(\frac{1}{4!}\sum_{\sigma\in S_4}\left(\sigma\circ G^{(\delta)}_{\boldsymbol{u}_1\boldsymbol{u}_2\boldsymbol{u}_3\boldsymbol{u}_4}\right)\left(\sigma\circ\delta^{a_1a_2}\delta^{a_3a_4}\right)\right)\left(\nabla^{a_1}_{\boldsymbol{u}_1}\nabla^{a_2}_{\boldsymbol{u}_2}\nabla^{a_3}_{\boldsymbol{u}_3}\nabla^{a_4}_{\boldsymbol{u}_4}+\overline{\nabla}^{a_1}_{\boldsymbol{u}_1}\overline{\nabla}^{a_2}_{\boldsymbol{u}_2}\overline{\nabla}^{a_3}_{\boldsymbol{u}_3}\overline{\nabla}^{a_4}_{\boldsymbol{u}_4}\right) \tag{C.3}$$

where we have chosen the notation for group algebra elements acting on arbitrary functions of the transverse coordinates and colour structures with colour indices:

$$\left(\sum_{\sigma\in S_n}\alpha_\sigma\sigma\right)\circ F_{\boldsymbol{u}_1\boldsymbol{u}_2\ldots\boldsymbol{u}_n}:=\sum_{\sigma\in S_n}\alpha_\sigma F_{\boldsymbol{u}_{\sigma(1)}\boldsymbol{u}_{\sigma(2)}\cdots\boldsymbol{u}_{\sigma(n)}} \tag{C.4}$$

for $\alpha_\sigma\in S_n$ and for any arbitrary function F that has n transverse coordinates and

$$\left(\sum_{\sigma\in S_n}\alpha_\sigma\sigma\right)\circ C^{a_1a_2\ldots a_n}:=\sum_{\sigma\in S_n}\alpha_\sigma C^{a_{\sigma(1)}a_{\sigma(2)}\cdots a_{\sigma(n)}} \tag{C.5}$$

for $\sigma \in S_n$ and for any arbitrary colour structure C that has n colour indices. We choose this notation to make the results easier to follow. Now, looking more closely at $\sigma \circ \delta^{a_1a_2}\delta^{a_3a_4}$ in Eq. C.3, we see that there are some permutations in S_4 that leave $\delta^{a_1a_2}\delta^{a_3a_4}$. For example, the permutation, (12)(34) acting on $\delta^{a_1a_2}\delta^{a_3a_4}$ gives:

$$\begin{aligned}(12)(34) \circ \delta^{a_1a_2}\delta^{a_3a_4} &= \delta^{a_2a_1}\delta^{a_4a_3} \\ &= \delta^{a_1a_2}\delta^{a_3a_4} \quad (\delta^{a_1a_2} \text{ is symmetric about an interchange of its indices})\end{aligned} \tag{C.6}$$

Permutations that preserve $\delta^{a_1a_2}\delta^{a_3a_4}$ include swapping a_1 with a_2, a_3 with a_4, or both. Additionally, swapping a_1a_2 indices on the left with a_3a_4 indices on the right (e.g., the (13)(24) permutation transforming $\delta^{a_1a_2}\delta^{a_3a_4}$ to $(13)(24) \circ \delta^{a_1a_2}\delta^{a_3a_4} = \delta^{a_3a_4}\delta^{a_1a_2} = \delta^{a_1a_2}\delta^{a_3a_4}$) combined with these swaps also maintains invariance. The invariance of $\delta^{a_1a_2}\delta^{a_3a_4}$ arises from the fact that, once again, $\delta^{a_1a_2}$, is invariant under an interchange of its indices and that $\delta^{a_1a_2}$ is a scalar and hence, it commutes multiplicatively. Thus, the generating set formed by the permutations (12), (34) and (13)(14) will give the subset of all permutations in S_4 that leave $\delta^{a_1a_2}\delta^{a_3a_4}$.

In fact, this subset also forms a subgroup of S_4 [1]. This subgroup is therefore given by (where we have labelled it as $S_{\delta\delta}$):

$$\begin{aligned}S_{\delta\delta} &= \{(), (12), (34), (1324), (1423), (12)(34), (13)(24), (14)(23)\} \\ &= \end{aligned} \tag{C.7}$$

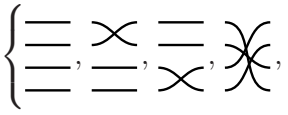

Since we have this subgroup $S_{\delta\delta}$, we can find all of its left- and right-cosets which partition the S_4 permutation group. Unfortunately, however, $S_{\delta\delta}$ is not a normal subgroup as can easily be verified. Nevertheless, we proceed and investigate how the elements in the left- and right-cosets act on $\delta^{a_1a_2}\delta^{a_3a_4}$. Each left-coset permutation defines a unique Kronecker product structure in its indices when acting on $\delta^{a_1a_2}\delta^{a_3a_4}$. Thus, the three left-cosets correspond to distinct Kronecker δ structures in their index permutations on $\delta^{a_1a_2}\delta^{a_3a_4}$. Permutations in the left-coset from acting the permutation $(24) =$  on subgroup $S_{\delta\delta}$ result in the $\delta^{a_1a_4}\delta^{a_2a_3}$ structure when acting on $\delta^{a_1a_2}\delta^{a_3a_4}$, as a_2 and a_4 indices swap, similar to the  permutation. This holds true for the left-coset from the $(23) =$  permutation on $S_{\delta\delta}$, where the  $\cdot\, S_{\delta\delta}$

[1] We suspect that this subgroup may in-fact be isomorphic to the dihedral group as it has 8 elements and is non-abelian but that is yet to be confirmed and is not important for our purposes.

left-coset gives the $\delta^{a_1a_3}\delta^{a_2a_4}$ structure when acting on $\delta^{a_1a_2}\delta^{a_3a_4}$.

Thus, since the left-cosets partition the S_4 group, we can in-turn express the sum over all permutations of S_4 in Eq. C.3 as 3 separate sums over the 3 left-cosets. I.e.

$$
\begin{aligned}
&\int_{\boldsymbol{u}_1\boldsymbol{u}_2\boldsymbol{u}_3\boldsymbol{u}_4} \left(\frac{1}{4!}\sum_{\sigma\in S_4}\left(\sigma\circ G^{(\delta)}_{\boldsymbol{u}_1\boldsymbol{u}_2\boldsymbol{u}_3\boldsymbol{u}_4}\right)\left(\sigma\circ\delta^{a_1a_2}\delta^{a_3a_4}\right)\right)\left(\nabla^{a_1}_{\boldsymbol{u}_1}\nabla^{a_2}_{\boldsymbol{u}_2}\nabla^{a_3}_{\boldsymbol{u}_3}\nabla^{a_4}_{\boldsymbol{u}_4}+\overline{\nabla}^{a_1}_{\boldsymbol{u}_1}\overline{\nabla}^{a_2}_{\boldsymbol{u}_2}\overline{\nabla}^{a_3}_{\boldsymbol{u}_3}\overline{\nabla}^{a_4}_{\boldsymbol{u}_4}\right)\\
&=\frac{1}{4!}\int_{\boldsymbol{u}_1\boldsymbol{u}_2\boldsymbol{u}_3\boldsymbol{u}_4}\left(\left(\sum_{\sigma_1\in S_{\delta\delta}}\left(\sigma_1\circ G^{(\delta)}_{\boldsymbol{u}_1\boldsymbol{u}_2\boldsymbol{u}_3\boldsymbol{u}_4}\right)\underbrace{\left(\sigma_1\circ\delta^{a_1a_2}\delta^{a_3a_4}\right)}_{\delta^{a_1a_2}\delta^{a_3a_4}}\right)\right.\\
&+\left(\sum_{\sigma_2\in(24)\cdot S_{\delta\delta}}\left(\sigma_2\circ G^{(\delta)}_{\boldsymbol{u}_1\boldsymbol{u}_2\boldsymbol{u}_3\boldsymbol{u}_4}\right)\underbrace{\left(\sigma_2\circ\delta^{a_1a_2}\delta^{a_3a_4}\right)}_{\delta^{a_1a_4}\delta^{a_2a_3}}\right)\\
&\left.+\left(\sum_{\sigma_3\in(23)\cdot S_{\delta\delta}}\left(\sigma_3\circ G^{(\delta)}_{\boldsymbol{u}_1\boldsymbol{u}_2\boldsymbol{u}_3\boldsymbol{u}_4}\right)\underbrace{\left(\sigma_3\circ\delta^{a_1a_2}\delta^{a_3a_4}\right)}_{\delta^{a_1a_3}\delta^{a_2a_4}}\right)\left(\nabla^{a_1}_{\boldsymbol{u}_1}\nabla^{a_2}_{\boldsymbol{u}_2}\nabla^{a_3}_{\boldsymbol{u}_3}\nabla^{a_4}_{\boldsymbol{u}_4}+\overline{\nabla}^{a_1}_{\boldsymbol{u}_1}\overline{\nabla}^{a_2}_{\boldsymbol{u}_2}\overline{\nabla}^{a_3}_{\boldsymbol{u}_3}\overline{\nabla}^{a_4}_{\boldsymbol{u}_4}\right)\right)\\
&=\frac{1}{4!}\int_{\boldsymbol{u}_1\boldsymbol{u}_2\boldsymbol{u}_3\boldsymbol{u}_4}\left(\left(\left(\sum_{\sigma_1\in S_{\delta\delta}}\sigma_1\right)\circ G^{(\delta)}_{\boldsymbol{u}_1\boldsymbol{u}_2\boldsymbol{u}_3\boldsymbol{u}_4}\right)\delta^{a_1a_2}\delta^{a_3a_4}\right.\\
&+\left(\left(\sum_{\sigma_2\in(24)\cdot S_{\delta\delta}}\sigma_2\right)\circ G^{(\delta)}_{\boldsymbol{u}_1\boldsymbol{u}_2\boldsymbol{u}_3\boldsymbol{u}_4}\right)\delta^{a_1a_4}\delta^{a_2a_3}\\
&\left.+\left(\left(\sum_{\sigma_3\in(23)\cdot S_{\delta\delta}}\sigma_3\right)\circ G^{(\delta)}_{\boldsymbol{u}_1\boldsymbol{u}_2\boldsymbol{u}_3\boldsymbol{u}_4}\right)\delta^{a_1a_3}\delta^{a_2a_4}\right)\left(\nabla^{a_1}_{\boldsymbol{u}_1}\nabla^{a_2}_{\boldsymbol{u}_2}\nabla^{a_3}_{\boldsymbol{u}_3}\nabla^{a_4}_{\boldsymbol{u}_4}+\overline{\nabla}^{a_1}_{\boldsymbol{u}_1}\overline{\nabla}^{a_2}_{\boldsymbol{u}_2}\overline{\nabla}^{a_3}_{\boldsymbol{u}_3}\overline{\nabla}^{a_4}_{\boldsymbol{u}_4}\right)\right)
\end{aligned}
\tag{C.8}
$$

where we have rewritten the each of the three sums of the relevant permutations acting on the colour structure function as a group algebra element acting on the colour structure function in Eq. C.8.

Now let us look at $\sum_{\sigma_1\in S_{\delta\delta}}\sigma_1$ in Eq. C.8. One can express this group algebra element in a different basis. Namely, we can express it in the projection and transition operator basis as was found in [23]. Doing so (incorporating a simple change of basis), we find that[2]

$$
\sum_{\sigma_1\in S_{\delta\delta}}\sigma_1 = 8\left(P_{\begin{array}{|c|c|c|c|}\hline 1&2&3&4\\\hline\end{array}}+P_{\begin{array}{|c|c|}\hline 1&2\\\hline 3&4\\\hline\end{array}}\right) \tag{C.9}
$$

which is a fairly simple expression. We can then naturally express $\sum_{\sigma_2\in(24)\cdot S_{\delta\delta}}\sigma_2$ and $\sum_{\sigma_3\in(23)\cdot S_{\delta\delta}}\sigma_3$ in Eq. C.8 in-terms of the projection operators in Eq. C.9 by simply multiplying with the $\overline{\times}$ and $\overline{\times}$ permutations from the left on the RHS of Eq. C.9 respectively (since these terms

[2] We will maintain the original notation for the HYPOs and transition operators in this section, as it clarifies the discussion.

arise from the other 2 left-cosets in question). Thus, we obtain that:

$$\sum_{\sigma_2 \in (24)\cdot S_{\delta\delta}} \sigma_2 = 8 \overline{\overline{\times}} \cdot \left(P_{\boxed{1}\boxed{2}\boxed{3}\boxed{4}} + P_{\begin{array}{|c|c|}\hline 1&2\\\hline 3&4\\\hline\end{array}} \right) \tag{C.10}$$

$$\sum_{\sigma_3 \in (23)\cdot S_{\delta\delta}} \sigma_3 = 8 \overline{\overline{\times}} \cdot \left(P_{\boxed{1}\boxed{2}\boxed{3}\boxed{4}} + P_{\begin{array}{|c|c|}\hline 1&2\\\hline 3&4\\\hline\end{array}} \right) \tag{C.11}$$

Putting this all together, we finally obtain that Eq. C.3 simplifies to:

$$\begin{aligned}
&\int_{\boldsymbol{u}_1\boldsymbol{u}_2\boldsymbol{u}_3\boldsymbol{u}_4} \left(\frac{1}{4!} \sum_{\sigma\in S_4} \left(\sigma \circ G^{(\delta)}_{\boldsymbol{u}_1\boldsymbol{u}_2\boldsymbol{u}_3\boldsymbol{u}_4} \right) (\sigma \circ \delta^{a_1a_2}\delta^{a_3a_4}) \right) \left(\nabla^{a_1}_{\boldsymbol{u}_1} \nabla^{a_2}_{\boldsymbol{u}_2} \nabla^{a_3}_{\boldsymbol{u}_3} \nabla^{a_4}_{\boldsymbol{u}_4} + \overline{\nabla}^{a_1}_{\boldsymbol{u}_1} \overline{\nabla}^{a_2}_{\boldsymbol{u}_2} \overline{\nabla}^{a_3}_{\boldsymbol{u}_3} \overline{\nabla}^{a_4}_{\boldsymbol{u}_4} \right) \\
&= \frac{1}{3} \int_{\boldsymbol{u}_1\boldsymbol{u}_2\boldsymbol{u}_3\boldsymbol{u}_4} \left(\left(\left(\left(P_{\boxed{1}\boxed{2}\boxed{3}\boxed{4}} + P_{\begin{array}{|c|c|}\hline 1&2\\\hline 3&4\\\hline\end{array}} \right) \right) \right) \circ G^{(\delta)}_{\boldsymbol{u}_1\boldsymbol{u}_2\boldsymbol{u}_3\boldsymbol{u}_4} \right) \delta^{a_1a_2}\delta^{a_3a_4} \\
&+ \left(\left(\overline{\overline{\times}} \cdot \left(P_{\boxed{1}\boxed{2}\boxed{3}\boxed{4}} + P_{\begin{array}{|c|c|}\hline 1&2\\\hline 3&4\\\hline\end{array}} \right) \right) \circ G^{(\delta)}_{\boldsymbol{u}_1\boldsymbol{u}_2\boldsymbol{u}_3\boldsymbol{u}_4} \right) \delta^{a_1a_4}\delta^{a_2a_3} \\
&+ \left(\left(\overline{\overline{\times}} \cdot \left(P_{\boxed{1}\boxed{2}\boxed{3}\boxed{4}} + P_{\begin{array}{|c|c|}\hline 1&2\\\hline 3&4\\\hline\end{array}} \right) \right) \circ G^{(\delta)}_{\boldsymbol{u}_1\boldsymbol{u}_2\boldsymbol{u}_3\boldsymbol{u}_4} \right) \delta^{a_1a_3}\delta^{a_2a_4} \right) \\
&\left(\nabla^{a_1}_{\boldsymbol{u}_1} \nabla^{a_2}_{\boldsymbol{u}_2} \nabla^{a_3}_{\boldsymbol{u}_3} \nabla^{a_4}_{\boldsymbol{u}_4} + \overline{\nabla}^{a_1}_{\boldsymbol{u}_1} \overline{\nabla}^{a_2}_{\boldsymbol{u}_2} \overline{\nabla}^{a_3}_{\boldsymbol{u}_3} \overline{\nabla}^{a_4}_{\boldsymbol{u}_4} \right) \Bigg)
\end{aligned} \tag{C.12}$$

That takes care of the first and fourth terms in Eq. C.2.

Now, examining the more complex second and third terms (inner terms), careful symmetrisation of the colour structure and function is essential. Unlike the first and fourth terms (outer terms) in Eq. C.2, these involve both left- and right-invariant vector fields. When symmetrising and commuting vector fields to ascending order, their initial arrangement can change. Let's clarify this by performing the calculation as we did for the outer terms. We get that:

$$\begin{aligned}
&\int_{\boldsymbol{u}_1\boldsymbol{u}_2\boldsymbol{u}_3\boldsymbol{u}_4} G^{(\delta)}_{\boldsymbol{u}_1\boldsymbol{u}_2\boldsymbol{u}_3\boldsymbol{u}_4} \delta^{a_1a_2}\delta^{a_3a_4} \left(\nabla^{a_1}_{\boldsymbol{u}_1} \nabla^{a_2}_{\boldsymbol{u}_2} \overline{\nabla}^{a_3}_{\boldsymbol{u}_3} \overline{\nabla}^{a_4}_{\boldsymbol{u}_4} + \overline{\nabla}^{a_1}_{\boldsymbol{u}_1} \overline{\nabla}^{a_2}_{\boldsymbol{u}_2} \nabla^{a_3}_{\boldsymbol{u}_3} \nabla^{a_4}_{\boldsymbol{u}_4} \right) \\
&= \frac{1}{4!} \sum_{\sigma\in S_4} \int_{\boldsymbol{u}_1\boldsymbol{u}_2\boldsymbol{u}_3\boldsymbol{u}_4} G^{(\delta)}_{\boldsymbol{u}_{\sigma(1)}\boldsymbol{u}_{\sigma(2)}\boldsymbol{u}_{\sigma(3)}\boldsymbol{u}_{\sigma(4)}} \delta^{a_1a_2}\delta^{a_3a_4} \Bigg(\nabla^{a_1}_{\boldsymbol{u}_{\sigma(1)}} \nabla^{a_2}_{\boldsymbol{u}_{\sigma(2)}} \overline{\nabla}^{a_3}_{\boldsymbol{u}_{\sigma(3)}} \overline{\nabla}^{a_4}_{\boldsymbol{u}_{\sigma(4)}} \\
&+ \nabla^{a_1}_{\boldsymbol{u}_{\sigma(1)}} \nabla^{a_2}_{\boldsymbol{u}_{\sigma(2)}} \overline{\nabla}^{a_3}_{\boldsymbol{u}_{\sigma(3)}} \overline{\nabla}^{a_4}_{\boldsymbol{u}_{\sigma(4)}} \Bigg)
\end{aligned} \tag{C.13}$$

Now let us illustrate the issue by means of an example. Take $\sigma = (1432) =$  and observe what happens when commute the vector fields back to ascending order in its term. We get that:

$$\frac{1}{4!}\int\limits_{\boldsymbol{u}_1\boldsymbol{u}_2\boldsymbol{u}_3\boldsymbol{u}_4} G^{(\delta)}_{\boldsymbol{u}_4\boldsymbol{u}_1\boldsymbol{u}_2\boldsymbol{u}_3}\delta^{a_1a_2}\delta^{a_3a_4}\left(\nabla^{a_1}_{\boldsymbol{u}_4}\nabla^{a_2}_{\boldsymbol{u}_1}\overline{\nabla}^{a_3}_{\boldsymbol{u}_2}\overline{\nabla}^{a_4}_{\boldsymbol{u}_3} + \nabla^{a_1}_{\boldsymbol{u}_4}\nabla^{a_2}_{\boldsymbol{u}_1}\overline{\nabla}^{a_3}_{\boldsymbol{u}_2}\overline{\nabla}^{a_4}_{\boldsymbol{u}_3}\right)$$

$$= \frac{1}{4!}\int\limits_{\boldsymbol{u}_1\boldsymbol{u}_2\boldsymbol{u}_3\boldsymbol{u}_4} G^{(\delta)}_{\boldsymbol{u}_4\boldsymbol{u}_1\boldsymbol{u}_2\boldsymbol{u}_3}\delta^{a_1a_2}\delta^{a_3a_4}\left(\nabla^{a_2}_{\boldsymbol{u}_1}\overline{\nabla}^{a_3}_{\boldsymbol{u}_2}\overline{\nabla}^{a_4}_{\boldsymbol{u}_3}\nabla^{a_1}_{\boldsymbol{u}_4} + \overline{\nabla}^{a_2}_{\boldsymbol{u}_1}\nabla^{a_3}_{\boldsymbol{u}_2}\nabla^{a_4}_{\boldsymbol{u}_3}\overline{\nabla}^{a_1}_{\boldsymbol{u}_4} + \text{commutator terms}\right)$$

(Commuting the vector fields back to ascending order in its transverse coordinates)

$$= \frac{1}{4!}\int\limits_{\boldsymbol{u}_1\boldsymbol{u}_2\boldsymbol{u}_3\boldsymbol{u}_4} G^{(\delta)}_{\boldsymbol{u}_4\boldsymbol{u}_1\boldsymbol{u}_2\boldsymbol{u}_3}\delta^{a_4a_1}\delta^{a_2a_3}\left(\nabla^{a_1}_{\boldsymbol{u}_1}\overline{\nabla}^{a_2}_{\boldsymbol{u}_2}\overline{\nabla}^{a_3}_{\boldsymbol{u}_3}\nabla^{a_4}_{\boldsymbol{u}_4} + \overline{\nabla}^{a_1}_{\boldsymbol{u}_1}\nabla^{a_2}_{\boldsymbol{u}_2}\nabla^{a_3}_{\boldsymbol{u}_3}\overline{\nabla}^{a_4}_{\boldsymbol{u}_4} + \text{commutator terms}\right)$$

(Relabelling all the colour indices)

$$= \frac{1}{4!}\int\limits_{\boldsymbol{u}_1\boldsymbol{u}_2\boldsymbol{u}_3\boldsymbol{u}_4} \left(\circ\, G^{(\delta)}_{\boldsymbol{u}_1\boldsymbol{u}_2\boldsymbol{u}_3\boldsymbol{u}_4}\right)\left(\circ\,\delta^{a_1a_2}\delta^{a_3a_4}\right)\left(\nabla^{a_1}_{\boldsymbol{u}_1}\overline{\nabla}^{a_2}_{\boldsymbol{u}_2}\overline{\nabla}^{a_3}_{\boldsymbol{u}_3}\nabla^{a_4}_{\boldsymbol{u}_4} + \overline{\nabla}^{a_1}_{\boldsymbol{u}_1}\nabla^{a_2}_{\boldsymbol{u}_2}\nabla^{a_3}_{\boldsymbol{u}_3}\overline{\nabla}^{a_4}_{\boldsymbol{u}_4}\right.$$

$$\left. + \text{commutator terms}\right) \tag{C.14}$$

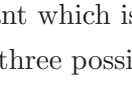

And so we see that although we still end up with the permutations acting on the colour structure function and the colour structure, the order in which the left- and right-invariant vector fields appear is not preserved; for the example above, we started off with something that looked like $\left(\nabla\nabla\overline{\nabla}\overline{\nabla} + \overline{\nabla}\overline{\nabla}\nabla\nabla\right)$ and ended up with something that looks like $\left(\nabla\overline{\nabla}\overline{\nabla}\nabla + \overline{\nabla}\nabla\nabla\overline{\nabla}\right)$. This is an issue as now the vector field operators do not factor as nicely as they do in Eq. C.12. However, we can still simplify Eq. C.13 significantly by considering the different types of structures that can arise in the vector fields once they are commuted back to ascending order in transverse coordinates (in the order in which the left- and right-invariant vector fields appear). We observe that there are 3 possible structures that can arise, namely the structure we started off with, $\left(\nabla\nabla\overline{\nabla}\overline{\nabla} + \overline{\nabla}\overline{\nabla}\nabla\nabla\right)$ and 2 other structures of the form $\left(\nabla\overline{\nabla}\nabla\overline{\nabla} + \overline{\nabla}\nabla\overline{\nabla}\nabla\right)$ and $\left(\overline{\nabla}\nabla\overline{\nabla}\nabla + \nabla\overline{\nabla}\nabla\overline{\nabla}\right)$. In-fact, the set of all permutations that preserve the $\left(\nabla\nabla\overline{\nabla}\overline{\nabla} + \overline{\nabla}\overline{\nabla}\nabla\nabla\right)$ structure (the set of permutations that reorder the vector fields back to the original $\left(\nabla\nabla\overline{\nabla}\overline{\nabla} + \overline{\nabla}\overline{\nabla}\nabla\nabla\right)$ structure after adjusting the transverse coordinates) is actually the subgroup that leaves $\delta^{a_1a_2}\delta^{a_3a_4}$ invariant which is not all too surprising. Similarly, each left-coset for $S_{\delta\delta}$ corresponds to one of the three possible vector field structures, analogous to how each left-coset yields a distinct Kronecker δ product. I.e. we have that:

$$\int\limits_{\boldsymbol{u}_1\boldsymbol{u}_2\boldsymbol{u}_3\boldsymbol{u}_4} G^{(\delta)}_{\boldsymbol{u}_{\sigma(1)}\boldsymbol{u}_{\sigma(2)}\boldsymbol{u}_{\sigma(3)}\boldsymbol{u}_{\sigma(4)}}\delta^{a_1a_2}\delta^{a_3a_4}\left(\nabla^{a_1}_{\boldsymbol{u}_{\sigma(1)}}\nabla^{a_2}_{\boldsymbol{u}_{\sigma(2)}}\overline{\nabla}^{a_3}_{\boldsymbol{u}_{\sigma(3)}}\overline{\nabla}^{a_4}_{\boldsymbol{u}_{\sigma(4)}}\right.$$

$$
\begin{aligned}
&+ \nabla^{a_1}_{\boldsymbol{u}_{\sigma(1)}} \nabla^{a_2}_{\boldsymbol{u}_{\sigma(2)}} \overline{\nabla}^{a_3}_{\boldsymbol{u}_{\sigma(3)}} \overline{\nabla}^{a_4}_{\boldsymbol{u}_{\sigma(4)}} \Bigg) \\
&= \begin{cases}
\int\limits_{\boldsymbol{u}_1\boldsymbol{u}_2\boldsymbol{u}_3\boldsymbol{u}_4} G^{(\delta)}_{\boldsymbol{u}_{\sigma(1)}\boldsymbol{u}_{\sigma(2)}\boldsymbol{u}_{\sigma(3)}\boldsymbol{u}_{\sigma(4)}} \delta^{a_1a_2}\delta^{a_3a_4} \Bigg(\nabla^{a_{\sigma^{-1}(1)}}_{\boldsymbol{u}_1} \nabla^{a_{\sigma^{-1}(2)}}_{\boldsymbol{u}_2} \overline{\nabla}^{a_{\sigma^{-1}(3)}}_{\boldsymbol{u}_3} \overline{\nabla}^{a_{\sigma^{-1}(4)}}_{\boldsymbol{u}_4} \\
+ \overline{\nabla}^{a_{\sigma^{-1}(1)}}_{\boldsymbol{u}_1} \overline{\nabla}^{a_{\sigma^{-1}(2)}}_{\boldsymbol{u}_2} \nabla^{a_{\sigma^{-1}(3)}}_{\boldsymbol{u}_3} \nabla^{a_{\sigma^{-1}(4)}}_{\boldsymbol{u}_4} \Bigg) \\
\text{if } \sigma \in S_{\delta\delta} \\
\int\limits_{\boldsymbol{u}_1\boldsymbol{u}_2\boldsymbol{u}_3\boldsymbol{u}_4} G^{(\delta)}_{\boldsymbol{u}_{\sigma(1)}\boldsymbol{u}_{\sigma(2)}\boldsymbol{u}_{\sigma(3)}\boldsymbol{u}_{\sigma(4)}} \delta^{a_1a_2}\delta^{a_3a_4} \Bigg(\nabla^{a_{\sigma^{-1}(1)}}_{\boldsymbol{u}_1} \overline{\nabla}^{a_{\sigma^{-1}(2)}}_{\boldsymbol{u}_2} \overline{\nabla}^{a_{\sigma^{-1}(3)}}_{\boldsymbol{u}_3} \nabla^{a_{\sigma^{-1}(4)}}_{\boldsymbol{u}_4} \\
+ \overline{\nabla}^{a_{\sigma^{-1}(1)}}_{\boldsymbol{u}_1} \nabla^{a_{\sigma^{-1}(2)}}_{\boldsymbol{u}_2} \nabla^{a_{\sigma^{-1}(3)}}_{\boldsymbol{u}_3} \overline{\nabla}^{a_{\sigma^{-1}(4)}}_{\boldsymbol{u}_4} \Bigg) \\
\text{if } \sigma \in \overline{\times} \cdot S_{\delta\delta} \\
\int\limits_{\boldsymbol{u}_1\boldsymbol{u}_2\boldsymbol{u}_3\boldsymbol{u}_4} G^{(\delta)}_{\boldsymbol{u}_{\sigma(1)}\boldsymbol{u}_{\sigma(2)}\boldsymbol{u}_{\sigma(3)}\boldsymbol{u}_{\sigma(4)}} \delta^{a_1a_2}\delta^{a_3a_4} \Bigg(\overline{\nabla}^{a_{\sigma^{-1}(1)}}_{\boldsymbol{u}_1} \nabla^{a_{\sigma^{-1}(2)}}_{\boldsymbol{u}_2} \overline{\nabla}^{a_{\sigma^{-1}(3)}}_{\boldsymbol{u}_3} \nabla^{a_{\sigma^{-1}(4)}}_{\boldsymbol{u}_4} \\
+ \nabla^{a_{\sigma^{-1}(1)}}_{\boldsymbol{u}_1} \overline{\nabla}^{a_{\sigma^{-1}(2)}}_{\boldsymbol{u}_2} \nabla^{a_{\sigma^{-1}(3)}}_{\boldsymbol{u}_3} \overline{\nabla}^{a_{\sigma^{-1}(4)}}_{\boldsymbol{u}_4} \Bigg) \\
\text{if } \sigma \in \underline{\overline{\times}} \cdot S_{\delta\delta}
\end{cases} \\
&= \begin{cases}
\int\limits_{\boldsymbol{u}_1\boldsymbol{u}_2\boldsymbol{u}_3\boldsymbol{u}_4} \left(\sigma \circ G^{(\delta)}_{\boldsymbol{u}_1\boldsymbol{u}_2\boldsymbol{u}_3\boldsymbol{u}_4}\right) \left(\sigma \circ \delta^{a_1a_2}\delta^{a_3a_4}\right) \left(\nabla^{a_1}_{\boldsymbol{u}_1} \nabla^{a_2}_{\boldsymbol{u}_2} \overline{\nabla}^{a_3}_{\boldsymbol{u}_3} \overline{\nabla}^{a_4}_{\boldsymbol{u}_4} + \overline{\nabla}^{a_1}_{\boldsymbol{u}_1} \overline{\nabla}^{a_2}_{\boldsymbol{u}_2} \nabla^{a_3}_{\boldsymbol{u}_3} \nabla^{a_4}_{\boldsymbol{u}_4} \right) \\
\text{if } \sigma \in S_{\delta\delta} \\
\int\limits_{\boldsymbol{u}_1\boldsymbol{u}_2\boldsymbol{u}_3\boldsymbol{u}_4} \left(\sigma \circ G^{(\delta)}_{\boldsymbol{u}_1\boldsymbol{u}_2\boldsymbol{u}_3\boldsymbol{u}_4}\right) \left(\sigma \circ \delta^{a_1a_2}\delta^{a_3a_4}\right) \left(\nabla^{a_1}_{\boldsymbol{u}_1} \overline{\nabla}^{a_2}_{\boldsymbol{u}_2} \overline{\nabla}^{a_3}_{\boldsymbol{u}_3} \nabla^{a_4}_{\boldsymbol{u}_4} + \overline{\nabla}^{a_1}_{\boldsymbol{u}_1} \nabla^{a_2}_{\boldsymbol{u}_2} \nabla^{a_3}_{\boldsymbol{u}_3} \overline{\nabla}^{a_4}_{\boldsymbol{u}_4} \right) \\
\text{if } \sigma \in \overline{\times} \cdot S_{\delta\delta} \\
\int\limits_{\boldsymbol{u}_1\boldsymbol{u}_2\boldsymbol{u}_3\boldsymbol{u}_4} \left(\sigma \circ G^{(\delta)}_{\boldsymbol{u}_1\boldsymbol{u}_2\boldsymbol{u}_3\boldsymbol{u}_4}\right) \left(\sigma \circ \delta^{a_1a_2}\delta^{a_3a_4}\right) \left(\overline{\nabla}^{a_1}_{\boldsymbol{u}_1} \nabla^{a_2}_{\boldsymbol{u}_2} \overline{\nabla}^{a_3}_{\boldsymbol{u}_3} \nabla^{a_4}_{\boldsymbol{u}_4} + \nabla^{a_1}_{\boldsymbol{u}_1} \overline{\nabla}^{a_2}_{\boldsymbol{u}_2} \nabla^{a_3}_{\boldsymbol{u}_3} \overline{\nabla}^{a_4}_{\boldsymbol{u}_4} \right) \\
\text{if } \sigma \in \underline{\overline{\times}} \cdot S_{\delta\delta}
\end{cases}
\end{aligned}
$$

Thus, similar to how we dealt with the outer terms, we can split the sum over all permutations in Eq. C.13 into 3 separate sums for each of the 3 left-cosets. This gives us

$$
\frac{1}{4!} \sum_{\sigma \in S_4} \int\limits_{\boldsymbol{u}_1\boldsymbol{u}_2\boldsymbol{u}_3\boldsymbol{u}_4} G^{(\delta)}_{\boldsymbol{u}_{\sigma(1)}\boldsymbol{u}_{\sigma(2)}\boldsymbol{u}_{\sigma(3)}\boldsymbol{u}_{\sigma(4)}} \delta^{a_1a_2}\delta^{a_3a_4} \Bigg(\nabla^{a_1}_{\boldsymbol{u}_{\sigma(1)}} \nabla^{a_2}_{\boldsymbol{u}_{\sigma(2)}} \overline{\nabla}^{a_3}_{\boldsymbol{u}_{\sigma(3)}} \overline{\nabla}^{a_4}_{\boldsymbol{u}_{\sigma(4)}}
$$

$$
\begin{aligned}
&+ \nabla^{a_1}_{\boldsymbol{u}_{\sigma(1)}} \nabla^{a_2}_{\boldsymbol{u}_{\sigma(2)}} \overline{\nabla}^{a_3}_{\boldsymbol{u}_{\sigma(3)}} \overline{\nabla}^{a_4}_{\boldsymbol{u}_{\sigma(4)}} \Bigg) \\
&= \frac{1}{4!} \int_{\boldsymbol{u}_1\boldsymbol{u}_2\boldsymbol{u}_3\boldsymbol{u}_4} \Bigg(\Bigg(\sum_{\sigma_1 \in S_{\delta\delta}} \left(\sigma_1 \circ G^{(\delta)}_{\boldsymbol{u}_1\boldsymbol{u}_2\boldsymbol{u}_3\boldsymbol{u}_4} \right) \underbrace{(\sigma_1 \circ \delta^{a_1a_2}\delta^{a_3a_4})}_{\delta^{a_1a_2}\delta^{a_3a_4}} \Bigg) \Bigg(\nabla^{a_1}_{\boldsymbol{u}_1} \nabla^{a_2}_{\boldsymbol{u}_2} \overline{\nabla}^{a_3}_{\boldsymbol{u}_3} \overline{\nabla}^{a_4}_{\boldsymbol{u}_4} \\
&+ \overline{\nabla}^{a_1}_{\boldsymbol{u}_1} \overline{\nabla}^{a_2}_{\boldsymbol{u}_2} \nabla^{a_3}_{\boldsymbol{u}_3} \nabla^{a_4}_{\boldsymbol{u}_4} \Bigg) \\
&+ \Bigg(\sum_{\sigma_2 \in (24)\cdot S_{\delta\delta}} \left(\sigma_2 \circ G^{(\delta)}_{\boldsymbol{u}_1\boldsymbol{u}_2\boldsymbol{u}_3\boldsymbol{u}_4} \right) \underbrace{(\sigma_2 \circ \delta^{a_1a_2}\delta^{a_3a_4})}_{\delta^{a_1a_4}\delta^{a_2a_3}} \Bigg) \Bigg(\nabla^{a_1}_{\boldsymbol{u}_1} \overline{\nabla}^{a_2}_{\boldsymbol{u}_2} \overline{\nabla}^{a_3}_{\boldsymbol{u}_3} \nabla^{a_4}_{\boldsymbol{u}_4} \\
&+ \overline{\nabla}^{a_1}_{\boldsymbol{u}_1} \nabla^{a_2}_{\boldsymbol{u}_2} \nabla^{a_3}_{\boldsymbol{u}_3} \overline{\nabla}^{a_4}_{\boldsymbol{u}_4} \Bigg) \\
&+ \Bigg(\sum_{\sigma_3 \in (23)\cdot S_{\delta\delta}} \left(\sigma_3 \circ G^{(\delta)}_{\boldsymbol{u}_1\boldsymbol{u}_2\boldsymbol{u}_3\boldsymbol{u}_4} \right) \underbrace{(\sigma_3 \circ \delta^{a_1a_2}\delta^{a_3a_4})}_{\delta^{a_1a_3}\delta^{a_2a_4}} \Bigg) \Bigg(\overline{\nabla}^{a_1}_{\boldsymbol{u}_1} \nabla^{a_2}_{\boldsymbol{u}_2} \overline{\nabla}^{a_3}_{\boldsymbol{u}_3} \nabla^{a_4}_{\boldsymbol{u}_4} \\
&+ \nabla^{a_1}_{\boldsymbol{u}_1} \overline{\nabla}^{a_2}_{\boldsymbol{u}_2} \nabla^{a_3}_{\boldsymbol{u}_3} \overline{\nabla}^{a_4}_{\boldsymbol{u}_4} \Bigg) \Bigg) \Bigg) \\
&= \frac{1}{3} \int_{\boldsymbol{u}_1\boldsymbol{u}_2\boldsymbol{u}_3\boldsymbol{u}_4} \Bigg(\Bigg(\Bigg(\Bigg(\Bigg(P_{\begin{array}{|c|c|c|c|}\hline 1&2&3&4\\\hline\end{array}} + P_{\begin{array}{|c|c|}\hline 1&2\\\hline 3&4\\\hline\end{array}} \Bigg) \circ G^{(\delta)}_{\boldsymbol{u}_1\boldsymbol{u}_2\boldsymbol{u}_3\boldsymbol{u}_4} \Bigg) \delta^{a_1a_2}\delta^{a_3a_4} \Bigg) \Bigg(\nabla^{a_1}_{\boldsymbol{u}_1} \nabla^{a_2}_{\boldsymbol{u}_2} \overline{\nabla}^{a_3}_{\boldsymbol{u}_3} \overline{\nabla}^{a_4}_{\boldsymbol{u}_4} \\
&+ \overline{\nabla}^{a_1}_{\boldsymbol{u}_1} \overline{\nabla}^{a_2}_{\boldsymbol{u}_2} \nabla^{a_3}_{\boldsymbol{u}_3} \nabla^{a_4}_{\boldsymbol{u}_4} \Bigg) \\
&+ \Bigg(\Bigg(\Bigg(\overline{\times} \cdot \left(P_{\begin{array}{|c|c|c|c|}\hline 1&2&3&4\\\hline\end{array}} + P_{\begin{array}{|c|c|}\hline 1&2\\\hline 3&4\\\hline\end{array}} \right) \Bigg) \circ G^{(\delta)}_{\boldsymbol{u}_1\boldsymbol{u}_2\boldsymbol{u}_3\boldsymbol{u}_4} \Bigg) \delta^{a_1a_4}\delta^{a_2a_3} \Bigg) \Bigg(\nabla^{a_1}_{\boldsymbol{u}_1} \overline{\nabla}^{a_2}_{\boldsymbol{u}_2} \overline{\nabla}^{a_3}_{\boldsymbol{u}_3} \nabla^{a_4}_{\boldsymbol{u}_4} \\
&+ \overline{\nabla}^{a_1}_{\boldsymbol{u}_1} \nabla^{a_2}_{\boldsymbol{u}_2} \nabla^{a_3}_{\boldsymbol{u}_3} \overline{\nabla}^{a_4}_{\boldsymbol{u}_4} \Bigg) \\
&+ \Bigg(\Bigg(\Bigg(\overline{\overline{\times}} \cdot \left(P_{\begin{array}{|c|c|c|c|}\hline 1&2&3&4\\\hline\end{array}} + P_{\begin{array}{|c|c|}\hline 1&2\\\hline 3&4\\\hline\end{array}} \right) \Bigg) \circ G^{(\delta)}_{\boldsymbol{u}_1\boldsymbol{u}_2\boldsymbol{u}_3\boldsymbol{u}_4} \Bigg) \delta^{a_1a_3}\delta^{a_2a_4} \Bigg) \Bigg(\overline{\nabla}^{a_1}_{\boldsymbol{u}_1} \nabla^{a_2}_{\boldsymbol{u}_2} \overline{\nabla}^{a_3}_{\boldsymbol{u}_3} \nabla^{a_4}_{\boldsymbol{u}_4} \\
&+ \nabla^{a_1}_{\boldsymbol{u}_1} \overline{\nabla}^{a_2}_{\boldsymbol{u}_2} \nabla^{a_3}_{\boldsymbol{u}_3} \overline{\nabla}^{a_4}_{\boldsymbol{u}_4} \Bigg) \Bigg)
\end{aligned}
\tag{C.15}
$$

Now we finally have a simplified expression for the Gaussian truncation squared with Eq. C.12 and Eq. C.15.

In-fact, we can even make these expressions simpler by only symmetrising over the permutations in the subgroup $S_{\delta\delta}$ in Eq. C.12 and Eq. C.15. I.e.

$$\begin{aligned}
&\int\limits_{\boldsymbol{u}_1\boldsymbol{u}_2\boldsymbol{u}_3\boldsymbol{u}_4} G^{(\delta)}_{\boldsymbol{u}_1\boldsymbol{u}_2\boldsymbol{u}_3\boldsymbol{u}_4}\delta^{a_1a_2}\delta^{a_3a_4}\left(\nabla^{a_1}_{\boldsymbol{u}_1}\nabla^{a_2}_{\boldsymbol{u}_2}\nabla^{a_3}_{\boldsymbol{u}_3}\nabla^{a_4}_{\boldsymbol{u}_4}+\overline{\nabla}^{a_1}_{\boldsymbol{u}_1}\overline{\nabla}^{a_2}_{\boldsymbol{u}_2}\overline{\nabla}^{a_3}_{\boldsymbol{u}_3}\overline{\nabla}^{a_4}_{\boldsymbol{u}_4}\right)\\
&=\frac{1}{8}\sum_{\sigma\in S_{\delta\delta}}\int\limits_{\boldsymbol{u}_1\boldsymbol{u}_2\boldsymbol{u}_3\boldsymbol{u}_4} G^{(\delta)}_{\boldsymbol{u}_{\sigma(1)}\boldsymbol{u}_{\sigma(2)}\boldsymbol{u}_{\sigma(3)}\boldsymbol{u}_{\sigma(4)}}\delta^{a_1a_2}\delta^{a_3a_4}\Bigg(\nabla^{a_1}_{\boldsymbol{u}_{\sigma(1)}}\nabla^{a_2}_{\boldsymbol{u}_{\sigma(2)}}\nabla^{a_3}_{\boldsymbol{u}_{\sigma(3)}}\nabla^{a_4}_{\boldsymbol{u}_{\sigma(4)}}\\
&+\overline{\nabla}^{a_1}_{\boldsymbol{u}_{\sigma(1)}}\overline{\nabla}^{a_2}_{\boldsymbol{u}_{\sigma(2)}}\overline{\nabla}^{a_3}_{\boldsymbol{u}_{\sigma(3)}}\overline{\nabla}^{a_4}_{\boldsymbol{u}_{\sigma(4)}}\Bigg)\\
&=\int\limits_{\boldsymbol{u}_1\boldsymbol{u}_2\boldsymbol{u}_3\boldsymbol{u}_4}\left(\left(\left(P_{\begin{array}{|c|c|c|c|}\hline 1&2&3&4\\\hline\end{array}}+P_{\begin{array}{|c|c|}\hline 1&2\\\hline 3&4\\\hline\end{array}}\right)\circ G^{(\delta)}_{\boldsymbol{u}_1\boldsymbol{u}_2\boldsymbol{u}_3\boldsymbol{u}_4}\right)\left(\left(P_{\begin{array}{|c|c|c|c|}\hline 1&2&3&4\\\hline\end{array}}+P_{\begin{array}{|c|c|}\hline 1&2\\\hline 3&4\\\hline\end{array}}\right)\circ\delta^{a_1a_2}\delta^{a_3a_4}\right)\right.\\
&\left.\left(\nabla^{a_1}_{\boldsymbol{u}_1}\nabla^{a_2}_{\boldsymbol{u}_2}\nabla^{a_3}_{\boldsymbol{u}_3}\nabla^{a_4}_{\boldsymbol{u}_4}+\overline{\nabla}^{a_1}_{\boldsymbol{u}_1}\overline{\nabla}^{a_2}_{\boldsymbol{u}_2}\overline{\nabla}^{a_3}_{\boldsymbol{u}_3}\overline{\nabla}^{a_4}_{\boldsymbol{u}_4}\right)\right.
\end{aligned}\tag{C.16}$$

and

$$\begin{aligned}
&\int\limits_{\boldsymbol{u}_1\boldsymbol{u}_2\boldsymbol{u}_3\boldsymbol{u}_4} G^{(\delta)}_{\boldsymbol{u}_1\boldsymbol{u}_2\boldsymbol{u}_3\boldsymbol{u}_4}\delta^{a_1a_2}\delta^{a_3a_4}\left(\nabla^{a_1}_{\boldsymbol{u}_1}\nabla^{a_2}_{\boldsymbol{u}_2}\overline{\nabla}^{a_3}_{\boldsymbol{u}_3}\overline{\nabla}^{a_4}_{\boldsymbol{u}_4}+\overline{\nabla}^{a_1}_{\boldsymbol{u}_1}\overline{\nabla}^{a_2}_{\boldsymbol{u}_2}\nabla^{a_3}_{\boldsymbol{u}_3}\nabla^{a_4}_{\boldsymbol{u}_4}\right)\\
&=\frac{1}{8}\sum_{\sigma\in S_{\delta\delta}}\int\limits_{\boldsymbol{u}_1\boldsymbol{u}_2\boldsymbol{u}_3\boldsymbol{u}_4} G^{(\delta)}_{\boldsymbol{u}_{\sigma(1)}\boldsymbol{u}_{\sigma(2)}\boldsymbol{u}_{\sigma(3)}\boldsymbol{u}_{\sigma(4)}}\delta^{a_1a_2}\delta^{a_3a_4}\Bigg(\nabla^{a_1}_{\boldsymbol{u}_{\sigma(1)}}\nabla^{a_2}_{\boldsymbol{u}_{\sigma(2)}}\overline{\nabla}^{a_3}_{\boldsymbol{u}_{\sigma(3)}}\overline{\nabla}^{a_4}_{\boldsymbol{u}_{\sigma(4)}}\\
&+\overline{\nabla}^{a_1}_{\boldsymbol{u}_{\sigma(1)}}\overline{\nabla}^{a_2}_{\boldsymbol{u}_{\sigma(2)}}\nabla^{a_3}_{\boldsymbol{u}_{\sigma(3)}}\nabla^{a_4}_{\boldsymbol{u}_{\sigma(4)}}\Bigg)\\
&=\int\limits_{\boldsymbol{u}_1\boldsymbol{u}_2\boldsymbol{u}_3\boldsymbol{u}_4}\left(\left(\left(P_{\begin{array}{|c|c|c|c|}\hline 1&2&3&4\\\hline\end{array}}+P_{\begin{array}{|c|c|}\hline 1&2\\\hline 3&4\\\hline\end{array}}\right)\circ G^{(\delta)}_{\boldsymbol{u}_1\boldsymbol{u}_2\boldsymbol{u}_3\boldsymbol{u}_4}\right)\left(\left(P_{\begin{array}{|c|c|c|c|}\hline 1&2&3&4\\\hline\end{array}}+P_{\begin{array}{|c|c|}\hline 1&2\\\hline 3&4\\\hline\end{array}}\right)\circ\delta^{a_1a_2}\delta^{a_3a_4}\right)\right.\\
&\left.\left(\nabla^{a_1}_{\boldsymbol{u}_1}\nabla^{a_2}_{\boldsymbol{u}_2}\overline{\nabla}^{a_3}_{\boldsymbol{u}_3}\overline{\nabla}^{a_4}_{\boldsymbol{u}_4}+\overline{\nabla}^{a_1}_{\boldsymbol{u}_1}\overline{\nabla}^{a_2}_{\boldsymbol{u}_2}\nabla^{a_3}_{\boldsymbol{u}_3}\nabla^{a_4}_{\boldsymbol{u}_4}\right)\right.
\end{aligned}\tag{C.17}$$

where we have written

$$\delta^{a_1a_2}\delta^{a_3a_4}=\left(P_{\begin{array}{|c|c|c|c|}\hline 1&2&3&4\\\hline\end{array}}+P_{\begin{array}{|c|c|}\hline 1&2\\\hline 3&4\\\hline\end{array}}\right)\circ\delta^{a_1a_2}\delta^{a_3a_4}$$

Symmetry groups and left-coset structures could simplify evolution equations for colour structure functions, but how to utilize these features remains unclear.

As such, this discussion proposes an alternative framework for truncating JIMWLK by examining adjoint color singlet symmetry groups and their interactions with HYPOs and transition operators. It questions whether left-coset structures appear for other color adjoint singlet states in 4-point or higher-order truncations, and whether these symmetry groups can simplify evolution equations for color structure functions. These questions are left for future

research, suggesting deeper mathematical insights in JIMWLK truncations.

Appendix D

Hermitian Young Projection Operators and Transition Operators

D.1 Hermitian Young Projection Operators

An immediate basis that one can think of for $\mathrm{API}\,(\mathrm{SU}(N), V^{\otimes m})$ are all the permutations in S_m (this is clear from Eq. 3.37). Nevertheless, this basis is cumbersome to utilize and does not facilitate clear physical interpretations. An obvious issue that arises quickly is the lack of orthogonality of such a basis with respect to the inner product defined in Eq. 3.17 and 3.22. To immediately see this, consider the inner product between the identity permutations (12 and (123) in S_3 as linear maps on $V^{\otimes 3}$:

$$\mathrm{tr}\left(\left(\;\right)^{\dagger}\right) = \mathrm{tr}\left(\right) = \mathrm{tr}\left(\right) = = N^2 \neq 0 \tag{D.1}$$

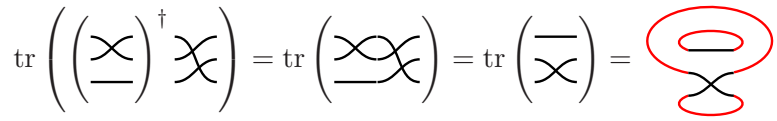

It is highly advantageous to have a basis that is orthogonal and conducive to clear physical interpretations, thereby enhancing our understanding of the space of linear invariants of $\mathrm{SU}(N)$ over $V^{\otimes m}$. This leads us to the consideration of Hermitian Young Projection Operators (HYPO) and Transition Operators.

Hermitian Young Projection Operators and the corresponding transition operators come from the Young tableaux. A Young tableau consisting of m boxes is a combinatorial arrangement of m boxes in rows and columns, adhering to the conditions that row lengths decrease progressively from the top downwards and column lengths decrease progressively from the left towards the right. Each box is labeled with a distinct number within the range from 1 to m, ensuring that the numbers ascend from left to right across each row and ascend from top to bottom down each column without any repetition. Young tableaux are highly intriguing entities that have been the subject of extensive study. They possess numerous significant applications, as detailed in [55, 61, 62], along with other standard references that provide

comprehensive expositions on the topic. We will denote the set of all Young tableau of size n by $\mathcal{Y}_n$ and as an example, $\mathcal{Y}_3$ is shown below:

$$\mathcal{Y}_3 := \left\{ \ydiagram{3}, \ydiagram{2,1}, \ydiagram{2,1}, \ydiagram{1,1,1} \right\} \tag{D.2}$$

A particular tableaux is denoted by an uppercase Greek letter such as Θ or Φ.

For our purposes, the important property of Young tableuax is this: **the set $\mathcal{Y}_m$ are in direct 1-1 correspondence with the irreducible representations of SU(N) over $V^{\otimes m}$ and in-fact, one can obtain projection operators, L_Θ, for each Θ corresponding to a Young tableau in $\mathcal{Y}_m$ onto the irreducible representations and thus, invariant subspaces of SU(N) over $V^{\otimes m}$ which satisfy three meaningful properties** [44, 55, 63–65]:

1. The projection operators are idempotent:

$$L_\Theta \cdot L_\Theta = L_\Theta \tag{D.3}$$

2. The operators are mutually transversal in that the intersection of the invariant subspaces they project onto is just the 0 element of the vector space, $V^{\otimes m}$. This then means that:

$$L_\Theta \cdot L_\Phi = 0 \quad \text{if } \Theta \neq \Phi. \tag{D.4}$$

3. The complete set of all projection operators sum up to the identity map on $V^{\otimes m}$:

$$\sum_{\Theta \in \mathcal{Y}_m} L_\Theta = \mathrm{id}_{V^{\otimes m}} \tag{D.5}$$

The direct one-to-one correspondence between $\mathcal{Y}_m$ and the irreducible representations of SU(N) over $V^{\otimes m}$ is derived from Schur-Weyl duality. This duality serves as a powerful tool in representation theory, enabling the establishment of a one-to-one correspondence between the irreducible representations of the general linear group GL(N) (and consequently SU(N)) over the vector space $V^{\otimes m}$ with $\dim(V) = N$, and the irreducible representations of the group S_m on $V^{\otimes m}$ (see [62, 66] and numerous other graduate-level texts in algebra). In representation theory, it is a well-established result that the number of irreducible representations of S_m on $V^{\otimes m}$ matches the number of Young diagrams with m boxes, and that Young tableaux are in a one-to-one correspondence with the irreducible representations of S_m on $V^{\otimes m}$ [61, 62, 64, 65]. Consequently, the Schur-Weyl duality implies a similar correspondence between Young diagrams and the irreducible representations of GL(N) (and hence SU(N))

over $V^{\otimes m}$, allowing for the construction of projection operators onto the irreducible representations of SU(N) over $V^{\otimes m}$ as delineated in Eqs. D.3, D.4 and D.5. Furthermore, Young diagrams that have the same shape such as:

$$\begin{array}{|c|c|}\hline 1 & 2 \\ \hline 3 \\ \cline{1-1}\end{array} \quad \text{and} \quad \begin{array}{|c|c|}\hline 1 & 3 \\ \hline 2 \\ \cline{1-1}\end{array} \tag{D.6}$$

correspond to equivalent irreducible representations of SU(N) over $V^{\otimes m}$ in that the projection operators corresponding to these Young tableaux project onto equivalent irreducible representations of SU(N) over $V^{\otimes m}$ [44, 55]. We will come back to this point later.

Considerable research has been dedicated to deriving projection operators from the Young tableaux that adhere to the properties outlined in Eqs. D.3, D.4, and D.5, with comprehensive discussions available in [44, 55, 61, 63–66], among others. The latest advancement in this area is the formulation of Hermitian Young Projection Operators (HYPO) by H. Weigert and J. Alcock-Zeilinger, as detailed in [23, 25], which constitutes the main focus of this thesis. In [23, 25], H. Weigert and J. Alcock-Zeilinger introduced a concise and efficient algorithm, known as the MOLD algorithm, to construct projection operators onto the irreducible representations of SU(N) over $V^{\otimes m}$ from the Young tableaux, $\mathcal{Y}_m$, which are compact and Hermitian and where their depiction in birdtrack notation clearly demonstrates their Hermiticity and which satisfies Eqs. D.3, D.4, and D.5. Hermitian Young Projection Operators (and really any such projection operator as discussed previously) are constructed from the symmetrisers and antisymmetrisers as in Eqs. 3.26 and 3.27[1] and as such, their Hermiticity is easy to see in birdtrack notation since they will have a mirror symmetry about its vertical axis a la Eq. 3.19.

The notation that we will use here (and the notation commonly used for HYPO's) is P_Θ which the HYPO corresponding to the Young tableaux Θ. We emphasise again that these HYPOs are elements of API$(\mathrm{SU}(N), V^{\otimes m})$. Due to the fact, these HYPOs satisfy the condition of transversality as in Eq. D.4, one can easily see that these HYPOs are orthogonal with respect to the inner product on GL$(V^{\otimes m})$. Furthermore, one can also easily see in Figure 3.1 that these HYPOs are Hermitian (via Eq. 3.19 and 3.31). However, these HYPOs do not form a complete basis for API$(\mathrm{SU}(N), V^{\otimes m})$ as the number of HYPOs for each m is less than $m!$ (the dimension of API$(\mathrm{SU}(N), V^{\otimes m})$), i.e.

$$|\mathcal{Y}_m| < m! \quad \forall m \geq 1, m \in \mathbb{N}$$

[1] This arises from the methodology that, to construct a Young projection operator (not necessarily Hermitian) that projects onto the irreducible representations of SU(N) over $V^{\otimes m}$ for $m < 5$, one must first form the product of all symmetrisers corresponding to the rows, followed by the multiplication of this product with the product of all antisymmetrisers corresponding to the columns, alongside an appropriate normalization constant. See [25, 44, 55] for more details on this.

We need additional elements in order to form a basis for API $(\mathrm{SU}(N), V^{\otimes m})$. Enter transition operators.

D.2 Transition Operators

Recall that Young tableaux that belong to the same Young diagram correspond to equivalent representations of $\mathrm{SU}(N)$ over $V^{\otimes m}$. As such, one can define transition operators such that [23, 24]:

Definition D.2.1 (Unitary transition operators)**.** Let $\Theta, \Phi \in \mathcal{Y}_m$ be two Young tableaux with the same underlying Young diagram and P_Θ and P_Φ be the corresponding Hermitian Young Projection Operators. Then, the operator, $T_{\Theta\phi}$, satisfying the following three properties

$$\begin{aligned} &T_{\Theta\Phi} P_\Phi = T_{\Theta\Phi} = P_\Theta T_{\Theta\Phi}, \\ &T^\dagger_{\Theta\Phi} = T_{\Phi\Theta}, \\ &T_{\Theta\Phi} T_{\Phi\Theta} = P_\Theta \end{aligned} \tag{D.7}$$

is called the transition operator between P_Θ and P_Φ.

Transition operators $T_{\Theta\Phi}$ project the image of $\mathrm{GL}\,(V^{\otimes m})$ onto P_Φ and map it surjectively onto P_Θ. Hence, they are named for transitioning between subspaces and equivalent irreducible representations projected by the HYPOs of Young tableaux with the same Young diagram. H. Weigert and J. Alcock-Zeilinger further developed an efficient algorithm for calculating transition operators given a complete set of HYPOs that is detailed in [23, 24]. These transition operators, together with the HYPOs form a complete basis for API $(\mathrm{SU}(N), V^{\otimes m})$ which we shall call $\mathfrak{G}_m$. This basis is now orthogonal due to the unitarity of the transition operators but more than that, it is useful for our purposes due to the fact that its elements consist of HYPOs and transition operators which lend themselves to the nice interpretations as above and also because these transition and projection operators have a convenient multiplication table.

The multiplication table of HYPOs and transition operators is given by Eqs. D.4, D.3 and D.7 along with Schur's lemma that tells us that transition operators between projectors that correspond to different Young diagrams (Young diagrams that do not have the same shape) are 0 [23, 24]. Thus, we see that the set of all projection and transition operators corresponding to Young diagrams that have the same shape, $\mathbf{Y}_i$, form a closed subalgebra, $\mathfrak{G}_{\mathbf{Y}_i}$ of API $(\mathrm{SU}(N), V^{\otimes m})$ [23, 24]. We can make this more evident by displaying all the projection and transition operators corresponding to a specific Young diagram $\mathbf{Y}_i$ in a matrix,

$\mathfrak{M}_{\mathbf{Y}_i}$, such that its diagonal elements are the HYPOs

$$\mathfrak{m}_{ii} = P_{\Theta_i} \quad \forall \Theta_i \in \mathcal{Y}_m \text{ with underlying diagram } \mathbf{Y}_i \tag{D.8}$$

and the off-diagonal elements are the transition operators

$$\mathfrak{m}_{ij} = T_{\Theta_i \Theta_j} \quad \forall \Theta_i, \Theta_j \in \mathcal{Y}_m \text{ with underlying diagram } \mathbf{Y}_i \tag{D.9}$$

Subsequently, a larger matrix, $\mathfrak{M}$, encompassing all the HYPOs and transition operators can be constructed by positioning the matrices $\mathfrak{M}_{\mathbf{Y}_i}$ along the diagonal corresponding to a specific m. The remaining entries are filled with zeros, given that transition operators between Young tableaux of differing shapes are null, thus resulting in a block diagonal matrix:

$$\mathfrak{M} = \begin{pmatrix} \mathfrak{M}_{\mathbf{Y}_1} & 0 & \cdots & 0 \\ 0 & \mathfrak{M}_{\mathbf{Y}_2} & \cdots & 0 \\ \vdots & \vdots & \ddots & \vdots \\ 0 & 0 & \cdots & \mathfrak{M}_{\mathbf{Y}_k} \end{pmatrix} \tag{D.10}$$

Equation D.10 thus makes it clear that the multiplication table of $\mathfrak{G}_m$ satisfies the following property:

$$\mathfrak{m}_{ij}\mathfrak{m}_{kl} = \delta_{jk}\mathfrak{m}_{il}. \tag{D.11}$$

and thus, we see why the basis, $\mathfrak{G}_m$ is much more convenient to work with even though it lacks the desired property of orthogonality. In the new notation, we have that:

$$\text{API}\left(\text{SU}(N), V^{\otimes m}\right) = \{\alpha_{ij}\mathfrak{m}_{ij} \mid \alpha_{ij} \in \mathbb{R}, \mathfrak{m}_{ij} \in S_m\}, \tag{D.12}$$

The complete set of all HYPOs and transition operators for $m = 1, 2, 3, 4$ is given in Figure 3.1 which is used throughout this thesis [23, 24]:

A comment on the size of m relative to N is needed. Notice that the total antisymmetriser for $m = 3$ becomes 0 if we have $N < 3$. This is because the dimension of the vector space V is now 2. When $P_{\begin{smallmatrix}1\\2\\3\end{smallmatrix}}$ acts on $V^{\otimes 3}$, say on $V^{\otimes 3}$ of the form $\mathbf{v} = v^{i_1 i_2 i_3}$, there are only two possible values for an i_n due to $\dim(V) = 2 < 3$, leading to repeats in the indices of $\mathbf{v}$. Thus, a total antisymmetriser acting on $\mathbf{v} = v^{i_1 i_2 i_3}$ always yields 0 if $N < 3$. Consequently, the dimension of the irreducible representation that $P_{\begin{smallmatrix}1\\2\\3\end{smallmatrix}}$ projects onto is 0, making $P_{\begin{smallmatrix}1\\2\\3\end{smallmatrix}}$ a null operator for $N < m$; this is a dimensional zero. Generally, when $N < m$, null operators appear for the HYPOs and transition operators [23, 24]. Therefore, one must consider this when using explicit values of N and m, and these dimensional zeroes naturally appear in the

matrix $\mathfrak{M}$ from Eq. D.11.

Bibliography

[1] R. Mann, *An Introduction to Particle Physics and the Standard Model*. Taylor & Francis, 2010.

[2] D. Griffiths, *Introduction to Elementary Particles*. John Wiley & Sons, New York, USA, 1987.

[3] S. Weinberg, *The quantum theory of fields. Vol. 2: Modern applications*. Cambridge University Press, 8, 2013.

[4] M. E. Peskin and D. V. Schroeder, *An Introduction to Quantum Field Theory*. Westview Press, 1995. Reading, USA: Addison-Wesley (1995) 842 p.

[5] W. Busza, K. Rajagopal, and W. van der Schee, *Heavy Ion Collisions: The Big Picture, and the Big Questions*, *Ann. Rev. Nucl. Part. Sci.* **68** (2018) 339–376, [arXiv:1802.04801].

[6] M. Riordan and W. A. Zajc, *The first few microseconds*, *Scientific American* **294** (May, 2006) 34–41.

[7] L. V. Gribov, E. M. Levin, and M. G. Ryskin, *Semihard Processes in QCD*, *Phys. Rept.* **100** (1983) 1–150.

[8] A. H. Mueller, *Parton saturation: An Overview*, in *Cargese Summer School on QCD Perspectives on Hot and Dense Matter*, pp. 45–72, 11, 2001. hep-ph/0111244.

[9] J. Jalilian-Marian and Y. V. Kovchegov, *Saturation physics and deuteron-Gold collisions at RHIC*, *Prog. Part. Nucl. Phys.* **56** (2006) 104–231, [hep-ph/0505052].

[10] Y. V. Kovchegov and E. Levin, *Quantum Chromodynamics at High Energy*, vol. 33. Oxford University Press, 2013.

[11] E. Iancu, A. Leonidov, and L. McLerran, *The Color Glass Condensate: An Introduction*, in *Cargese Summer School on QCD Perspectives on Hot and Dense Matter*, pp. 73–145, 2, 2002. hep-ph/0202270.

[12] E. Iancu and R. Venugopalan, *The Color Glass Condensate and high-energy scattering in QCD*, pp. 249–3363. 3, 2003. hep-ph/0303204.

[13] H. Weigert, *Evolution at small x(bj): The Color glass condensate*, *Prog. Part. Nucl. Phys.* **55** (2005) 461–565, [hep-ph/0501087].

[14] F. Gelis, E. Iancu, J. Jalilian-Marian, and R. Venugopalan, *The Color Glass Condensate*, *Ann. Rev. Nucl. Part. Sci.* **60** (2010) 463–489, [arXiv:1002.0333].

[15] L. McLerran, *The Color Glass Condensate and Glasma*, arXiv:0804.1736.

[16] F. Gelis, *Color Glass Condensate and Glasma*, *Int. J. Mod. Phys. A* **28** (2013) 1330001, [arXiv:1211.3327].

[17] C. Marquet and H. Weigert, *New observables to test the Color Glass Condensate beyond the large- N_c limit*, *Nucl. Phys. A* **843** (2010) 68–97, [arXiv:1003.0813].

[18] E. Iancu, A. H. Mueller, and D. N. Triantafyllopoulos, *CGC factorization for forward particle production in proton-nucleus collisions at next-to-leading order*, *JHEP* **12** (2016) 041, [arXiv:1608.05293].

[19] I. O. Cherednikov, T. Mertens, and F. F. V. der Veken, *Wilson Lines in Quantum Field Theory*. De Gruyter, Berlin, München, Boston, 2014.

[20] F. Fiorani, G. Marchesini, and L. Reina, *Soft-gluon factorization and multi-gluon amplitude*, *Nuclear Physics B* **309** (1988), no. 3 439–460.

[21] F. Dominguez, C. Marquet, B.-W. Xiao, and F. Yuan, *Universality of Unintegrated Gluon Distributions at small x*, *Phys. Rev. D* **83** (2011) 105005, [arXiv:1101.0715].

[22] S. Munier, S. Peigné, and E. Petreska, *Medium-induced gluon radiation in hard forward parton scattering in the saturation formalism*, *Phys. Rev. D* **95** (2017), no. 1 014014, [arXiv:1603.01028].

[23] J. M. Alcock-Zeilinger, *Symmetry Implications for Wilson Line Correlators in QCD at High Energies*. PhD thesis, Cape Town U., 2017.

[24] J. Alcock-Zeilinger and H. Weigert, *Transition Operators*, *J. Math. Phys.* **58** (2017), no. 5 051703, [arXiv:1610.08802].

[25] J. Alcock-Zeilinger and H. Weigert, *Compact Hermitian Young Projection Operators*, *J. Math. Phys.* **58** (2017), no. 5 051702, [arXiv:1610.10088].

[26] J. Alcock-Zeilinger and H. Weigert, *Simplification Rules for Birdtrack Operators*, *J. Math. Phys.* **58** (2017), no. 5 051701, [arXiv:1610.08801].

[27] H. Weigert, *Unitarity at small Bjorken x*, *Nucl. Phys. A* **703** (2002) 823–860, [hep-ph/0004044].

[28] Y. V. Kovchegov, *Small x F(2) structure function of a nucleus including multiple pomeron exchanges*, *Phys. Rev. D* **60** (1999) 034008, [hep-ph/9901281].

[29] Y. V. Kovchegov, *Unitarization of the BFKL pomeron on a nucleus*, *Phys. Rev. D* **61** (2000) 074018, [hep-ph/9905214].

[30] I. Balitsky, *Operator expansion for high-energy scattering*, *Nucl. Phys. B* **463** (1996) 99–160, [hep-ph/9509348].

[31] I. Balitsky, *Operator expansion for diffractive high-energy scattering*, *AIP Conf. Proc.* **407** (1997), no. 1 953, [hep-ph/9706411].

[32] I. Balitsky, *Factorization and high-energy effective action*, *Phys. Rev. D* **60** (1999) 014020, [hep-ph/9812311].

[33] R. Moerman, "A gauge-invariant, symmetry-preserving truncation of JIMWLK." Master's thesis, University of Cape Town, January, 2018. Available at: https://open.uct.ac.za/items/87c3c3a9-435e-4895-bb87-3bb0bf0c7f01.

[34] M. D. Schwartz, *Quantum Field Theory and the Standard Model*. Cambridge University Press, 3, 2014.

[35] T. J. Hobbs, *The Nonperturbative Structure of Hadrons*. PhD thesis, Indiana U., 8, 2014. arXiv:1408.5463.

[36] A. Bacchetta, *Probing the Transverse Spin of Quarks in Deep Inelastic Scattering*. PhD thesis, Vrije U., Amsterdam, 2002. hep-ph/0212025.

[37] D. Adamiak, "Rapidity evolution of observables at high energies using the gaussian truncation." Master's thesis, University of Cape Town, November, 2018. Available at: https://open.uct.ac.za/items/296b7089-c2a8-4ea2-a41e-45788c33fa11.

[38] Y. V. Kovchegov, J. Kuokkanen, K. Rummukainen, and H. Weigert, *Subleading-N(c) corrections in non-linear small-x evolution*, *Nucl. Phys. A* **823** (2009) 47–82, [arXiv:0812.3238].

[39] T. Lappi, A. Ramnath, K. Rummukainen, and H. Weigert, *JIMWLK evolution of the odderon*, *Phys. Rev. D* **94** (2016), no. 5 054014, [arXiv:1606.00551].

[40] J. Rayner, "Reps for JIMWLK: Applications of representation theory to a novel approach to the JIMWLK equation." Master's thesis, University of Cape Town, January, 2018. Available at: https://open.uct.ac.za/items/feee451c-cd28-460b-a851-d1256386f90a.

[41] J. Bohra, "The Jet/CGC Correspondence: A Conformal Perspective.." Master's thesis, University of Cape Town, March, 2023. Available at: https://open.uct.ac.za/items/ed57df55-94ad-4673-bb00-dd2f7e2c8de6.

[42] T. Becher, T. Rauh, and X. Xu, *Two-loop anomalous dimension for the resummation of non-global observables*, *JHEP* **08** (2022) 134, [arXiv:2112.02108].

[43] S. Plätzer, *Amplitude and colour evolution*, *SciPost Phys. Proc.* **15** (2024) 007, [arXiv:2210.09178].

[44] P. Cvitanovic, *Group Theory: Birdtracks, Lie's, and Exceptional Groups*. Princeton University Press, 5, 2020.

[45] J. Jalilian-Marian, A. Kovner, L. D. McLerran, and H. Weigert, *The Intrinsic glue distribution at very small x*, *Phys. Rev. D* **55** (1997) 5414–5428, [hep-ph/9606337].

[46] J. N. Guenther, *Overview of the QCD phase diagram*, *The European Physical Journal A* **57** (Apr, 2021) 136.

[47] E. Rutherford, *Lxxix. the scattering of α and β particles by matter and the structure of the atom*, *The London, Edinburgh, and Dublin Philosophical Magazine and Journal of Science* **21** (1911), no. 125 669–688, [https://doi.org/10.1080/14786440508637080].

[48] **ATLAS** Collaboration, M. Aaboud et al., *Measurement of the Inelastic Proton-Proton Cross Section at $\sqrt{s} = 13$ TeV with the ATLAS Detector at the LHC*, *Phys. Rev. Lett.* **117** (2016), no. 18 182002, [arXiv:1606.02625].

[49] M. Srednicki, *Quantum field theory*. Cambridge University Press, 1, 2007.

[50] J. Alcock-Zeilinger and H. Weigert, *Compact construction algorithms for the singlets of SU(N) over mixed tensor product spaces*, arXiv:1812.11223.

[51] J. M. Alcock-Zeilinger, "The Special Unitary Group, Birdtracks, and Applications in QCD." Lecture Notes, University of Tübingen, 2018. Available at: https://www.math.uni-tuebingen.de/de/forschung/maphy/lehre/ss-2018/sun/dateien/birdtracks-sun-qcd-lecturenotes.pdf.

[52] S. Keppeler, *Birdtracks for SU(N)*, *SciPost Phys. Lect. Notes* **3** (2018) 1, [arXiv:1707.07280].

[53] N. Jacobson, *Basic Algebra II: Second Edition*. Dover Books on Mathematics. Dover Publications, 2012.

[54] S. Lang, *Linear Algebra*. Undergraduate Texts in Mathematics. Springer New York, 2013.

[55] W. Tung, *Group Theory in Physics*. G - Reference,Information and Interdisciplinary Subjects Series. World Scientific, 1985.

[56] S. Keppeler and M. Sjodahl, *Orthogonal multiplet bases in SU(Nc) color space*, *JHEP* **09** (2012) 124, [arXiv:1207.0609].

[57] M. Sjodahl and J. Thorén, *Decomposing color structure into multiplet bases*, *JHEP* **09** (2015) 055, [arXiv:1507.03814].

[58] R. Graham, M. Grötschel, and L. Lovász, *Handbook of Combinatorics*. No. v. 1 in Handbook of Combinatorics. Elsevier Science, 1995.

[59] I. Goulden and D. Jackson, *Combinatorial Enumeration*. Dover Books on Mathematics. Dover Publications, 2004.

[60] W. Research, "Sort." https://reference.wolfram.com/language/ref/Sort.html, 2017.

[61] W. Fulton, *Young Tableaux: With Applications to Representation Theory and Geometry*. London Mathematical Society Student Texts. Cambridge University Press, 1997.

[62] B. Sagan, *The Symmetric Group: Representations, Combinatorial Algorithms, and Symmetric Functions*. Graduate Texts in Mathematics. Springer New York, 2013.

[63] S. Keppeler and M. Sjödahl, *Hermitian Young Operators*, *J. Math. Phys.* **55** (2014) 021702, [arXiv:1307.6147].

[64] D. Littlewood, *The Theory of Group Characters and Matrix Representations of Groups*. AMS Chelsea Publishing Series. University Microfilms, 1977.

[65] W. Fulton and J. Harris, *Representation Theory: A First Course*. Graduate texts in mathematics. Springer, 1991.

[66] R. Goodman and N. Wallach, *Symmetry, Representations, and Invariants*. Graduate Texts in Mathematics. Springer New York, 2009.

[67] J. M. Maldacena, *The Large N limit of superconformal field theories and supergravity*, *Adv. Theor. Math. Phys.* **2** (1998) 231–252, [hep-th/9711200].

[68] S. Weinberg, *The Quantum Theory of Fields, Volume 1: Foundations*. Cambridge University Press, 2005.

[69] S. M. Carroll, *Spacetime and Geometry: An Introduction to General Relativity*. Cambridge University Press, 7, 2019.

[70] M. Artin, *Algebra*. Pearson Education, 2011.

[71] H. Weigert. Personal Communication.

[72] J. M. Campbell et al., *Event generators for high-energy physics experiments*, *SciPost Phys.* **16** (2024), no. 5 130, [arXiv:2203.11110].

[73] G. Bewick et al., *Herwig 7.3 release note*, *Eur. Phys. J. C* **84** (2024), no. 10 1053, [arXiv:2312.05175].